Addendum and Errata

Addendum

All experiments were performed on a Varian XL-200 spectrometer. The static magnetic field is provided by a superconducting solenoid with a strength of 4.7 Tesla. At this field strength proton resonance occurs at 200 MHz, carbon-13 at 50.3 MHz and nitrogen-15 at 20.3 MHz. All experimental results reported in this thesis are in frequency units of Hz. Axes are labelled in frequency units of offset from the transmitter/receiver frequency.

Errata

Chapter 3

p. 89, line 12: '$\alpha < \frac{\pi}{2}$' should be written as '$\frac{(n-1)\pi}{2} < \alpha < \frac{(n+1)\pi}{2}$; $n = 0,4,8,\ldots$'

p. 89, line 13: '$\alpha > \frac{\pi}{2}$' should be written as '$\frac{(n+1)\pi}{2} < \alpha < \frac{(n+3)\pi}{2}$; $n = 0,4,8,\ldots$'

Chapter 4

p. 131, line 20: '2,3-dibromothiophene' should be written as '2,3-dibromopropionic acid'

Microfilmed
by BLLD
D45841/83

Ph.D. C 1276 : RSL

New Techniques in Fourier Transform Nuclear Magnetic Resonance

A thesis submitted for the degree of
Doctor of Philosophy
of the University of Oxford

by

Thomas Harold Mareci

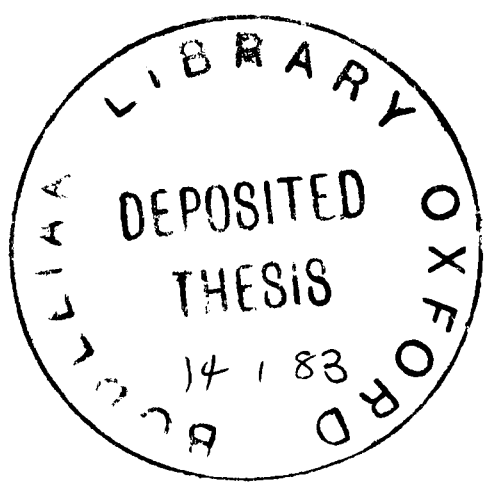

Magdalen College
Trinity Term, 1982

New Techniques in Fourier Transform Nuclear Magnetic Resonance

A thesis submitted for the degree of
Doctor of Philosophy

by

Thomas Harold Mareci

Magdalen College
Trinity Term, 1982

Abstract

New techniques in Fourier transform nuclear magnetic resonance spectroscopy are introduced with chemical applications to the study of molecules in the liquid state.

Recently a theoretical description of magnetic resonance in terms of single transition operators has been introduced which provides a geometric interpretation of the behaviour of a spin system. This formalism is developed further and extended to the general description of a system of nonequivalent spin-1/2 nuclei. Operator combinations are introduced which allow extension of the convenient geometric representation to the concerted behaviour of coupled spins. The operator formalism is applied to the excitation and detection of multiple quantum transitions, providing a description of the processes in terms of rotating vectors.

The process of coherence transfer in two-dimensional Fourier transform experiments is studied in detail and single transition operators are used to derive a general expression for the tip angle dependence of the detection process. A method of discriminating the sense of precession of double quantum coherence is presented and applied to the correlation of chemical shifts of carbon-13 spins in natural abundance. A new technique is presented for the correlation of chemical shift information in coupled proton spin systems in which excitation and indirect detection of double quantum transitions is used to assign coupling patterns in complex spectra. The tip angle dependence of the detection process is used to suppress all but direct correlation of spins.

Methods for the measurement of heteronuclear coupling constants in proton spectra are introduced which discriminate the heteronuclear satellites from the parent proton resonance. The technique provides a sensitivity advantage over direct measurement of coupling in the heteronuclear spectrum. Ambiguities are encountered when the proton-proton and proton-heteronuclear coupling constants are of the same order of magnitude. This problem is overcome by extension of the basic experiment to its two-dimensional analogue.

Acknowledgement

It is a pleasure to acknowledge the help and support of my coworkers; Ad Bax, Tom Frenkiel, James Keeler, Stewart Kempsell, Malcolm Levitt, Gareth Morris, Pei Feng-kui, Regina Schuck and A. J. Shaka. Their work and my own are so intimately tied that specific acknowledgement is difficult. However I would particularly like to thank my supervisor, Dr. Ray Freeman, for his support and encouragement. His experience and advice have proved a constant source of enlightenment during this research and I would like to thank him for the opportunity to work in his research group in Oxford.

I would also like to thank my family for their help and support with special thanks extended to my wife, Debra, for providing the artwork for this thesis and financial support while this work was in progress. This thesis would not have been possible without her love and encouragement.

For Joseph Robert

Table of Contents

1 Introduction

1.1 Introduction 1

1.2 The phenomenological equations of Bloch 3

1.3 Fourier transform spectroscopy 6

1.4 Two-dimensional Fourier transform spectroscopy 10

1.4.1 Application of two-dimensional spectroscopy 13

References 19

2 Density operator formalism

2.1 Introduction 21

2.2 The density operator formalism 22

2.2.1 Transformation to the rotating frame 25

2.2.2 RF pulses in the rotating frame 27

2.3 Introduction to operator formalism 31

2.3.1 Two level system, single spin-1/2 33

2.3.2 Single transition operators 44

2.3.3 Multiple level system 45

2.4 The density operator in terms of single transition operators 50

2.4.1 General discussion of time evolution 54

2.4.2 Free precession 54

2.4.3 Pulsed excitation 57

2.4.4 Phase shifts 59

2.4.5 Observable magnetization 60

2.5 Linear combinations of single transition operators 61

2.6 Application to a system of two coupled spin-1/2 particles 68

2.6.1 The Carr-Purcell spin echo pulse sequence 72

2.6.2 Combination operators for an AX spin system 76

2.6.3 Excitation and detection of double quantum coherence 78

References 81

3 Coherence transfer in two-dimensional spectroscopy

3.1 Introduction 83

3.2 Coherence transfer echoes 84

3.3 Coherence transfer for a single spin-1/2 system 87

3.4 Coherence transfer for coupled spins: AX spin system 89

3.4.1 Transfer of single quantum coherences 90

3.4.2 Transfer of zero quantum coherence 94

3.4.3 Transfer of double quantum coherence 98

3.5 General coherence transfer formulation 104

References 111

4 Homonuclear correlation through double quantum coherences

4.1 Introduction 112

4.2 Excitation of double quantum coherence in an AMX spin system 117

4.3 Indirect detection of double quantum coherence in an AMX spin system 122

4.4 Folding for optimum use of data space 129

4.5 Broadband decoupling in the F_1 dimension 130

4.6 Practical application of correlation through double quantum coherence 132

References 134

5 Heteronuclear coupling constants measured in proton spectra

5.1 Introduction 135

5.2 Heteronuclear satellites in proton spectra 137

5.3 Two-dimensional observation of satellites in proton spectra 143

References 146

Appendix

A.1 The density operator at thermal equilibrium in the high temperature limit 147

A.2 Reduced density operator 149

Chapter 1

Introduction

1.1. Introduction

Since the early measurement of nuclear magnetic resonance (NMR) in molecular beams [1.1] and later in bulk material [1.2,1.3], research in NMR spectroscopy has continued to expand to the point where substances as diverse as liquid helium [1.4] and the entire human body [1.5] are being studied with the same basic technique. In the middle ground between these two extremes lies the rich and varied field of chemical applications of nuclear magnetic resonance.

NMR finds itsuse in chemistry mainly through the study of molecular structure. This is made possible by three types of interactions for nuclear magnetic moments in a molecule [1.6,1.7]. The first is the direct effect of neighbouring nuclear magnetic dipoles. In liquid samples, because of the rapid tumbling of the molecules, the anisotropy of dipolar interaction is averaged to zero leaving only an average isotropic contribution. The effect of the rapidly tumbling dipoles is to provide a mechanism for the nuclear spins to reach an equilibrium with their surroundings with the rate determined by the environment of each spin. The approach to equilibrium is termed relaxation and the reciprocal of the rate constants are called relaxation times. The second type of interaction is the result of the presence of electrons near the nuclear spins. A contribution to the magnetic field experienced by the nuclear spin is induced in the circulating motion of the electrons by the application of a static magnetic field. The

effective magnetic field at the nucleus can be written as,

$$B = B_0(1 - \sigma) \tag{1.1}$$

where σ represents the strength of the perturbation due to the surrounding electrons and B_0 is the applied static magnetic field. The field dependent effect, σ, is called the chemical shift and is sensitive to the nature and geometry of bonding and the presence of substituents near a nuclear spin. The final effect is the result of the presence of spin on the electron with an accompanying magnetic moment. The nuclear magnetic moment affects the surrounding electron magnetic dipoles and therefore indirectly affects the energy states of other nuclear spins. The nuclear spins are thus effectively coupled by the electronic magnetic moments. The strength of the coupling is independent of the strength of the applied field and is termed the spin-spin or indirect coupling constant denoted by J. The relaxation times, chemical shift and coupling constants of a nuclear spin are indicative of molecular structure and are used as assignment tools by chemists. This thesis will be concerned mainly with new methods for the correlation of chemical shifts and coupling constants among spins to provide information about molecular structure.

In this chapter the semi-classical description of NMR by the Bloch equations [1.8] is presented and properties of Fourier transform NMR spectroscopy reviewed. The general aspects of two-dimensional Fourier spectroscopy are discussed and an application is presented.

In chapter 2 the formal quantum mechanical description of the NMR experiment is developed from the point of view of the statistical density operator. The relationship between the quantum description of a system with a single spin-1/2 and the Bloch model is presented and a geometric representation of the quantum process introduced. Extension

to more complicated spin systems is possible using the recently developed single transition operator formalism [1.9]. In the past these operators have been used to provide a geometric interpretation of experiments for spin-1 particles and transition selective excitation. In chapter 2 it is shown that a geometric description of experiments for coupled nonequivalent spin-1/2 particles is also possible using the single transition operator formalism. The excitation of the spin system is not required to be transition selective and the operator formalism leads to a geometric interpretation of the equations of motion.

1.2. The phenomenological equations of Bloch

In 1946 Bloch introduced a description of magnetic resonance based on arguments from classical physics [1.8]. The model assumes that the magnetization of bulk material under the influence of a magnetic field can be described by classical electrodynamics. The magnetic energy for such a system can be written as,

$$E = - M.B \tag{1.2}$$

where M is the magnetic moment and B the applied magnetic field. The magnetic moment of bulk material is the resultant of the magnetic moment, μ, of each spin. The magnetic moment of a nucleus lies parallel to its angular momentum, $\hbar I$, with proportionality constant, γ, called the gyromagnetic ratio. From classical mechanics the rate of change of angular momentum is equal to the applied torque so the equation of motion of a spin which has an angular momentum and a magnetic moment in an applied field can be written as,

$$\hbar \frac{dI}{dt} = \mu \times B \tag{1.3}$$

or since $\mu = \gamma\hbar I$,

$$\frac{d\mu}{dt} = \gamma(\mu \times B) \quad . \tag{1.4}$$

For noninteracting spins in bulk material the equation of motion for the magnetization can be written as,

$$\frac{dM}{dt} = \gamma(M \times B) \quad . \tag{1.5}$$

This equation can be interpreted geometrically as a rotation of the magnetic moment about the applied field at the Larmor precession frequency, $|\omega| = |\gamma B|$.

In the development of equation 1.5 it was assumed that the magnetic moment only interacts with the applied field. To include the interaction of the spins among themselves and with the surrounding environment the effect of thermal motion and spin-spin interaction must be considered.

For a static field applied along the z-axis the magnetic energy can be written as,

$$E = - M_z B_0 \quad . \tag{1.6}$$

Exchanges of energy between the magnetic moments and their surroundings (called the lattice) will cause a change in only the z-component of magnetic moment. The energy exchange will allow the spins to reach equilibrium with the lattice. The equilibrium value of M_z will be denoted M_0 and z-magnetization will be assumed to approach M_0 exponentially with a time constant T_1 called the spin-lattice relaxation time.

The interaction of spins within the system cannot cause a change in the overall magnetic energy of the spin system but is assumed to cause a loss of magnetization in the plane transverse to the applied static field and will therefore effect only the x- and y-components of magnetic moment. The decay of magnetization is assumed to be exponential with time constant T_2 called the spin-spin relaxation time.

The effects of relaxation can be included in equation 1.5 to give the component equations first introduced by Bloch.

$$\frac{dM_x}{dt} = \gamma(M \times B)_x - \frac{M_x}{T_2}$$

$$\frac{dM_y}{dt} = \gamma(M \times B)_y - \frac{M_y}{T_2} \qquad (1.7)$$

$$\frac{dM_z}{dt} = \gamma(M \times B)_z - \frac{(M_0 - M_z)}{T_1}.$$

The original resonance experiments involve measurement at a fixed frequency with the static magnetic field swept through resonance [1.2,1.3]. A weak excitation field is applied in a plane transverse to the static field and transverse magnetization is detected in the phase sensitive mode at the resonance frequency. The solution of the Bloch equations 1.7 under these conditions represent Lorentzian absorption and dispersion lineshapes depending on the phase of the detector.

In chapter 2 it is shown that equation of motion 1.4 for a single spin can be derived from quantum mechanical principles using the Schroedinger equation. An operator form of description is developed which can be seen to represent rotating components of magnetic moment when there is a definite phase coherence between states of the spin system. Consider the case of an isolated spin-1/2 nucleus. If there exists a finite probability of the spin being in both states, a

transverse component of magnetization will be detected when the states have a coherence of phase. The concept of transverse magnetization and coherence are intimately related, however a clear distinction must be drawn. A coherence can be present even if an observable component of magnetization is not. The concept of coherence is more general and can apply to any possible transition between two states of a multiple level system. Thus a coherence can exist between two levels of a system which represent a simultaneous transition of more than one spin or for spin ≥ 1 a multiple quantum transition. This would not correspond to an observable magnetization because it violates the selection rule, $\Delta m_z = \pm 1$ [1.10].

As will be shown later, it is possible to indirectly detect normally unobservable coherences with the technique of two-dimensional spectroscopy. The concept of a coherence transfer is involved and will be discussed in detail in chapter 3. The idea is to transfer coherence existing between two levels to a state of coherence for two other levels which represent observable magnetization. Care must be taken with the terminology to avoid confusion. A common expression is to speak of a coherence transfer from coherence to coherence. Perhaps a better way of expressing this is to speak of a coherence transfer from one transition to another transition.

1.3. Fourier transform spectroscopy

In contrast to measurements at a fixed frequency performed by sweeping the applied field, it is possible to observe the time response of a spin system following a period of excitation and extract the frequency spectrum by Fourier transformation [1.11]. The information is collected in discrete steps separated by a fixed interval of time. The sampling rate determines the spectral width and the total acquisition

time determines the frequency resolution.

The acquisition of signal in the time domain allows the excitation to be repeated as soon as the system has recovered toward equilibrium [1.12]. This permits efficient signal averaging for improved sensitivity with the frequency spectrum calculated at a convenient time at the end of the experiment [1.11b]. This improvement in sensitivity has extended the range of spins accessible to observation by NMR so that most of the spins encountered in organic molecules are routinely observed.

In magnetic resonance the amplitude of the time response decays due to loses in coherence from magnetic field inhomogeneity and spin-spin relaxation processes. The time response is termed a free induction decay. Consider a system consisting of a single spin, the observed free induction decay can be written as,

$$S(t) = M_0 \, e^{-\lambda t} \, e^{i\Omega t + \phi} \qquad (1.8)$$

where M_0 is the initial amplitude of the magnetization, $\lambda = (T_2^*)^{-1}$ is the reciprocal of the effective relaxation time, T_2^*, representing field inhomogeneity effects and spin-spin relaxation processes, Ω is the precessional frequency and ϕ is the initial phase of the signal. This represents a complex signal determined by quadrature detection of the magnetization [1.13]. The use of quadrature detection will be assumed throughout this thesis.

In practice the Fourier transformation is carried out by a digital transformation of the discrete data, however the essence of the relationship between time and frequency response can be represented by a continuous transformation. Assume that the signal is measured for a time, $T \gg T_2^*$, then the complex Fourier transformation can be written as

[1.14],

$$S(\omega) = \int_0^\infty dt\ e^{-i\omega t}\ S(t)$$

$$= M_0\ e^{i\emptyset}\ \left(\frac{\lambda + i\Delta\omega}{\lambda^2 + \Delta\omega^2}\right)$$

$$= M_0\ e^{i\emptyset}\ [A(\omega) + iD(\omega)] \qquad (1.9)$$

where $\Delta\omega = \Omega - \omega$ and,

$$A(\omega) = \frac{\lambda}{\lambda^2 + \Delta\omega^2} \qquad (1.10)$$

and

$$D(\omega) = \frac{\Delta\omega}{\lambda^2 + \Delta\omega^2}\ . \qquad (1.11)$$

The terms A and D represent absorption and dispersion Lorentzian lineshapes. The amount of absorption or dispersion present in the real and imaginary portion of the frequency spectrum is determined by the phase angle, $\emptyset$. A phase correction can be applied to the spectrum so that the real part is in pure absorption and the imaginary in pure dispersion. The correction is effected by multipling the spectrum by $e^{-i\emptyset}$.

Two commonly used modes of spectral display are the phase sensitive mode given by equation 1.9 and the absolute value mode. The absolute value is defined as the square root of the sum of the squares of the real and imaginary part of a complex quantity [1.15] so the absolute value of the spectrum is given by,

$$|S(\omega)| = M_0\ [A^2(\omega) + D^2(\omega)]^{1/2}$$

$$= M_0 \, (\lambda^2 + \Delta\omega^2)^{-1/2}. \qquad (1.12)$$

This mode of display is independent of the initial phase of the signal and has the same peak height as the absorption component of the phase sensitive mode. The linewidth at half height for the absolute value lineshape is a factor of $(3)^{1/2}$ larger than for the absorption lineshape.

The frequency spectrum derived from Fourier transformation of the time domain signal represents the frequency response of the spin system during the period of observation. The history of the spin system prior to observation is transmitted to the spectrum through the initial amplitude and phase of the free induction decay. Since the entire frequency range of a spectrum is observed simultaneously in the time domain it is possible to follow the time development of complicated spin systems with the Fourier transformation process. For example it is possible to measure relaxation times, T_1 and T_2, for all the spins in a complex molecule [1.16].

Spin-lattice relaxation is usually observed with the inversion-recovery sequence first proposed by Hahn [1.17]. In this pulse sequence the spins initially at thermal equilibrium are inverted by a π pulse, allowed to relax for a time, τ, then a free induction decay is measured following a monitoring pulse. After Fourier transformation the intensity of each line in the spectrum represents the recovery of the associated spin back to equilibrium as a function of τ. In this way accurate measurement of T_1 can be made in a complex spectrum.

The spin-spin relaxation time can be determined using the spin echo sequence proposed by Carr and Purcell [1.18]. The spin system initially at thermal equilibrium is rotated into a state of transverse magnetization by a $\frac{\pi}{2}$ pulse. The system freely precesses for a time τ

Basic two-dimensional experiment

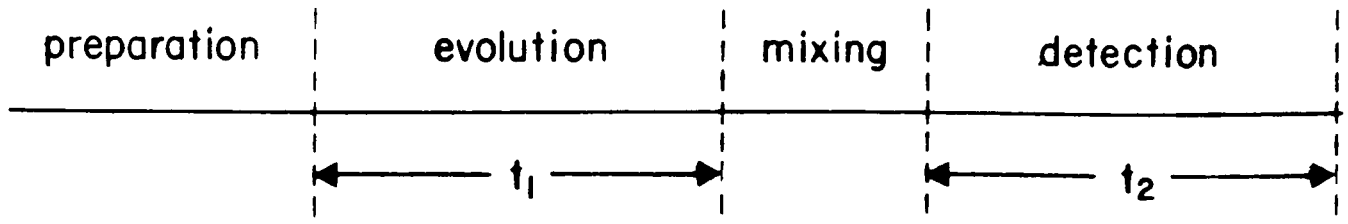

Basic two-dimensional spectrum

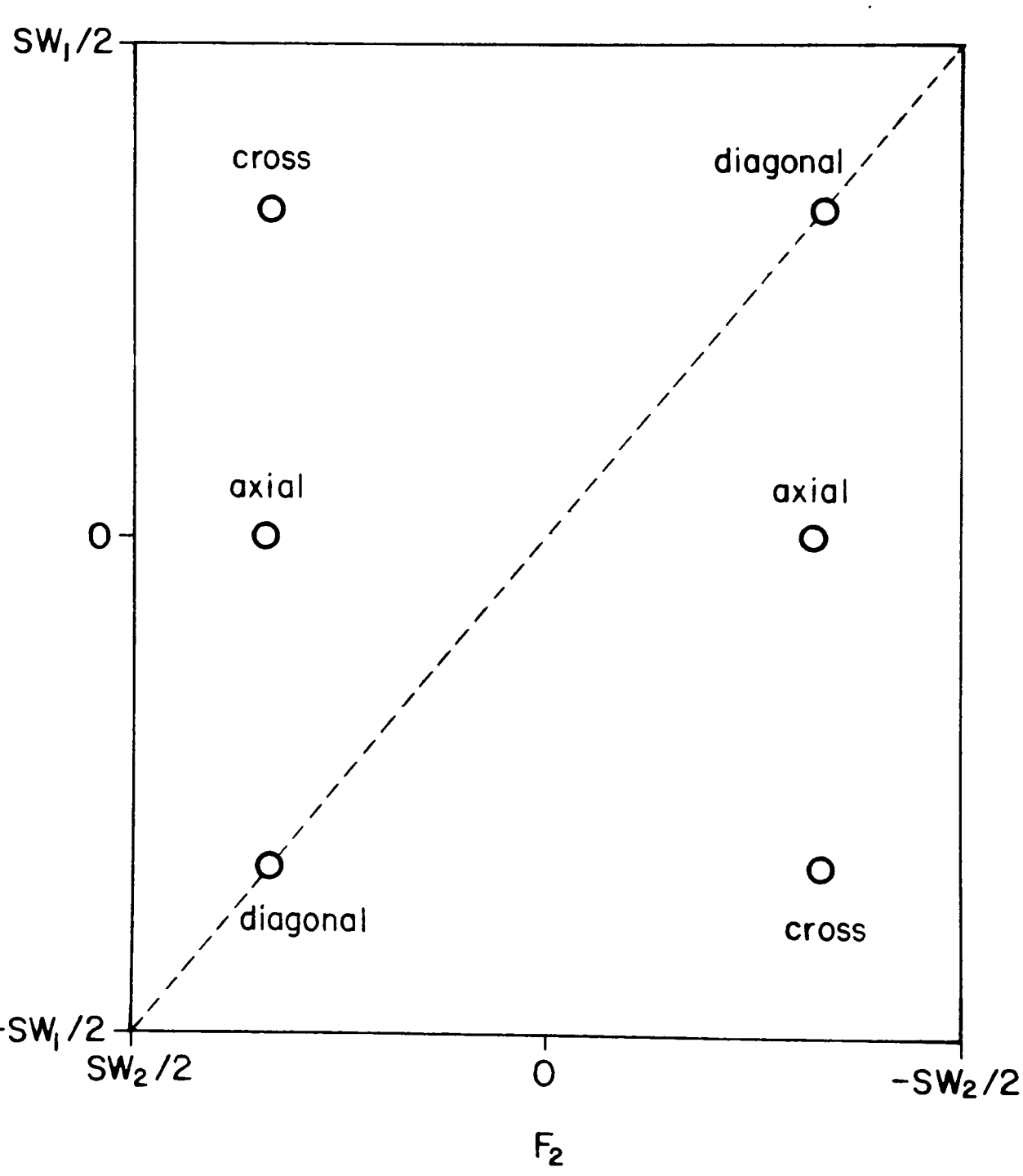

Figure 1.1 General nomenclature for two-dimensional Fourier transform spectroscopy. The basic elements of the two-dimensional experiment are diagrammed at the top. An idealized two-dimensional spectrum is shown at the bottom.

losing coherence due to field inhomogeneity and spin-spin relaxation processes. The application of a π pulse refocusses inhomogeneity effects at time 2τ resulting in a loss of signal intensity due to only spin-spin relaxation processes in the absence of diffusion. A free induction decay is acquired starting at 2τ and Fourier transformed with the resulting line intensities reflecting the transverse relaxation as a function of τ.

1.4. Two-dimensional Fourier transform spectroscopy

An extension of Fourier spectroscopy into two frequency dimensions was proposed by Jeener in 1971 [1.19]. The basic idea is to record a series of free induction decays as a function of a time parameter which reflects the history of the spin system before acquisition. This procedure provides a method of indirectly detecting the evolution of the spin system prior to observation. The information is transmitted through the initial amplitude and phase of each free induction decay. After Fourier transforming the free induction decays, the resulting matrix of spectral data points can be transposed into a series of 'interferograms'; one for each frequency point in the spectrum [1.20,1.21]. These interferograms are functions of the time parameter of prior evolution so that a further transformation constructs a spectrum which is a function in two frequency dimensions. The meaning of the time parameter is determined by each experiment.

A general nomenclature can be introduced to describes a two-dimensional experiment [1.20]. The experiment can be divided into four intervals as shown at the top of figure 1.1. The detection time, t_2, is the time required for observation of each free induction decay and is the time variable of the first Fourier transformation. The resulting frequency dimension is referred to as F_2. The evolution time, t_1, is

constant for each observation of a free induction decay and is incremented to form a series of F_2 spectra with the incremental step size determining the spectral width in the second frequency dimension called F_1. All four intervals may contain a mixture of pulses and delays. The preparation period is used to establish the initial condition of the system at the beginning of the evolution time. The effective interactions of the system during the evolution period determine the information available in the F_1 spectrum and the mixing period establishes the nature of the correlation of information between frequency dimensions.

The history of the spin system during evolution is transmitted to the detection interval through phase and amplitude modulation of the F_2 spectrum. In most two-dimensional experiments involving amplitude modulation the functional dependence of amplitude on t_1 has a sinusoidal form [1.22,1.23]. Since sinusoidal modulation can be considered as a combination of two components of phase modulation with opposite frequencies the fundamental mode of information transfer is through phase modulation. In general the observed signal in a two-dimensional experiment can be written as,

$$S(t_1,t_2) = C\, e^{-\lambda_1 t_1}\, e^{-\lambda_2 t_2}\, e^{i(\Omega_1 t_1+\phi_1)}\, e^{i(\Omega_2 t_2+\phi_2)}. \qquad (1.13)$$

The coefficient C is dependent on the mixing of information among the two frequency dimensions. The relaxation rates, λ_1 and λ_2, are defined as for equation 1.8 and Ω_1, ϕ_1 and Ω_2, ϕ_2 are the precession frequencies and initial phases for the evolution and detection periods. Two-dimensional Fourier transformation produces the following spectrum:

$$S(\omega_1,\omega_2) = C\, e^{i(\phi_1+\phi_2)}\, [A(\omega_1) + iD(\omega_1)][A(\omega_2) + iD(\omega_2)]$$

$$= C\, e^{i(\phi_1+\phi_2)} \{[A(\omega_1)A(\omega_2) - D(\omega_1)D(\omega_2)]$$

$$+i[A(\omega_1)D(\omega_2) + A(\omega_2)D(\omega_1)]\}. \qquad (1.14)$$

It is not possible to produce pure absorption or dispersion in the real and imaginary portions of the spectrum by a simple phase correction of the type used in one-dimensional Fourier spectroscopy. The resulting two-dimensional lineshape is a complex mixture of absorptive and dispersive contributions termed a 'phase twist' lineshape [1.22,1.23]. A simple method which avoids the problems of displaying this lineshape in a phase sensitive mode is to calculate the absolute value mode. This mode of display will be used throughout this thesis to present the results of two-dimensional experiments. The lineshape function for the absolute value mode is given by,

$$|S(\omega_1,\omega_2)| = C\,[(\lambda_1^2 + \Delta\omega_1^2)(\lambda_2^2 + \Delta\omega_2^2)]^{-1/2}. \qquad (1.15)$$

This lineshape is independent of the initial phase at the beginning of evolution and detection intervals and has the same peak height as the 'phase twist' lineshape on resonance in both dimensions if the 'phase twist' spectrum is corrected for initial phase values.

Most two-dimensional experiments produce a mixture of phase and amplitude modulation as a function of t_1. Pure phase modulation allows the sign of the precession frequency in t_1 to be determined thus allowing the transmitter to be positioned in the middle of the spectral width for more efficient use of experimental time [1.23]. Several methods of assuring phase modulation have been proposed [1.24]. In chapter 3 the effect of static field inhomogeneity on two-dimensional spectra is discussed and a new method introduced that allows the discrimination of the sign of the precession frequency for a new class of two-dimensional experiments involving multiple quantum transitions

[1.25]. In one-dimensional Fourier spectroscopy, measurable frequencies are restricted to those for the transition of a single spin. With two-dimensional NMR it is possible to indirectly detect the frequency of simultaneous transition of more than one spin thus allowing correlation of spin-spin interaction through multiple quantum transitions.

Loss of coherence due to the effect of static magnetic field inhomogeneity during evolution can be refocussed by a mixing pulse [1.26]. The observed magnetization echoes for a particular sense of precession in t_1. Phase modulation with this sense of precession is chosen to take advantage of the echo effect (see chapter 3). With this choice the two-dimensional spectrum is oriented as shown at the bottom of figure 1.1. Three types of peaks are identified on the spectrum; axial peaks with $F_1 = 0$, diagonal peaks for $F_2 = -F_1$ and cross peaks with $F_2 \neq F_1$. Axial peaks result from parts of the spin system which have no effective evolution in t_1. Diagonal peaks correspond to parts of the system that precess with the same frequencies but opposite sign in t_1 and t_2. The definition of diagonal peaks is generalized to include all the peaks of a coupled multiplet for a particular spin centred on the main diagonal. Hence for a system of coupled spins, cross peaks will indicate a correlation between spins that precess at different frequencies during evolution and detection periods.

1.4.1. Application of two-dimensional spectroscopy

Three experiments will be discussed briefly and applied to the same molecular system to illustrate the usefulness of the two-dimensional technique and show their interrelationship. Two of the experiments involve correlation of homonuclear spins of two different types, hydrogen and carbon-13. The other experiment correlates heteronuclear spins, in this case hydrogen and carbon-13, and provides a method of

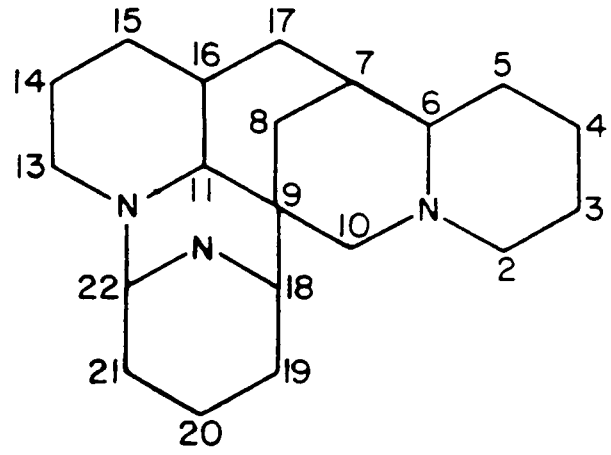

Panamine (NB 1)

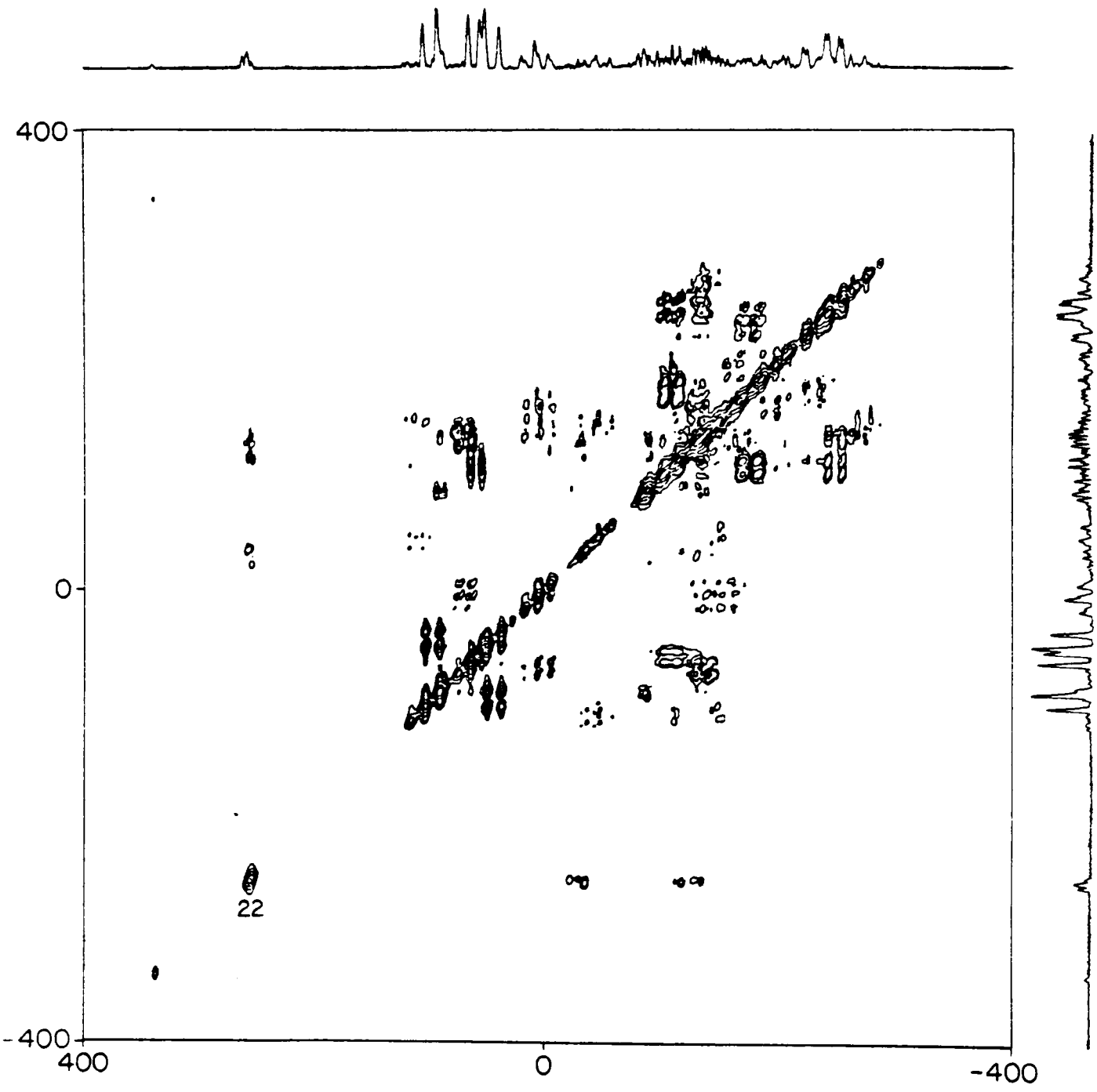

Figure 1.2 Proton-proton chemical shift correlation of panamine in $CDCL_3$. One-dimensional high resolution proton spectra are included parallel to the F_1 and F_2 axes.

relating the information in both homonuclear experiments.

The first experiment is of the type initially proposed by Jeener to demonstrate the concepts of two-dimensional spectroscopy [1.19,1.20]. The sequence is diagrammed as follows with the last pulse reduced from $\frac{\pi}{2}$ to $\frac{\pi}{4}$ to simplify the information transfer among frequency components [1.27] (also see chapter 3).

$$\frac{\pi}{2} - t_1 - \frac{\pi}{4} - t_2$$

The first pulse creates transverse magnetization which evolves for t_1 and is then detected following the $\frac{\pi}{4}$ mixing pulse. The resulting spectrum provides homonuclear chemical shift correlation in a J-coupled spin system. An example is shown in figure 1.2. This is the proton spectrum of panamine (shown at the top) with the one-dimensional spectrum included parallel to the F_1 and F_2 axes. The diagonal peaks running from bottom left to top right correspond to autocorrelation of each spin. No axial peaks are present in the spectrum. The cross peaks represent shift correlations among the coupled protons in the molecule and are symmetrically placed about the diagonal. Although the correlation pattern is complex a few specific assignments can be made easily from this spectrum. Because of shift effects from the surrounding nitrogens, the lowest field multiplet can be assigned to the single proton at position 22. The cross peaks to 22 indicate the resonance positions of the geminal protons at position 21. Other correlations can be identified and assigned to the structure in a straight forward fashion however determination of an unknown structure from the information in this type of spectrum alone would be a difficult if not impossible task.

More information about molecular structure could be obtained if it were possible to correlate carbon-13 spins thus providing the

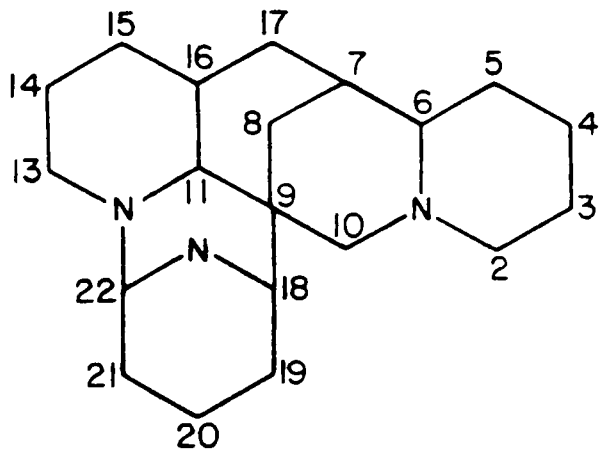

Panamine (NB 1)

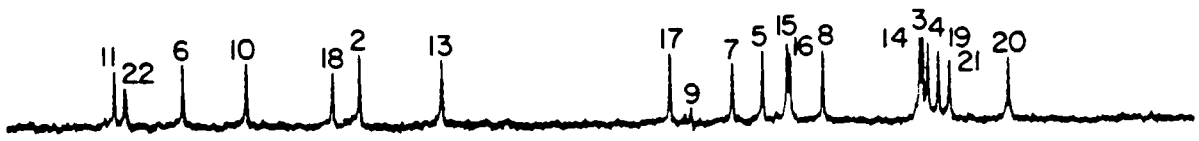

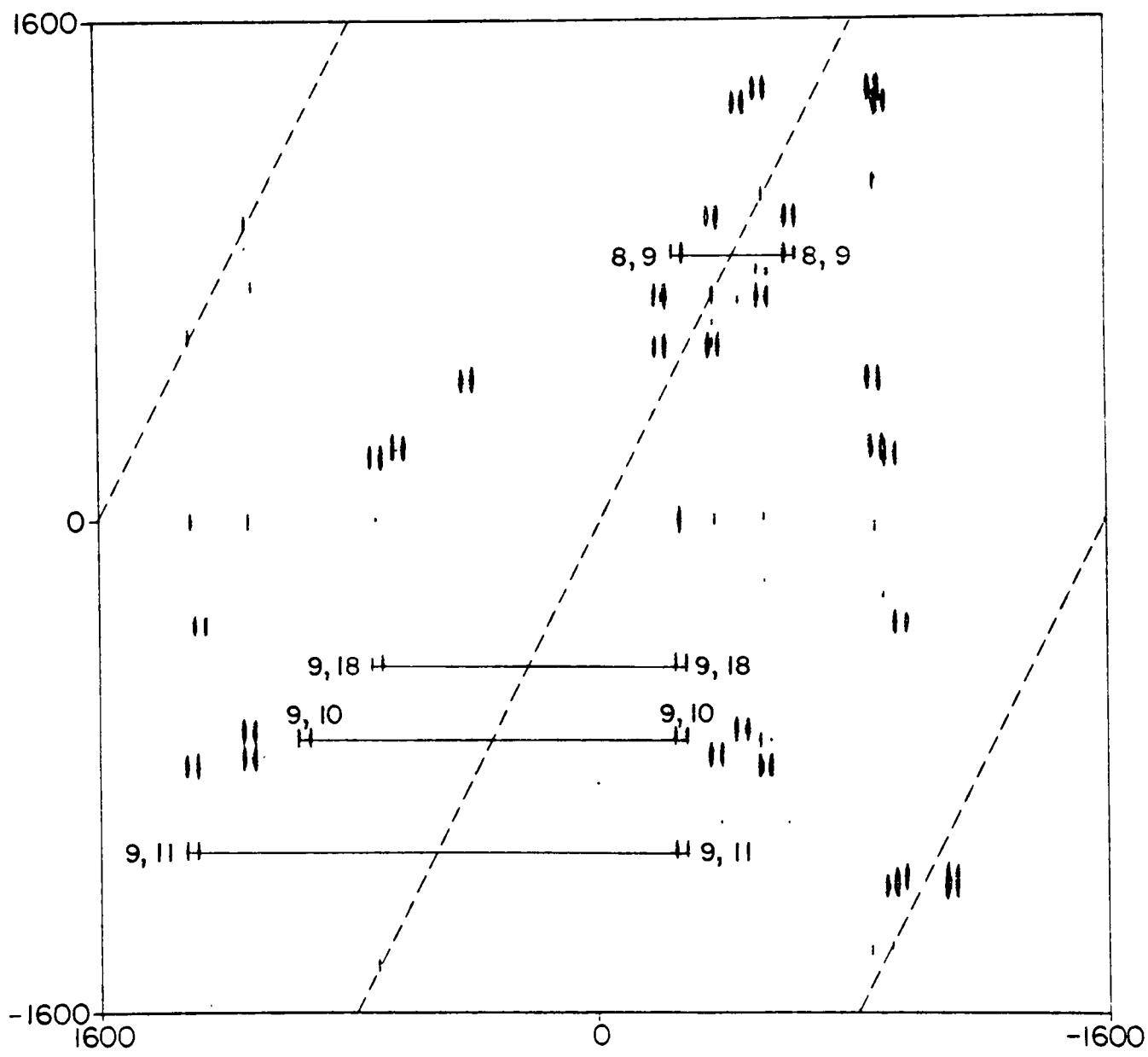

Figure 1.3 Carbon-carbon chemical shift correlation through double quantum coherence for panamine in $CDCL_3$. One dimensional proton-decoupled carbon spectrum is shown to the top parallel to the F_2 axis.

identification of specific carbons with positions in the hydrocarbon framework. This is possible for carbon-13 in natural abundance using the INADEQUATE sequence diagrammed below [1.28],

$$(\frac{\pi}{2})_x - \tau - (\pi)_y - \tau - (\frac{\pi}{2})_x - t_1 - (\alpha)_\phi - \text{detect}_\xi$$

Proton broadband decoupling is applied continuously during the experiment. This sequence relies on the fact that for a particular carbon atom in a molecule, a carbon-13 isotope in natural abundance only occurs for approximately one molecule in a hundred. Hence the probability of two carbon-13 isotopes occurring on adjacent carbon sites will be ~ 10^{-4} and three ~ 10^{-6}, thus two such carbon-13 isotopes effectively form an isolated pair. In the normal one-dimensional carbon spectrum these appear as weak satellites of the parent carbon line. The INADEQUATE sequence prepares the two spin system into a state of double quantum coherence which then evolves for t_1 and is transferred to and detected as single quantum coherences by the final pulse. By combining the results of several experiments with cycling of the phase of the detection pulse and receiver it is possible to suppress signal from the single isolated carbon-13 spins of the parent line and detect only signal from the coupled spin pairs. The amount of double quantum coherence created is dependent on the creation delay, τ, with the optimum setting of $\tau = 1/4J_{CC}$. In the two-dimensional spectrum the double quantum precession frequency appears at the F_2 frequency of each spin in the pair thus providing a direct correlation though carbon-carbon coupling.

The INADEQUATE spectrum of panamine is shown in figure 1.3. Indirectly detected double quantum frequencies lie on traces parallel to the F_1 axis and the carbon-carbon satellite spectra parallel to F_2. The normal broadband decoupled carbon single quantum spectrum is shown at

the top. Specific carbon assignments can be developed quite easily from the spectrum. For example the molecule has only one quaternary carbon at position 9 and only the carbon resonance labelled 9 has four associated double quantum frequencies. Starting from this position the connectivity can be mapped with breaks occurring at the nitrogen positions. In many systems the resonances of carbons next to heteronuclear atoms such as oxygen or nitrogen can be identified from chemical shift effects. The panamine carbon one-dimensional spectrum is divided into two regions with a gap between 13 and 17. All the resonances low field from 17 are next to a nitrogen atom so these can be correlated with specific positions in the molecular structure.

There are two possible correlations which do not appear in this spectrum. One between 15 and 16 and one between 3 and 4. These resonances are strongly coupled and the setting of $\tau = 1/4J_{CC}$ is not optimum [1.29]. Another experiment could be performed optimised for strong coupling to assure complete correlation.

The INADEQUATE experiment provides a method of 'drawing' the carbon-carbon connectivity of a hydrocarbon framework in a simple, straight forward fashion. In chapter 3 the optimum choice of the detection pulse α is discussed with the result that a simple setting of $\alpha = 135^0$ provides an increase in sensitivity and allows the discrimination of the sign of the double quantum precession frequency. This reduces the phase cycling required by a factor of two and simplifies the pulse sequence.

Finally a method of correlating the information in both homonuclear two-dimensional spectra is possible through the direct correlation of the chemical shifts of protons and carbons with the following pulse sequence [1.22].

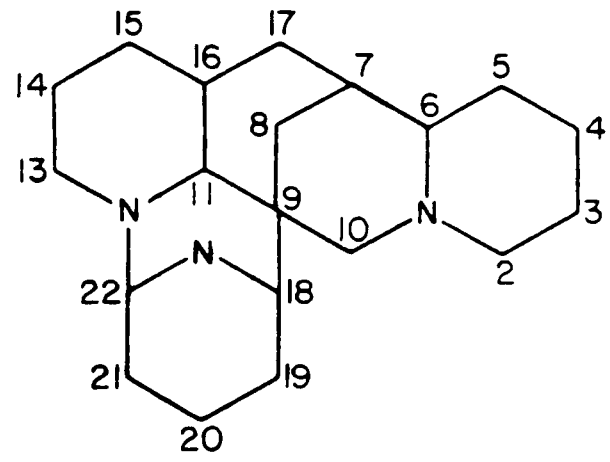

Panamine (NB 1)

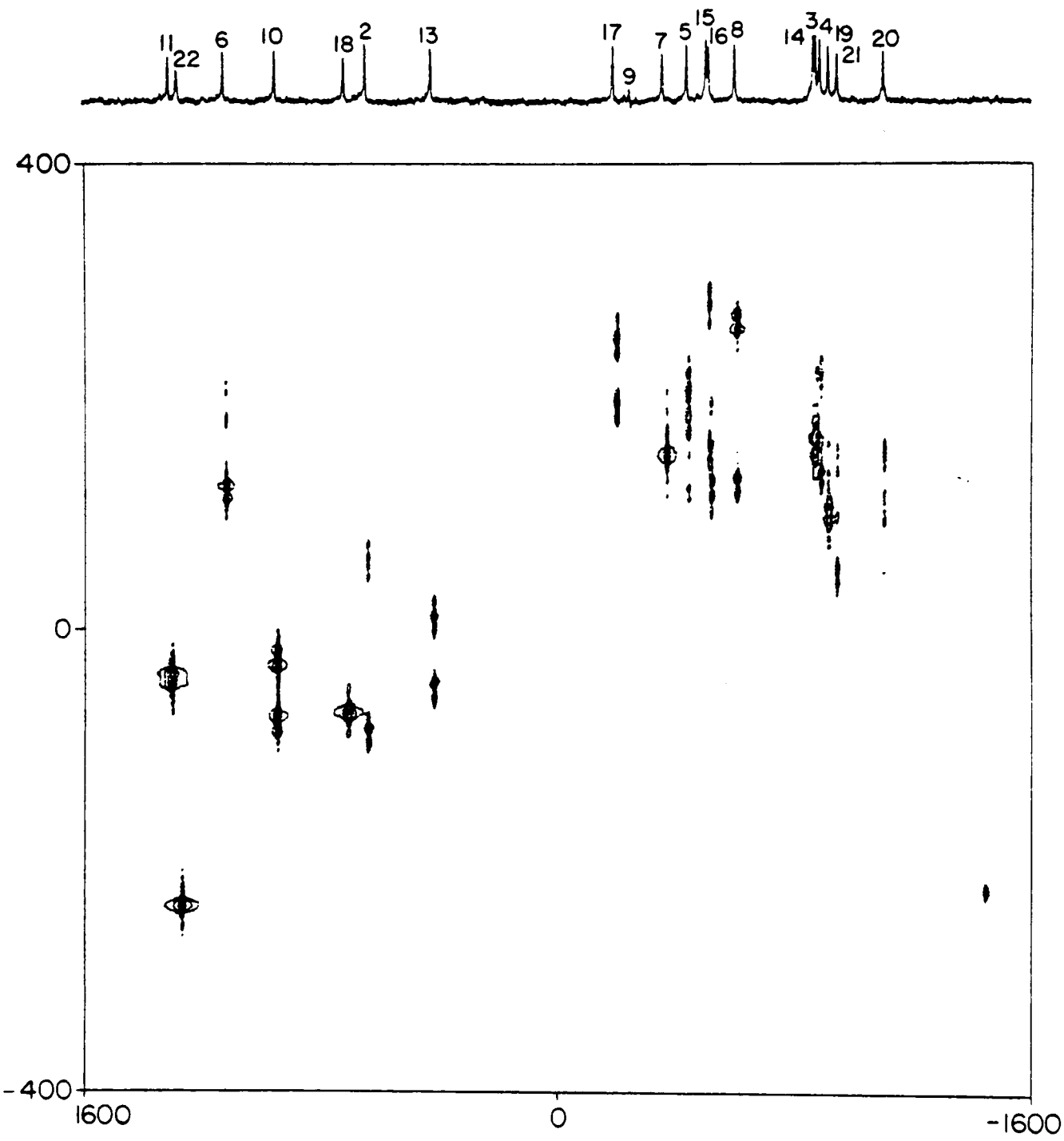

Figure 1.4 Carbon-proton chemical shift correlation of panamine in $CDCL_3$. The one dimensional proton-decoupled carbon spectrum is shown at the top parallel to F_2.

Carbon-13 $- (\pi)_x -$ $- \Delta_1 - (\frac{\pi}{2})_{\pm x} - \Delta_2 -$ detect

Proton $(\frac{\pi}{2})_{\pm x} - t_1/2 -$ $- t_1/2 - \Delta_1 - (\frac{\pi}{2})_y - \Delta_2 -$ decouple

The basic idea is to create proton transverse magnetization which evolves during t_1, effectively decoupled from carbon-13 by the π pulse in the middle of the evolution period, and transfer the proton transverse coherence to directly bonded carbons with the mixing pulses and delays. The carbon spectrum is observed in the presence of proton broadband decoupling. With this method, evolution of the proton spins is indirectly detected on the carbons and the two chemical shifts correlated in a two-dimensional spectrum. The proton-carbon shift correlation spectrum for panamine is shown in figure 1.4. Proton shifts lie parallel to F_1 and carbon shifts parallel to F_2. The one-dimensional carbon spectrum is included at the top. This clearly separates the crowded proton spectra over the carbon chemical shift range.

The results of the three experiments are combined in figure 1.5. Starting with the information in the carbon-carbon correlation spectrum at the bottom right and using the carbon-proton correlation spectrum at the top right it is possible to begin to unravel the complex coupling pattern presented by the proton-proton correlation spectrum on the top left. This will lead to a conformation of the structure of panamine illustrated at the bottom left of the figure.

In chapter 4 a new method of proton-proton shift correlation is presented. A modified INADEQUATE sequence [1.30] is used to create and indirectly detect double quantum coherence between coupled protons by two-dimensional Fourier transform techniques. The resulting spectrum contains no 'diagonal' peaks from autocorrelation of spins and only half the multiplet fine structure of the two-pulse sequence proposed by

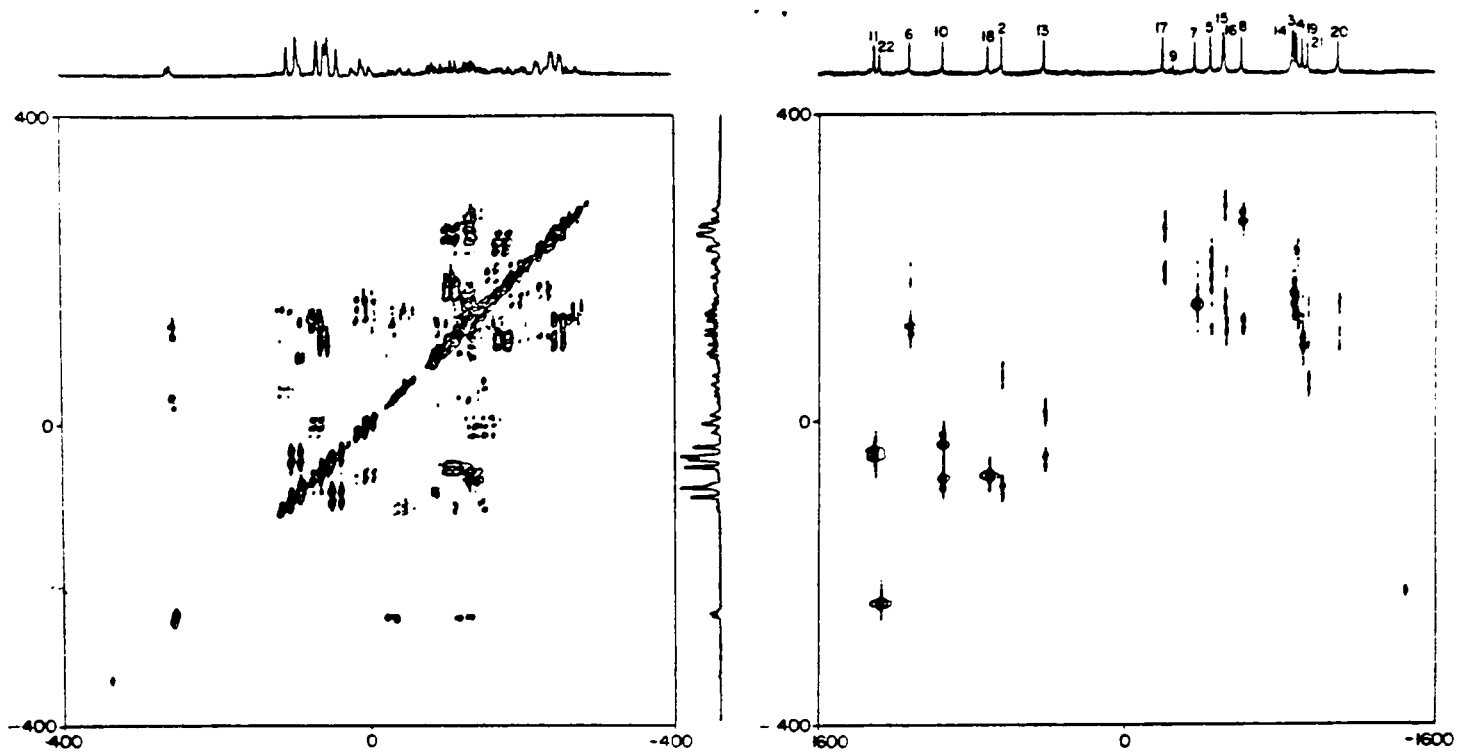

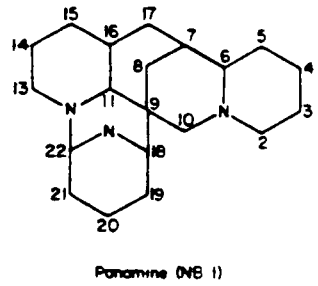

Panamine (NB 1)

Figure 1.5 Combined result of the three spectra of figure 1.2, 1.3 and 1.4 for panamine in $CDCL_3$. Carbon-carbon correlation shown at the bottom right, carbon-proton correlation at the top right and proton-proton correlation at the top left of the figure.

Jeener [1.19].

New methods for the observation of heteronuclear satellites in proton spectra are presented in chapter 5 which can provide a great sensitivity advantage over the direct measurement of the proton coupled heteronuclear spectrum of spins such as carbon-13 and nitrogen-15. All the techniques rely on a modulation of the satellites by heteronuclear coupling constants to provide discrimination from the main proton resonance peak. The basic idea is extended to a two-dimensional experiment which allows the observation of heteronuclear coupling in proton spectra where the proton-proton coupling is of the same order of magnitude as the heteronuclear coupling to protons.

References

[1.1] I. I. Rabi, J. R. Zacharias, S. Millman and P. Kusch, Phys. Rev. 53, 318 (1938)

[1.2] E. M. Purcell, H. C. Torry and R. V. Pound, Phys. Rev. 69, 37 (1946)

[1.3] F. Bloch, W. W. Hansen and M. Packard, Phys. Rev. 70, 474 (1946)

[1.4] M. G. Richards, Adv. Magn. Reson. 5, 305 (1971)

[1.5] I. L. Pykett, Scientific American 246, 54, May (1982)

[1.6] A. Abragram, The Principles of Nuclear Magnetism, Oxford University Press, London (1961)

[1.7] C. P. Slichter, Principles of Magnetic Resonance, Springer-Verlag, Berlin (1980)

[1.8] F. Bloch, Phys. Rev. 70, 460 (1946)

[1.9] S. Vega and A. Pines, J. Chem. Phys. 66, 5624 (1977), A. Wokaun and R. R. Ernst, J. Chem. Phys. 67, 1752 (1977), S. Vega, J. Chem. Phys. 68, 5518 (1978), M. Mehring, E. K. Wolff and M. E. Stoll, J. Magn. Reson. 37, 475 (1980), R. Kaiser, J. Magn. Reson. 40, 439 (1980)

[1.10] P. L. Corio, Structure of High-Resolution NMR spectra, Academic Press, New York (1967)

[1.11] (a) I. J. Lowe and R. E. Norberg, Phys. Rev. 107, 46 (1957), (b) R. R. Ernst and W. A. Anderson, Rev. Sci. Instr. 37, 93 (1966)

[1.12] J. S. Waugh, J. Mol. Spectrosc. 35, 298 (1970)

[1.13] E. O. Stejskal and J. Schaefer, J. Magn. Reson. 13, 249 (1974)

[1.14] R. Bracewell, The Fourier Transform and Its Applications, McGraw-Hill, New York (1965)

[1.15] R. V. Churchill, Complex Variables and Applications, McGraw-Hill, New York (1960)

[1.16] R. L. Vold, J. S. Waugh, M. P. Klein and D. E. Phelps, Jr., J. Chem. Phys. 48, 3831 (1968), R. Freeman and H. D. W. Hill, J. Chem. Phys. 54, 301 (1971)

[1.17] E. L. Hahn, Phys. Rev. 76, 145 (1949)

[1.18] H. Y. Carr and E. M. Purcell, Phys. Rev. 94, 630 (1954)

[1.19] J. Jeener, Ampere International Summer School, Basko Polje, Yugoslavia 1971

[1.20] W. P. Aue, E. Bartholdi and R. R. Ernst, J. Chem. Phys. 64, 2229 (1976)

[1.21] G. Bodenhausen, R. Freeman, R. Niedermeyer and D. L. Turner, J. Magn. Reson. 26, 133 (1977)

[1.22] R. Freeman, Proc. Roy. Soc. London A 373, 149 (1980)

[1.23] A. Bax, Two-Dimensional Nuclear Magnetic Resonance in Liquids, Delft University Press, Dordrecht Holland, 1982

[1.24] K. Nagayama, A. Kumar, K. Wutrich and R. R. Ernst, J. Magn. Reson. 40, 321 (1980), A. Bax, R. Freeman and G. A. Morris, J. Magn. Reson. 42, 164 (1981), A. Bax and G. A. Morris, J. Magn. Reson. 42, 501 (1981)

[1.25] A. Wokaun and R. R. Ernst, Chem. Phys. Letts. 52, 407 (1977), G. Bodenhausen, Prog. NMR Spectrosc. 14, 137 (1981)

[1.26] A. A. Maudsley, A. Wokaun and R. R. Ernst, Chem. Phys. Letts. 55, 9 (1978)

[1.27] A. Bax and R. Freeman, J. Magn. Reson. 44, 542 (1981)

[1.28] A. Bax, R. Freeman and S. P. Kempsell, J. Amer. Chem. Soc. 102, 4849 (1980), A. Bax, R. Freeman, T. A. Frenkiel and M. H. Levitt, J. Magn. Reson. 43, 478 (1981)

[1.29] A. Bax and R. Freeman, J. Magn. Reson. 41, 507 (1980)

[1.30] T. H. Mareci and R. Freeman, J. Magn. Reson. 48, 158 (1982)

Chapter 2

Density operator formalism

2.1. Introduction

In this chapter a quantum mechanical description of the magnetic resonance experiment is presented in terms of the density matrix formulation [2.1]. In the second section the general properties of the density matrix operator are discussed and the density operator is written in a form appropriate for magnetic resonance. In the third section a convenient set of operators are developed. These are the single transition operators which under certain conditions allow a pictorial description of the evolution of the system during an experiment. In the fourth section the density operator is written in terms of these operators and the evolution of the system is studied in detail and explicit expressions are developed for pulsed excitation and free precession in terms of the single transition operators. In the fifth section the effect of considering combinations of single transition operators is presented. It is possible to define combinations of operators which behave as a vector in an appropriately defined coordinate frame and allow a pictorial interpretation of the evolution of these operator combinations. Finally in the last section the single transition operator formulation of the density operator is applied to the system of two spin-1/2 nuclei with scalar coupling. The evolution of the system is studied in detail and a description of the excitation and detection of double quantum coherence is presented. This allows the visualization of the creation and detection of double quantum coherence in a vector frame where the operators rotate in the manner of

angular momentum operators.

2.2. The density operator formalism

The result of an experiment is determined by making observations of some dynamic variable of the system under study. Therefore a description of the observation process is central to understanding the connection between theory and experiment. In quantum mechanics an observation is described as the expectation value of some observable, Q,

$$\langle Q \rangle = \langle \xi | Q | \xi \rangle \tag{2.1}$$

where $|\xi\rangle$ is the state function for the system in a pure state. The state function can be expanded in terms of eigenvectors of a complete set of operators as

$$|\xi\rangle = \sum_n c_n |u_n\rangle. \tag{2.2}$$

By choice the coefficients, c_n, are time dependent, and eigenfunctions, $|u_n\rangle$, are time independent. The observation can then be described by

$$\langle Q \rangle = \sum_m \sum_n c_m^* c_n \langle u_m | Q | u_n \rangle. \tag{2.3}$$

When the system can be represented by a statistical ensemble of pure states the observation is then described by the superposition of the expectation values of the operator, Q, for the system to be in any of the possible pure states, $|\xi_i\rangle$, with an appropriate statistical weight, p_i. The observable for the statistical ensemble can be written as

$$\langle Q\rangle = \sum_i p_i \langle Q\rangle_i$$

$$= \sum_m \sum_n \langle u_m|Q|u_n\rangle \sum_i p_i \,(c_m^* c_n)_i \qquad (2.4)$$

where the sum, $\sum_i$, is over all possible pure states in the ensemble. One can then define elements of the density matrix as [2.1]

$$\sigma_{nm} = \sum_i p_i \,(c_m^* c_n)_i . \qquad (2.5)$$

These matrix elements represent a density operator of the form

$$\sigma = \sum_i |\xi_i\rangle p_i \langle \xi_i| . \qquad (2.6)$$

Finally equation 2.4 can be written as

$$\langle Q\rangle = \sum_m \sum_n \langle u_m|Q|u_n\rangle \langle u_n|\sigma|u_m\rangle$$

$$= \sum_m \langle u_m|Q\sigma|u_m\rangle$$

$$= \mathrm{Tr}(Q\sigma) = \mathrm{Tr}(\sigma Q) . \qquad (2.7)$$

The description of the system by a density operator with the form of σ provides a method of describing the state of the system at any point during an experiment. The time dependence of the state of the system is governed by the Schroedinger equation,

$$i\hbar \frac{\partial}{\partial t}|\xi\rangle = H|\xi\rangle \qquad (2.8)$$

where H is the Hamiltonian of the system and it is assumed to be the same for all the pure states in the statistical ensemble. Using equation 2.8 the equation of motion for the density operator can be

written as

$$\frac{\partial \sigma}{\partial t} = \sum_i \left[\, |\xi_i\rangle p_i \left(\frac{\partial}{\partial t}\langle \xi_i|\right) + \left(\frac{\partial}{\partial t}|\xi_i\rangle\right) p_i \langle \xi_i| \, \right]$$

$$= \sum_i \left[\, |\xi_i\rangle p_i \langle \xi_i| (H i\hbar^{-1}) - (i\hbar^{-1} H) |\xi_i\rangle p_i \langle \xi_i| \, \right]$$

$$\frac{\partial \sigma}{\partial t} = -\frac{i}{\hbar} [\, H \, , \, \sigma \,]. \qquad (2.9)$$

Now the description of the system at all times during an experiment is essentially complete. All that is necessary is a knowledge of the Hamiltonian operators that govern the interactions of the system and a description of the system by a density operator at some initial point in time. Obtaining knowledge of the Hamiltonians and boundary conditions is of course the central problem of quantum mechanics. The appropriate Hamiltonian operators for an experiment are usually known or have been chosen by design of the experiment. It is the description of the system in terms of eigenvectors for a complete set of operators which determines the ease of obtaining a solution to the problem. A particularly useful set of operators for magnetic resonance problems are the single transition operators and these will be described in a later section of this chapter and used throughout this thesis to treat the experimental situations considered. In using the density operator to describe experiments it will be assumed that the system can be adequately described as being in a pure state. This will simplify the calculations without any loss in generality if it is assumed that the observed quantity will eventually be calculated by taking a statistically weighted sum of the probability that the observable will be in each possible pure state of the system. With this in mind the system can be described by the density operator for a pure state as

$$\sigma = |\xi\rangle\langle\xi| = \sum_m \sum_n |u_m\rangle \sigma_{mn} \langle u_n| . \qquad (2.10)$$

2.2.1. Transformation to the rotating frame

In magnetic resonance experiments the observable is the magnetization of an ensemble of nuclei which each possess a magnetic moment, μ. For a nucleus to exhibit a magnetic moment it must have a nonvanishing spin angular momentum denoted by I where the relationship between magnetic moment and spin angular momentum is given by $\mu = \gamma\hbar I$.

The magnetic moment is a vector quantity which interacts with an applied magnetic field. This interaction is described by the Hamiltonian,

$$\begin{aligned} H &= -\mu . B = -\gamma\hbar I . B \\ &= -\gamma\hbar \left(I_x B_x + I_y B_y + I_z B_z \right) \end{aligned} \qquad (2.11)$$

which is written in terms of the usual Cartesian coordinate frame.

In magnetic resonance, the system is usually viewed in a rotating coordinate frame [2.2]. Near resonance, transformation to a rotating frame of reference simplifies the motion of the spins and makes it easier to visualize the effect of pulses and precession. For a time independent Hamiltonian, equation 2.9 has the solution,

$$\sigma(t) = e^{-iHt/\hbar}\, \sigma(0)\, e^{iHt/\hbar} \qquad (2.12)$$

Now we define a new density operator in a frame rotating about the z-axis with angular frequency, ω, as

$$\rho(t) = e^{i\omega t I_z}\, \sigma(t)\, e^{-i\omega t I_z} . \qquad (2.13)$$

The equation of motion of equation 2.9 can be rewritten as

$$\frac{\partial \rho}{\partial t} = \frac{i}{\hbar} [H' , \rho] \tag{2.14}$$

where

$$H'(t) = e^{-i\omega t I_z} (H - \hbar\omega I_z) e^{i\omega t I_z}. \tag{2.15}$$

Equation 2.12 can be rewritten as

$$\rho(t) = e^{i(\omega I_z - \hbar^{-1} H)t} \rho(0) e^{-i(\omega I_z - \hbar^{-1} H)t} \tag{2.16}$$

where from equation 2.13 it should be noted that $\rho(0) = \sigma(0)$.

If the Hamiltonian, H, has the form of a static magnetic field aligned along the z-axis,

$$H = -\hbar\gamma B_0 I_z = \hbar\omega_0 I_z \tag{2.17}$$

where $\omega_0 = -\gamma B_0$, then equation 2.16 can be written as

$$\rho(t) = e^{-i\Delta\omega t I_z} \rho(0) e^{i\Delta\omega t I_z} \tag{2.18}$$

where $\Delta\omega = (\omega_0 - \omega)$. This represents free precession in the rotating frame about the effective field, $B_{eff} = B_0 + \frac{\omega}{\gamma}$. Note that on resonance, $\Delta\omega = 0$, the density operator is stationary.

2.2.2. RF pulses in the rotating frame

The effect of magnetic field pulses on the spin system can be described in a straight forward manner once a Hamiltonian operator can be defined which represents the time varying field. The most common NMR experiments involve the application of a linearly polarized rf field. Choosing as a reference the x-axis, the Hamiltonian can be written as,

$$\hbar^{-1}H = \omega_0 I_z + 2\omega_1 I_x \cos(\omega t) \qquad (2.19)$$

where $\omega_1 = -\gamma B_1$. The rf field can be decomposed into two counter-rotating components [2.3]. The component rotating in the same sense as rotation of the spin about B_0 is the most effective in exciting the spin so that the other component of the field can be neglected [2.3] and the Hamiltonian becomes,

$$\hbar^{-1}H = \omega_0 I_z + \omega_1 (e^{-i\omega t I_z} I_x e^{i\omega t I_z}) \qquad (2.20)$$

Now in a reference frame rotating at the rf frequency, ω, using equation 2.15. the Hamiltonian becomes,

$$\hbar^{-1}H' = (\omega_0 - \omega) I_z + \omega_1 I_x \qquad (2.21)$$

and finally the density operator during the application of an rf field can be written as,

$$\rho(t) = e^{-i[(\omega_0-\omega)I_z + \omega_1 I_x]t} \rho(0) e^{i[(\omega_0-\omega)I_z + \omega_1 I_x]t}. \qquad (2.22)$$

For a field applied on resonance, $\Delta\omega = 0$, or if the B_1 field is strong such that $|\omega_1| \gg |(\omega_0 - \omega)|$ equation 2.22 can be rewritten as,

(a)

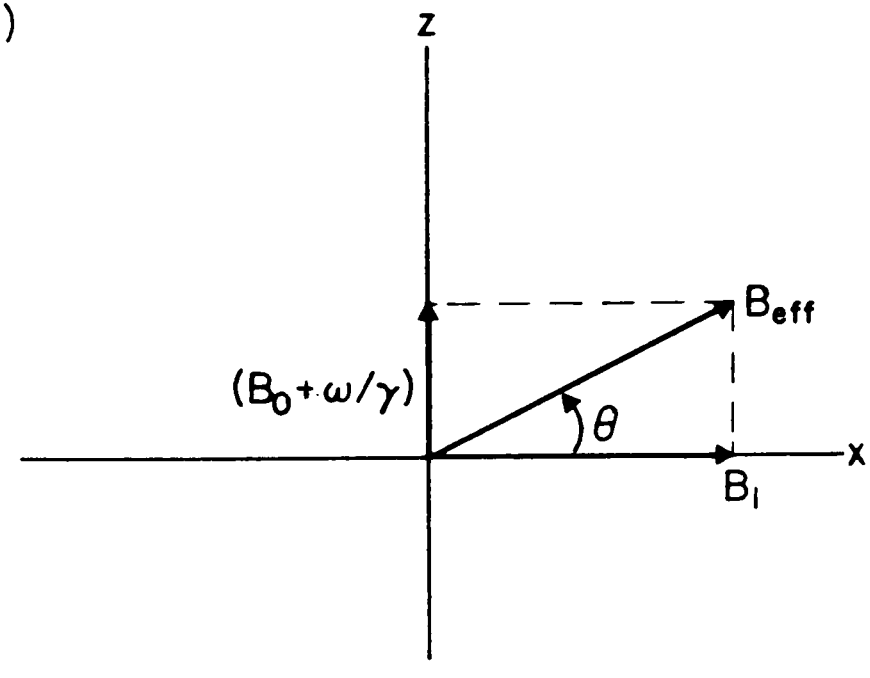

$$\tan\theta = \frac{(B_0+\omega/\gamma)}{B_1}$$

$$= \frac{(\omega_0-\omega)}{\omega}$$

(b)

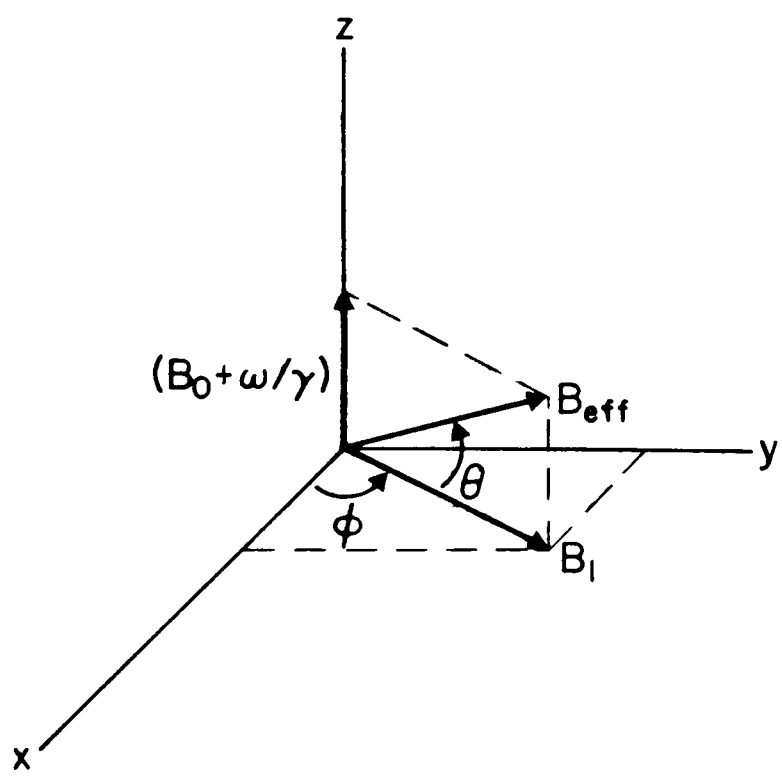

Figure 2.1 Magnetic field in the rotating frame of reference. (a) B_1 field applied off resonance aligned along the x-axis. (b) B_1 field applied off resonance with phase $\emptyset$ with respect to the x-axis.

$$\rho(t) = e^{-i\omega_1 t I_x} \rho(0) e^{i\omega_1 t I_x}. \qquad (2.23)$$

Let $\alpha = \omega_1 t$ be the angle of rotation about the applied rf field (commonly called the tip angle) and adopt the simplified notation,

$$\rho' = R_x(\alpha) \rho R_x^+(\alpha) \qquad (2.24)$$

where $R_x(\alpha) = e^{-i\alpha I_x}$ is called the rotation operator for rotation about the x-axis [2.4].

The application of rf fields off resonance requires a generalization of the rotation operator in equation 2.24. By simple geometric considerations illustrated in figure 2.1a, the rotation operator of the form in equation 2.24 can be written,

$$R(\alpha,\theta) = e^{-i\alpha(I_x\cos\theta + I_z\sin\theta)} \qquad (2.25)$$

where α is now the angle of rotation about the effective field in the rotating frame, $B_{eff} = [(B_1)^2 + (B_0 + \frac{\omega}{\gamma})^2]^{1/2}$, given by $\alpha = \omega_{eff} t = -\gamma B_{eff} t$. These ideas can be extended to show that the most general form of the rotation operator for a time varying field applied in the transverse plane at an angle, ϕ, with respect to the x-axis in the rotating frame of reference (see figure 2.1b) is given by,

$$R(\alpha,\theta,\phi) = e^{-i\alpha[(I_x\cos\phi + I_y\sin\phi)\cos\theta + I_z\sin\theta]}. \qquad (2.26)$$

Using the properties of exponential operators [2.5] this can be rewritten as,

$$R(\alpha,\theta,\phi) = e^{-i\phi I_z} e^{i\theta I_y} e^{-i\alpha I_x} e^{-i\theta I_y} e^{i\phi I_z}. \qquad (2.27)$$

A general rotation about any axis in the rotating frame of reference can be parameterized by the angles α, θ and $\emptyset$ just as the Euler angles parameterize a general rotation for an operator of the rotation group [2.6]. The state of the system after a pulse is described by the density operator,

$$\rho' = R(\alpha,\theta,\emptyset)\ \rho\ R^{+}(\alpha,\theta,\emptyset). \qquad (2.28)$$

This equation along with equation 2.18 for free precession completes the formal description of the evolution of the system. Since the trace is invariant to a unitary transformation, the expectation value of observable operators in the rotating frame is the same as in the lab frame so that,

$$\begin{aligned} \langle Q' \rangle &= Tr(Q'\rho) = Tr(UQU^{+}U\sigma U^{+}) \\ &= Tr(UQ\sigma U^{+}) \\ &= Tr(Q\sigma) = \langle Q \rangle \end{aligned} \qquad (2.29)$$

and all calculations will henceforth be carried out in terms of the rotating frame of reference.

For a system of N interacting spins the total spin angular momentum components can be expressed as,

$$F_{\alpha} = \sum_{n=1}^{N} (I_{\alpha})_{n} \quad ; \quad \alpha = x,y \text{ or } z. \qquad (2.30)$$

For this case the rotation operator of equation 2.27 should be written as,

$$R(\alpha,\theta,\emptyset) = e^{-i\emptyset F_z}\, e^{i\theta F_y}\, e^{-i\alpha F_x}\, e^{-i\theta F_y}\, e^{i\emptyset F_z}. \qquad (2.31)$$

For the system described in terms of the eigenfunctions of the Hamiltonian given in equation 2.17, a given matrix element of the density operator after a pulse is given by,

$$\rho_{rs}' = \langle r|\ R(\alpha,\theta,\phi)\ \rho\ R^{+}(\alpha,\theta,\phi)\ |s\rangle$$

$$= \sum_{k}\sum_{l} R_{rk}\rho_{kl}R^{+}_{ls}. \qquad (2.32)$$

Assume that the rf field is strong enough compared to the spectral width of interest to justify ignoring off resonance effects so set $\theta = 0$ and write the pulse operator of equation 2.31 as,

$$R(\alpha,\phi) = e^{-i\phi F_z}\, e^{-i\alpha F_x}\, e^{i\phi F_z}. \qquad (2.33)$$

Let $\Delta m_{pq} = m_p - m_q$ and call its value the order of a transition, then the matrix elements of the rotation operator assume the simplified form,

$$R_{pq} = e^{-i\Delta m_{pq}\phi}\ \langle p|\ e^{-i\alpha F_x}\ |q\rangle. \qquad (2.34)$$

Expressing F_x in terms of raising and lowering operators and expanding the exponential it is possible to show that the following relation holds [2.4],

$$e^{-i\alpha F_x} = \prod_{n=1}^{N} (e^{-i\alpha I_x})_n$$

$$= \prod_{n=1}^{N} [\cos\tfrac{\alpha}{2}\, I + i \sin\tfrac{\alpha}{2}\, (I_+ + I_-)]_n \qquad (2.35)$$

where here I is the identity operator. The matrix elements of equation 2.34 become,

$$R_{pq} = e^{-i\Delta m_{pq}\phi}\,(i)^{\delta_{pq}}$$

$$x\ (\cos\tfrac{\alpha}{2})^{N-\delta_{pq}}\ (\sin\tfrac{\alpha}{2})^{\delta_{pq}}. \qquad (2.36)$$

The term δ_{pq} is the number of spins that flip in the transition from state $|p\rangle$ to state $|q\rangle$. The important product of matrix elements of the rotation operator becomes,

$$R_{rk}R^{+}_{ls} = (-1)^{\delta_{ls}}(i)^{\delta_{rk}+\delta_{ls}}\ e^{-i(\Delta m_{rk}+\Delta m_{ls})\phi}$$

$$x\ (\cos\tfrac{\alpha}{2})^{2N-\delta_{rk}-\delta_{ls}}\ (\sin\tfrac{\alpha}{2})^{\delta_{rk}+\delta_{ls}}. \qquad (2.37)$$

This important result will be discussed in a later section after the introduction of the single transition operators to describe magnetic resonance experiments. The density operator will be expanded in terms of these operators and equation 2.37 will be used to describe the transfer of coherence represented by these operators.

The single transition operator formalism will be introduced in the next section. The basic form will be developed from the representation of a single isolated particle with spin-1/2. Then extension to more complicated systems will be considered. The general description of the spin system by Hamiltonian operators and the density operator will be expanded in terms of the single transition operators and a specific example treated.

2.3. Introduction to operator formalism

The purpose of this section is to introduce the use of an operator formalism to describe magnetic resonance in terms of a geometric representation. The result can be stated in an abstract form and then the development of the ideas can be illustrated with specific examples.

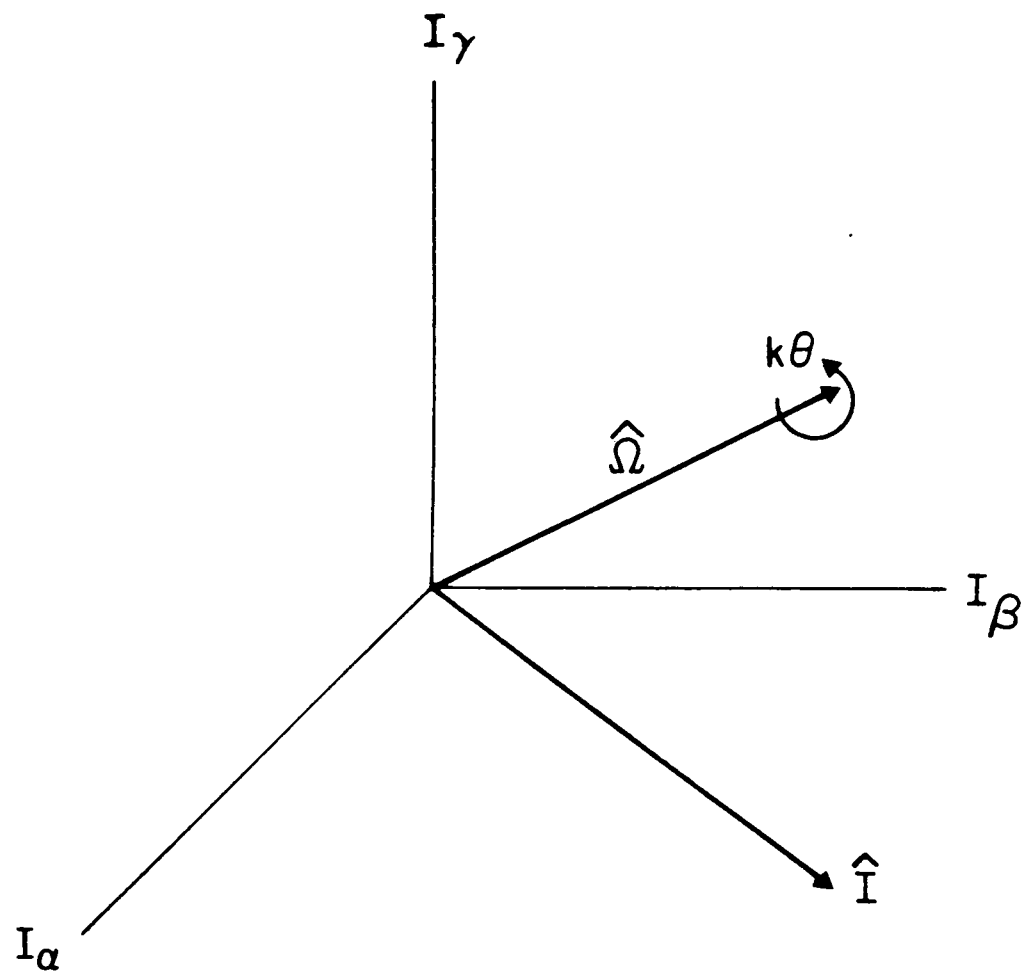

Figure 2.2 General form of a vector frame defined by the operators, I_α, I_β and I_γ which have a cyclic commutator property.

Assume the three operators, I_α, I_β and I_γ have a cyclic commutation relationship of the following form,

$$[\ I_\alpha\ ,\ I_\beta\ ] = ikI_\gamma \tag{2.38}$$

with cyclic permutations of α, β and γ. The factor k is a constant which remains the same under cyclic permutations of the operators. Also assume the operators obey the equation of motion,

$$\frac{\partial I_\delta}{\partial t} = \frac{i}{\hbar}[\ H\ ,\ I_\delta\ ] \quad , \delta = \alpha,\beta \text{ or } \gamma. \tag{2.39}$$

For a time independent Hamiltonian equation 2.39 has the solution,

$$I_\delta(t) = e^{-iHt/\hbar}\ I_\delta(0)\ e^{iHt/\hbar}. \tag{2.40}$$

If the Hamiltonian, H, has the form

$$H = \hbar\ (\ \omega_\alpha I_\alpha + \omega_\beta I_\beta + \omega_\gamma I_\gamma\ ) \tag{2.41}$$

the operator equation of motion can be written in a vector form such that

$$\frac{\partial I}{\partial t} = k\ (\ \Omega \times I\ ) \tag{2.42}$$

where $I = (I_\alpha, I_\beta, I_\gamma)$ and $\Omega = (\omega_\alpha, \omega_\beta, \omega_\gamma)$. This vector equation of motion has the form of a classical equation describing the rotation of a vector quantity, I, about an axis aligned along Ω with angular velocity, $k|\Omega|$. The constant, k, is determined from the commutator properties of the operators, I_δ in equation 2.38. Therefore the vector equation of motion can be interpreted geometrically in a frame defined by the components of the vector I as diagrammed in figure 2.2.

If the Hamiltonian acts for a time, t, the components of I have transformation properties of the general form,

$$e^{-i\theta I_\alpha} I_\beta e^{i\theta I_\alpha} = I_\beta \cos(k\theta) + I_\gamma \sin(k\theta) \qquad (2.43)$$

where $\theta = |\Omega| t = (\omega_\alpha{}^2+\omega_\beta{}^2+\omega_\gamma{}^2)^{1/2} t$.

The evolution of the system can be interpreted in terms of a vector representation if operators with the above properties (equations 2.38 through 2.42) can be defined for the system. For magnetic resonance this is easily accomplished using the single transition operators [2.7] and linear combinations of the single transition operators [2.7d]. The basic form of the single transition operators can be developed from the solution of the Schroedinger equation for a spin-1/2 particle in a magnetic field.

2.3.1. Two level system, single spin-1/2

In the presence of a static magnetic field the behaviour of an isolated particle with spin angular momentum of $\frac{1}{2}\hbar$ and a magnetic moment can be described by a phenomenological vector equation introduced by Bloch [2.8]. A simple extension of the phenomenological equation is not possible for more complicated spin systems, however starting from the simple case of an isolated spin-1/2 system definite mathematical operators can be developed which describe the physical situation in a vector model [2.9] and allow extension to more complicated systems.

Feynman et al. [2.9] have shown that a geometric representation of the Schroedinger equation is possible for a two-level system. Their approach can be applied to nuclear magnetic resonance for an isolated single nucleus of spin-1/2 in a static magnetic field. Consider a general two-level system represented by the wavefunction,

$$|\xi(t)\rangle = a(t)|a\rangle + b(t)|b\rangle \tag{2.44}$$

where a(t) and b(t) are complex coefficients. Specifically consider the system of a single spin-1/2 particle in a magnetic field, B_0, and choose as a basis set the eigenfunctions of the Zeeman Hamiltonian,

$$\begin{aligned} H_0 &= -\mu.B = -\gamma\hbar I_z B_0 \\ &= \hbar\omega_0 I_z \qquad , \omega_0 = -\gamma B_0. \end{aligned} \tag{2.45}$$

Therefore define $|a\rangle = |m_z\rangle_+ = |\frac{1}{2}\rangle$ and $|b\rangle = |m_z\rangle_- = |-\frac{1}{2}\rangle$. The eigenvalues for this system are found by solving the time-independent Schroedinger equation with the results,

$$\begin{aligned} H_0|a\rangle &= \hbar\frac{\omega_0}{2}|a\rangle, \\ H_0|b\rangle &= -\hbar\frac{\omega_0}{2}|b\rangle. \end{aligned} \tag{2.46}$$

The energy of the system is given by

$$\begin{aligned} E_0 &= \langle\xi(t)|H_0|\xi(t)\rangle \\ &= (a^*\langle a| + b^*\langle b|)\ H_0\ (a|a\rangle + b|b\rangle) \\ &= \frac{1}{2}(a^*a - b^*b)\hbar\omega_0. \end{aligned} \tag{2.47}$$

Now recall the form, $H_0 = \hbar\omega_0 I_z$, then the identification can be made,

$$\langle I_z\rangle = \langle\xi(t)|I_z|\xi(t)\rangle = \frac{1}{2}(a^*a - b^*b). \tag{2.48}$$

Equation 2.48 represents the z-component of magnetic moment aligned along the magnetic field, B_0. Therefore the energy of the system can be written as,

$$E_0 = \hbar\omega_0\langle I_z\rangle = -\hbar\gamma B_0\langle I_z\rangle = -\langle\mu_z\rangle B_0 \qquad (2.49)$$

where $\langle\mu_z\rangle = \gamma\hbar\langle I_z\rangle$.

Let the probability of finding the system in state $|a\rangle$ be p_a and in state $|b\rangle$ be p_b. Using the normalization condition, $a^*a + b^*b = 1$, the probabilities can be identified as $p_a = a^*a$ and $p_b = b^*b$. The z-component of magnetic moment is now seen to be proportional to the difference in the probabilities of finding the system in either state $|a\rangle$ or state $|b\rangle$ and can be written as

$$\langle I_z\rangle = \frac{1}{2}(p_a - p_b). \qquad (2.50)$$

In the classical picture a 90^0 pulse along either the x- or y-axis is interpreted as causing a rotation of the z-magnetization into the transverse plane leaving the z-component equal to zero. Using the above equation this can be seen to represent a state of the system where both levels are equally populated. Analogously, a 180° pulse would invert the magnetization aligning it along the - z-axis which in terms of probabilities would represent the situation where the populations are reversed.

The components of magnetization transverse to the Zeeman field become important when the system is perturbed from its equilibrium position. The Hamiltonian, H, for the system with a perturbation can be separated into a sum of unperturbed and perturbed parts, $H = H_0 + V$. The time-dependent Schroedinger equation for the system becomes,

$$i\hbar\frac{\partial}{\partial t}|\xi(t)\rangle = H|\xi(t)\rangle = (H_0 + V)|\xi(t)\rangle. \qquad (2.51)$$

Equations of motion for the coefficients can be calculated by multiplying from the left by the appropriate basis function. The

resulting equations and complex conjugates are given below.

$$
\begin{aligned}
i\hbar\frac{\partial a}{\partial t} &= aH_{aa} + bH_{ab} = a(\hbar\frac{\omega_0}{2} + V_{aa}) + bV_{ab} \\
-i\hbar\frac{\partial a^*}{\partial t} &= a^*H_{aa} + b^*H_{ba} = a^*(\hbar\frac{\omega_0}{2} + V_{aa}) + b^*V_{ba} \\
i\hbar\frac{\partial b}{\partial t} &= aH_{ba} + bH_{bb} = aV_{ba} + b(-\hbar\frac{\omega_0}{2} + V_{bb}) \\
-i\hbar\frac{\partial b^*}{\partial t} &= a^*H_{ab} + b^*H_{bb} = a^*V_{ab} + b^*(-\hbar\frac{\omega_0}{2} + V_{bb})
\end{aligned}
\tag{2.52}
$$

where in general for any operator, O ; $O_{ij} = \langle i|O|j\rangle$.

For most cases of interest $V_{aa}=V_{bb}=0$. This corresponds to the situation where the perturbation only causes transitions from one state to another state and does not cause a change in any observable property of the system without a change of state of the system. Also these terms can be neglected if they are small compared to $\hbar\frac{\omega_0}{2}$. The above system of equations then reduce to the following,

$$
\begin{aligned}
i\hbar\frac{\partial a}{\partial t} &= a\hbar\frac{\omega_0}{2} + bV_{ab} \\
-i\hbar\frac{\partial a^*}{\partial t} &= a^*\hbar\frac{\omega_0}{2} + b^*V_{ba} \\
i\hbar\frac{\partial b}{\partial t} &= aV_{ba} - b\hbar\frac{\omega_0}{2} \\
-i\hbar\frac{\partial b^*}{\partial t} &= a^*V_{ab} - b^*\hbar\frac{\omega_0}{2}.
\end{aligned}
\tag{2.53}
$$

Now the time development of the z-magnetization in the presence of a perturbation can be calculated from the above equations as follows,

$$\frac{\partial\langle I_z\rangle}{\partial t} = \frac{1}{2}\frac{\partial}{\partial t}(a^*a - b^*b)$$

$$= \frac{1}{2}(a^*\frac{\partial a}{\partial t} + \frac{\partial a^*}{\partial t}a - b^*\frac{\partial b}{\partial t} - \frac{\partial b^*}{\partial t}b) \qquad (2.54)$$

$$= \frac{1}{i\hbar}(a^*bV_{ab} - b^*aV_{ba}).$$

This equation can be seen to represent the time development of one component of an ordered triplet of numbers if the following definitions are made.

$$r_x = \frac{1}{2}(a^*b + b^*a) \quad , \quad \Omega_x = (V_{ab} + V_{ba})/\hbar$$

$$r_y = -\frac{i}{2}(a^*b - b^*a) \quad , \quad \Omega_y = i(V_{ab} - V_{ba})/\hbar \qquad (2.55)$$

$$r_z = \frac{1}{2}(a^*a - b^*b) \quad , \quad \Omega_z = \omega_0$$

therefore

$$\frac{\partial r_z}{\partial t} = \Omega_x r_y - r_x \Omega_y. \qquad (2.56)$$

The ordered triplets can be represented as vectors in a mathematical space so that the following equation is satisfied.

$$\frac{\partial r}{\partial t} = \Omega \times r \qquad (2.57)$$

where $r = (r_x, r_y, r_z)$ and $\Omega = (\Omega_x, \Omega_y, \Omega_z)$.

Note that $|r| = (a^*a + b^*b)$ which is equal to one for a normalized wavefunction so r is a vector of unit length in this mathematical space.

The mathematical vector space can take on a more physical meaning by considering the following properties of the components of the spin operator, I.

$$\langle \xi(t) | I_x | \xi(t) \rangle = \langle \xi(t) | \frac{1}{2}(I_+ + I_-) | \xi(t) \rangle$$

$$= \frac{1}{2}(a^* b + b^* a) \tag{2.58}$$

and

$$\langle \xi(t) | I_y | \xi(t) \rangle = \langle \xi(t) | -\frac{i}{2}(I_+ - I_-) | \xi(t) \rangle$$

$$= -\frac{i}{2}(a^* b - b^* a). \tag{2.59}$$

Now the choice of subscripts on the components of the vector r seem more reasonable and can be identified as the components of the spin, I.

$$\begin{aligned} r_x &= \frac{1}{2}(a^* b + b^* a) = \langle I_x \rangle \\ r_y &= -\frac{i}{2}(a^* b - b^* a) = \langle I_y \rangle \\ r_z &= \frac{1}{2}(a^* a - b^* b) = \langle I_z \rangle . \end{aligned} \tag{2.60}$$

The components of magnetic moment, μ, are given by

$$\begin{aligned} \langle \mu_x \rangle &= \gamma \hbar \langle I_x \rangle = \gamma \hbar r_x \\ \langle \mu_y \rangle &= \gamma \hbar \langle I_y \rangle = \gamma \hbar r_y \\ \langle \mu_z \rangle &= \gamma \hbar \langle I_z \rangle = \gamma \hbar r_z \end{aligned} \tag{2.61}$$

therefore the vector equation of motion for r can be rewritten in terms of the magnetic moment as

$$\frac{\partial \mu}{\partial t} = \Omega \times \mu. \tag{2.62}$$

If the perturbation is a magnetic field applied in the xy-plane, the perturbing Hamiltonian can be written as

$$V = -\gamma\hbar(B_x I_x + B_y I_y) = \hbar(\omega_x I_x + \omega_y I_y) \tag{2.63}$$

where $\omega_x = -\gamma B_x$ and $\omega_y = -\gamma B_y$. The expectation value of the perturbation becomes,

$$\begin{aligned} V_{ab} &= \hbar\langle a|(\omega_x I_x + \omega_y I_y)|b\rangle \\ &= \hbar\langle a|[\omega_x \tfrac{1}{2}(I_+ + I_-) + \omega_y \tfrac{1}{2i}(I_+ - I_-)]|b\rangle \\ &= \tfrac{1}{2}\hbar(\omega_x - i\omega_y) \end{aligned} \tag{2.64}$$

and

$$\begin{aligned} V_{ba} &= \hbar\langle b|[\omega_x \tfrac{1}{2}(I_+ + I_-) + \omega_y \tfrac{1}{2i}(I_+ - I_-)]|a\rangle \\ &= \tfrac{1}{2}\hbar(\omega_x + i\omega_y). \end{aligned} \tag{2.65}$$

Therefore the components of Ω are given by

$$\Omega_x = \omega_x \quad , \quad \Omega_y = \omega_y \quad , \quad \Omega_z = \omega_0 \tag{2.66}$$

and for a Hamiltonian of the form

$$\begin{aligned} H &= H_0 + V = \hbar(\omega_x I_x + \omega_y I_y + \omega_0 I_z) \\ &= \hbar\, \Omega.I = -\hbar\, \gamma B.I \end{aligned} \tag{2.67}$$

where $\Omega = -\gamma B$, the vector equation of motion for the magnetic moment can be written as,

$$\frac{\partial \mu}{\partial t} = (-\gamma B) \times \mu = \gamma\, (\, \mu \times B\,). \tag{2.68}$$

This is the classical equation of motion of the magnetic moment in a magnetic field [2.8].

The observable transverse magnetization can now be interpreted in terms of combinations of the coefficients associated with each state. In order to make this more explicit let

$$a(t) = a_0 e^{i\omega_\alpha t}$$

$$b(t) = b_0 e^{i\omega_\beta t}. \tag{2.69}$$

Therefore the components of the magnetic moment μ become,

$$\langle \mu_x \rangle = \gamma\hbar a_0 b_0 \cos(\omega_\alpha - \omega_\beta)t$$

$$\langle \mu_y \rangle = -\gamma\hbar a_0 b_0 \sin(\omega_\alpha - \omega_\beta)t \tag{2.70}$$

$$\langle \mu_z \rangle = \gamma\hbar\tfrac{1}{2}(a_0^2 - b_0^2).$$

If the states have a random distribution of phases the x- and y-components of magnetization will average to zero. Therefore transverse magnetization is observed only when there exists a definite phase coherence between the states. In the situation where a definite phase coherence is present the x- and y-components vary sinusoidally in time.

The probability for occupation of each state is given by $p_a = a_0^2$ and $p_b = b_0^2$. The magnitude of the observable magnetic moment in the xy-plane is given by

$$|\langle \mu_{xy} \rangle| = (\langle \mu_x \rangle^2 + \langle \mu_y \rangle^2)^{1/2}$$

$$= \gamma\hbar a_0 b_0 = \gamma\hbar(p_a p_b)^{1/2}. \tag{2.71}$$

Therefore the maximum observable transverse magnetization occurs when the states are equally populated so that $p_a = p_b$. As discussed previously, this corresponds to a state with zero z-component of

magnetization.

The time evolution of the transverse magnetization can be illustrated by considering the following situation. Assume that a perturbation acting at t = 0 creates a state with only transverse magnetization hence $p_a = p_b = 1/2$ and one possible choice is $a_0 = b_0 = 2^{-1/2}$. Using the time evolution operator the state at a time, t, can be written as

$$\begin{aligned} |\xi(t)\rangle &= e^{-iH_0 t/\hbar} |\xi(0)\rangle \\ &= e^{-iH_0 t/\hbar} 2^{-1/2}(|a\rangle + |b\rangle) \\ &= 2^{-1/2}(e^{-i\omega_0 t/2}|a\rangle + e^{i\omega_0 t/2}|b\rangle). \end{aligned} \tag{2.72}$$

For this example $a(t) = 2^{-1/2}\, e^{-i\omega_0 t/2}$ and $b(t) = 2^{-1/2}\, e^{i\omega_0 t/2}$. The components of transverse magnetization can be written as

$$\begin{aligned} \langle \mu_x \rangle &= \gamma\hbar\tfrac{1}{2}(a^* b + b^* a) = \tfrac{1}{2}\gamma\hbar \cos(\omega_0 t) \\ \langle \mu_y \rangle &= -\gamma\hbar\tfrac{i}{2}(a^* b - b^* a) = \tfrac{1}{2}\gamma\hbar \sin(\omega_0 t). \end{aligned} \tag{2.73}$$

Hence the observed signal oscillates in a sinusoidal manner at the Larmor frequency, $\omega_0 = -\gamma B_0$. In terms of the vector picture developed in this section the transverse magnetization can be thought of as rotating about the z-axis in the space defined by the components of the spin angular momentum.

The vector picture can also be written in an operator formulation as follows. The components of the spin angular momentum operator, I, in terms of the basis set can be written in the following form.

$$I_x = \frac{1}{2}(|a\rangle\langle b| + |b\rangle\langle a|)$$

$$I_y = -\frac{i}{2}(|a\rangle\langle b| - |b\rangle\langle a|) \qquad (2.74)$$

$$I_z = \frac{1}{2}(|a\rangle\langle a| - |b\rangle\langle b|).$$

These operators have commutation properties such that

$$[I_x , I_y] = iI_z \quad , \quad \text{and cyclic permutations.} \qquad (2.75)$$

They also obey the following equation of motion,

$$\frac{dI_\alpha}{dt} = \frac{i}{\hbar}[H , I_\alpha] \quad , \quad \alpha = x,y,z \qquad (2.76)$$

or more properly

$$\frac{d\langle I_\alpha\rangle}{dt} = \frac{i}{\hbar}\langle[H , I_\alpha]\rangle \quad , \quad \alpha = x,y,z. \qquad (2.77)$$

Now if the Hamiltonian has the form

$$H = \hbar(\omega_x I_x + \omega_y I_y + \omega_z I_z) \qquad (2.78)$$

equation 2.76 can be written as

$$\frac{dI_\alpha}{dt} = i\,[(\omega_x I_x + \omega_y I_y + \omega_z I_z) , I_\alpha]$$

$$= \omega_x i[I_x,I_\alpha] + \omega_y i[I_y,I_\alpha] + \omega_z i[I_z,I_\alpha]. \qquad (2.79)$$

For $\alpha = x$

$$\frac{dI_x}{dt} = \omega_y I_z - I_y \omega_z \qquad (2.80)$$

$\alpha = y$

$$\frac{dI_y}{dt} = \omega_z I_x - I_z \omega_x \tag{2.81}$$

and $\alpha = z$

$$\frac{dI_z}{dt} = \omega_x I_y - I_x \omega_y . \tag{2.82}$$

These equations can be seen to represent the time development of a vector in a space defined by the components of the spin angular momentum so that the spin operator, I, obeys the following vector equation of motion.

$$\frac{\partial I}{\partial t} = \Omega \times I \tag{2.83}$$

where $I = (I_x, I_y, I_z)$ and $\Omega = (\omega_x, \omega_y, \omega_z)$.

These operators can be used to provide a geometric representation of processes for a single spin-1/2 system. In a coordinate frame defined by the components of spin I, the effect of the application of a magnetic field of strength $|\Omega|/\gamma$ can be viewed as a rotation of the spin vector I about the applied field vector Ω. These operators also fulfill the conditions outlined in the introduction in equations 2.38 to 2.42 and demonstrate the usefulness of defining such a set of operators. An equation of the type of equation 2.43 can be used to predict the effect of an applied field where here the constant k has unit value.

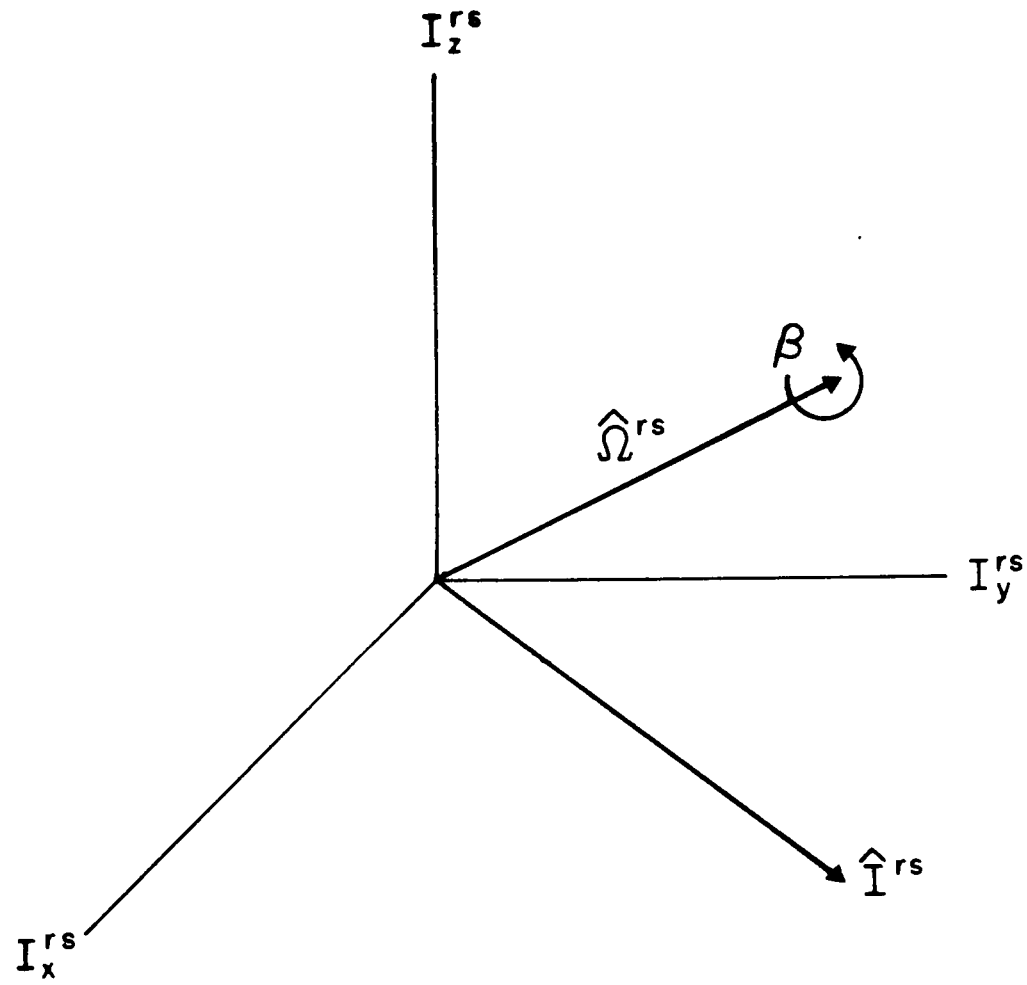

Figure 2.3 Vector frame defined by the components of the single transition operator for any two levels.

2.3.2. Single transition operators

The operator development of the preceding section can be generalized to include any two-level subsystem of a multiple-level system by defining a set of single transition operators for each two-level subsystem as follows [2.7].

$$I_x^{rs} = \frac{1}{2}(|r\rangle\langle s| + |s\rangle\langle r|) \quad , \quad I_x^{rs} = I_x^{sr}$$

$$I_y^{rs} = -\frac{i}{2}(|r\rangle\langle s| - |s\rangle\langle r|) \quad , \quad I_y^{rs} = -I_y^{sr} \qquad (2.84)$$

$$I_z^{rs} = \frac{1}{2}(|r\rangle\langle r| - |s\rangle\langle s|) \quad , \quad I_z^{rs} = -I_z^{sr}.$$

They have the same commutation properties and obey the same equations of motion as defined in the previous section.

$$[I_x^{rs} \, , \, I_y^{rs}] = iI_z^{rs} \quad , \text{ and cyclic permutations} \qquad (2.85)$$

and

$$\frac{\partial I^{rs}}{\partial t} = \Omega^{rs} \times I^{rs} \qquad (2.86)$$

where $I^{rs} = (I_x^{rs}, I_y^{rs}, I_z^{rs})$ and $\Omega^{rs} = (\omega_x^{rs}, \omega_y^{rs}, \omega_z^{rs})$.

The equation of motion can be interpreted as a rotation of the vector I^{rs} about Ω^{rs} with the effective rotational frequency,

$$|\Omega^{rs}| = \omega_e{}^{rs} = [\omega_x^{rs} + \omega_y^{rs} + \omega_z^{rs}]^{1/2} \qquad (2.87)$$

and if Ω^{rs} is applied for a time, t, the vector I^{rs} rotates about Ω^{rs} by an angle, $\beta = \omega_e{}^{rs} t$, or in a graphical form this can be represented as shown in figure 2.3. These operators have a transformation property of the general form [2.5],

$$e^{-i\beta I_y^{rs}} I_z^{rs} e^{i\beta I_y^{rs}} = I_z^{rs} \cos(\beta) + I_x^{rs} \sin(\beta). \qquad (2.88)$$

This equation can be used for calculation of the process illustrated graphically in figure 2.3.

2.3.3. Multiple level system

In this section the concept of single transition operators is generalized to include systems with more than two levels. A three level system will be considered which exhibits the basic properties of a multiple level system.

Any multi-level system can be decomposed into a set of two-level subsystems which have the properties of an isolated two-level system. Two-level subsystems will be referred to as transitions and are considered connected if they have an energy level in common and nonconnected if they are totally separate. The operators between nonconnected transitions commute, so that

$$[I_\alpha^{rs} , I_\beta^{tu}] = 0 \quad ; \quad \alpha,\beta = x,y,z. \qquad (2.89)$$

For operators associated with different transitions yet having one level in common, a multi-level system can be decomposed into a set of three-level subsystems for which the x- and y-components of the associated single transition operators have the commutator property,

$$[I_\alpha^{rs} , I_\beta^{st}] = i \frac{1}{2} \varepsilon_{\alpha\beta\gamma} I_\gamma^{rt} \qquad (2.90)$$

and cyclic permutations of α,β,γ. For $\alpha = \beta$,

$$\gamma = y \quad \text{and} \quad \varepsilon_{\alpha\beta\gamma} = \begin{cases} 1 , & \text{if } \alpha = \beta = x \\ -1 , & \text{if } \alpha = \beta = y \end{cases} \qquad (2.91)$$

and for $\alpha \neq \beta$,

$$\gamma = x \quad \text{and} \quad \varepsilon_{\alpha\beta\gamma} = -1. \tag{2.92}$$

As introduced in the last section the single transition operators obey an equation of motion of the form,

$$\frac{dI_{\alpha}^{rs}}{dt} = \frac{i}{\hbar}[H\ ,\ I_{\alpha}^{rs}] \quad , \alpha = x,y,z. \tag{2.93}$$

For the connected x- and y-components of the single transition operators, the cyclic commutation property and above equation of motion can be combined in a vector equation of motion if the Hamiltonian has the following form,

$$H = \hbar(\omega_{\alpha}^{rs} I_{\alpha}^{rs} + \omega_{\beta}^{st} I_{\beta}^{st} + \omega_{\gamma}^{rt} I_{\gamma}^{rt}). \tag{2.94}$$

The vector equation has the form

$$\frac{dI_{\alpha\beta\gamma}}{dt} = \frac{1}{2}\,\varepsilon_{\alpha\beta\gamma}\,\Omega_{\alpha\beta\gamma} \times I_{\alpha\beta\gamma} \tag{2.95}$$

where $I_{\alpha\beta\gamma} = (I_{\alpha}^{rs}, I_{\beta}^{st}, I_{\gamma}^{rt})$ and $\Omega_{\alpha\beta\gamma} = (\omega_{\alpha}^{rs}, \omega_{\beta}^{st}, \omega_{\gamma}^{rt})$. Note that the angle of rotation during the time, t, is given by half the angle of an isolated two-level system. The rotation angle is given by

$$\theta = \frac{\beta}{2} = \frac{1}{2}\omega_e t = \frac{1}{2}[(\omega_{\alpha}^{rs})^2 + (\omega_{\beta}^{st})^2 + (\omega_{\gamma}^{rt})^2]^{1/2} t. \tag{2.96}$$

The vector equation 2.95 defines a set of operators for each connected three-level subsystem which behaves as a classical vector under rotation. The number of possible nondegenerate three-dimensional frames for the x- and y-components of each three-level subsystem can be shown

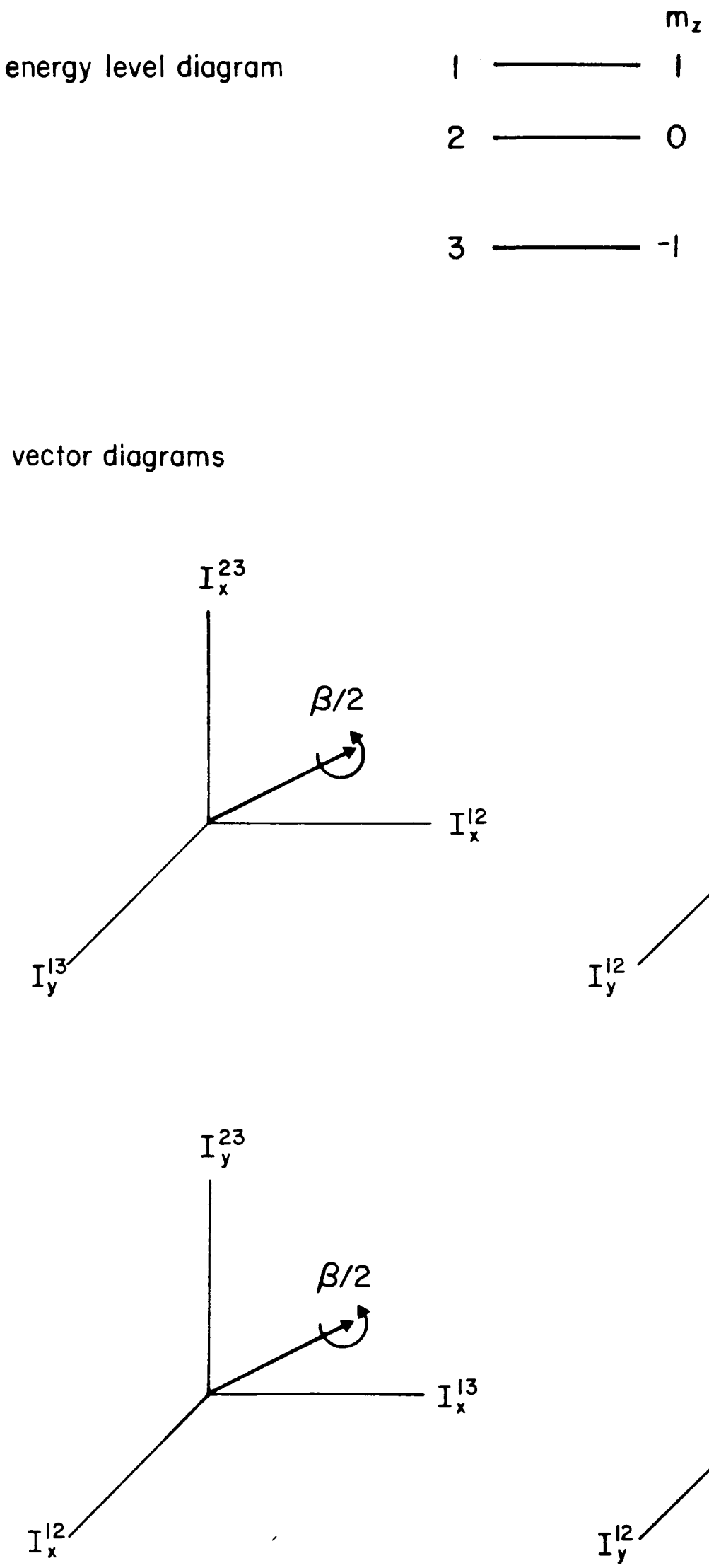

Figure 2.4 The top of the figure shows the energy level diagram for a spin-1 system with quadrupolar coupling. The bottom shows the four vector diagrams appropriate for a three level system.

to be equal to four. As a specific example consider an isolated three-level system which can represent a spin-1 nucleus with a quadrupolar coupling [2.10]. This exhibits all the characteristics of any three-level subsystem. The energy level diagram and four vector frames for a three level system are represented graphically in figure 2.4.

These vector frames illuminate several interesting properties of the three-level system. These can be illustrated by considering the top left vector frame in detail. In terms of exponential operators the rotation of I_x^{23} about I_x^{12} can be written as,

$$e^{-i\beta I_x^{12}} I_x^{23} e^{i\beta I_x^{12}} = I_x^{23} \cos(\tfrac{\beta}{2}) + I_y^{13} \sin(\tfrac{\beta}{2}). \qquad (2.97)$$

This vector frame points out one method of exciting double quantum coherence by creating I_y^{13}. This could be accomplished by appling a $(\frac{\pi}{2})_y$ pulse to the 23-transition at equilibrium which would selectively create I_x^{23}. Then a $(\pi)_x$ pulse to the 12-transition rotates the I_x^{23} coherence into the double quantum coherence, I_y^{13}. This is equivalent to appling a $(\frac{\pi}{2})_{-x}$ pulse to I_x^{13} rotating the I_z^{13} vector into I_y^{13} [2.10a].

Also this vector frame exhibits the properties of a spinor if the behaviour of I_x^{23} is followed as a function of the rotation angle applied along I_x^{12}, i.e. it returns to its original position only after a rotation of a multiple of 4π [2.10a].

The z-component of the single transition operators associated with different transitions having one level in common does not have cyclic commutator properties with either x-, y-, or z-components of any connected transition. Therefore no vector equation of motion or geometric representation can be defined in a straightforward manner. The z-component does have the following noncyclic commutation properties,

$$[I_x^{rs} , I_z^{st}] = \frac{i}{2} I_y^{rs}$$

$$[I_y^{rs} , I_z^{st}] = -\frac{i}{2} I_x^{rs} \qquad (2.98)$$

$$[I_z^{rs} , I_z^{st}] = 0.$$

The z-components of a set of connected transitions are not linearly independent. For a group of levels which form a closed loop, the sum of the z-components of the single transition operators will vanish.

$$I_z^{pq} + I_z^{pr} + \ldots + I_z^{up} = 0. \qquad (2.99)$$

The z-components for a three level subsystem are related by,

$$I_z^{rs} + I_z^{st} + I_z^{tr} = 0 \qquad (2.100)$$

and the 'tr' component can be rewritten,

$$I_z^{rt} = \frac{1}{2}(I_z^{rt} + I_z^{rs} + I_z^{st}). \qquad (2.101)$$

This provides a useful method of treating the z-component operator for by using equation 2.98 it can be shown that any component operator associated with the 'rs' transition commutes with the sum of the first and last terms in equation 2.101.

$$[I_\alpha^{rs} , (I_z^{rt} + I_z^{st})] = 0 \quad , \quad \alpha = x,y \text{ or } z. \qquad (2.102)$$

Therefore the commutator of any component operator of a transition with the z-component operator of a connected transition can be written as the sum of two commutators. One commutator will be zero as noted in equation 2.102 and the other will be cyclic and therefore interpretable in a vector picture. As an illustration consider a pulse to the 'rs' transition in the transverse plane represented by the pulse operator,

$$R^{rs}(\alpha,\phi) = e^{-i\alpha(I_x^{rs}\cos\phi + I_y^{rs}\sin\phi)} . \qquad (2.103)$$

The effect of this pulse on the component operator I_z^{rt} can be written as, using equation 2.101 and equation 2.102,

$$R^{rs}(\alpha,\phi)\ I_z^{rt}\ R^{rs}(\alpha,\phi)^+$$

$$= \frac{1}{2}(I_z^{rt} + I_z^{st})$$

$$+ \frac{1}{2}[I_z^{rs}\cos\alpha + (I_x^{rs}\sin\phi - I_y^{rs}\cos\phi)\sin\alpha] . \qquad (2.104)$$

Note that the effective rotation angle is α with a scaling factor of unity. This is a result of the commutator property of equation 2.85 as illustrated in figure 2.3.

In this section the general properties of the single transition operators have been presented. The idea of a coherence between states has been developed and represented in terms of component operators in a mathematical vector space. A pictorial representation of the transformation among the single transition operators is possible whenever a cyclic commutator can be defined among a group of operators. This leads to a simplified method of calculation for some experiments. In particular it is possible to calculate the result of a transition selective experiment in detail. The example of the quadrupolar coupled spin-1 nucleus has been mentioned and several other experiments have been performed which illustrate the usefulness of these ideas [2.11].

Experiments which pulse all the transitions associated with a single spin or group of spins can be treated using the concept of a pulse cascade [2.12]. A non-selective pulse can be considered a cascade of pulses to each spin separately because the pulse operators for each individual spin commute. Hence the pulse to each spin can be taken in any order. Also a pulse to each spin can be considered a cascade of

separate pulses to each transition associated with the spin. Again the order of applying the pulse to each transition within a spin multiplet is immaterial. However the order of operation for transitions associated with different spins will not commute if the transitions are connected, in which case the order must be preserved. Using this approach, a pulse operator expressed in terms of single transition operators can be written as a cascade of pulses to each individual single transition operator and the result can be predicted using the appropriate vector rotation properties for the operators.

In section 2.5 it will be shown that in certain situations the description of the experiments with non-selective pulses can be simplified by considering linear combinations of the single transition operators. This will reduce the amount of calculation necessary to follow an experiment and illustrate the usefulness of the single transition operators in representing the coherent processes involved in an experiment.

2.4. The density operator in terms of single transition operators

The single transition operators provide a natural set of operators for the representation of a spin system in a magnetic resonance experiment. As outlined previously the description of the system proceeds from the point of view of the density operator so expressing the density operator in terms of the single transition operators provides a simplified method of following the evolution of the spin system in the experiment.

Transforming equation 2.10 into the rotating frame of reference, the density operator for a system of spins in a pure state can be written as,

$$\rho = \sum_k \sum_l |k\rangle \rho_{kl} \langle l| \tag{2.105}$$

which has the following properties,

$$\rho_{kl} = \rho^*_{lk} \quad , \quad \text{Hermitian} \tag{2.106}$$

and

$$\begin{aligned} Tr(\rho) &= \sum_s \sum_k \sum_l \langle s|k\rangle \rho_{kl} \langle l|s\rangle \\ &= \sum_s \rho_{ss} = 1. \end{aligned} \tag{2.107}$$

As is shown in the Appendix, a reduced density operator, ρ_r, can be defined in the high temperature limit by,

$$\rho = (Tr\ 1)^{-1} + \rho_r. \tag{2.108}$$

Now equation 2.107 becomes,

$$\begin{aligned} Tr(\rho) &= 1 + Tr(\rho_r) = 1 \\ Tr(\rho_r) &= 0. \end{aligned} \tag{2.109}$$

For experiments in high resolution nuclear magnetic resonance at room temperature, the high temperature limit is a valid approximation so that the reduced density operator contains all the time dependence of the system and provides a complete description of the system (see the Appendix). Hence only the reduced density operator will be considered and the subscript will be dropped in all subsequent calculations with the implicit understanding that it is the reduced form of the operator with the trace property outlined in equation 2.109 which will be used in calculations.

By requiring the trace to vanish, the diagonal elements of the density operator are related by,

$$Tr(\rho) = \sum_k \rho_{kk} = 0 \qquad (2.110)$$

which can be written as,

$$\rho_{ll} = - \sum_{k \neq l} \rho_{kk}. \qquad (2.111)$$

Using this relationship the density operator of equation 2.105 can be written as,

$$\rho = \rho_{ll}|l\rangle\langle l| + \sum_{k \neq l} \rho_{kk}|k\rangle\langle k| + \sum_{k \neq l} \sum_l \rho_{kl}|k\rangle\langle l|$$

$$= \sum_{k \neq l} [\, \rho_{kk}(|k\rangle\langle k| - |l\rangle\langle l|)$$

$$+ \sum_{k<l} \sum_l \mathrm{Re}\rho_{kl}(|k\rangle\langle l| + |l\rangle\langle k|) + i\mathrm{Im}\rho_{kl}(|k\rangle\langle l| - |l\rangle\langle k|)]. \qquad (2.112)$$

For a system of N particles of spin I the number of states is given by $(2I+1)^N$. The diagonal elements of the density operator can be summed over all possible values of the state 'l' and the sum divided by the number of possible states. Also, recalling the definition of the single transition operators from equation 2.84, the density operator can be written as,

$$\rho = \sum_{k<l} \sum_l [\, 2\,\mathrm{Re}\rho_{kl} I_x^{kl} - 2\,\mathrm{Im}\rho_{kl} I_y^{kl} + (2I+1)^{-N}\, 2(\rho_{kk} - \rho_{ll}) I_z^{kl}]. \qquad (2.113)$$

This represents the relationship between elements of the density matrix and the components of the single transition operators. Clearly an x-coherence is present if an off-diagonal element of the density matrix has a real component and similarly a y-coherence exists if an imaginary

component is present in an off-diagonal element. Finally z-magnetization is seen to be present whenever there is a population difference between energy levels of the spin system represented by a finite difference between diagonal elements of the density matrix. To simplify the notation, equation 2.113 will be written as,

$$\rho = \sum_{k<l} \sum_{l} (c_x^{kl} I_x^{kl} + c_y^{kl} I_y^{kl} + c_z^{kl} I_z^{kl}) \qquad (2.114)$$

where c_α^{kl} is a real-valued coefficient identified with terms in equation 2.113.

The matrix elements of the density operator are expressed in terms of the above coefficients as,

$$\rho_{kl} = \frac{1}{2} (c_x^{kl} - i c_y^{kl})$$

and

$$\rho_{kk} = \frac{1}{2} \sum_{l \neq k} c_z^{kl}.$$

These equations represent the connection between the matrix representation of the density operator and the expansion of the density operator in terms of the single transition operators.

The system under study is initially assumed to be in thermal equilibrium with its surroundings. In the appendix it is shown that the reduced density operator at thermal equilibrium in the high temperature limit is proportional to the z-component of spin angular momentum described by a Boltzmann distribution of states. Therefore the starting point for the calculation of the response of the spin system to an experiment will be the thermal equilibrium density operator of equation

A.15. For each spin the z-component of spin angular momentum operator can be expanded in terms of single transition operators. The density operator during an experiment can be written in the form of equation 2.114 and this provides a geometric representation of the state of the system.

2.4.1. General discussion of time evolution

With the density operator represented in terms of single transition operators it is possible to follow the evolution of the system in terms of the evolution of these operators. Recall the general equation of motion 2.39,

$$\frac{\partial I_\alpha}{\partial t} = \frac{i}{\hbar}[\, H \,,\, I_\alpha \,]. \qquad (2.115)$$

the
If Hamiltonian is not an explicit function of time this equation has the solution,

$$I_\alpha(t) = e^{-iHt/\hbar}\, I_\alpha(0)\, e^{iHt/\hbar}. \qquad (2.116)$$

Equations of this form will be used extensively to calculate the response of the system to perturbation and to determine the evolution of the system is the absence of perturbations. The general procedure for the single transition operators is illustrated below.

2.4.2. Free precession

Assume that the Hamiltonian for free precession, H_0, is diagonal in the chosen basis set then H_0 can be expanded in terms of the z-components of the single transition operators for this set as,

$$\hbar^{-1}H_0 = \sum_{(kl)} \emptyset_{kl} I_z^{kl}. \qquad (2.117)$$

The sum is over pairs of transitions such that $m_l = m_k - 1$.

The transition frequency between any two energy levels is given by,

$$\begin{aligned}\omega_{rs} &= \hbar^{-1}\Delta E_{rs} \\ &= [\sum_{(kl)} \emptyset_{kl}\langle r|I_z^{kl}|r\rangle - \sum_{(pq)} \emptyset_{pq}\langle s|I_z^{pq}|s\rangle] \\ &= \frac{1}{2}[\sum_{(rl)} \emptyset_{rl} - \sum_{(kr)} \emptyset_{kr} - \sum_{(sq)} \emptyset_{sq} + \sum_{(ps)} \emptyset_{ps}]. \qquad (2.118)\end{aligned}$$

The free precession of a component of a single transition operator can be calculated using equation 2.116. The z-components are stationary during free precession so we need only consider the x- and y-components. The x- and y-components can be expressed in terms of the raising and lowering operators as,

$$\begin{aligned}I_x^{rs} &= \tfrac{1}{2}(I_+^{rs} + I_-^{rs}) \\ I_y^{rs} &= \tfrac{1}{2}(I_+^{rs} - I_-^{rs}). \qquad (2.119)\end{aligned}$$

To simplify the calculation we will only consider the effect of the free precession Hamiltonian on the raising and lowering operators and from the result infer the precession property for the x- and y-components of the single transition operators.

From equation 2.116, the equation for free precession becomes,

$$\begin{aligned}&e^{-iH_0t/\hbar} I_{\pm}^{rs} e^{iH_0t/\hbar} \\ &= e^{-i\sum_{(kl)} \emptyset_{kl} I_z^{kl} t} I_{\pm}^{rs} e^{i\sum_{(pq)} \emptyset_{pq} I_z^{pq} t}\end{aligned}$$

$$= \left(\prod_{(kl)} e^{-i\phi_{kl} I_z^{kl} t} \right) I_{\pm}^{rs} \left(\prod_{(pq)} e^{i\phi_{pq} I_z^{pq} t} \right) \tag{2.120}$$

where use has been made of the property $[I_z^{rs}, I_z^{tu}] = 0$ for any transition, rs and tu. By expanding the operators in terms of their defining relationships, equations 2.84 and 2.119, it is possible to show that,

$$\begin{aligned} & e^{-iH_0 t/\hbar} I_{\pm}^{rs} e^{iH_0 t/\hbar} \\ & = I_{\pm}^{rs} e^{\mp i\frac{1}{2}\left(\sum_{(rl)} \phi_{rl} - \sum_{(kr)} \phi_{kr} - \sum_{(sq)} \phi_{sq} + \sum_{(ps)} \phi_{ps} \right)} \\ & = I_{\pm}^{rs} e^{\mp i\omega_{rs} t} . \end{aligned} \tag{2.121}$$

Equation 2.118 has been used to derive the result in the final line of equation 2.121. Expanding the exponential and using equation 2.119 the above result can be rewritten in terms of x- and y-components of the single transition operators as

$$\begin{aligned} e^{-iH_0 t/\hbar} I_x^{rs} e^{iH_0 t/\hbar} &= e^{-i\omega_{rs} t\, I_z^{rs}} I_x^{rs} e^{i\omega_{rs} t\, I_z^{rs}} \\ e^{-iH_0 t/\hbar} I_y^{rs} e^{iH_0 t/\hbar} &= e^{-i\omega_{rs} t\, I_z^{rs}} I_y^{rs} e^{i\omega_{rs} t\, I_z^{rs}} . \end{aligned} \tag{2.122}$$

This result allows the use of the vector picture to represent the free precession of each coherence about the static magnetic field, B_0. Each coherence rotates about B_0 at its transition frequency determined by the energy eigenvalues of the spin system as represented by equation 2.118. It is important to note that these relations hold for any order of coherence so that a multiple quantum coherence can be thought of as rotating about the static field at its appropriate transition frequency.

This provides a pictorial representation of the free precession process for any state of coherence of the spin system.

2.4.3. Pulsed excitation

Consider the effect of a pulse on the density operator now expressed in terms of single transition operators as in equation 2.114. The general equation of motion is given by,

$$\rho' = R\,\rho\,R^{+}. \tag{2.123}$$

The coefficients for each component of the density operator after the pulse can be determined by taking the trace of each component operator with the density operator,

$$\langle I_{\alpha}^{rs}\rho'\rangle = (c_{\alpha}^{rs})'\ \mathrm{Tr}[(I_{\alpha}^{rs})^{2}] = \tfrac{1}{2}(c_{\alpha}^{rs})' \tag{2.124}$$

so that the coefficient for the x-component is given by,

$$\begin{aligned}(c_{x}^{rs})' &= 2\ \mathrm{Tr}(I_{x}^{rs}R\,\rho\,R^{+})\\ &= \langle s|\ R\,\rho\,R^{+}\ |r\rangle + \langle r|\ R\,\rho\,R^{+}\ |s\rangle\\ &= 2\ \mathrm{Re}\ (\langle r|\ R\,\rho\,R^{+}\ |s\rangle).\end{aligned} \tag{2.125}$$

For the y-component,

$$\begin{aligned}(c_{y}^{rs})' &= 2\ \mathrm{Tr}(I_{y}^{rs}\ R\,\rho\,R^{+}\ )\\ &= -2\ \mathrm{Im}\ (\langle r|\ R\,\rho\,R^{+}\ |s\rangle)\end{aligned} \tag{2.126}$$

and for the z-component,

$$I_x^{rs} \leftarrow I_x^{pq}$$

$$(c_x^{rs})' = c_x^{pq}[\,\mathrm{Re}(R_{rp}R_{qs}^{+}) + \mathrm{Re}(R_{rq}R_{ps}^{+})]$$

$$I_y^{rs} \leftarrow I_x^{pq}$$

$$(c_y^{rs})' = -c_x^{pq}[\,\mathrm{Im}(R_{rp}R_{qs}^{+}) + \mathrm{Im}(R_{rq}R_{ps}^{+})]$$

$$I_z^{rs} \leftarrow I_x^{pq}$$

$$(c_z^{rs})' = c_x^{pq}[\,\mathrm{Re}(R_{rp}R_{qr}^{+}) - \mathrm{Re}(R_{sp}R_{qs}^{+})]$$

$$I_x^{rs} \leftarrow I_y^{pq}$$

$$(c_x^{rs})' = c_y^{pq}[\,\mathrm{Im}(R_{rp}R_{qs}^{+}) - \mathrm{Im}(R_{rq}R_{ps}^{+})]$$

$$I_y^{rs} \leftarrow I_y^{pq}$$

$$(c_y^{rs})' = c_y^{pq}[\,\mathrm{Re}(R_{rp}R_{qs}^{+}) - \mathrm{Re}(R_{rq}R_{ps}^{+})]$$

$$I_z^{rs} \leftarrow I_y^{pq}$$

$$(c_z^{rs})' = c_y^{pq}[\,\mathrm{Im}(R_{rp}R_{qr}^{+}) - \mathrm{Im}(R_{sp}R_{qs}^{+})]$$

$$I_x^{rs} \leftarrow I_z^{pq}$$

$$(c_x^{rs})' = c_z^{pq}[\,\mathrm{Re}(R_{pr}R_{rq}^{+}) - \mathrm{Re}(R_{ps}R_{sq}^{+})]$$

$$I_y^{rs} \leftarrow I_z^{pq}$$

$$(c_y^{rs})' = -c_z^{pq}[\,\mathrm{Im}(R_{pr}R_{rq}^{+}) - \mathrm{Im}(R_{ps}R_{sq}^{+})]$$

$$I_z^{rs} \leftarrow I_z^{pq}$$

$$(c_z^{rs})' = \tfrac{1}{2}c_z^{pq}[\,(R_{pr}R_{rp}^{+} - R_{ps}R_{sp}^{+}) - (R_{qr}R_{rq}^{+} - R_{qs}R_{sq}^{+})]$$

Table 2.1 The table shows the coefficients in the expansion of the density operator after a pulse. The coefficients are grouped according to the component of coherence transferred by the pulse. The first three represent transfer from the x-component of coherence pq to the x-, y- and z-components of coherence rs. The second three represent the y-component transfer and the last three the z-component transfer.

$$(c_z^{rs})' = 2\ \mathrm{Tr}\ (I_z^{rs}\ R\ \rho\ R^+)$$

$$= \langle r|\ R\ \rho\ R^+\ |r\rangle - \langle s|\ R\ \rho\ R^+\ |s\rangle. \qquad (2.127)$$

Now expressions for the effect of the pulse operator on individual components of the density operator before the pulse can be developed. This will provide a completely general method of studying the transfer of coherence affected by a pulse.

The matrix elements of the components of the system after the pulse are given by,

$$c_x^{pq}\langle r|\ R\ I_x^{pq}\ R^+\ |s\rangle = c_x^{pq}\ \frac{1}{2}\ (R_{rp}R_{qs}^+ + R_{rq}R_{ps}^+)$$

$$c_y^{pq}\langle r|\ R\ I_y^{pq}\ R^+\ |s\rangle = -c_y^{pq}\ \frac{i}{2}\ (R_{rp}R_{qs}^+ - R_{rq}R_{ps}^+) \qquad (2.128)$$

$$c_z^{pq}\langle r|\ R\ I_z^{pq}\ R^+\ |s\rangle = c_z^{pq}\ \frac{1}{2}\ (R_{rp}R_{ps}^+ - R_{rq}R_{qs}^+).$$

Using equation 2.125 to equation 2.128 the transfer of individual components of coherence as represented by the single transition operators can be calculated explicitly. The resulting transfer coefficients are given in table 2.1. This rather daunting result will be used in the next chapter to derive a simple expression for the transfer of coherence among connected transitions of the same and different orders of coherence.

In many situations it is not necessary to calculate the transfer coefficients in detail for each individual coherence in the spin system. In section 2.5 it is shown that combinations of single transition operators can be used to represent the state of the spin system in such a way that each individual coherence need not be considered separately. Appropriate combinations of operators can be used to represent the state of the system in terms of vectors which behave as angular momentum

vectors under rotations and lead to a simple vector picture.

2.4.4. Phase shifts

In general, the effect of shifting the phase of a pulse can be interpreted as affecting a rotation about the z-axis. The pulse operator of equation 2.33 can be considered in three parts. A given coherence of the spin system is first rotated about the -z-axis for the phase angle, $\emptyset$. Then the pulse about the x-axis for the tip angle, α, affects a coherence transfer among the states of the system. Finally the transferred coherence is rotated about the z-axis for the phase angle, $\emptyset$. Also it is possible to apply a composite z-pulse [2.13] to rotate a coherence about the z-axis so the effect of z-rotations on coherences represented by the single transition operators is considered in detail in this section.

Consider rotations about the z-axis applied to a single spin of a multiple spin system. It is a simple matter to generalize to rotations applied to all the spins. The rotation can be represented by,

$$e^{-i\emptyset(I_z)_j} I_\alpha^{rs} e^{i\emptyset(I_z)_j} \quad ; \quad \alpha = x, y \text{ or } z \tag{2.129}$$

where $(I_z)_j$ is the jth spin of a multiple spin system with total spin, $F_z = \sum_j (I_z)_j$. The z-component of the single transition operator is uneffected by the z-rotation. The effect on the x- and y-components can most easily be calculated using the raising and lowering operators defined in equation 2.119. Now equation 2.129 can be written as,

$$e^{-i\emptyset(I_z)_j} I_{\pm}^{rs} e^{i\emptyset(I_z)_j}$$

$$= \sum_k \sum_l \left[e^{-i\emptyset(I_z)_j} |k\rangle\langle k| I_{\pm}^{rs} |l\rangle\langle l| e^{i\emptyset(I_z)_j} \right]$$

$$= I_{\pm}^{rs} \, e^{\mp i(\Delta m_{rs})_j \emptyset} \qquad (2.130)$$

where $(\Delta m_{rs})_j = (m_r)_j - (m_s)_j$ and $(m_k)_j$ is the kth eigenvalue of z-component of spin for the jth spin. This can be expanded in terms of x- and y-components to give the general form,

$$e^{-i\emptyset(I_z)_j} \, I_\alpha^{rs} \, e^{i\emptyset(I_z)_j}$$

$$= e^{-i(\Delta m_{rs})_j \emptyset \, I_z^{rs}} \, I_\alpha^{rs} \, e^{i(\Delta m_{rs})_j \emptyset \, I_z^{rs}} \qquad (2.131)$$

for α = x or y. A phase shift or rotation about the z-axis is dependent on the order of the coherence as represented by the change in magnetic quantum number, $(\Delta m_{rs})_j$. This provides a method of distinguishing between different orders of coherence by combining different experiments with appropriately chosen phases to cancel all but the desired order of coherence [2.14]. This property will be of use later in an experiment to observe magnetization derived from double quantum coherence selectively.

2.4.5. Observable magnetization

The observable transverse magnetization can be calculated by taking the trace of a component of magnetic moment with the density operator. Using equations 2.7 and 2.30, the x-component of magnetization is given by,

$$\langle \mu_x \rangle = \gamma\hbar \, Tr(F_x \rho) = \gamma\hbar \sum_{n=1}^{N} Tr[(I_x)_n \rho]. \qquad (2.132)$$

For the density operator of equation 2.114 this becomes,

$$\langle \mu_x \rangle = \gamma\hbar \sum_{n=1}^{N} \sum_{k<l} \sum_{l} c_x^{kl} \, \mathrm{Tr}[(I_x)_n I_x^{kl}] \qquad (2.133)$$

where the following properties have been used.

$$\mathrm{Tr}[(I_x)_n I_y^{kl}] = 0 \qquad (2.134)$$

and

$$\mathrm{Tr}[(I_x)_n I_z^{kl}] = 0. \qquad (2.135)$$

Finally the result becomes,

$$\langle \mu_x \rangle = \gamma\hbar \sum_{n=1}^{N} \left(\sum_{k<l} \sum_{l} c_x^{kl} \, \frac{1}{2}[I(I+1) - m_k(m_k \pm 1)]^{1/2} \delta_{k,l\pm1} \right)_n \qquad (2.136)$$

and a similar result can be derived for the y-component. From equation 2.136 it can be seen that the observable magnetization is derived from single transition operator terms in the density operator which represent transitions with $\Delta m = \pm 1$. Hence only single transition operators which represent single quantum coherences with the appropriate phase are observable. The observable magnetization is thus the sum of magnetization originating from each single quantum coherence represented by a single transition operator.

2.5. Linear combination of single transition operators

Under certain conditions it is possible to simplify the formal treatment of an experiment by considering appropriate single transition operators in combinations. If operator combinations can be identified that behave in the manner of angular momentum operators under rotations it is possible to interpret the motion of these combination operators in a vector picture without recourse to a detailed calculation.

As was shown in section 2.3, the equation of motion for operators which form a cyclic commutation relationship can be interpreted in a vector equation of motion. The effect of an appropriate Hamiltonian can be illustrated in a vector picture as a rotation about an applied field represented by the components of the Hamiltonian in the coordinate frame defined by the operators. Similarly this notion can be extended to operator combinations which form cyclic commutation relationships.

When this approach is possible it greatly simplifies the calculation and provides some 'feel' for the nature of the process being considered. The vector approach is more easily visualized and hence the outcome of an experiment simpler to predict.

A specific example of the usefulness of linear combinations of single transition operators is the following. The total spin angular momentum components of a multi-level system can be written as [2.14],

$$\begin{aligned} F_x &= \sum_{n=1}^{N} (I_x)_n = \sum_{rs} (C^{rs})^{1/2} I_x^{rs} \\ F_y &= \sum_{n=1}^{N} (I_y)_n = \sum_{rs} (C^{rs})^{1/2} I_y^{rs} \\ F_z &= \sum_{n=1}^{N} (I_z)_n = \sum_{rs} C^{rs} I_z^{rs} \end{aligned} \tag{2.137}$$

where the sum is over ordered pairs with decreasing quantum number such that $m_s = m_r - 1$ and $C^{rs} = I(I+1) - m_r m_s$. Using the previously defined commutation properties for the single transition operators it follows that the total spin angular momentum components obey the following commutation relation,

$$[F_x , F_y] = iF_z \quad , \quad \text{cyclic permutations.} \tag{2.138}$$

(a)

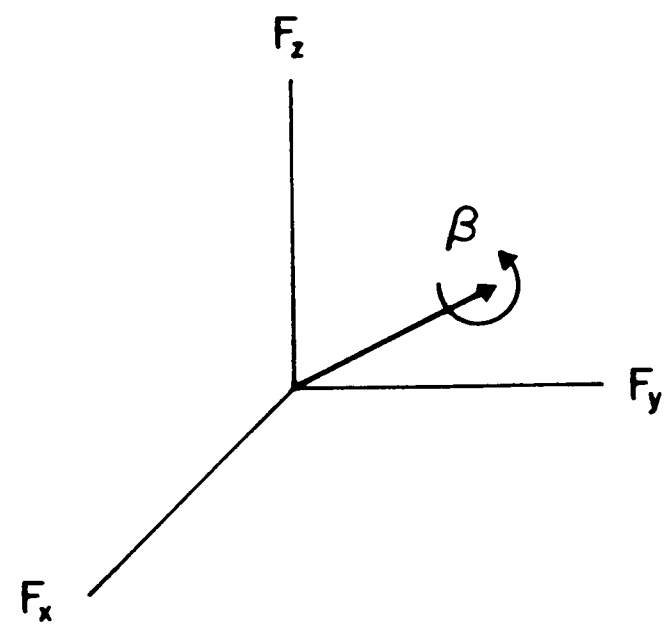

(b)

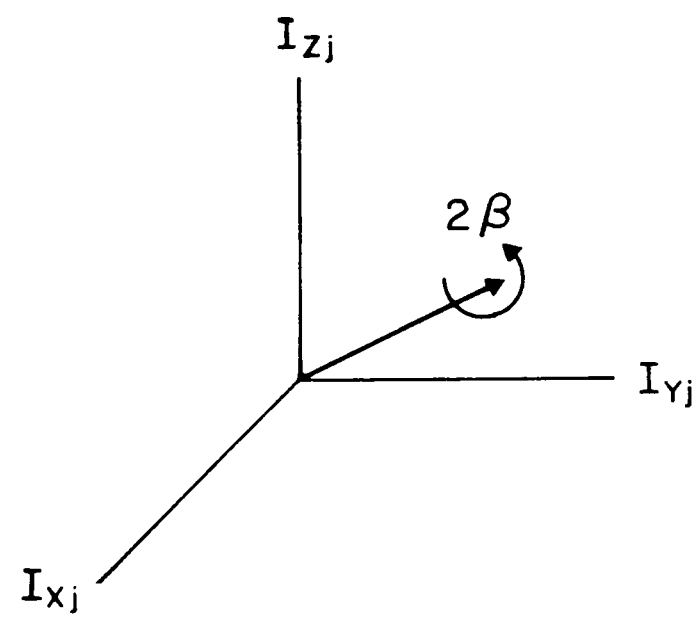

(c)

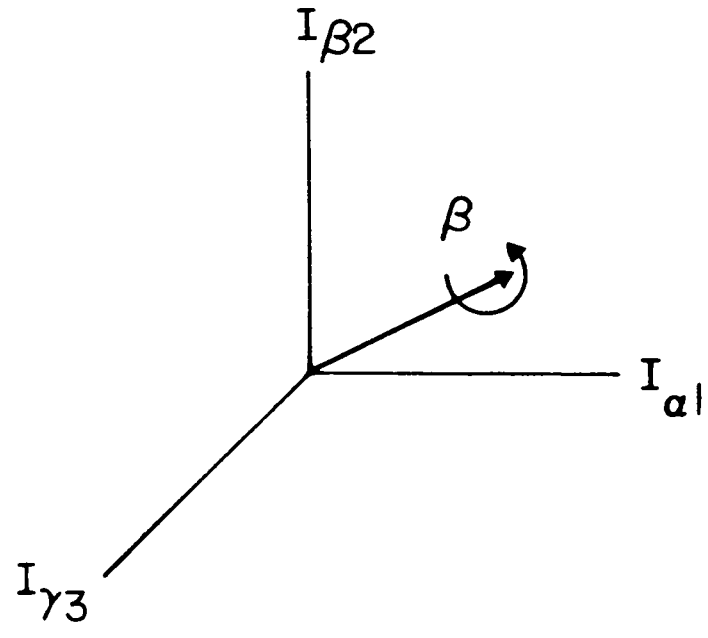

Figure 2.5 Vector frames for combination operators of table 2.2. (a) Vector frame for total spin angular momentum. (b) and (c) The two general vector frames defined by the operators of table 2.2.

For a Hamiltonian of the form

$$H = \hbar(\omega_x F_x + \omega_y F_y + \omega_z F_z) \tag{2.139}$$

the following vector equation applies,

$$\frac{\partial F}{\partial t} = \Omega \times F \tag{2.140}$$

where $F = (F_x, F_y, F_z)$ and $\Omega = (\omega_x, \omega_y, \omega_z)$. This can be interpreted in a geometric picture as illustrated in figure 2.5a. The transformation properties can be written in the form,

$$e^{-i\beta F_x} F_y e^{i\beta F_x} = F_y \cos\beta + F_z \sin\beta. \tag{2.141}$$

where $\beta = |\Omega| t = (\omega_x^2+\omega_y^2+\omega_z^2)^{1/2} t$.

Vega and Pines [2.7b] introduced another useful set of operators constructed from combinations of the total spin angular momentum operators which are tabulated in table 2.2. These operators were used to interpret experiments for the excitation and detection of double quantum transitions of a spin-1 nucleus with quadrupolar coupling in the solid state. These operators obey the following cyclic commutation properties,

$$[I_{Xj} , I_{Yj}] = 2iI_{Zj} \quad , \quad \text{for } j = 1,2 \text{ or } 3 \tag{2.142}$$

with cyclic permutations of X, Y and Z.

Also the following,

$$[I_{\alpha 1} , I_{\beta 2}] = i\, \varepsilon_{\alpha\beta\gamma}\, I_{\gamma 3} \tag{2.143}$$

$$I_{X1} = F_x$$

$$I_{Y1} = F_y F_z + F_z F_y$$

$$I_{Z1} = F_z^2 - F_y^2$$

$$I_{X2} = F_x F_z + F_z F_x$$

$$I_{Y2} = F_y$$

$$I_{Z2} = F_z^2 + F_x^2$$

$$I_{X3} = F_x^2 - F_y^2$$

$$I_{Y3} = F_x F_y + F_y F_x$$

$$I_{Z3} = F_z$$

Table2.2 Combination operators as defined by Vega and Pines [2.7b].

with cyclic permutations of the operators where,

$$\alpha = \beta = X \text{ or } Y \quad \text{then } \gamma = Y \quad \text{and} \quad \varepsilon_{\alpha\beta\gamma} = -1$$

$$\alpha = X \ , \ \beta = Y \quad \text{then } \gamma = Z \quad \text{and} \quad \varepsilon_{\alpha\beta\gamma} = 1.$$

The pseudo tensor $\varepsilon_{\alpha\beta\gamma}$ changes sign when the ordering of α, β and γ is not a cyclic permutation of the above ordering.

Consider any of the groups of three operators in table 2.2. For a Hamiltonian of the form,

$$H = \hbar(\omega_{Xj} I_{Xj} + \omega_{Yj} I_{Yj} + \omega_{Zj} I_{Zj}) \ , \tag{2.144}$$

the commutation property of equation 2.142 along with the equation of motion for the operators define several vector equations of motion. As an example any of the groups of operators in table 2.2 obey the following equation,

$$\frac{\partial I_j}{\partial t} = 2 \ \Omega_j \times I_j \tag{2.145}$$

where $I_j = (I_{Xj}, I_{Yj}, I_{Zj})$ and $\Omega_j = (\omega_{Xj}, \omega_{Yj}, \omega_{Zj})$ and this can be interpreted in a geometric picture as shown in figure 2.5b. The transformation properties can be written in the form

$$e^{-i\beta I_{Xj}} \ I_{Yj} \ e^{i\beta I_{Xj}} = I_{Yj} \cos 2\beta + I_{Zj} \sin 2\beta \tag{2.146}$$

where $\beta = |\Omega_j| t = (\omega_{Xj}^2 + \omega_{Yj}^2 + \omega_{Zj}^2)^{1/2} t$. Note that the angle of rotation of any component operator about another is twice the effective angle, β. This is a consequence of the commutation properties of these operators and is a general relationship between the constant in a cyclic commutator and the defined vector equation of motion as outlined in

equations 2.38 to 2.42. In a similar manner, equation 2.143 can be interpreted in a vector equation of motion which is illustrated in figure 2.5c.

Using the relationships of equation 2.137, the operators defined in table 2.2 can be expanded in terms of a linear combination of single transition operators for a particular spin system. These rather abstract vector operators will be used in a later section to simplify the interpretation of an experiment for the excitation of double quantum coherence in a coupled two spin-1/2 system. They provide a simple geometric picture of the experiment and allow a more clear visualization of the processes involved.

Linear combinations of single transition operators can be defined for a system of weakly coupled nonequivalent spin-1/2 nuclei; each pair of spins can be treated as a separate isolated spin system for each fixed state of the other spins in the system. For example in a AMX spin system the AM subsystem can be treated as an isolated pair for each state spin X. This would allow six possible subsystems for the AMX spin system, two for each pair of spins. From the definition of the single transition operators given in equation 2.84 the following properties can be developed. For operators associated with the same spin,

$$[(I_\alpha^{ij} + I_\alpha^{kl}) \, , \, (I_\alpha^{ij} \pm I_\alpha^{kl})] = 0 \qquad (2.147)$$

for $\alpha = x, y,$ or z. Also,

$$[(I_\alpha^{ij} + I_\alpha^{kl}) \, , \, (I_\beta^{ij} \pm I_\beta^{kl})] = i\varepsilon_{\alpha\beta\gamma} \, (I_\gamma^{ij} \pm I_\gamma^{kl}) \qquad (2.148)$$

where

(a)

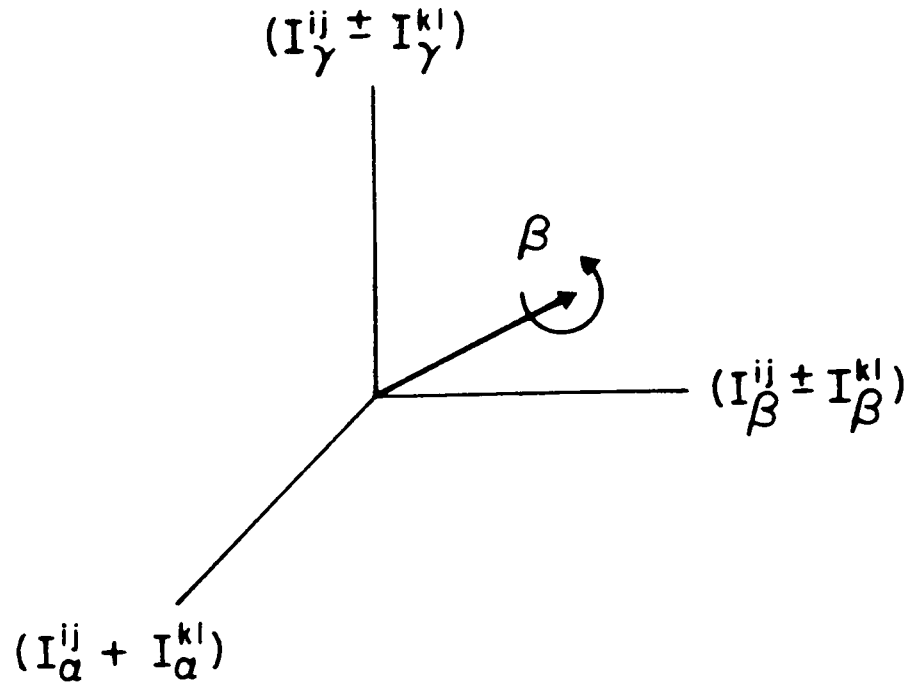

(b)

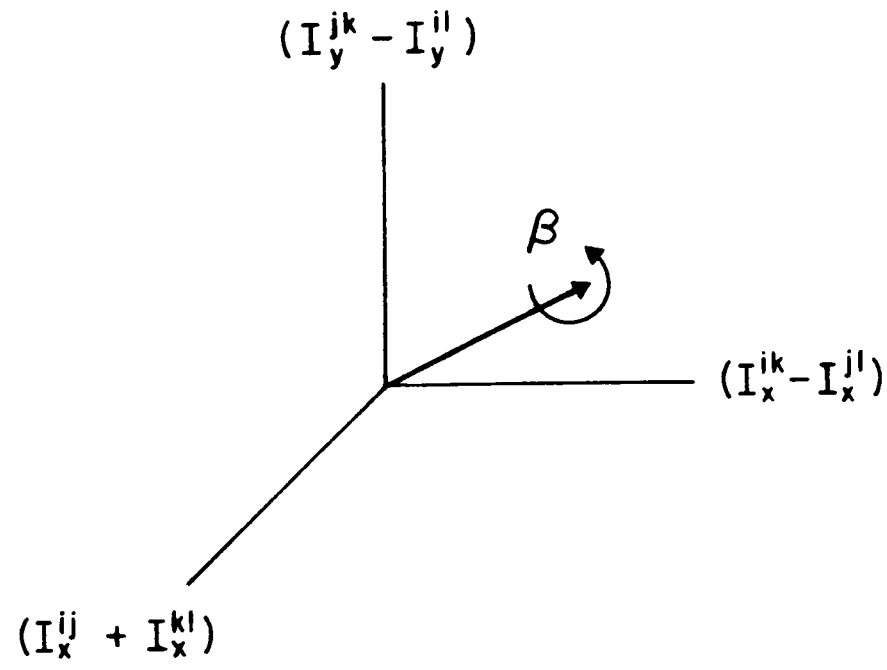

(c)

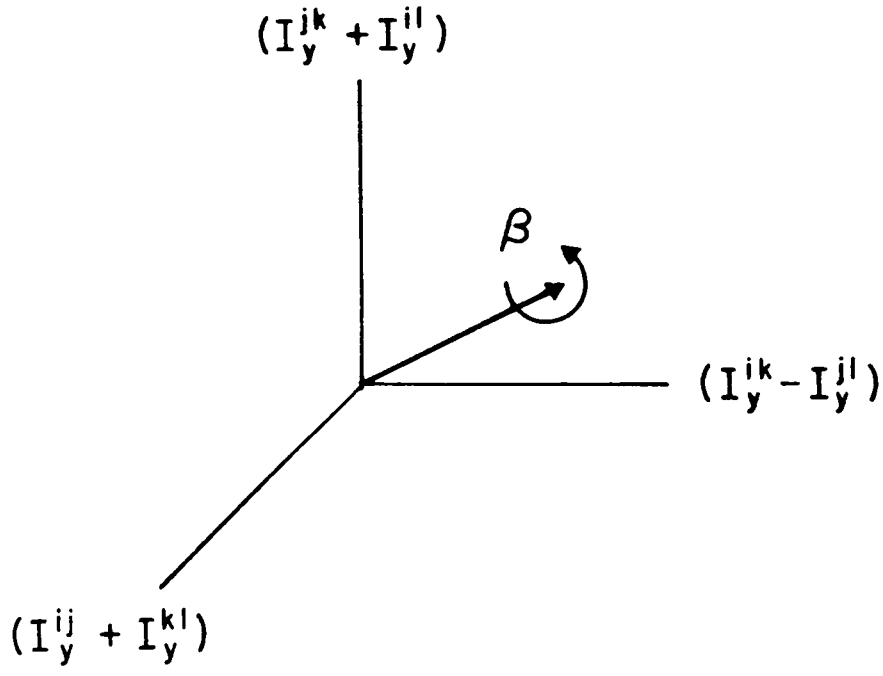

Figure 2.6 General vector diagrams for a system of weakly coupled nonequivalent spin-1/2 particles. (a) Vector diagram for the operator combinations for a single spin. (b) and (c) Vector diagrams for the operator combinations for two coupled spins.

$$\varepsilon_{\alpha\beta\gamma} = \begin{cases} 1 & ; \alpha, \beta, \gamma \text{ cyclic permutations of x, y, z} \\ -1 & ; \alpha, \beta, \gamma \text{ noncyclic permutations of x, y, z.} \end{cases}$$

For operators associated with different spins forming a coupled pair,

$$[(I_x^{ij} + I_x^{kl}) , (I_x^{ik} - I_x^{jl})] = i(I_y^{jk} - I_y^{il}) \qquad (2.149)$$

and

$$[(I_y^{ij} + I_y^{kl}) , (I_y^{ik} - I_y^{jl})] = i(I_y^{jk} + I_y^{il}). \qquad (2.150)$$

The commutation properties of equations 2.149 and 2.150 hold for cyclic permutations of the linear combination of operators but the commutators for any other sign combinations vanish. Since the commutation properties of equations 2.148 to 2.150 hold for cyclic permutations of the operator combinations, with an appropriately defined Hamiltonian it is possible to interpret the equation of motion for these operator combinations in a vector frame as illustrated in figure 2.6.

The commutation property of equation 2.148 connects coherence of the same order associated with the same spin. In contrast, the commutation properties of equations 2.149 and 2.150 represent a transformation among different orders of coherence. The order of transition jk can be written, $\Delta m_{jk} = \Delta m_{ik} - \Delta m_{ij}$ and il as $\Delta m_{il} = \Delta m_{jl} + \Delta m_{ij}$. Thus for single quantum coherences these commutation properties represent transformation to zero and double quantum coherence.

Important properties between the z-components of the single transition operators for such a spin pair are given by the following,

$$(I_z^{ij} - I_z^{kl}) = (I_z^{ik} - I_z^{jl}) \qquad (2.151)$$

(a)

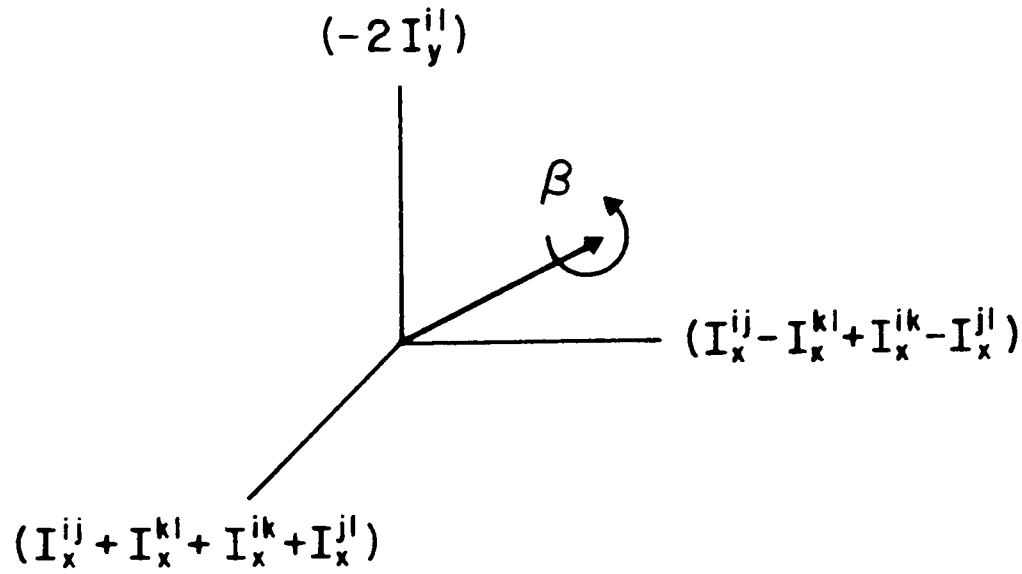

(b)

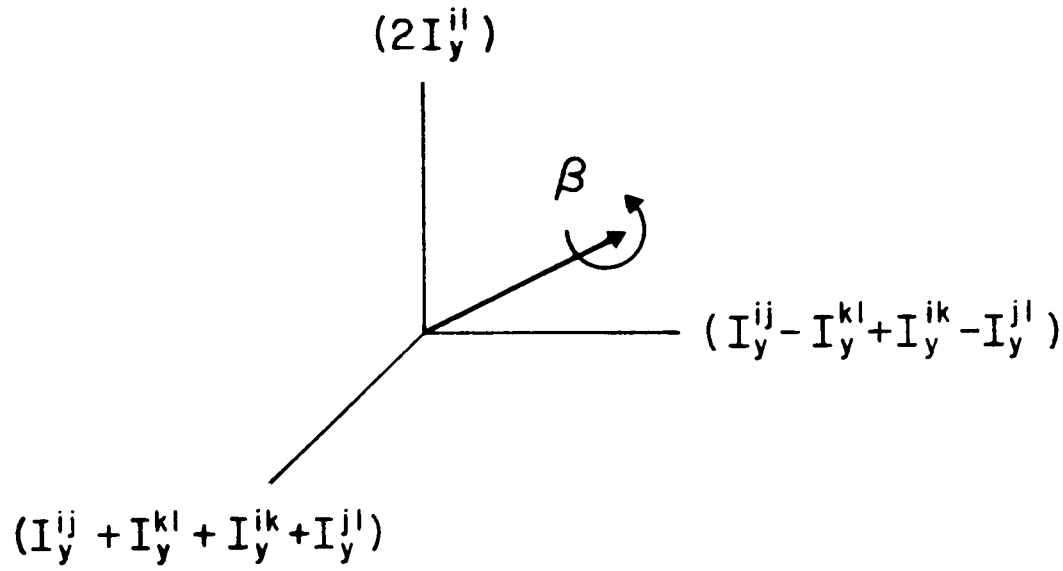

(c)

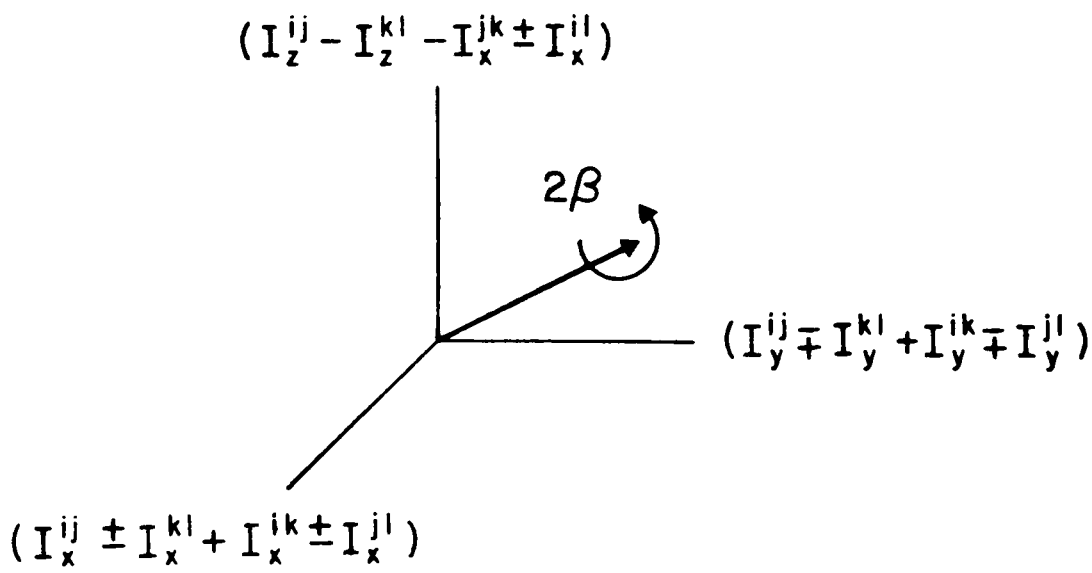

Figure 2.7 General vector diagrams for a pair of spins in a system of weakly coupled spin-1/2 particles. The diagrams in (a) and (b) have an effective rotation angle of β. The effective rotation angle in (c) is 2β.

$$(I_z^{ij} + I_z^{kl} + I_z^{ik} + I_z^{jl}) = 2I_z^{il}. \qquad (2.152)$$

Using the commutator properties of equations 2.147 to 2.150 the following general commutator properties can be developed for each spin pair.

$$[(I_x^{ij}+I_x^{kl}+I_x^{ik}+I_x^{jl}),(I_x^{ij}-I_x^{kl}+I_x^{ik}-I_x^{jl})] = i\ (-2I_y^{il}) \qquad (2.153)$$

$$[(I_x^{ij}+I_x^{kl}+I_x^{ik}+I_x^{jl}),(I_x^{ij}-I_x^{kl}-I_x^{ik}+I_x^{jl})] = i\ (-2I_y^{jk}) \qquad (2.154)$$

$$[(I_y^{ij}+I_y^{kl}+I_y^{ik}+I_y^{jl}),(I_y^{ij}-I_y^{kl}+I_y^{ik}-I_y^{jl})] = i\ (\ 2I_y^{il}) \qquad (2.155)$$

$$[(I_y^{ij}+I_y^{kl}+I_y^{ik}+I_y^{jl}),(I_y^{ij}-I_y^{kl}-I_y^{ik}+I_y^{jl})] = i\ (-2I_y^{jk}) \qquad (2.156)$$

$$[(I_x^{ij}\pm I_x^{kl}+I_x^{ik}\pm I_x^{jl}),(I_y^{ij}\mp I_y^{kl}+I_y^{ik}\mp I_y^{jl})]$$

$$= 2\ i\ (I_z^{ij}-I_z^{kl}-I_x^{jk}\pm I_x^{il}) \qquad (2.157)$$

and cyclic permutations among the linear combinations of operators in the parentheses. With an appropriately defined Hamiltonian the linear combinations of equations 2.153 to 2.157 can be represented in vector frames. Three are illustrated in figure 2.7. Note that the first four commutators in the above equations have a constant factor of unity multiplying the commutator result. Hence a rotation among these combinations would be of the magnitude of the effective rotation angle as illustrated in figures 2.7a and 2.7b. The last commutator has a factor of two so that a rotation would be of twice the magnitude of the effective angle as illustrated in figure 2.7c. The commutators of equations 2.153 to 2.157 represent transformations among orders of coherences as outlined for equation 2.149 and 2.150.

Examples of the use of operator combinations of this form will be given in the next section where a system of two coupled spin-1/2 nuclei will be considered. Other examples will be given in later chapters.

2.6. Application to a system of two coupled spin-1/2 particles

In order to illustrate the usefulness of the operator formalism consider the specific example of two coupled spin-1/2 particles. The eigenfunctions for the system can be expressed in a product basis set which results in the association of transitions 1 -> 3 and 2 -> 4 with the first particle, denote it A, and transitions 1 -> 2 and 3 -> 4 with the second particle, denote it X. For this numbering scheme the components of total spin can be written as,

$$F_\alpha = (I_\alpha)_A + (I_\alpha)_X \tag{2.158}$$

where

$$(I_\alpha)_A = I_\alpha^{13} + I_\alpha^{24}$$

$$(I_\alpha)_X = I_\alpha^{12} + I_\alpha^{34} \tag{2.159}$$

and α = x, y or z.

For the high temperature limit, the reduced density operator in thermal equilibrium can be written as,

$$\begin{aligned}\rho &= (2I+1)^{-1}(kT)^{-1}[\omega_A(I_z)_A + \omega_X(I_z)_X] \\ &= c_A(I_z^{13} + I_z^{24}) + c_X(I_z^{12} + I_z^{34})\end{aligned} \tag{2.160}$$

where $c_m = (2I+1)^{-1}(kT)^{-1}\omega_m$. When considering equilibrium populations the coupling between the spins can be ignored because the coupling interaction is negligible compared to the Zeeman interaction of the spins with the static magnetic field.

For a homonuclear spin system the coefficients can be written as $\omega_A = \omega_0 + \pi\delta_{AX}$ and $\omega_X = \omega_0 - \pi\delta_{AX}$ where δ_{AX} is the chemical shift difference

between the spins. The chemical shift term can be neglected provided $2\pi\delta_{AX} \ll \omega_0$ so in this approximation the density operator can be written as,

$$\rho = c_0 \, (I_z^{13} + I_z^{24} + I_z^{12} + I_z^{34})$$

$$= c_0 \, F_z \qquad (2.161)$$

where $c_0 = (2I+1)^{-1}(kT)^{-1}\omega_0$.

The above forms of the density operator in equation 2.160 and equation 2.161 provide a representation of the initial state of the system in thermal equilibrium which will be used as a starting point in calculating the response of the spin system to the experimental situation.

The Hamiltonian operator which describes the interaction of the spins with the applied magnetic field and the coupling among the spins is given by,

$$\hbar^{-1}H_0 = \omega_A(I_z)_A + \omega_X(I_z)_X + 2\pi J \, (I)_A.(I)_X. \qquad (2.162)$$

This can be expanded in terms of single transition operators. The coupling terms can be written using the following products,

$$(I_x)_A(I_x)_X = \tfrac{1}{2}(I_x^{23} + I_x^{14})$$

$$(I_y)_A(I_y)_X = \tfrac{1}{2}(I_x^{23} - I_x^{14}) \qquad (2.163)$$

$$(I_z)_A(I_z)_X = \tfrac{1}{4}(I_z^{13} - I_z^{24} + I_z^{12} - I_z^{34})$$

so that equation 2.162 becomes,

$$\hbar^{-1}H_0 = \phi_{13}I_z^{13} + \phi_{24}I_z^{24} + \phi_{12}I_z^{12} + \phi_{34}I_z^{34} + 2\pi J I_x^{23} \qquad (2.164)$$

where

$$\phi_{13} = \omega_A + 2\pi\frac{J}{4}$$

$$\phi_{24} = \omega_A - 2\pi\frac{J}{4}$$

$$\phi_{12} = \omega_X + 2\pi\frac{J}{4}$$

$$\phi_{34} = \omega_X - 2\pi\frac{J}{4}. \qquad (2.165)$$

The Hamiltonian in this form is not diagonal in the simple product basis set. The off-diagonal term containing the operator I_x^{23} has the magnitude, $2\pi J$. The determination of the energy eigenvalues requires an expression for the Hamiltonian which is diagonal in the chosen basis set. The Hamiltonian becomes diagonal in the weak coupling limit where the I_x^{23} term can be ignored. In the limit of weak coupling the strength of the coupling is weak compared to the chemical shift difference between the two spins. The weak coupling limit can be derived by considering second order perturbation theory [2.15]. Assume that the Hamiltonian, H_0, can be written as a sum of unperturbed and perturbed parts as, $H_0 = H_0' + H_0''$, where

$$\hbar^{-1}H_0' = \phi_{13}I_z^{13} + \phi_{24}I_z^{24} + \phi_{12}I_z^{12} + \phi_{34}I_z^{34} \qquad (2.166)$$

and

$$\hbar^{-1}H_0'' = 2\pi J I_x^{23}. \qquad (2.167)$$

Now consider the perturbation calculation for the energy eigenvalue of the third state.

$$\hbar^{-1}E_3^{(2)} = \hbar^{-1}E_3^{(0)} + \sum_{n\neq 3} \left(\frac{\langle 3|\hbar^{-1}H_0''|n\rangle\langle n|\hbar^{-1}H_0''|3\rangle}{(E_3^{(0)})^2 - (E_n^{(0)})^2}\right) \qquad (2.168)$$

where

$$\hbar^{-1}E_m^{(0)} = \langle m|H_0'|m\rangle \qquad (2.169)$$

and

$$\begin{aligned}
\hbar^{-1}E_1^{(0)} &= \tfrac{1}{2}(\emptyset_{13} + \emptyset_{12}) = \tfrac{1}{2}(\omega_A + \omega_X) + \tfrac{\pi}{2}J \\
\hbar^{-1}E_2^{(0)} &= \tfrac{1}{2}(\emptyset_{24} - \emptyset_{12}) = \tfrac{1}{2}(\omega_A - \omega_X) - \tfrac{\pi}{2}J \\
\hbar^{-1}E_3^{(0)} &= \tfrac{1}{2}(-\emptyset_{13} + \emptyset_{34}) = -\tfrac{1}{2}(\omega_A - \omega_X) - \tfrac{\pi}{2}J \\
\hbar^{-1}E_4^{(0)} &= \tfrac{1}{2}(-\emptyset_{24} - \emptyset_{34}) = -\tfrac{1}{2}(\omega_A + \omega_X) + \tfrac{\pi}{2}J
\end{aligned} \qquad (2.170)$$

Using equations 2.166 to 2.168 the perturbed energy is given by,

$$\hbar^{-1}E_3^{(2)} = [-\tfrac{1}{2}(\omega_A - \omega_X) - \tfrac{\pi}{2}J] + \frac{2\pi J}{(\omega_A - \omega_X)} \qquad (2.171)$$

The second term represents the perturbation to the energy eigenvalue due to strong coupling. Therefore the weak coupling limit is reached when $|(2\pi J)| \ll |(\omega_A - \omega_X)|$ and the second term in the above equation can be neglected. The Hamiltonian is diagonal in this limit and can be written as,

$$\hbar^{-1}H_0 = \emptyset_{13}I_z^{13} + \emptyset_{24}I_z^{24} + \emptyset_{12}I_z^{12} + \emptyset_{34}I_z^{34} \qquad (2.172)$$

with energy eigenvalues given by equation 2.170.

In this limit the transition frequencies are given by $\omega_{ij} = \hbar^{-1}\Delta E_{ij}$,

$$\omega_{13} = \omega_A + 2\pi\frac{J}{2}$$

$$\omega_{24} = \omega_A - 2\pi\frac{J}{2}$$

$$\omega_{12} = \omega_X + 2\pi\frac{J}{2}$$

$$\omega_{34} = \omega_X - 2\pi\frac{J}{2}. \qquad (2.173)$$

2.6.1. The Carr-Purcell spin echo pulse sequence

The Carr-Purcell spin echo sequence [2.17] is the basis for many experiments in both one-dimensional and two-dimensional NMR and will provide a starting point for the analysis of experiments on the AX-spin system in terms of the single transition operators. The pulse sequence with the Meiboom-Gill modification [2.17] is written as,

$$(\tfrac{\pi}{2})_x - \tau - (\pi)_y - \tau.$$

The analysis will be for a weakly coupled homonuclear system but can easily be generalized to the heteronuclear case.

Assume the system is in thermal equilibrium at the high temperature limit. Recalling equation 2.161, the density operator can be written,

$$\rho_0 = c_0(I_z^{13} + I_z^{24} + I_z^{12} + I_z^{34}) = c_0 F_z \qquad (2.174)$$

Using the commutator properties of the single transition operators and vector representations where they apply, the pulse sequence can be analysed in operator form. For the $(\frac{\pi}{2})_x$ pulse, the density operator becomes,

$$\rho_+ = e^{-i\frac{\pi}{2}F_x}\ \rho_0\ e^{i\frac{\pi}{2}F_x} = -c_0 F_y$$

$$= -c_0(I_y^{13} + I_y^{24} + I_y^{12} + I_y^{34}). \qquad (2.175)$$

The vector picture for the total spin angular momentum has been used as outlined previously.

The spin system is allowed to precess for a time, τ, and the density operator becomes,

$$\begin{aligned}
\rho(\tau) &= e^{-iH_0\tau/\hbar}\ \rho_+\ e^{iH_0\tau/\hbar} \\
&= -c_0[\ e^{-i\omega_{13}\tau I_z^{13}}\ I_y^{13}\ e^{i\omega_{13}\tau I_z^{13}} \\
&\quad + e^{-i\omega_{24}\tau I_z^{24}}\ I_y^{24}\ e^{i\omega_{24}\tau I_z^{24}} \\
&\quad + e^{-i\omega_{12}\tau I_z^{12}}\ I_y^{12}\ e^{i\omega_{12}\tau I_z^{12}} \\
&\quad + e^{-i\omega_{34}\tau I_z^{34}}\ I_y^{34}\ e^{i\omega_{34}\tau I_z^{34}}\ ] \qquad (2.176)
\end{aligned}$$

where the free precession relationship of equation 2.122 has been used. Expanding this in terms of the precession frequencies of equation 2.173 results in the following form for the density operator.

$$\begin{aligned}
\rho(\tau) = -c_0[\ &(I_y^{13} + I_y^{24})\cos\omega_A\tau\ \cos\pi J\tau + (I_y^{12} + I_y^{34})\cos\omega_X\tau\ \cos\pi J\tau \\
&- (I_x^{13} + I_x^{24})\sin\omega_A\tau\ \cos\pi J\tau - (I_x^{12} + I_x^{34})\sin\omega_X\tau\ \cos\pi J\tau \\
&- (I_y^{13} - I_y^{24})\sin\omega_A\tau\ \sin\pi J\tau - (I_y^{12} - I_y^{34})\sin\omega_X\tau\ \sin\pi J\tau \\
&- (I_x^{13} - I_x^{24})\cos\omega_A\tau\ \sin\pi J\tau - (I_x^{12} - I_x^{34})\cos\omega_X\tau\ \sin\pi J\tau\ ] \qquad (2.177)
\end{aligned}$$

The effect of the $(\pi)_y$-pulse on the density operator can be calculated using the vector properties of the combination operators

defined in equations 2.147 to 2.150 and figure 2.6. To illustrate this first note that the pulse operator can be written in terms of these combination operators as

$$R_y(\pi) = e^{-i\pi F_y} = e^{-i\pi (I_y)_A} e^{-i\pi (I_y)_X}. \qquad (2.178)$$

These exponential operators can be written in either order because the components, $(I_y)_A$ and $(I_y)_X$, commute. Using the commutation property of equations 2.147 to 2.150, it can be seen that the first two terms are uneffected by the pulse. The effect of the pulse on the other terms can be calculated using the vector frames of figure 2.6 which show that all the remaining terms change sign except the last two terms. These terms have their sign effectively unchanged by successive π rotations about the $(I_y)_A$ and $(I_y)_X$ axes.

Recombining terms for the density operator after the pulse results in the following,

$$\begin{aligned}
\rho_+(\tau) &= R_y(\pi)\ \rho(\tau)\ R_y^+(\pi) \\
&= -c_0[\ e^{+i\omega_{24}\tau I_z^{13}}\ I_y^{13}\ e^{-i\omega_{24}\tau I_z^{13}} \\
&\quad + e^{+i\omega_{13}\tau I_z^{24}}\ I_y^{24}\ e^{-i\omega_{13}\tau I_z^{24}} \\
&\quad + e^{+i\omega_{34}\tau I_z^{12}}\ I_y^{12}\ e^{-i\omega_{34}\tau I_z^{12}} \\
&\quad + e^{+i\omega_{12}\tau I_z^{34}}\ I_y^{34}\ e^{-i\omega_{12}\tau I_z^{34}}\ ].
\end{aligned} \qquad (2.179)$$

By comparing equations 2.176 and 2.179 it can be seen that the effect of the $(\pi)_y$-pulse is to interchange precession frequencies and reverse the effective sense of precession among coherences associated with each

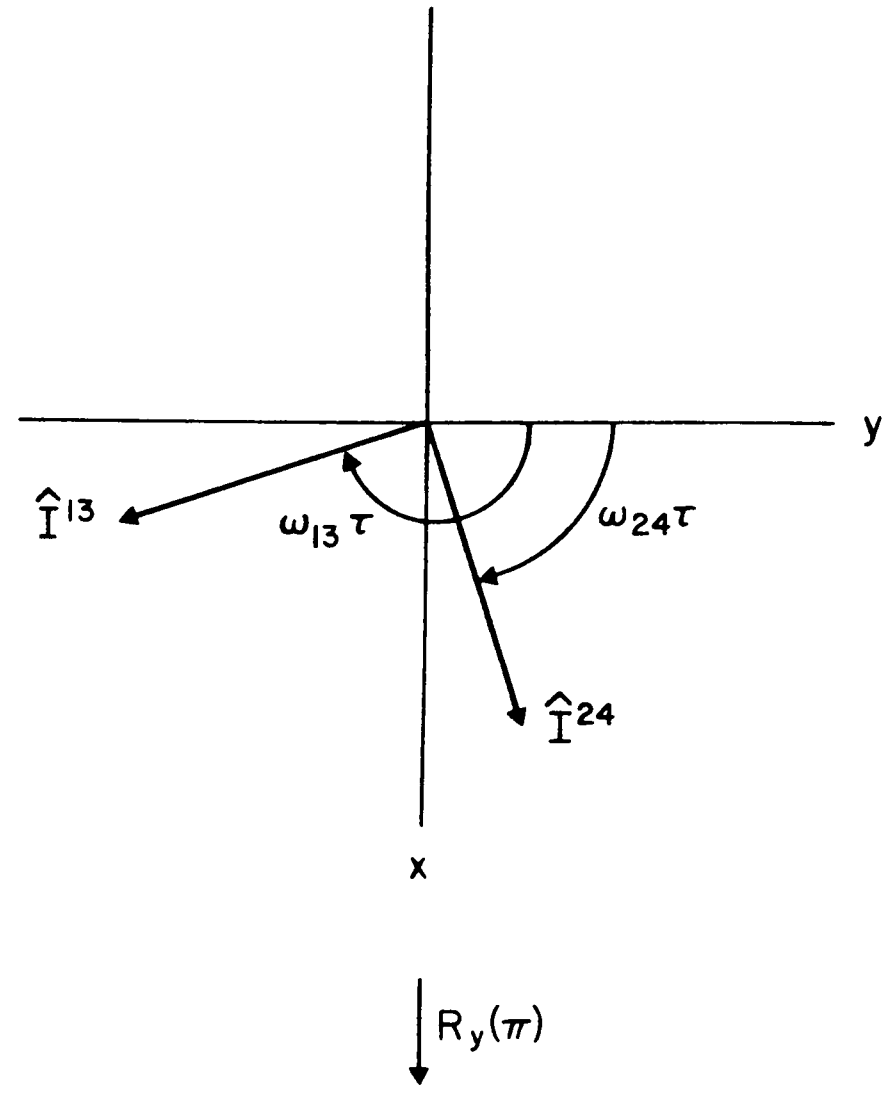

Figure 2.8 Effect of a $(\pi)_y$ pulse represented by the operator $R_y(\pi)$. The A spin coherences are represented by the vectors I^{13} and I^{24}.

spin. This is illustrated for the A-spin in figure 2.8. This can also be viewed as a reflection of each coherence through the y-axis and an interchange of 'labels' among the coherences associated with each spin.

The spin system is now allowed to precess for another interval of length, τ. The density operator at the end of this time becomes,

$$\begin{aligned}\rho(2\tau) = -c_0[\ & e^{-i(\omega_{13}-\omega_{24})\tau I_z^{13}}\ I_y^{13}\ e^{i(\omega_{13}-\omega_{24})\tau I_z^{13}} \\ & + e^{-i(\omega_{24}-\omega_{13})\tau I_z^{24}}\ I_y^{24}\ e^{i(\omega_{24}-\omega_{13})\tau I_z^{24}} \\ & + e^{-i(\omega_{12}-\omega_{34})\tau I_z^{12}}\ I_y^{12}\ e^{i(\omega_{12}-\omega_{34})\tau I_z^{12}} \\ & + e^{-i(\omega_{34}-\omega_{12})\tau I_z^{34}}\ I_y^{34}\ e^{i(\omega_{34}-\omega_{12})\tau I_z^{34}}\ ]. \end{aligned} \tag{2.180}$$

Expanding the transition frequencies using equation 2.173, the density operator can be written in the form,

$$\begin{aligned}\rho(2\tau) = -c_0[\ & (I_y^{13} + I_y^{24} + I_y^{12} + I_y^{34})\ \cos(2\pi J\tau) \\ & - (I_x^{13} - I_x^{24} + I_x^{12} - I_x^{34})\ \sin(2\pi J\tau)]. \end{aligned} \tag{2.181}$$

The single transition operator representation of this spin system in equation 2.181 shows the result of J-modulation of the observable coherences and provides a geometric interpretation of the state of the system at the end of the pulse sequence. Each of the two coherences in a spin multiplet is phase modulated in an equal and opposite sense. This is also the basis for the phase modulation in a two-dimensional J-spectrum where the time 2τ is allowed to vary as the evolution time t_1 in a two-dimensional experiment [2.18].

$$I_{X1} = F_x = I_x^{13} + I_x^{24} + I_x^{12} + I_x^{34}$$

$$I_{Y1} = F_yF_z + F_zF_y = I_y^{13} - I_y^{24} + I_y^{12} - I_y^{34}$$

$$I_{Z1} = F_z^2 - F_y^2 = I_z^{13} - I_z^{24} - I_x^{23} + I_x^{14}$$

$$I_{X2} = F_xF_z + F_zF_x = I_x^{13} - I_x^{24} + I_x^{12} - I_x^{34}$$

$$I_{Y2} = F_y = I_y^{13} + I_y^{24} + I_y^{12} + I_y^{34}$$

$$I_{Z2} = F_z^2 + F_x^2 = I_z^{13} - I_z^{24} - I_x^{23} - I_x^{14}$$

$$I_{X3} = F_x^2 - F_y^2 = 2I_x^{14}$$

$$I_{Y3} = F_xF_y + F_yF_x = 2I_y^{14}$$

$$I_{Z3} = F_z = 2I_z^{14} = I_z^{13} + I_z^{24} + I_z^{12} + I_z^{34}$$

Table 2.3 Combination operators of table 2.2 for an AX spin system expanded in terms of single transition operators.

2.6.2. Combination operators for an AX spin system

The density operator of equation 2.181 has a relatively simple form when the linear combinations of operators in parentheses are compared with the general operator combinations discussed previously. The first term in equation 2.181 can be identified as the y-component of total spin, F_y. The second term has the form of the combinations discussed in equations 2.153 and 2.157. The effect of a pulse on the density operator in this state can be interpreted in vector pictures using figure 2.5a and 2.7.

It is also possible to identify the combinations of operators in equations 2.153, 2.155 and 2.157 with the operators of table 2.2 for an AX spin system. Using the definitions of equation 2.159, the operators of table 2.2 can be expanded in terms of single transition operators for an AX spin system. It is shown here that the operators defined by Vega and Pines [2.7b] can be applied to the case of two coupled spin-1/2 nuclei and the vector representation used to interpret the results of experiments. The operators for the AX spin system are given in table 2.3. Now the spin system at the end of the Carr-Purcell pulse sequence described by the density operator of equation 2.181 can be written in terms of these combination operators as,

$$\rho(2\tau) = -c_0 \, [I_{Y2} \cos(2\pi J\tau) - I_{X2} \sin(2\pi J\tau)]. \qquad (2.182)$$

The effect of applying a pulse at time 2τ can be interpreted in terms of the vector pictures developed previously for the operators of table 2.3.

A pulse along the x-axis can be represented as a rotation about the I_{X1} axis in figure 2.5c with effective rotation angle of β. Using equation 2.143, the pulse rotates I_{Y2} into I_{Z3} as follows,

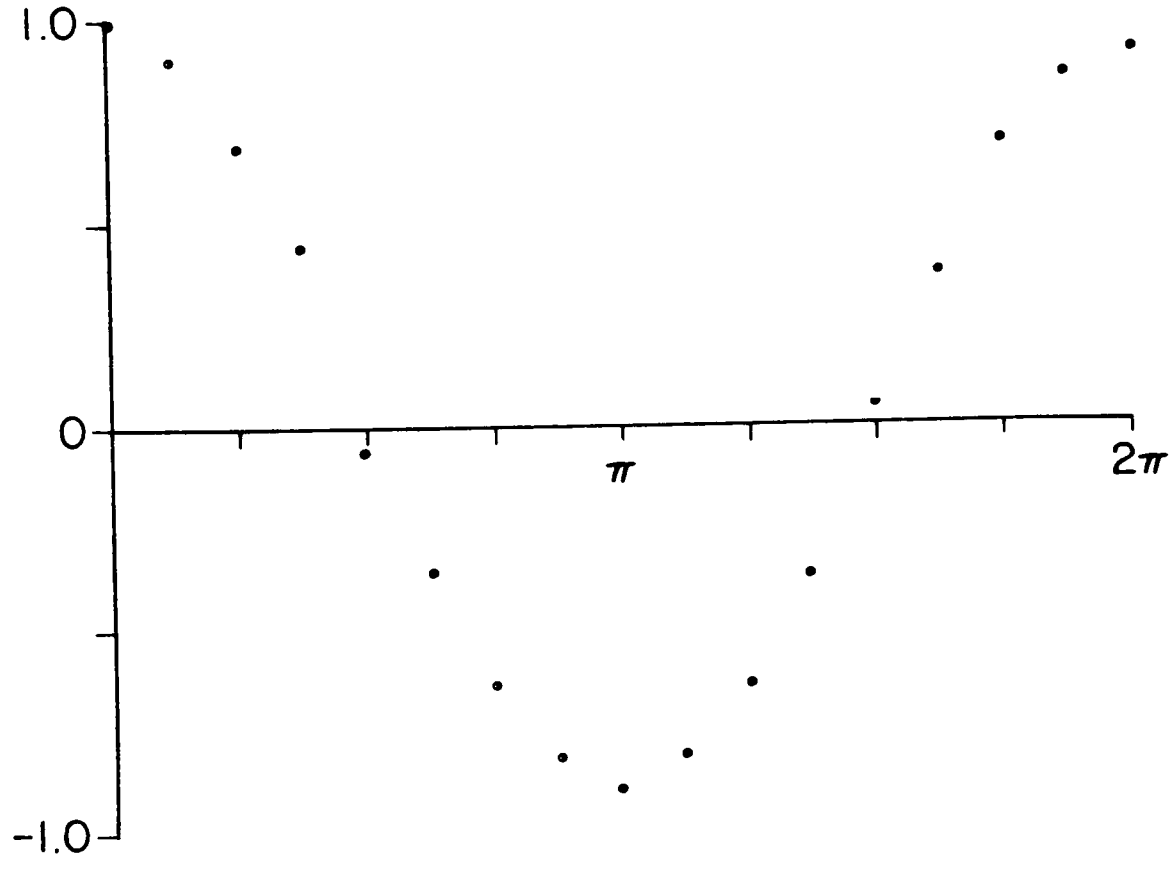

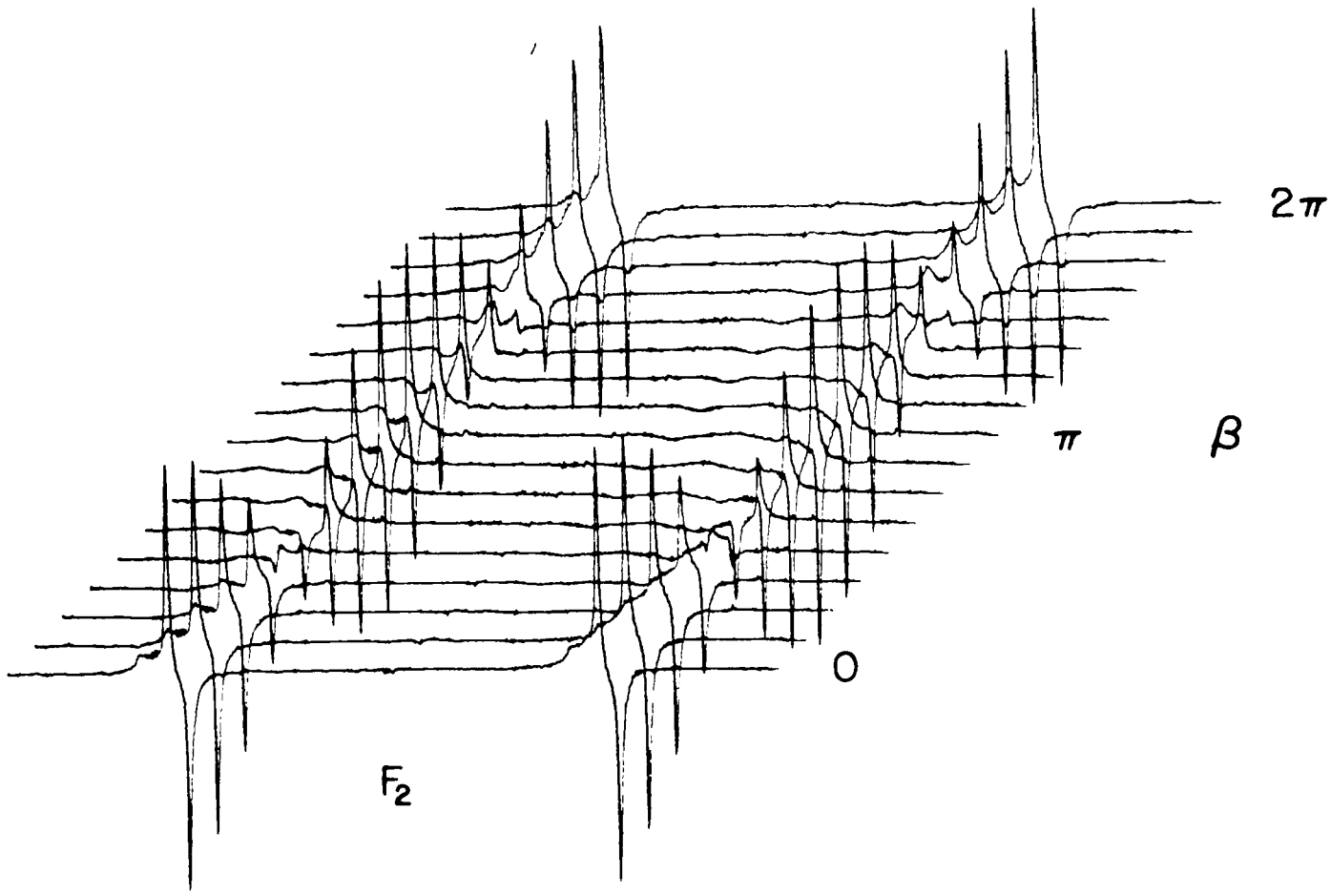

Figure 2.9 Tip angle effect on the J-modulated state of a pulse along the x-axis after a Carr-Purcell pulse sequence. The graph represents the average peak height versus tip angle, β.

$$e^{-i\beta I_{X1}} I_{Y2} e^{i\beta I_{X1}}$$

$$= I_{Y2}\cos\beta + I_{Z3}\sin\beta. \qquad (2.183)$$

The pulse also rotates the I_{X2} component in a similar manner. Using equation 2.143, the rotation can be written as,

$$e^{-i\beta I_{X1}} I_{X2} e^{i\beta I_{X1}}$$

$$= I_{X2}\cos\beta - I_{Y3}\sin\beta. \qquad (2.184)$$

The pulse rotates the J-modulated state, I_{X2}, into a state of double quantum coherence represented by I_{Y3}.

An example of this rotation property is shown in figure 2.9. At time 2τ a pulse to the x-axis has been applied as follows,

$$(\tfrac{\pi}{2})_x - \tau - (\pi)_y - \tau - (\beta)_x.$$

The tip angle, β, has been incremented in steps of $\pi/8$ from 0 to 2π. The proton AX spin system 2,3-dibromothiophene in acetone-d_6 with $\tau = 1/4J$ is shown at the bottom of the figure. The average peak height as a function of tip angle is plotted at the top of the figure. As illustrated in figure 2.5c the spin system returns to its original position after a rotation of $\beta = 2\pi$.

A pulse applied along the y-axis to the system described by equation 2.182 can be represented as a rotation about the I_{Y2} axis in figure 2.5b. The I_{Y2} component is uneffected by a rotation about the I_{Y2} axis so the first term in equation 2.182 remains the same after the pulse. However the I_{X2} component rotates as,

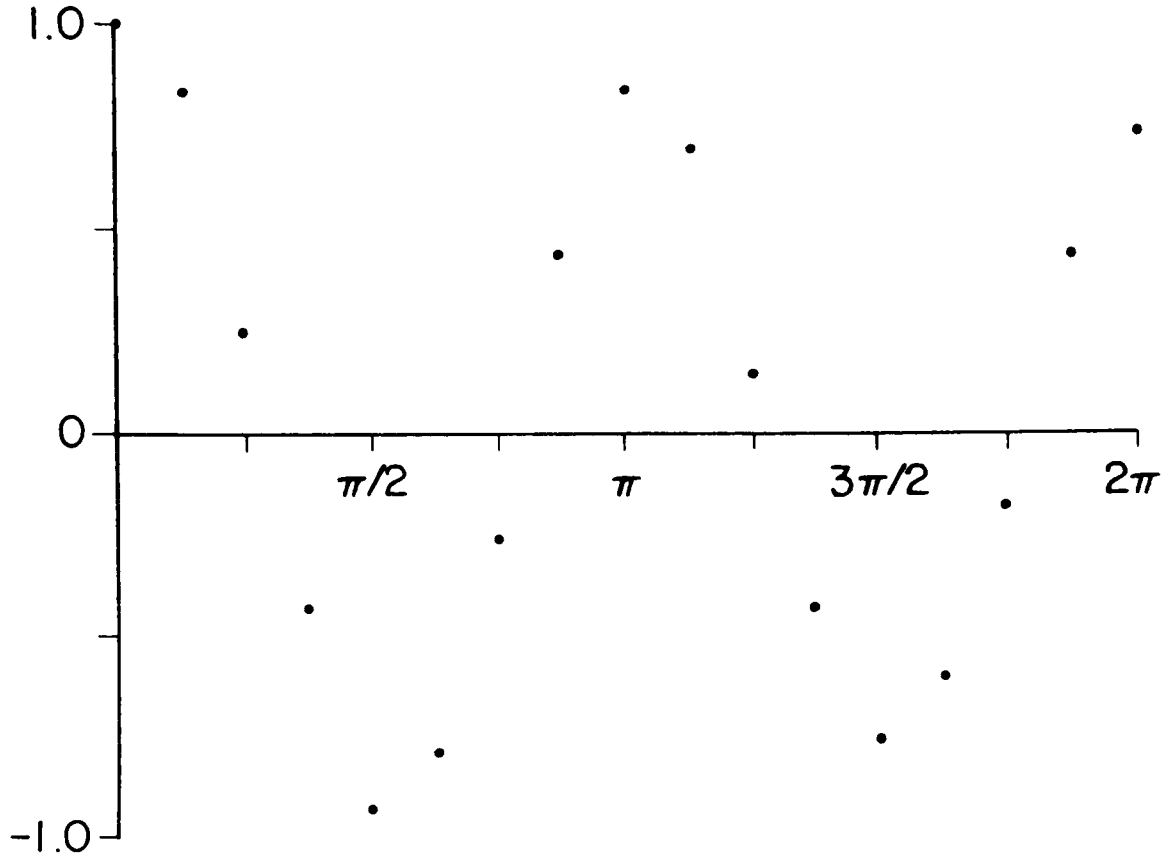

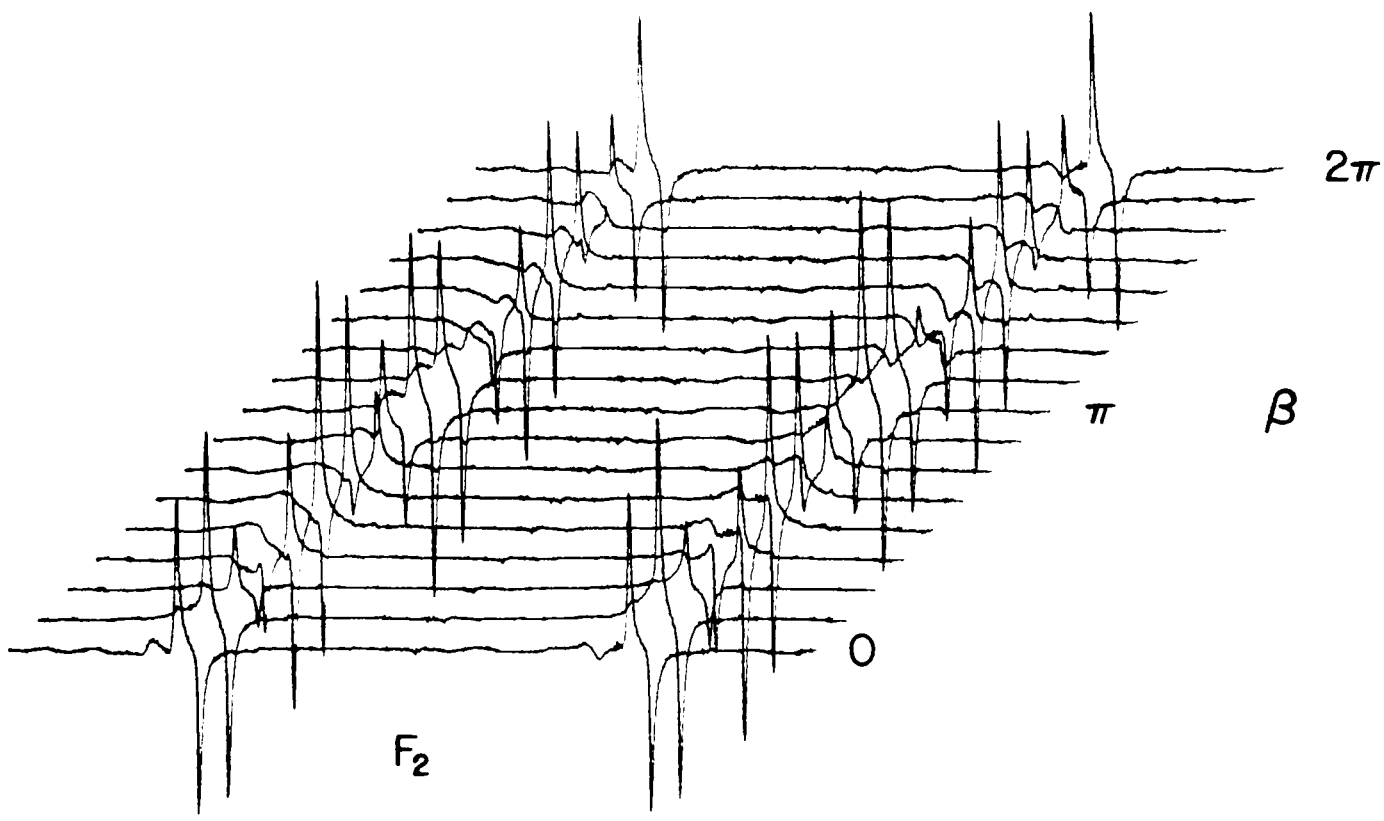

Figure 2.10 Tip angle effect on the J-modulated state of a pulse to the y-axis after a Carr-Purcell pulse sequence. The graph represents the average peak height versus tip angle, β.

$$e^{-i\beta I_{Y2}} I_{X2} e^{i\beta I_{Y2}}$$

$$= I_{X2}\cos 2\beta - I_{Z2}\sin 2\beta. \qquad (2.185)$$

The effective rotation angle is twice that for an isolated particle with spin-1/2.

This rotation property is illustrated in figure 2.10 for the proton AX spin system described above. The pulse sequence is given by,

$$(\tfrac{\pi}{2})_x - \tau - (\pi)_y - \tau - (\beta)_y.$$

The third pulse is now applied along the y-axis and the results as β is varied are shown at the bottom of the figure. The average peak height versus β is plotted at the top and clearly shows that the spin system returns to its original position for $\beta = \pi$. This is the expected result for a rotation described by the vector picture shown in figure 2.5b. The effective rotation angle is 2β which returns the vectors to their original position for $\beta = \pi$.

The combination operators of table 2.3 form a convenient set for the interpretation of the action of these pulse sequences and provide a pictorial representation of the processes involved.

2.6.3. Excitation and indirect detection of double quantum coherence

As an example of the use of the operators of table 2.3 consider the preparation of the AX-spin system into a state containing double quantum coherence. Several methods of excitation have been described [2.19], however the simplest method is the INADEQUATE sequence [2.20] where the excitation only depends on the value of the coupling constant as outlined below.

Double quantum coherence is created using the INADEQUATE sequence diagrammed below [2.20],

$$(\tfrac{\pi}{2})_x - \tau - (\pi)_y - \tau - (\tfrac{\pi}{2})_x - \Delta - (\tfrac{\pi}{2})_\phi - \text{detect}_\xi$$

where the phase, ϕ, of the last pulse and the phase, ξ, of the detector are to be chosen in an appropriate manner [2.20]. The time, Δ, is an extremely short delay to allow phase switching between the last two pulses. Its value is typically around 10 μsecs.

The system is first prepared in a state with x-components of coherence in antiphase by a Carr-Purcell spin echo sequence. At the time 2τ the system is described by the density operator of equation 2.181 and in terms of combination operators in equation 2.182. The result of applying a $(\frac{\pi}{2})_x$-pulse at 2τ can be predicted in terms of equation 2.182 using the vector picture of figure 2.5c. Hence the density operator after the pulse can be written as,

$$\rho_+(2\tau) = -c_0\,[I_{Z3}\cos(2\pi J\tau) + I_{Y3}\sin(2\pi J\tau)]. \qquad (2.186)$$

Using table 2.3 this can be written for an AX-spin system as,

$$\rho_+(2\tau) = -c_0[F_z\cos(2\pi J\tau) + 2I_y^{14}\sin(2\pi J\tau)]. \qquad (2.187)$$

The single transition operator I_y^{14} represents the y-component of double quantum coherence for this spin system. For a choice of $\tau = 1/4J$ the system before the pulse is entirely in a state with x-components of coherence in antiphase represented by I_{X2} and the effect of the $(\frac{\pi}{2})_x$-pulse is to rotate this state into the state of double quantum coherence. Maximum creation of double quantum coherence is achieved with a $\pi/2$ pulse.

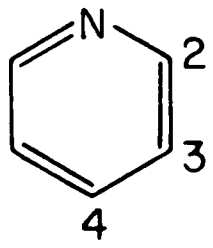

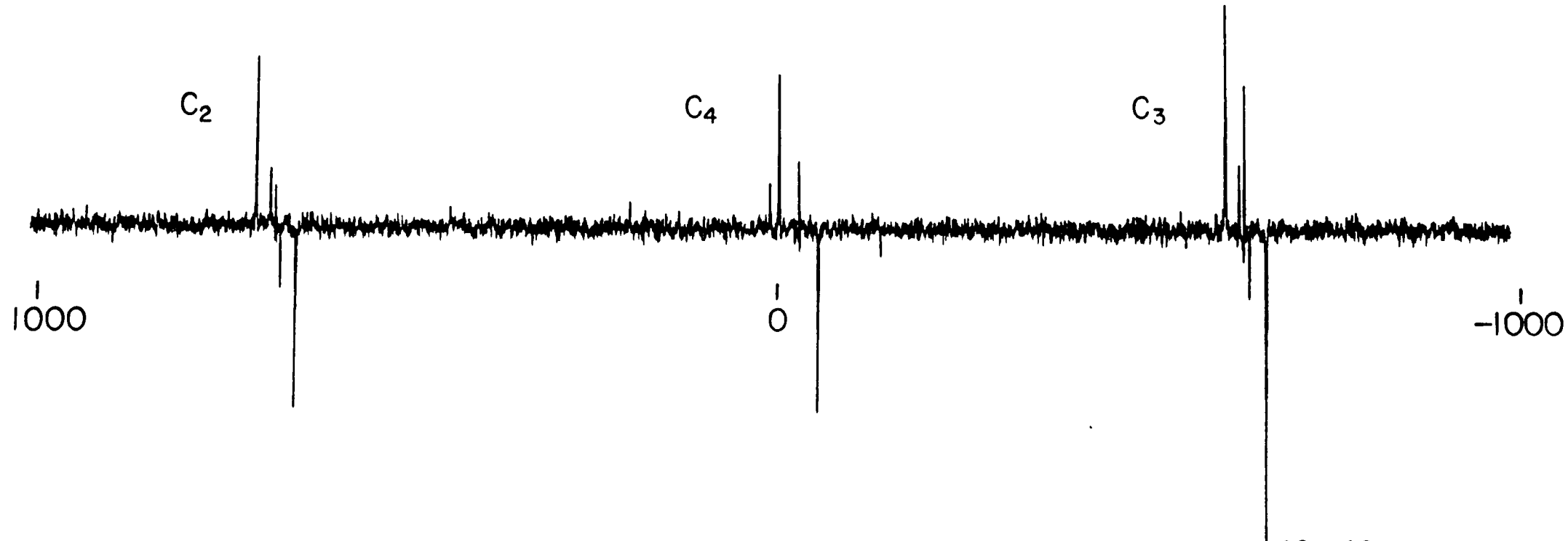

Figure 2.11 Carbon-13 spectrum of pyridine with 10% acetone-d_6. ^{13}C-^{13}C coupling in natural abundance observed with the INADEQUATE sequence. Delay τ optimized for one-bond coupling constants of ~ 54 Hz. Spectrum obtained in 1.7 hours with 256 transients. Broadband proton decoupling applied continuously.

Since the delay Δ is very short we can assume it can be set approximately equal to zero and the system will remain in the initial state of double quantum coherence during the delay. The double quantum coherence can be transferred back to observable single quantum coherence by the application of the last $\frac{\pi}{2}$ pulse. Using equation 2.143 and figure 2.5c it is seen that the phase of the last pulse determines the phase of the detected signal. The general dependence of a coherence on phase is given by equation 2.131 which shows that the phase dependence can be exploited to distinguish orders of coherence.

For ^{13}C in natural abundance, the strongest resonance comes from a ^{13}C surrounded by ^{12}C nuclei. This corresponds to an isolated spin-1/2 system which can only be in a state of single quantum coherence or z-magnetization. Two ^{13}C spins in natural abundance only occur for one molecule in ~ 10^4 and three ^{13}C spins for one molecule in ~ 10^6 so two ^{13}C spins form an effectively isolated AX or AB spin system. This pair can be excited into a state of double quantum coherence with the INADEQUATE sequence described above. With the proper choice of the phase of the detection pulse and receiver it is possible to suppress the ^{13}C-(^{12}C) signal and observe only the signal derived from the excited double quantum coherence [2.20]. An example of the observation of ^{13}C-^{13}C coupling in natural abundance by the INADEQUATE sequence is shown in figure 2.11. This is a spectrum of pyridine in acetone-d_6. The experiment was optimized to observe one bond carbon-carbon coupling constants.

It has been shown that the single transition operator formalism provides for a geometric interpretation of the excitation and indirect detection of double quantum coherence in an AX spin system. Extension to more complicated systems is straightforward and applications will be presented in the next chapters.

References

[2.1] U. Fano, Rev. Mod. Phys. 29, 74 (1957)

[2.2] I. I. Rabi, N. F. Ramsey and J. Schwinger, Rev. Mod. Phys. 26, 167 (1954)

[2.3] A. Abragam, Principles of Nuclear Magnetism, Oxford University Press, London (1961)

[2.4] S. Schaeublin, H. Hoehener and R. R. Ernst, J. Magn. Reson. 13, 196 (1974), W. P. Aue, E. Bartholdi and R. R. Ernst, J. Chem. Phys. 64, 2229 (1976)

[2.5] C. P. Slichter, Principles of Magnetic Resonance, Springer-Verlag, Berlin (1980)

[2.6] D. M. Brink and G. R. Satchler, Angular Momentum, Oxford University Press, Oxford (1968)

[2.7] (a) S. Vega, J. Chem. Phys. 63, 3769 (1975), (b) S. Vega and A. Pines, J. Chem. Phys. 66, 5624 (1977), (c) A. Wokaun and R. R. Ernst, J. Chem. Phys. 67, 1752 (1977), (d) S. Vega, J. Chem. Phys. 68, 5518 (1978)

[2.8] F. Bloch, Phys. Rev. 70, 460 (1946)

[2.9] R. P. Feymann, F. L. Vernon, Jr. and R. W. Hellwarth, J. Appl. Phys. 28, 49 (1957)

[2.10] M. Mehring, E. K. Wolff and M. E. Stoll, J. Magn. Reson. 37, 475 (1980) and G. I. Hoatson and K. J. Packer, Mol. Phys. 40, 1153 (1980)

[2.11] E. Y. C. Lu and L. E. Wood, Phys. Lett. 44A, 68 (1973), H. Hatanaka, T. Terao and T. Hashi, J. Phys. Soc. Japan 39, 835 (1975), H. Hatanaka and T. Hashi, J. Phys. Soc. Japan 39, 1139 (1975), R. G. Brewer and E. L. Hahn, Phys. Rev. A 11, 1641 (1975)

[2.12] G. Bodenhausen and R. Freeman, J. Magn. Reson. 36, 221 (1979)

[2.13] R. Freeman, T. A. Frenkiel and M. H. Levitt, J. Magn. Reson. 44, 409 (1981)

[2.14] A. Wokaun and R. R. Ernst, Chem. Phys. Lett. 52, 407 (1977)

[2.15] P. M. Morse and H. Feshbach, Methods of Theoretical Physics, Part II, McGraw-Hill, New York (1953)

[2.16] R. Kaiser, J. Magn. Reson. 40, 439 (1980)

[2.17] H. Y. Carr and E. M. Purcell, Phys. Rev. 94, 630 (1954), S. Meiboom and D. Gill, Rev. Sci. Instr. 29, 688 (1958)

[2.18] W. P. Aue, J. Karhan and R. R. Ernst, J. Chem. Phys. 64, 4226 (1976), G. Bodenhausen, R. Freeman and D. L. Turner, J. Chem. Phys. 65, 839 (1976)

[2.19] G. Bodenhausen, Prog. Nucl. Mag. Res. Spect. 14, 137 (1980)

[2.20] A. Bax, R. Freeman and S. P. Kempsell, J. Amer. Chem. Soc. 102, 4849 (1980)

Chapter 3

Coherence transfer in two-dimensional spectroscopy

3.1. Introduction

In this chapter the process of coherence transfer by rf pulses is studied in detail with emphasis on two-dimensional spectroscopy. The effects of inhomogeneities in the static magnetic field must be considered and the idea of coherence transfer echoes is introduced. The transfer process is described in terms of the single transition operator formalism which allows a geometric interpretation of the results. Specific expressions for coherence transfer in a single spin system and coupled homonuclear AX spin system will be developed and applied to the indirect observation of zero and double quantum coherence by two-dimensional Fourier transform methods. The dependence of coherence transfer on the tip angle of the detection pulse in a two-dimensional experiment can be used to enhance or suppress portions of the detected magnetization. A tip angle dependent method of discriminating the sign of double quantum precession frequencies is developed and applied to the determination of carbon-carbon connectivity in molecules of natural carbon-13 abundance. Finally a general expression for coherence transfer from any order of coherence will be derived and its properties discussed.

3.2. Coherence transfer echoes

For ensemble of spins precessing in an inhomogeneous magnetic field, each spin will rotate at a sightly different frequency dependent on its position in the magnetic field. An initially coherent system will gradually lose this coherence as a function of time leading to a seemingly incoherent or random state. However this coherent state can be regained, as was demonstrated by Hahn [3.1]. The effect of defocussing of the coherence by the inhomogeneous magnetic field can be refocussed leading to an apparent 'echo' of the original coherence. The idea of coherence transfer echoes has recently been generalized by Maudsley et al. [3.2] to include defocussing and refocussing of coherences at two different transition frequencies.

To understand the echo phenomena the idea of free precession must be extended to include field inhomogeneity. In the presence of an inhomogeneous static magnetic field, $B = B_0 + \Delta B$, the Hamiltonian for free precession can be written as,

$$\hbar^{-1}H_0' = \hbar^{-1}H_0 - \sum_{n=1}^{N} \gamma_n (I_z)_n \Delta B \qquad (3.1)$$

where the sum is over all N spins of the system and the precession frequency of equation 2.122 becomes,

$$\omega_{pq}' = \omega_{pq} - \sum_{n=1}^{N} \gamma_n (\Delta m_{pq})_n \Delta B. \qquad (3.2)$$

For a distribution of field inhomogeneities, each member of an ensemble precessing at ω_{pq} in the absence of ΔB will precess at a different frequency depending on its position in the field. At zero time the members of the ensemble will be phase coherent. However as time increases the field distribution will cause a loss of coherence among

the members of the ensemble as they continue to precess at different frequencies.

The lost phase coherence can be regained by the application of a coherent pulse which affects all the members of the ensemble equally. Let the system precess for a time t_1 before the pulse and a time t_2 after the pulse. Assume the magnetization is detected during t_2. The pulse transfers coherence from pq to some transition rs. In the absence of a pulse the detected magnetization would be phase modulated as a function of t_1 and the observable magnetization can be written as,

$$M_{rs,pq}(t_1,t_2) \sim e^{i\omega'_{pq} t_2} e^{i\omega'_{rs} t_1}, \quad \text{where } \omega_{pq} = \omega_{rs}. \tag{3.3}$$

The effect of the pulse is to mix varying amounts of x- and y-components of coherence pq into the rs coherence. The mixing is dependent on the phase of the pulse and the value of the tip angle as is implicit in table 2.1. If the pulse only transferred one component of coherence pq the observable magnetization would be amplitude modulated as a sinusoidal function of t_1. When both components are mixed the observed magnetization is a mixture of phase and amplitude modulation where in general the magnetization can be written as,

$$\begin{aligned} M_{rs,pq}(t_1,t_2) &= e^{i\omega'_{rs} t_2} \left(a\, e^{i\omega'_{pq} t_1} + b\, e^{-i\omega'_{pq} t_1} \right) \\ &= a\, e^{i(\omega'_{rs} t_2 + \omega'_{pq} t_1)} + b\, e^{i(\omega'_{rs} t_2 - \omega'_{pq} t_1)}. \end{aligned} \tag{3.4}$$

The coefficients 'a' and 'b' indirectly determine the amount of phase and amplitude modulation present. For the first term the effect of the field inhomogeneity will add and this portion of the magnetization will continue to dephase during both time intervals. This term will be

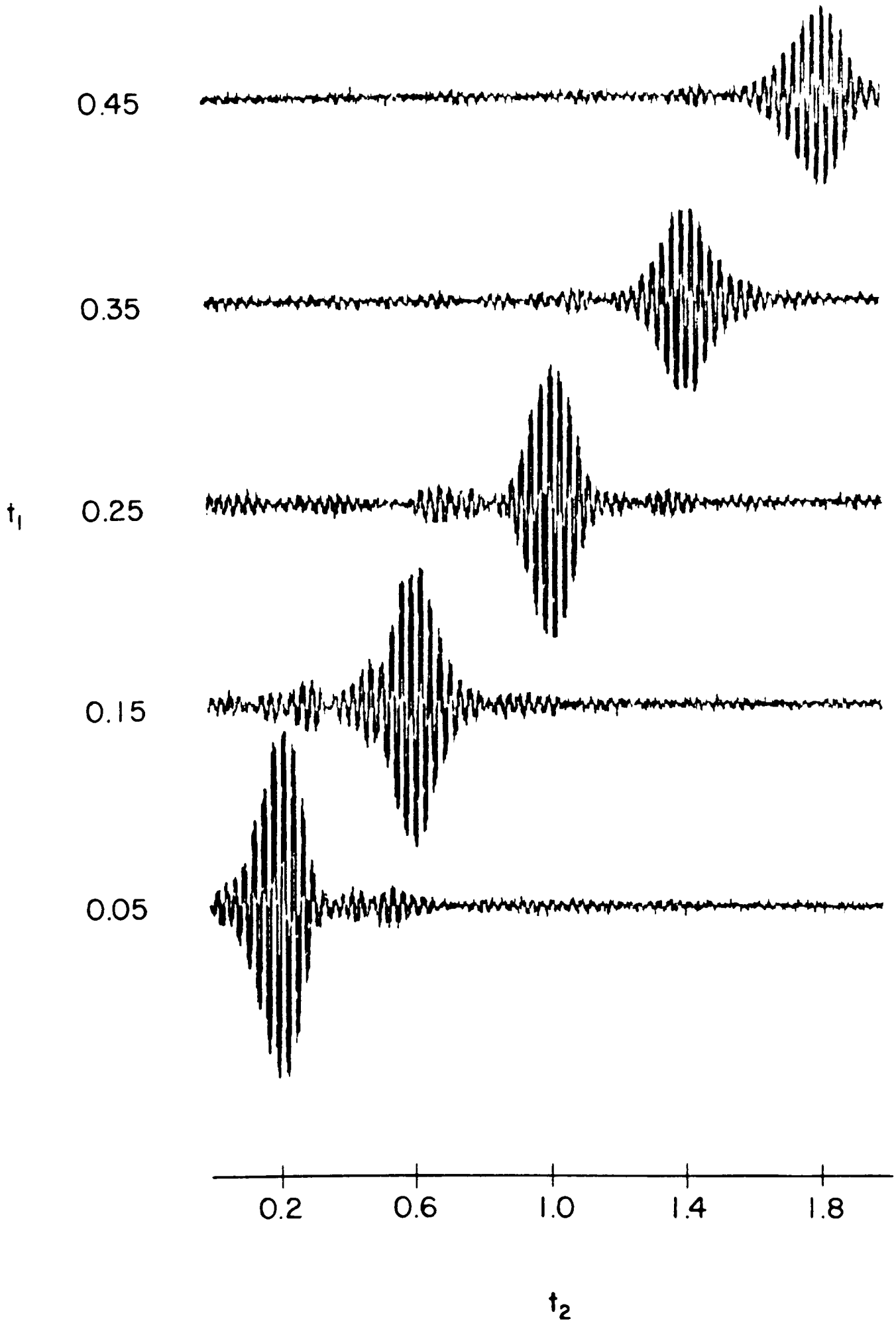

Figure 3.1 Coherence transfer echoes for Carbon-13 magnetization after a heteronuclear shift correlation pulse sequence. Carbon magnetization detected for a time, t_2, and proton evolution for a time, t_1. Static field homogeneity has been degraded to enhance the echo effect.

referred to as an 'antiecho'. For the second term the inhomogeneity effects will cancel at some point during t_2 leading to an apparent rephasing of the lost coherence. This term will be referred to as the 'echo' term. To make this explicit write the argument of the echo term as,

$$\omega'_{rs}\, t_2 - \omega'_{pq}\, t_1 = (\omega_{rs} t_2 - \omega_{pq} t_1) - \left[\sum_{k=1}^{N} \gamma_k (\Delta m_{rs})_k t_2 - \sum_{l=1}^{N} \gamma_l (\Delta m_{pq})_l t_1\right] \Delta B. \qquad (3.5)$$

This expression becomes independent of field inhomogeneity when,

$$t_2 = \frac{\sum_{l=1}^{N} \gamma_l (\Delta m_{pq})_l}{\sum_{k=1}^{N} \gamma_k (\Delta m_{rs})_k} t_1. \qquad (3.6)$$

An example of coherence transfer echoes consider figure 3.1. This is the detected carbon-13 magnetization after a heteronuclear shift correlation sequence [3.3]. In the sequence proton coherence evolves for time t_1 then is transferred to carbon-13 coherence where the magnetization is detected for a time t_2. This process involves only single quantum coherence so the time of the echo in equation 3.6 is determined by the ratio γ_H/γ_C. The echo should occur at $t_2 \simeq 4t_1$. The result agrees very well with this prediction. The homogeneity has been intentionally degraded to accentuate the echo effect.

Now a more detailed treatment will be given of coherence transfer in two-dimensional spectroscopy. Starting from the single spin case the ideas will be extended to more complicated spin systems. The prime will be dropped from the notation for the precession frequency in all subsequent calculations with the understanding that equation 3.2 is

being implied for the precession frequency.

3.3. Coherence transfer for a single spin-1/2 system

Assume that the spin is initially in thermal equilibrium with its surroundings. The state of the system can be represented by the density operator,

$$\rho_0 = aI_z \tag{3.7}$$

where $a = -\hbar\gamma B_0/kT$ is the Boltzmann population factor. A $(\frac{\pi}{2})_y$ preparation pulse rotates the spin angular momentum vector into the transverse plane aligning it along the x-axis. After the pulse the system undergoes free precession for a time, t_1, where the state of the system can be expressed by the density operator,

$$\rho(t_1) = a(I_x\cos\omega_0 t_1 + I_y\sin\omega_0 t_1) \tag{3.8}$$

where $\omega_0 = -\gamma B_0$ is the Larmor precession frequency.

The coherence transfer process is effected by an $(\alpha)_y$ detection pulse. For a single spin-1/2 a pulse along the y-axis will not effect the y-component of spin. However the x-component will be rotated about the y-axis transferring to the -z-axis and over to the -x-axis dependent on the value of the detection pulse, α. The density operator following the pulse is given by,

$$\begin{aligned}\rho'(t_1) &= e^{-i\alpha I_y}\,\rho(t_1)\,e^{i\alpha I_y} \\ &= a\,[\,\cos\omega_0 t_1 (I_x\cos\alpha - I_z\sin\alpha) \\ &\quad + \sin\omega_0 t_1\, I_y\,].\end{aligned} \tag{3.9}$$

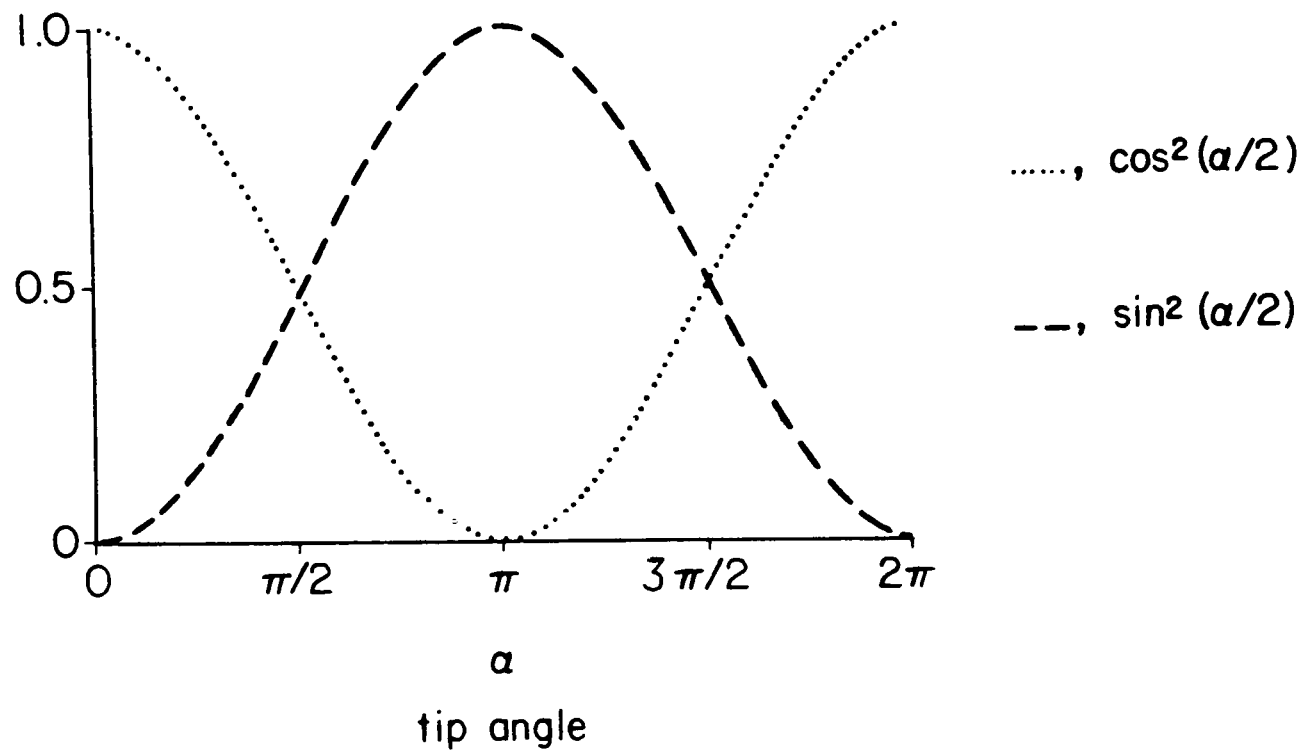

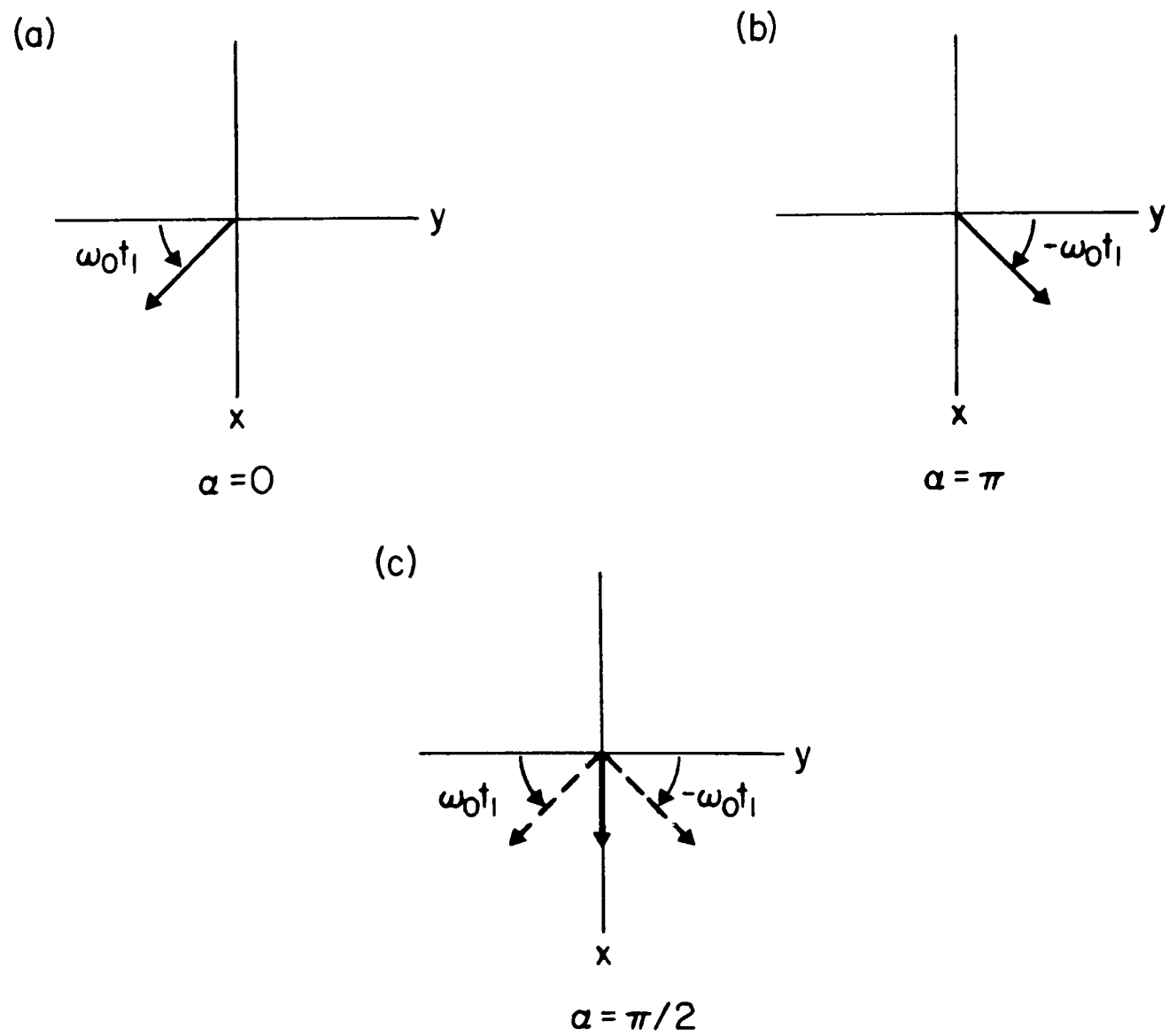

Figure 3.2 Tip angle effect of coherence transfer for a single spin. Specific aspects of the transfer process illustrated in the figure are discussed in the text. For the graph at the top, the antiecho portion is represented by the dotted curve and the echo portion by the dashed curve.

The observable magnetization detected for a time t_2 is given by,

$$M(t_1,t_2) = \langle \mu_x \rho(t_1,t_2) \rangle + i\langle \mu_y \rho(t_1,t_2) \rangle$$

$$= \gamma\hbar \left[\langle I_x \rho'(t_1) \rangle + i\langle I_y \rho'(t_1) \rangle \right] e^{i\omega_0 t_2}$$

$$= \gamma\hbar a \left[\cos^2(\tfrac{\alpha}{2})\, e^{i(\omega_0 t_2 + \omega_0 t_1)} \right.$$

$$\left. - \sin^2(\tfrac{\alpha}{2})\, e^{i(\omega_0 t_2 - \omega_0 t_1)} \right]. \qquad (3.10)$$

The first term represents the 'antiecho' portion of the detected signal and the second term the 'echo' portion.

When the two-dimensional Fourier transformation process is applied to the detected magnetization, given by equation 3.10, the F_1 trace at $\omega_2 = \omega_0$ will have two resonances at $\omega_1 = \pm\omega_0$ corresponding to the antiecho and echo portions of the magnetization. The dependence of the magnitude of each resonance on the tip angle, α, is plotted at the top of figure 3.2 in the absence of field inhomogeneity. For $\alpha = 0$ there is no coherence transfer due to the detection pulse so the system simply precesses freely for t_1 and then is detected for t_2. In this case there is only one resonance in the two-dimensional spectrum at $\omega_2 = \omega_0$ and $\omega_1 = \omega_0$. For $\alpha = \pi$ the x-component of spin will be transferred over to the $-x$ axis. As t_1 is incremented there appears to be a negative rotation of the magnetization vector which results in only one resonance in the two-dimensional spectrum at $\omega_2 = \omega_0$ and $\omega_1 = -\omega_0$. The position of the spin vector is illustrated in figure 3.2a and figure 3.2b for these two values of the tip angle, α. For a $\frac{\pi}{2}$ detection pulse only the y-component is transferred to observable coherence, therefore the observed magnetization is amplitude modulated by $\sin(\omega_0 t_1)$ which can be represented as two counter rotating vectors of equal magnitude as illustrated in figure 3.2c. The positively rotating component

represents the antiecho term and the negatively rotating component the echo term in equation 3.10. Therefore the resulting two dimensional spectrum would have two resonances of equal magnitude at $\omega_2 = \omega_0$ and $\omega_1 = \pm\omega_0$.

In the presence of an inhomogeneous B_0 field the antiecho term would continue to lose phase coherence during both times, t_1 and t_2. No echo would form and the intensity of the associated resonance peak in the two-dimensional spectrum would be reduced. The echo term would form an echo at $t_2 = t_1$ and the associated resonance peak would be larger than the antiecho peak in the two-dimensional spectrum.

As illustrated in figure 3.2 the tip angle effect of equation 3.10 will determine which portion of the signal in favoured. For $\alpha < \frac{\pi}{2}$ the antiecho term is largest and for $\alpha > \frac{\pi}{2}$ the echo term is dominant. The fact that only the echo term appears for $\alpha = \pi$ is consistent with the expected result for the one-dimensional Carr-Purcell spin echo sequence [3.4].

3.4. Coherence transfer for coupled spins: AX spin system

The coherence transfer process for coupled spin systems is more involved than for a single spin. Coherence can be transferred among components of a multiplet associated with a given spin and also transferred to the other spins involved in a coupling pattern. In addition coherence can be transferred between different orders in a multiple level system. In the following treatment the specific example of a homonuclear AX spin system is considered. The general ideas developed here can be extended to more complicated spin systems with the method outlined in section 3.5.

3.4.1. Transfer of single quantum coherence in an AX spin system

After some initial creation pulse sequence each single quantum coherence associated with a spin evolves for a time t_1. For simplicity consider only the 13 coherence assumed to be initially in the state, $a(I_x^{13})$. The density operator for this coherence is given by

$$\rho(t_1) = a \left(I_x^{13} \cos\omega_{13} t_1 + I_y^{13} \sin\omega_{13} t_1 \right) \qquad (3.11)$$

where 'a' is the appropriate coefficient for occurrence of the 13 coherence. At the end of the evolution time an $(\alpha)_y$ detection pulse transfers the 13 coherence in the following manner where the x- and y-components are considered separately.

Using the pulse cascade approach [3.5] a pulse operator $R_\beta = e^{-i\alpha F_\beta}$ applied to the spin system can be treated as a pulse to each spin separately. Furthermore the pulse to each spin can be treated separately as a pulse to each coherence associated with the spin. The order of operating on each spin can be interchanged because the operators for each spin commute. Also the order of operating on each coherence associated with a particular spin can be interchanged because these operators commute. However, care must be taken in changing the order of operation among coherences associated with different spins as these operators might not commute. Within these restrictions a convenient choice of order is possible to simplify the calculation.

Using the pulse cascade approach, the coherence transfer for the I_x^{13} term becomes,

$$e^{-i\alpha F_y} I_x^{13} e^{i\alpha F_y}$$

$$= \cos\alpha \left[\left(I_x^{13} \cos^2\left(\frac{\alpha}{2}\right) + I_x^{24} \sin^2\left(\frac{\alpha}{2}\right) \right) \right.$$

$$+ \left(I_x^{23} + I_x^{14} \right)\cos\left(\frac{\alpha}{2}\right) \sin\left(\frac{\alpha}{2}\right)]$$

$$- \sin\alpha \left[\left(I_z^{13} + I_z^{24} \right) + \left(I_z^{12} - I_z^{34} \right)\cos\alpha \right.$$

$$\left. + \frac{1}{2}\left(I_x^{12} - I_x^{34} \right)\cos\left(\frac{\alpha}{2}\right) \sin\left(\frac{\alpha}{2}\right) \right]. \qquad (3.12)$$

The coherence transfer among the A-spin transition 13 and 24 is in phase so that the 13 coherence is redistributed among these transitions and the zero and double quantum transitions 23 and 14. The the X-spin coherences 12 and 34 appear in antiphase indicating that there is no net coherence transfer between spins by the detection pulse. The observable coherences are given by the first and last lines of equation 3.12.

Again using the pulse cascade approach, the transferred coherence from the I_y^{13} term becomes,

$$e^{-i\alpha F_y} I_y^{13} e^{i\alpha F_y}$$

$$= I_y^{13}\cos^2\left(\frac{\alpha}{2}\right) + I_y^{24}\sin^2\left(\frac{\alpha}{2}\right)$$

$$+ \left(I_y^{23} + I_y^{14} \right)\cos\left(\frac{\alpha}{2}\right) \sin\left(\frac{\alpha}{2}\right). \qquad (3.13)$$

As for the I_x^{13} term, I_y^{13} coherence is redistributed among the A-spin coherences and zero and double quantum coherences. The observable coherences are given by the first two terms in equation 3.13.

During the detection interval, t_2, the observable signal transferred from the 13 coherence must be considered in three parts: Two diagonal coherences 13 and 24 and one cross coherence, either 12 or 34. As can be seen from equation 3.12 the 12 and 34 coherences transfer with the same dependence on α but with opposite phase so only one of these two coherences need be considered to study the transfer process. The 12 coherence will be used to illustrate the result for both 12 and 34

Figure 3.3 Tip angle effect of coherence transfer for single quantum coherences in an AX spin system. (a) Transfer to 'diagonal' peak 13. (b) and (c) Transfer to 'cross' peaks 24 and 12. In each diagram, the antiecho portion is represented by the dotted curve and the echo portion by the dashed curve.

coherences.

In a two-dimensional spectrum the diagonal resonances occur along two main diagonal lines for $\omega_2 = \omega_1$ and $\omega_2 = -\omega_1$. For the AX spin system this corresponds to coherence transfer of the 13 component to the antiecho and echo portion of the 13 magnetization. The detectable magnetization due to coherence 13 is given by,

$$M_{13}(t_1,t_2) = \langle (\mu_x)_{13}\rho(t_1,t_2) \rangle + i\langle (\mu_y)_{13}\rho(t_1,t_2) \rangle$$

$$= \gamma\hbar \left[\langle I_x^{13} R\rho(t_1)R^+ \rangle + i\langle I_y^{13} R\rho(t_1)R^+ \rangle \right] e^{i\omega_{13}t_2}. \qquad (3.14)$$

Using the results from equations 3.11, 3.12 and 3.13 the magnetization can be written as,

$$M_{13}(t_1,t_2) = \gamma\hbar a \left[\cos^4(\tfrac{\alpha}{2})\, e^{i(\omega_{13}t_2 + \omega_{13}t_1)} \right.$$

$$\left. - \cos^2(\tfrac{\alpha}{2})\, \sin^2(\tfrac{\alpha}{2})\, e^{i(\omega_{13}t_2 - \omega_{13}t_1)} \right]. \qquad (3.15)$$

The first term corresponds to the antiecho portion which appears in the two-dimensional spectrum at $\omega_2 = \omega_1$. The second term represents the echo portion and will appear at $\omega_2 = -\omega_1$. The magnitude of each portion is illustrated in figure 3.3a. If the 13 coherence represented an isolated spin the α dependence of the coherence transfer process would be like the single spin system described previously. For $\alpha = \pi$ the antiecho term would be zero and the echo term maximum in that situation. However both antiecho and echo terms go to zero at $\alpha = \pi$ for the 13 coherence. As will be shown next the 13 coherence is transferred to the 24 coherence for $\alpha = \pi$.

For the AX spin system the 24 diagonal peak resonance also occurs near the main diagonal at $\omega_2 = \omega_{24} = \omega_A - \pi J$ and $\omega_1 = \omega_{13} = \pm(\omega_A + \pi J)$.

The 24 coherence is associated with the same spin as the 13 coherence so the two resonances have the same phase. However the dependence on α is different for coherences 13 and 24. Using a procedure similar to equation 3.14 the detectable magnetization due to coherence 24 is given by,

$$M_{24}(t_1,t_2) = \gamma\hbar a \left[\cos^2(\tfrac{\alpha}{2}) \sin^2(\tfrac{\alpha}{2}) \, e^{i(\omega_{24}t_2 + \omega_{13}t_1)} - \sin^4(\tfrac{\alpha}{2}) \, e^{i(\omega_{24}t_2 - \omega_{13}t_1)} \right]. \qquad (3.16)$$

The first term represents the antiecho portion and the second the echo portion. The magnitude of each term is illustrated in figure 3.3b. For the echo portion of the 24 coherence the transfer from 13 to 24 is most effective for $\alpha = \pi$. This is the result expected for J-modulated spin echoes for the $(\frac{\pi}{2})_y - \tau - (\pi)_y - \tau$ Carr-Purcell pulse sequence. The $(\pi)_y$ pulse refocusses the inhomogeneity and inverts the spin labels leading to J-modulation of the echo result.

The coherence transfer to the cross peak coherence 12 can be calculated in a similar manner to the above calculations. This represents coherence transfer among different spins in a coupled system. The observable magnetization due to the 12 coherence transferred from coherence 13 is given by,

$$M_{12}(t_1,t_2) = -\gamma\hbar a \cos^2(\tfrac{\alpha}{2}) \sin^2(\tfrac{\alpha}{2}) \left[e^{i(\omega_{12}t_2 + \omega_{13}t_1)} + e^{i(\omega_{12}t_2 - \omega_{13}t_1)} \right]. \qquad (3.17)$$

The first term in square brackets represents the antiecho portion of the 12 coherence and will appear in the two-dimensional spectrum at $\omega_2 = \omega_A + \pi J$ and $\omega_1 = \omega_X + \pi J$. The second term in square brackets is the echo portion and will appear at $\omega_2 = \omega_A + \pi J$ and $\omega_1 = -(\omega_X + \pi J)$.

Both portions of the 12 coherence have the same dependence on the detection pulse, α. This is illustrated in figure 3.3c. From the figure it can be seen that the maximum amount of transfer occurs when $\alpha = \frac{m\pi}{2}$ for m = 1,3,5,... and the minimum where $\alpha = \frac{n\pi}{2}$ for n = 0,2,4,....

The maximum amount of coherence is transferred among the transitions of the spin system when α is set equal to an odd multiple of $\frac{\pi}{2}$. As can be seen in figure 3.3 all the observable magnetization components have equal intensity for this value of α. By varying α one can choose to enhance or suppress portions of the resonances in a two-dimensional spectrum. This has been used by Bax and Freeman [3.6] to simplify the spectrum of the two pulse sequence proposed by Jeener by reducing the relative size of the diagonal peaks within a multiplet lying on the main diagonal. In addition the tip angle effect provides additional information on the relative sign of the coupling constants in more complicated spin systems by suppressing portions of a multiplet of cross peaks correlating two coupled spins.

3.4.2. Transfer of zero quantum coherence in an AX spin system

Assume that the AX spin system has been prepared into a state which contains the zero quantum coherence, 23 , and has evolved for a time t_1. The density operator for the zero quantum coherence can be written as,

$$\rho(t_1) = a \left(I_x^{23} \cos\omega_{23} t_1 + I_y^{23} \sin\omega_{23} t_1 \right) \qquad (3.18)$$

where 'a' is an appropriate coefficient for the occurrence of the 23 coherence. After the evolution time t_1 a $(\alpha)_y$ detection pulse is applied to the spin system and the 23 coherence transferred to observable single quantum coherence as follows.

Using the pulse cascade approach and considering each element of

the zero quantum coherence separately, the I_x^{23} coherence transfers as,

$$e^{-i\alpha F_y} I_x^{23} e^{i\alpha F_y}$$

$$= I_x^{23} + (I_z^{13} - I_z^{24} - I_x^{23} - I_x^{14}) \, 2 \cos^2(\tfrac{\alpha}{2}) \sin^2(\tfrac{\alpha}{2})$$

$$- (I_x^{13} - I_x^{24} + I_x^{12} - I_x^{34}) \, \tfrac{1}{2} \cos\alpha \sin\alpha. \qquad (3.19)$$

Observable single quantum coherence is represented by the last line in equation 3.19. All single quantum elements transfer with the same dependence on α and are in antiphase for each spin doublet. For spin A element 13 is of the opposite phase to element 24 while for spin X element 12 is of opposite phase to element 34.

The transfer of the I_y^{23} coherence can be calculated most easily by using the appropriate vector picture for the cyclic commutator property of the combinations of operators given in equation 2.156. This approach gives the simple result,

$$e^{-i\alpha F_y} I_y^{23} e^{i\alpha F_y}$$

$$= I_y^{23} \cos\alpha$$

$$- (I_y^{13} - I_y^{24} - I_y^{12} + I_y^{34}) \, \tfrac{1}{2} \sin\alpha. \qquad (3.20)$$

The observable single quantum coherences of the last line of equation 3.20 will all receive coherence with the same dependence on α and with opposite phase for each spin doublet and with opposite phase between the doublets for each spin. Because of the antiphase relationship between the two spin doublets, coherence transfer to each spin must be considered separately. Consider transfer to single quantum coherence 13 for spin A and coherence 12 for spin X.

coherence 13

antiecho ....., $\cos^3(\alpha/2)\sin(\alpha/2)$

echo – –, $\cos(\alpha/2)\sin^3(\alpha/2)$

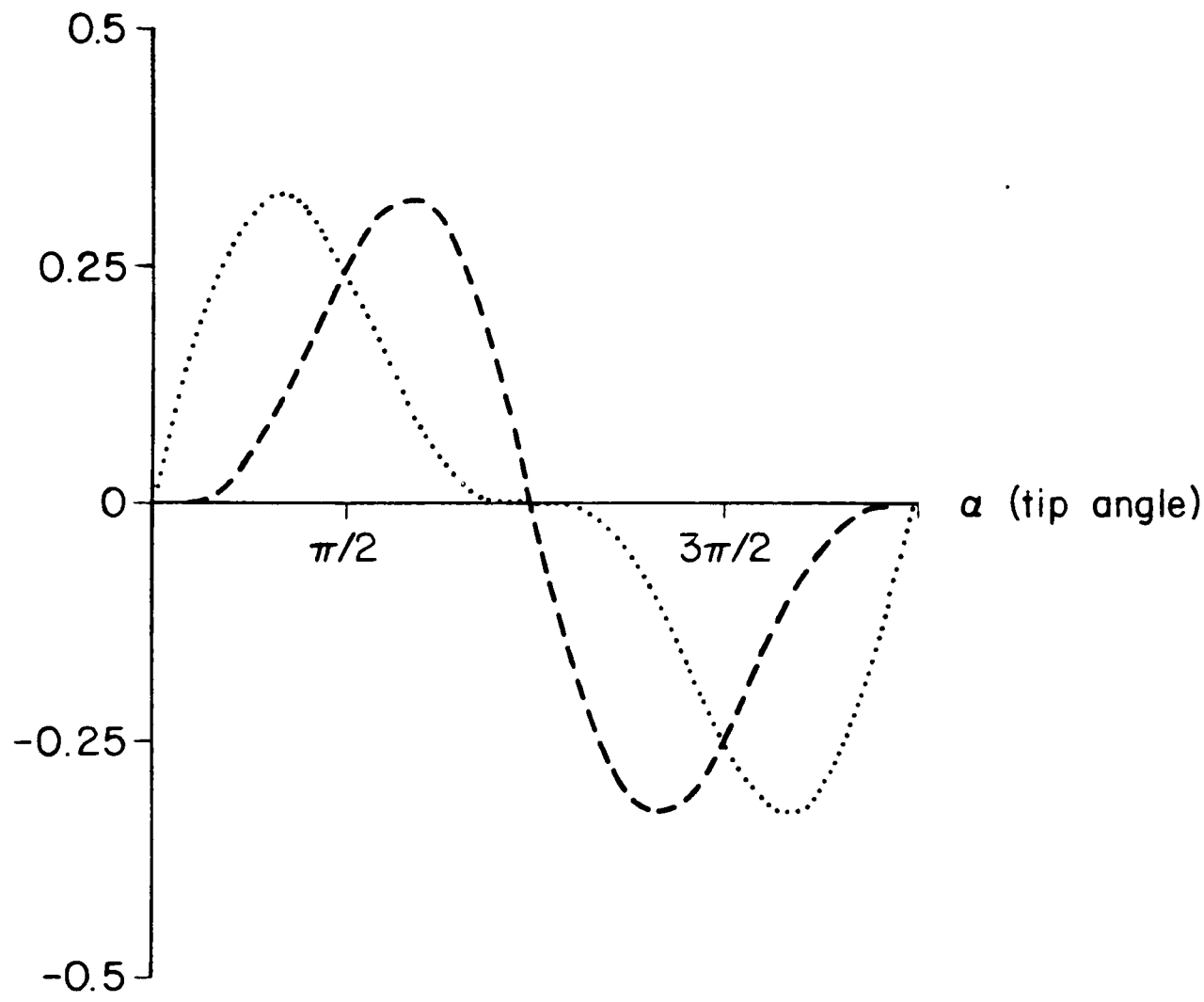

coherence 12

antiecho – –, $\cos(\alpha/2)\sin^3(\alpha/2)$

echo ....., $\cos^3(\alpha/2)\sin(\alpha/2)$

Figure 3.4 Tip angle effect of coherence transfer from zero or double quantum coherence to single quantum coherence in an AX spin system. The antiecho is represented by the dotted curve and the echo portion by the dashed curve.

Using the same procedure as outline in section 3.4.1 for the transfer among single quantum coherences, the observable magnetization due to the 13 coherence can be calculated using equation 3.14 and the results of equations 3.18, 3.19 and 3.20.

$$M_{13}(t_1,t_2) = \gamma\hbar a \left[-\cos^3(\tfrac{\alpha}{2}) \sin(\tfrac{\alpha}{2}) e^{i(\omega_{13}t_2 + \omega_{23}t_1)} + \cos(\tfrac{\alpha}{2}) \sin^3(\tfrac{\alpha}{2}) e^{i(\omega_{13}t_2 - \omega_{23}t_1)} \right]. \qquad (3.21)$$

The first term in square brackets represents the antiecho and the second the echo portion of the observable magnetization. In a similar manner the transfer to the 12 coherence can be calculated with the following result.

$$M_{12}(t_1,t_2) = \gamma\hbar a \left[\cos(\tfrac{\alpha}{2}) \sin^3(\tfrac{\alpha}{2}) e^{i(\omega_{13}t_2 + \omega_{23}t_1)} - \cos^3(\tfrac{\alpha}{2}) \sin(\tfrac{\alpha}{2}) e^{i(\omega_{13}t_2 - \omega_{23}t_1)} \right]. \qquad (3.22)$$

Again the first and second terms correspond to the antiecho and echo portions.

The tip angle dependence for the antiecho and echo portions of the 13 magnetization of spin A is opposite to the dependence for the 12 magnetization of spin X. The antiecho and echo portions are equal for $\alpha = \frac{\pi}{2}$ and in antiphase. For α not equal to some odd integer multiple of $\frac{\pi}{2}$ the echo will predominate for one spin and the antiecho for the other spin. The predominate role of the antiecho or echo for each spin will reverse as the tip angle is increased of decreased past the next odd integer multiple of $\frac{\pi}{2}$. The α dependence is plotted in figure 3.4 for the 13 coherence. This graph also applies to the 12 coherence if the roles of the antiecho and echo coefficients are reversed.

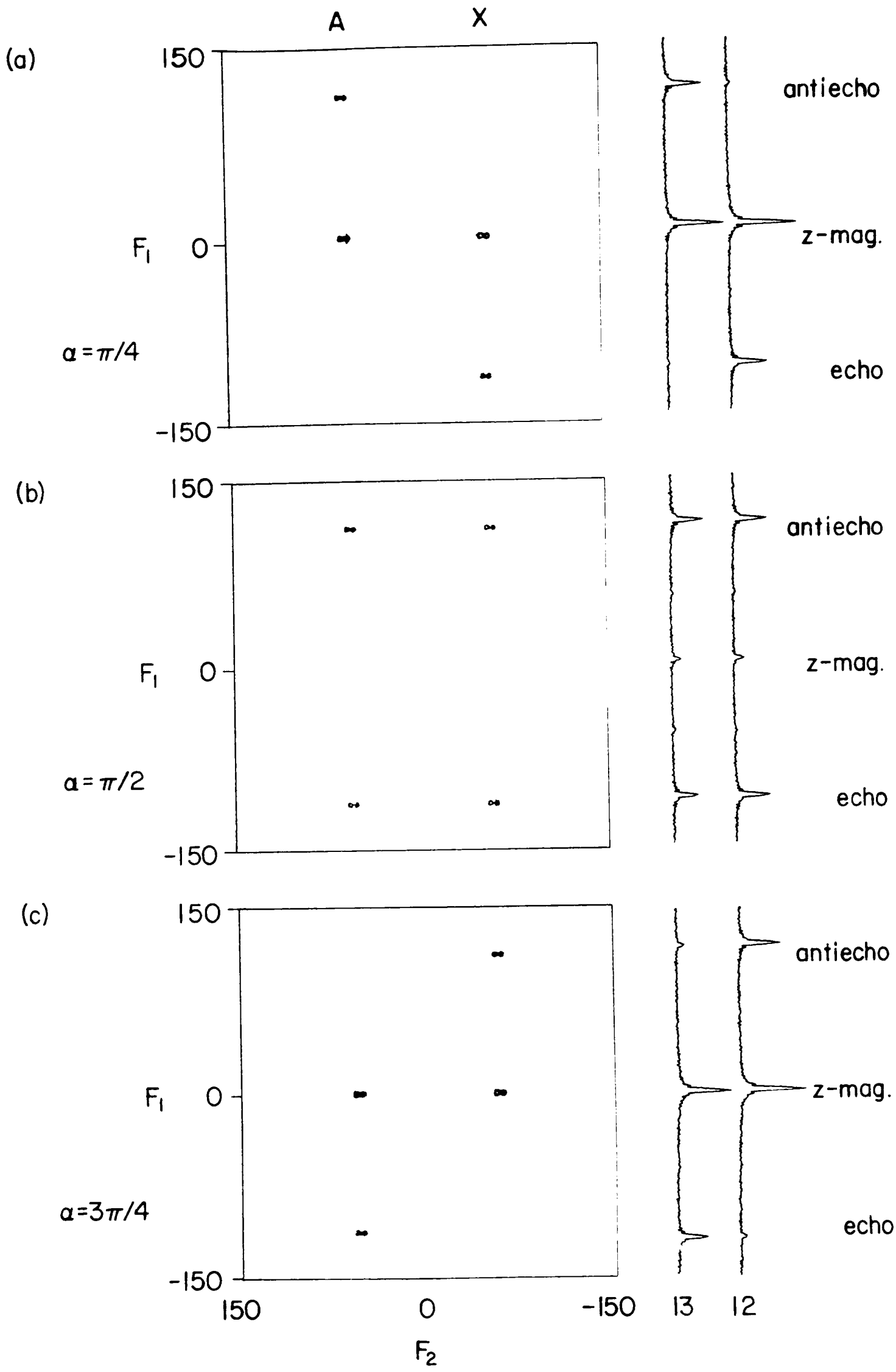

Figure 3.5 Tip angle effect for zero quantum coherence of the AX spin system 2,3-dibromothiophene in acetone-d_6. The two-dimensional spectrum for (a) $\alpha = \pi/4$, (b) $\pi/2$ and $3\pi/4$ are shown. Traces for coherence 13 and 12 are plotted at the right of the contour plots with the same vertical scale.

The transfer of zero quantum coherence to observable single quantum coherence is shown in figure 3.5 for the proton AX spin system 2,3-dibromothiophene in acetone-d_6. The spin system has been excited into a state containing zero quantum coherence, allowed to evolve for t_1 and thendetected for t_2 using the following pulse sequence.

$$(\frac{\pi}{2})_x - \tau - (\pi)_y - \tau - (\frac{\pi}{4})_y - t_1 - (\alpha)_y - t_2$$

The delay τ is chosen as $1/4J$ and the creation scheme follows that outlined in chapter 2. The phase of the last pulse is cycled through a four step sequence to suppress single quantum coherence derived from all orders of coherence except zero quantum and z-magnetization [3.7]. The z-magnetization peaks in the two-dimensional spectrum lie along a line parallel to the F_2 axis at $\omega_1 = 0$ since z-magnetization will not have precessed during t_1. The zero quantum peaks can easily be distinguished because they appear at $F_1 = \pm(\omega_A - \omega_X)$. The two-dimensional spectra for three values of α are illustrated in figure 3.5 and the traces corresponding to the observable magnetization from coherences 13 and 12 are plotted parallel to the F_1 axis. For $\alpha = \frac{\pi}{4}$ the antiecho term dominates for spin A and the echo term is largest for spin X as can be seen in figure 3.5a. For $\alpha = \frac{\pi}{2}$ all four terms are of equal intensity as shown in figure 3.5b. With α chosen as $\frac{3\pi}{4}$ the echo term dominates for the A spin and the antiecho for the X spin in figure 3.5c. For a value of the tip angle which selectively enhances one term over the other the number of peaks appearing in the contour map due to the zero quantum coherence will be reduced from four to two. The zero quantum peaks for each pair of spins will appear on opposite sides of the line $\omega_1 = 0$ and a line joining the two peaks will have a slope of ± 2.

The expressions 'antiecho' and 'echo' are a misnomer for the two portions of the observable magnetization for zero quantum coherence for

in general zero order coherences are not affected by field inhomogeneities [3.7]. This is illustrated in figure 3.5b for $\alpha = \frac{\pi}{2}$ where all four peaks are approximately equal in intensity. Thus for a well digitized F_1 trace the linewidth of the zero quantum peak will accurately reflect the transverse decay rate of the zero quantum coherence.

3.4.3. Transfer of double quantum coherence in an AX spin system

The analysis of coherence transfer for the AX spin system will be complete with the consideration of double quantum coherence transfer. Assume that the AX spin system has been prepared into a state containing the double quantum coherence, 14. After an evolution time t_1 the density operator for this coherence can be written as,

$$\rho(t_1) = a \left(I_y^{14} \cos\omega_{14} t_1 - I_x^{14} \sin\omega_{14} t_1 \right) \qquad (3.23)$$

where 'a' is an appropriate coefficient. The phase of the 14 coherence represented in the above equation is shifted by $\frac{\pi}{2}$ with respect to the phase of the zero quantum coherence 23 represented in equation 3.18. This is in line with the phase of the zero and double quantum coherences created by the methods outlined in chapter 2. A $(\alpha)_x$ detection pulse is applied at t_1 transferring the 14 coherence among the other levels of the spin system. Coherence transfer for each component of the double quantum coherence 14 will be treated separately.

The transfer of the double quantum coherence follows quite similar lines to that for the zero quantum coherence. The transfer of the I_y^{14} component can be calculated using the vector picture of figure 2.5c or 2.7a which are equivalent representations for the AX spin system. The result of the use of the vector picture can be written mathematically as,

$$e^{-i\alpha F_x} I_y^{14} e^{i\alpha F_x}$$

$$= I_y^{14} \cos\alpha$$

$$+ (I_x^{13} - I_x^{24} + I_x^{12} - I_x^{34}) \frac{1}{2} \sin\alpha. \qquad (3.24)$$

As represented by the last line in this equation, all the observable single quantum coherences transfer with the same α dependence and are in antiphase for each spin.

Applying the pulse cascade argument to the pulse operator, the transfer of the I_x^{14} component can be calculated, with the result,

$$e^{-i\alpha F_x} I_x^{14} e^{i\alpha F_x}$$

$$= I_x^{14} - (I_z^{13} - I_z^{24} - I_x^{23} + I_x^{14}) \, 2 \cos^2(\tfrac{\alpha}{2}) \sin^2(\tfrac{\alpha}{2})$$

$$- (I_y^{13} - I_y^{24} + I_y^{12} - I_y^{34}) \frac{1}{2} \cos\alpha \sin\alpha. \qquad (3.25)$$

In the last line of the above equation the observable single quantum coherences appear in antiphase for each spin and all transfer with the same dependence on α. In contrast to the zero quantum transfer process there is no difference in phase between spins in the form of the transfer process for the double quantum coherence. Hence it is sufficient to consider transfer to only one element of the single quantum coherence; choose the 13 element.

The observable magnetization of coherence 13 can be determined using equation 3.14 and the results of equations 3.23, 3.24 and 3.25.

$$M_{13}(t_1,t_2) = \gamma\hbar a \, [\cos^3(\tfrac{\alpha}{2}) \sin(\tfrac{\alpha}{2}) \, e^{i(\omega_{13}t_2 + \omega_{14}t_1)}$$

$$+ \cos(\tfrac{\alpha}{2}) \sin^3(\tfrac{\alpha}{2}) \, e^{i(\omega_{13}t_2 - \omega_{14}t_1)}]. \qquad (3.26)$$

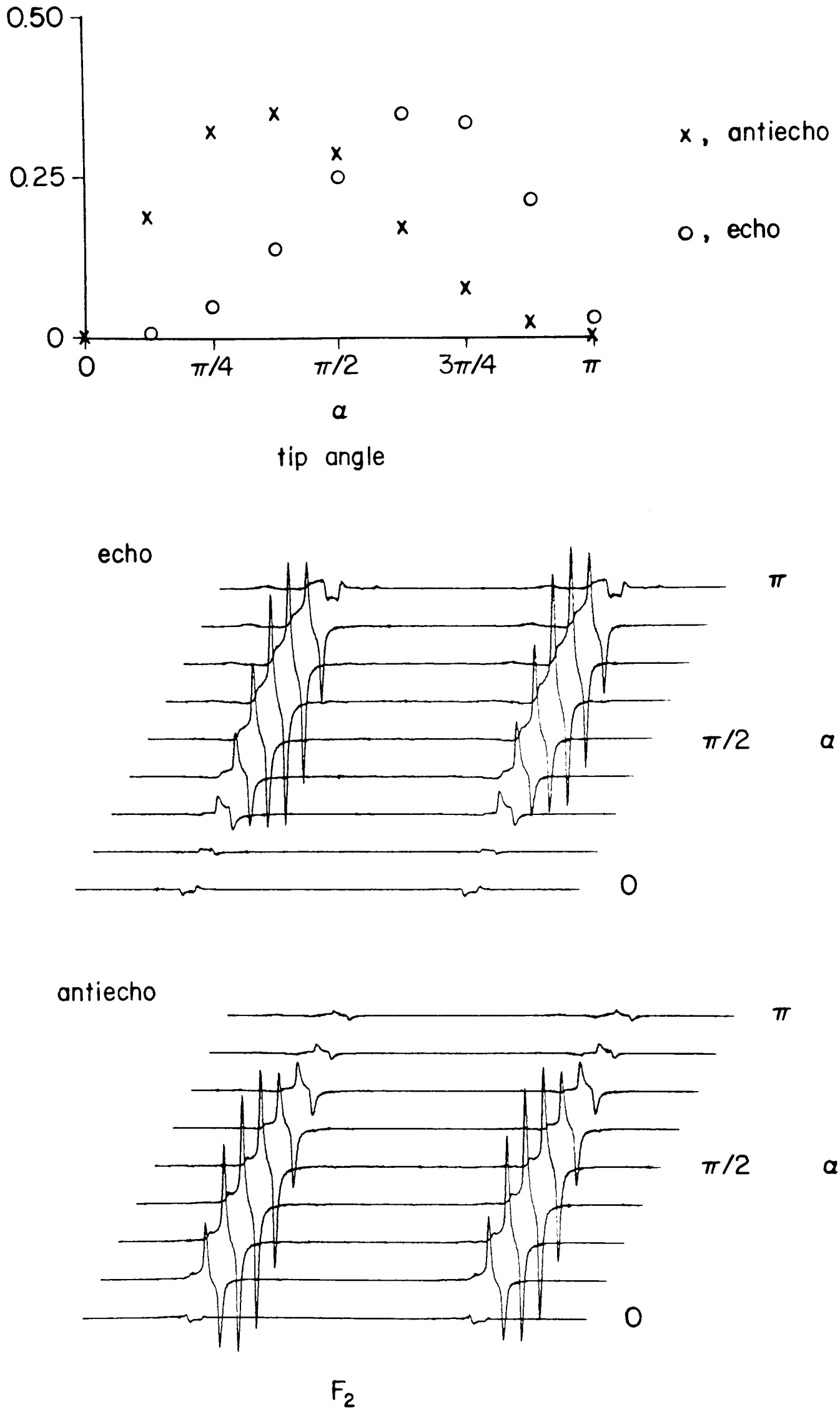

Figure 3.6 The tip angle dependence of the antiecho and echo portions of the observed magnetization for the proton AX spin system described in the text. The average peak height versus detection pulse tip angle is shown at the top of the figure. The evolution time, t_1 was set to zero.

The first term in the square brackets is the antiecho and the second the echo portion of the observable magnetization. The dependence of the antiecho and echo coefficients on the tip angle, α, is also represented by figure 3.4.

An experimental verification of the tip angle effect for double quantum coherence is provided by the proton AX spin system used previously; 2,3-dibromothiophene in acetone-d_6. The system is prepared into a state of double quantum coherence using a modified INADEQUATE sequence [3.8].

$$(\frac{\pi}{2})_x - \tau - (\pi)_y - \tau - (\frac{\pi}{2})_x - t_1 - (\alpha)_x - t_2$$

As outlined in chapter 2, for $\tau = 1/4J$ the third pulse creates double quantum coherence proportional to I_y^{14}. The evolution is described by equation 3.23 and the detected magnetization for the 13 element by equation 3.26. The double quantum coherence is selectively detected by cycling the phases of the creation and detection pulses [3.7,3.9]. The antiecho and echo portions of the magnetization are shown separately in figure 3.6. The two portions have been separated by using an additional $\frac{\pi}{4}$ z-pulse at the beginning of the evolution time and phase cycling of the receiver [3.10]. The experimental result is compiled in the graph at the top of the figure which is a plot of the average peak height for the four resonances versus tip angle. The evolution time t_1 has been set equal to zero so the portions should be of the same intensity because the field inhomogeneity has not caused any dephasing during the evolution. The same experiment was performed with $t_1 = 0.05$ secs. and the results are shown in figure 3.7. Because of the field inhomogeneity the antiecho has lost peak height and the echo has gained in height due to refocussing for these terms. The experimental results shown in figure 3.6 and 3.7 are plotted on the same scale. The values on both graphs

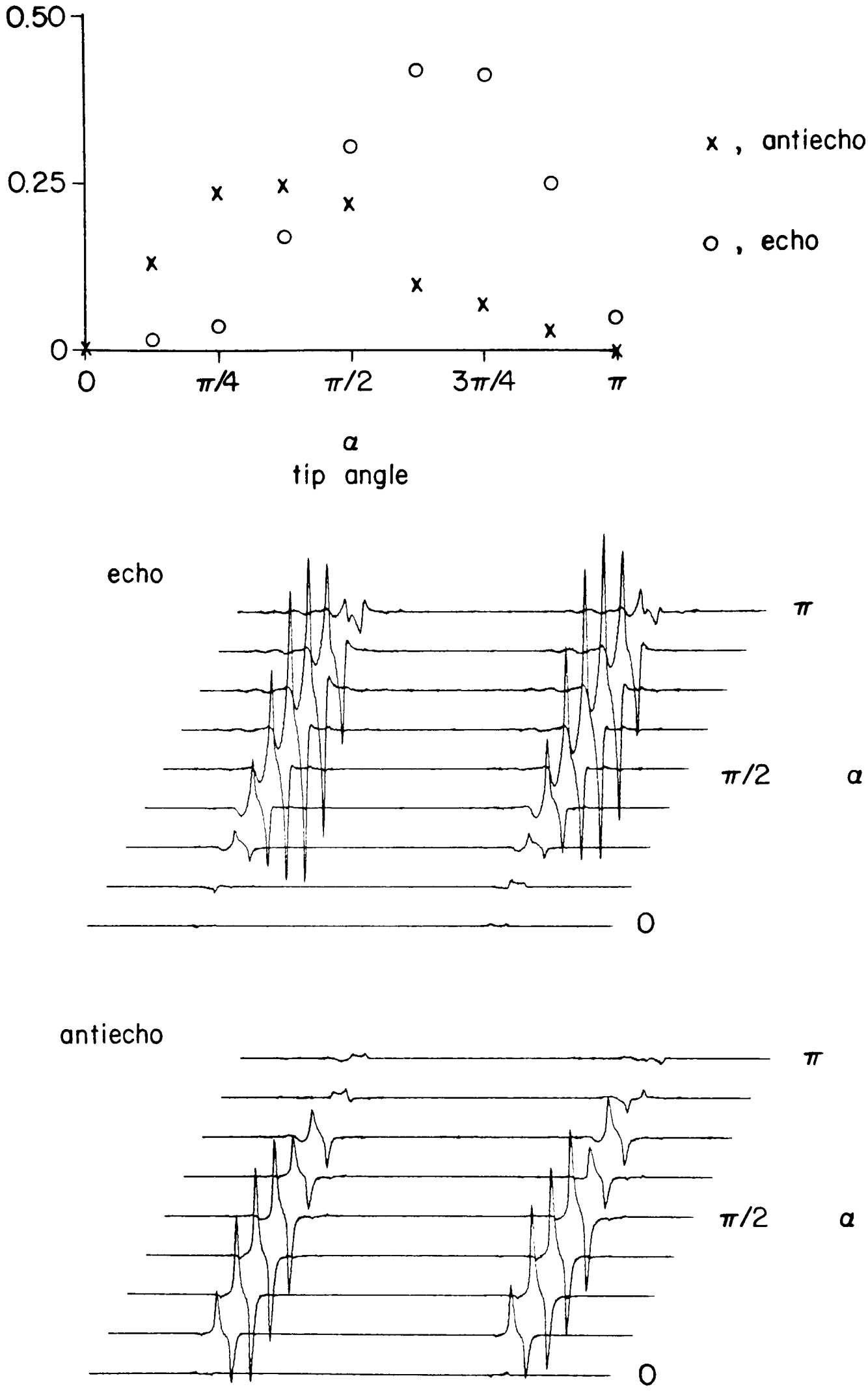

Figure 3.7 Tip angle dependence of the antiecho and echo portions of the observable magnetization for the AX spin system. Peak height versus detection pulse tip angle is shown at the top for an evolution time, t_1, was set to 0.05 sec.

have been normalized to 0.25 for the echo portion of the result for $\alpha = \frac{\pi}{2}$, $t_1 = 0$ so that the results can be compared to the theoretical curve of figure 3.4.

Evolution in an inhomogeneous field during t_1 causes a dephasing of the double quantum coherence. The detection pulse refocusses the effect of inhomogeneity for the echo portion of the observed magnetization whereas the antiecho portion continues to loose phase coherence during the detection time. This effect is illustrated in figure 3.8 for the proton AX spin system described above. The Fourier transform of the detected magnetization is plotted as a function of the evolution time, t_1. The detection time, t_2, is 2.56 secs so the coherence transfer echo for the maximum evolution time, $t_1 = 1.0$ secs, occurs within the detection interval. The spectra are plotted in the absolute value mode of display for a $\frac{\pi}{2}$ detection pulse. The refocussing effect results in an increased peak height for the echo over the antiecho portion.

A two-dimensional Fourier transformation of the time dependent signal of equation 3.26 will produce a spectrum with two resonances symmetric about $\omega_1 = 0$ at $\omega_1 = \pm\omega_{14}$ on a trace parallel to the F_1 axis at $\omega_2 = \omega_{13}$. The intensity of the two symmetrically placed resonances will depend on the value of α in the manner described by the coefficients in equation 3.26. The antiecho will appear at $\omega_1 = \omega_{14}$ and the echo at $\omega_1 = -\omega_{14}$. By choosing α other than $\frac{\pi}{2}$ it is possible to enhance the antiecho or echo while suppressing the other. In this way it is possible to discriminate the sign of the double quantum precession frequency because the antiecho represents precession in a positive and the echo precession in a negative sense with respect to precession during t_2. The echo is preferred over the antiecho because of the increased peak height in the presence of field inhomogeneity as illustrated in figure 3.8. The graph in figure 3.4 has a maximum for

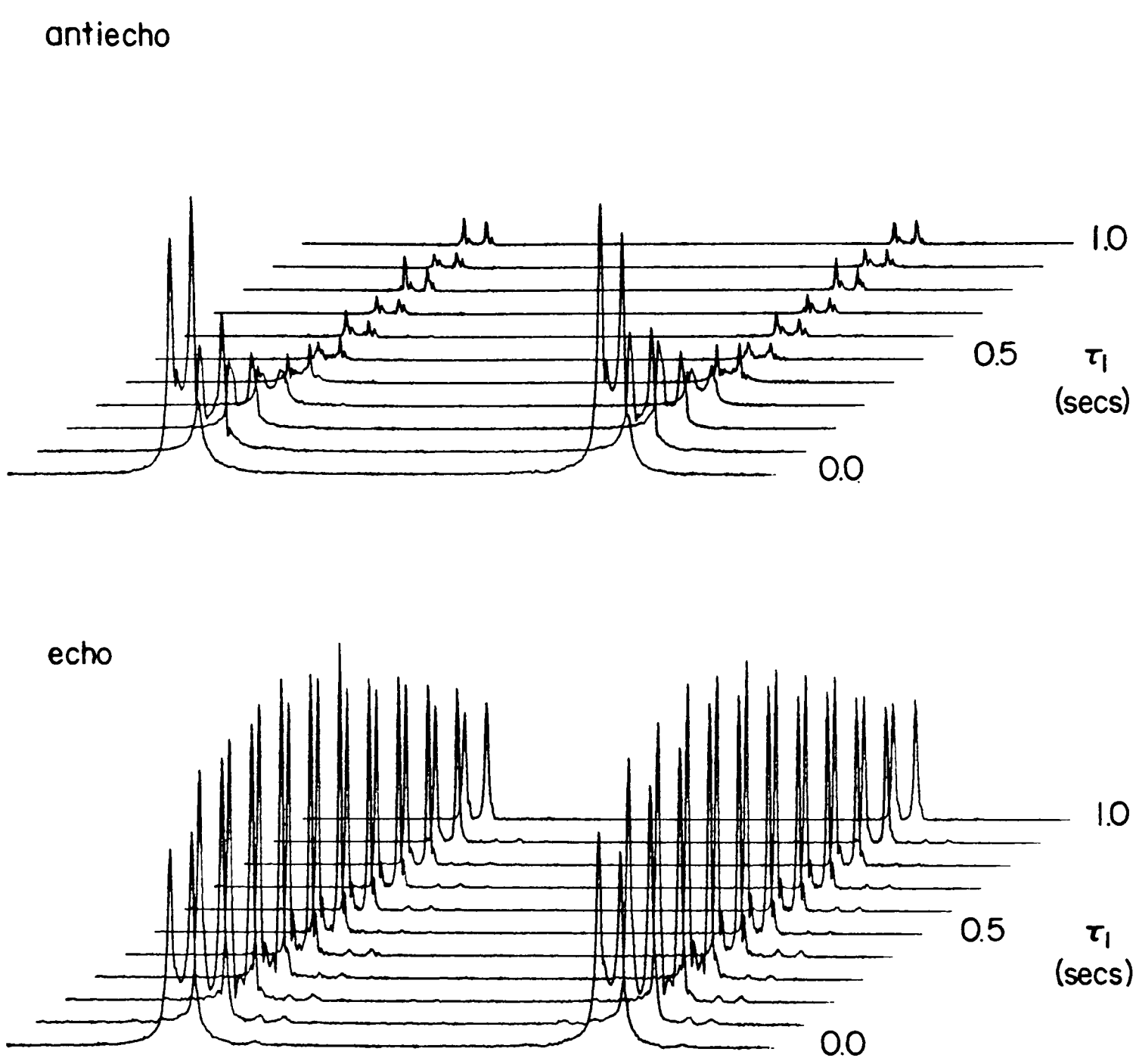

Figure 3.8 The effect of the evolution of double quantum coherence during t_1 in an inhomogeneous magnetic field. The observable magnetization for the proton AX spin system is plotted as a function of t_1. The spectra are displayed in the absolute value mode for the antiecho and echo portions with the same vertical scale.

the echo term at 120° and this value of the tip angle would give a 30% increase in the intensity of the echo peak in the two-dimensional spectrum over the same experiment with a 90° detection pulse [3.8]. If more discrimination between echo and antiecho is desired a larger tip angle can be chosen as a compromise between sensitivity and discrimination. A good choice is 135° which give a discrimination ratio of 6 to 1 between antiecho and echo peaks and still a 20% improvement in sensitivity over a 90° detection pulse if field inhomogeneity effects are not taken into consideration. This choice would provide even better discrimination in the presence of an inhomogeneous field as can be seen in figure 3.7.

Some understanding of the tip angle effect can be obtained by considering the modulation of the detected magnetization introduced by equations 3.24 and 3.25. In the two-dimensional Fourier transform process, if the F_2 spectrum is amplitude modulated by a sinusoidal function of the evolution time, the transformed F_1 trace will have peaks of equal intensity at both the positive and negative frequency of evolution. For a tip angle of $\frac{\pi}{2}$ the real part of the double quantum coherence, I_x^{14} does not transfer to observable single quantum coherence. Only the imaginary element, I_y^{14}, is transferred and the observed magnetization is amplitude modulated by $\cos\omega_{14}t_1$ hence the sign of the precession frequency during evolution cannot be determined. However for $\alpha \neq \frac{n\pi}{2}$, where n is an integer, the real part of the double quantum coherence is transferred to observable single quantum transitions leading to a phase modulation of the F_2 spectrum after the first Fourier transform. Fourier transformation of a phase modulated signal then allows discrimination of the sign of the frequency of evolution. The amount of phase and amplitude modulation present depends on the value of the tip angle as indicated by the antiecho and echo coefficients of equation 3.26.

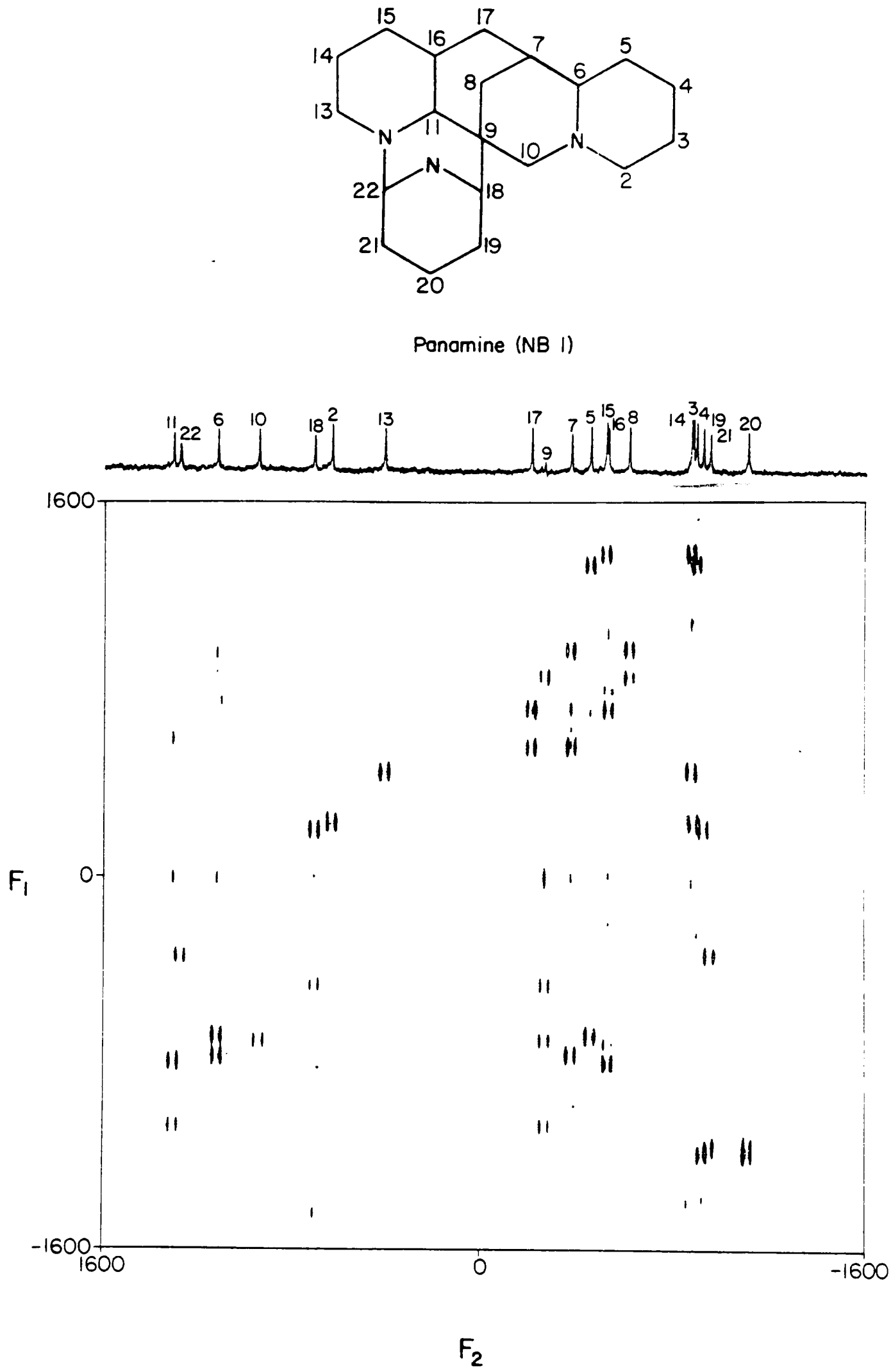

Figure 3.9 Two-dimensional carbon-carbon connectivity spectrum for panamine using the modified INADEQUATE sequence described in the text. The structure of panamine is shown at the top of the figure. The normal proton broadband decoupled carbon spectrum is included at the top of the two-dimensional spectrum.

This method of determining the sign of the double quantum frequency is illustrated by studying the carbon-carbon connectivity pattern in a natural abundance sample of panamine, an Ormosia alkaloid. The modified INADEQUATE sequence described above was used with a the tip angle of the last pulse set to 135°. The experiment was run over a period of 10 hours. The sample concentration was approximately 1.2 M. With α set to 135° responses from the antiecho are too small to appear on the contour map and it is possible to set the transmitter frequency near the centre of the carbon-13 shift range without introducing ambiguity about the sign of the double quantum frequencies.

Figure 3.9 shows the two-dimensional contour map. Each pair of directly coupled carbon atoms gives rise to a four-line AX or AB type spectrum running in the F_2 dimension, the satellites of the conventional carbon-13 spectrum (shown along the top of the chart). The F_1 ordinate of each subspectrum is the double quantum frequency, the sum of the chemical shifts of the two carbon resonances involved. Since the midpoint of each subspectrum is at the mean chemical shift in the F_2 dimension, all these midpoints must lie on a diagonal line of slope 2 passing through the origin. The spectrum has been allowed to fold to make optimum use of the data space as described in section 4.4 of chapter 4.

Although in many types of NMR experiment a 90° read pulse elicits the strongest signals, it is shown here that for the reconversion of double quantum coherence in a two-dimensional experiment larger peak heights are obtained with tip angles of either 60° for the antiecho or 120° for the echo portions. This comes about because the 90° pulse fails to convert the real component of double quantum coherence, whereas larger or smaller read pulses mix some of this real component as well as the imaginary component. Thus by an extremely simple change in the

basic INADEQUATE pulse sequence for carbon-carbon connectivity determination, larger peak heights are obtained in the two-dimensional spectrum and the signs of the double quantum frequencies are established unambiguously.

3.5. General coherence transfer formulation

A general expression for transfer among coherences of a given spin system can be derived using the formulation detailed in chapter 2. In a two-dimensional experiment assume coherence pq initially aligned along the x-axis evolves during t_1 as follows.

$$\rho(t_1) = a(I_x^{pq} \cos\omega_{pq} t_1 + I_y^{pq} \sin\omega_{pq} t_1). \qquad (3.27)$$

After a detection pulse the coherence pq has been transferred to coherence rs. The observable magnetization originating from coherence rs can be written as,

$$\begin{aligned} M_{rs,pq}(t_1,t_2) &= \langle \mu_x^{rs} \rho(t_1,t_2) \rangle + i\langle \mu_y^{rs} \rho(t_1,t_2) \rangle \\ &= \gamma\hbar [\langle I_x^{rs} \rho'(t_1) \rangle + i\langle I_y^{rs} \rho'(t_1) \rangle] e^{i\omega_{rs} t_2} \\ &= \gamma\hbar a [(\langle I_x^{rs} R I_x^{pq} R^+ \rangle \cos\omega_{pq} t_1 \\ &\quad + \langle I_x^{rs} R I_y^{pq} R^+ \rangle \sin\omega_{pq} t_1) \\ &\quad + i(\langle I_y^{rs} R I_x^{pq} R^+ \rangle \cos\omega_{pq} t_1 \\ &\quad + \langle I_y^{rs} R I_y^{pq} R^+ \rangle \sin\omega_{pq} t_1)] e^{i\omega_{rs} t_2}. \end{aligned} \qquad (3.28)$$

The transfer coefficients of table 2.1 can be used to rewrite equation 3.28 in a simplified form. After some rearrangement and combination of terms the result becomes,

$$M_{rs,pq}(t_1,t_2) = \gamma\hbar a \left[(R_{sq}R^{+}_{pr})\, e^{i(\omega_{rs}t_2 + \omega_{pq}t_1)} + (R_{sp}R^{+}_{qr})\, e^{i(\omega_{rs}t_2 - \omega_{pq}t_1)} \right]. \qquad (3.29)$$

This is a general result for any coherences of a spin system. Also the phase of the detection pulse is implicit in the operator form $R(\alpha,\emptyset)$ of equation 2.33. Thus using equation 2.37, the tip angle and phase dependence of any coherence transfer process can be considered in detail using the equation 3.29.

As an example consider the transfer of triple quantum coherence to single quantum coherence in an AMX spin system. Using the energy level diagram and numbering scheme of figure 4.1 in chapter 4, the triple quantum coherence will be denoted 18 and assume transfer to the A spin single quantum coherence 15.

The transfer coefficients can be written explicitly using equation 2.37. The antiecho term becomes,

$$R_{58}R^{+}_{11} = (-1)^{\delta_{11}}(i)^{\delta_{58}+\delta_{11}}\, e^{-i(\Delta m_{58}+\Delta m_{11})\emptyset} \times (\cos\tfrac{\alpha}{2})^{6-\delta_{58}-\delta_{11}}\, (\sin\tfrac{\alpha}{2})^{\delta_{58}+\delta_{11}}.$$

$$= -e^{-i2\emptyset}\cos^4(\tfrac{\alpha}{2})\sin^2(\tfrac{\alpha}{2}) \qquad (3.30)$$

and for the echo coefficient,

$$R_{51}R^{+}_{81} = (-1)^{\delta_{18}}(i)^{\delta_{51}+\delta_{81}}\, e^{-i(\Delta m_{51}+\Delta m_{81})\emptyset} \times (\cos\tfrac{\alpha}{2})^{6-\delta_{51}-\delta_{81}}\, (\sin\tfrac{\alpha}{2})^{\delta_{51}+\delta_{81}}.$$

$$= -e^{i4\emptyset}\cos^2(\tfrac{\alpha}{2})\sin^4(\tfrac{\alpha}{2}). \qquad (3.31)$$

Finally the observable magnetization of equation 3.29 can be written as,

$$M_{15,18}(t_1,t_2)$$

$$= \gamma\hbar a \left[- e^{-i2\phi} \cos^4(\tfrac{a}{2}) \sin^2(\tfrac{a}{2}) e^{i(\omega_{15}t_2 + \omega_{18}t_1)} \right.$$

$$\left. - e^{i4\phi} \cos^2(\tfrac{a}{2}) \sin^4(\tfrac{a}{2}) e^{i(\omega_{15}t_2 - \omega_{18}t_1)} \right]. \qquad (3.32)$$

If two experiments are performed, the dependence of the transfer coefficients on the phase of the pulse can be used to observe selectively either the antiecho or echo terms. Perform two experiments; one with $\phi = 0$ and one with $\phi = \frac{\pi}{2}$. The two experimental results can be subtracted to give the antiecho and added to give the echo portion of the observable magnetization.

Also the tip angle dependence can be used to discriminate the sign of the triple quantum precession frequency. The antiecho and echo portions of equation 3.32 are maximum at ~ 70.5° and ~ 109.5°. As the tip angle increases from 0° the antiecho portion increases to its maximum at ~ 70.5° and then decreases to zero at 180°. The echo portion initially increases more slowly than the antiecho reaching a maximum at ~ 109.5° and then decreases more rapidly to a zero at 180°. If the tip angle is chosen to be ~ 135°, the echo portion has six times the intensity of the antiecho which results in an effective sign discrimination of triple quantum precession frequency.

It is possible to generalize further the formulation to include the initial phase of the coherence at the beginning of the evolution period and the phase of the receiver. Let the phase of the coherence at the beginning of the evolution be given by the angle ε with respect to the x-axis. The density operator can be written as,

$$\rho(t_1) = a\,[(\, I_x^{pq}\cos\varepsilon + I_y^{pq}\sin\varepsilon\,)\cos\omega_{pq}t_1 + (\, I_y^{pq}\cos\varepsilon - I_x^{pq}\sin\varepsilon\,)\sin\omega_{pq}t_1]$$

$$= a\,[\, I_x^{pq}\cos(\omega_{pq}t_1 + \varepsilon) + I_y^{pq}\sin(\omega_{pq}t_1 + \varepsilon)] \qquad (3.33)$$

At the end of the evolution time a detection pulse is applied to the spin system and magnetization detected for a time t_2. For an arbitrary receiver phase setting of ξ with respect to the x-axis in the rotating frame, the observable magnetization due to coherence rs can be written as

$$M_{rs}(t_1,t_2) = \gamma\hbar\,[\langle\, (I_x^{rs}\cos\xi + I_y^{rs}\sin\xi)\;\rho(t_1,t_2)\,\rangle + i\,\langle\, (I_y^{rs}\cos\xi - I_x^{rs}\sin\xi)\;\rho(t_1,t_2)\,\rangle]$$

$$= \gamma\hbar\,[\langle I_x^{rs}\rho'(t_1)\rangle + i\langle I_y^{rs}\rho'(t_1)\rangle]\; e^{\,i(\omega_{rs}t_2 - \xi)}. \qquad (3.34)$$

Now for arbitrary phase of the initial coherence during evolution and arbitrary receiver phase equation 3.29 can be written as

$$M_{rs,pq}(t_1,t_2) = \gamma\hbar a\,[\;(R_{sq}R_{pr}^{+})\; e^{\,i(\omega_{rs}t_2 + \omega_{pq}t_1 - \xi + \varepsilon)} + (R_{sp}R_{qr}^{+})\; e^{\,i(\omega_{rs}t_2 - \omega_{pq}t_1 - \xi - \varepsilon)}\;]. \qquad (3.35)$$

This result shows that the transfer coefficients are independent of the initial phase of the coherence during evolution and receiver phase. These only enter as an overall phase factor in the final result.

It is possible to control the initial phase of the coherence at the beginning of the evolution in the following manner. Assume the spin system is initially in a state of thermal equilibrium described by density operator of equation A.15 in the appendix. The initial density operator is a function of only the z-component of spin angular momentum

for each spin. Starting from equilibrium a sequence of pulses and periods of free precession will create the system into some specific state of coherences. Write a creation sequence of this type as a general operator, C,

$$C = R(\alpha_n,\phi_n)\ e^{-iH_0\tau_{n-1}/\hbar}\ \ldots\ R(\alpha_2,\phi_2)\ e^{-iH_0\tau_1/\hbar}\ R(\alpha_1,\phi_1).$$

Now if all the pulses are phase shifted by the same amount, θ, the creation operator can be written as,

$$C(\theta) = R(\alpha_n,\phi_n+\theta)\ e^{-iH_0\tau_{n-1}/\hbar}\ \ldots\ R(\alpha_2,\phi_2+\theta)\ e^{-iH_0\tau_1/\hbar}\ R(\alpha_1,\phi_1+\theta)$$

Applying this phase shifted creation sequence to the initial density operator gives

$$\rho' = C(\theta)\ \rho_0\ C^+(\theta) = e^{-i\theta F_z}\ C\ \rho_0\ C^+\ e^{i\theta F_z} \qquad (3.36)$$

To derive the final result use has been made of the fact that the pulse operator can be written in the form of equation 2.33 and the following commutation properties have been used,

$$[\ F_z\ ,\ H_0\ ] = 0 \qquad (3.37)$$

and

$$[\ F_z\ ,\ (I_z)_j\ ] = 0 \quad , \quad \text{for any spin } j. \qquad (3.38)$$

The result of equation 3.36 is equivalent to applying a z-pulse of angle θ at the end of the creation sequence. Using the properties of phase shifts developed in section 2.4.4 the evolution of the pq coherence of the density operator can be written as,

$$\rho(t_1) = a\ [\ I_x^{pq}\cos(\omega_{pq}t_1 + \Delta m_{pq}\theta) + I_y^{pq}\sin(\omega_{pq}t_1 + \Delta m_{pq}\theta)\ ] \qquad (3.39)$$

where it has been assumed that the system is initially created into a state proportional to I_x^{pq} in the absence of phase shifts.

Following the same procedure as in equation 3.35 the observable magnetization can written as,

$$M_{rs,pq}(t_1,t_2) = \gamma\hbar a\ [\ (R_{sq}R_{pr}^{+})\ e^{i(\omega_{rs}t_2 + \omega_{pq}t_1 - \xi + \Delta m_{pq}\theta)} + (R_{sp}R_{qr}^{+})\ e^{i(\omega_{rs}t_2 - \omega_{pq}t_1 - \xi - \Delta m_{pq}\theta)}\ ]. \qquad (3.40)$$

This completes the formal description and represents quite an explicit expression for coherence transfer processes in two-dimensional spectroscopy. Two examples will illustrate the usefulness of equation 3.40.

If the sign of the precession frequency during the evolution is desired two experiments can be performed with different phase setting of the initial coherences and receiver and the results combined to cancel either the antiecho or echo portion of the observed magnetization. For the evolution of single quantum coherence during t_1 set $\xi = \theta = 0$ for the first experiment and then set $\xi = -\theta = \frac{\pi}{2}$ for the second and add the results of the two experiments. The resulting combination will contain only the echo portion of the magnetization. The two-dimensional spectrum will contain only peaks from the echo portion thus effectively determining the sign of the precession frequency. It is possible to discriminate the sign of the precession frequency during t_1 for any order of coherence with only two values of the phase shift θ assuming that ξ can be incremented in $\frac{\pi}{2}$ steps. For even order coherences it is sufficient to combine two experiments with $\theta = 0$, $\xi = 0$ and $\theta = \frac{\pi}{4}$, $\xi = -\frac{\pi}{2}$ and for odd order coherences combine two experiments with $\theta = 0$,

$\xi = 0$ and $\theta = -\xi = \frac{\pi}{2}$ to discriminate between antiecho and echo and hence determine the sign of the precession.

The phase cycling technique can also be used to discriminate between orders of coherence indirectly detected by the two-dimensional method. If a coherence of order $n = \Delta m_{pq}$ is desired, the phases θ and ξ should be cycled through a 2n step sequence. Start with $\theta = 0$ and $\xi = 0$ then increment θ by $\frac{\pi}{\Delta m_{pq}}$ and ξ by π for each step and add the result of each step of the sequence. This will remove all orders lower than n [3.7]. The zero quantum coherence must be treated differently. All orders except zero order up to and including order n can be suppressed with the same phase cycling sequence as above however to select only zero order hold ξ constant at $\xi = 0$ and add the results of each step.

Since the antiecho and echo terms of equation 3.40 have different dependence on the tip angle α, it is possible to selectively enhance or suppress portions of the coherence transfer to observable magnetization. The exact effect of a tip angle variation is dependent of the type of spin system and coherence being correlated in a two-dimensional experiment.

References

[3.1] E. L. Hahn, Phys. Rev. 80, 580 (1950)

[3.2] A. A. Maudsley, A. Wokaun and R. R. Ernst, Chem. Phys. Letters 55, 9 (1978)

[3.3] R. Freeman and G. A. Morris, J. Chem. Soc. Chem. Common., 684 (1978)

[3.4] H . Y. Carr and E. M. Purcell, Phys. Rev. 94, 630 (1954)

[3.5] G. Bodenhausen and R. Freeman, J. Magn. Reson. 36, 221 (1979)

[3.6] A. Bax and R. Freeman, J. Magn. Reson. 44, 542 (1981)

[3.7] A. Wokaun and R. R. Ernst, Chem. Phys. Letters 52, 407 (1977)

[3.8] T. H. Mareci and R. Freeman, J. Magn. Reson. 48, 158 (1982)

[3.9] A. Bax, R. Freeman and S. P. Kempsell, J. Amer. Chem. Soc. 102, 4849 (1980)

[3.10] A. Bax, R. Freeman, T. A. Frenkiel and M. H. Levitt, J. Magn. Reson. 43, 478 (1981)

Chapter 4

Homonuclear correlation through double quantum coherences

4.1. Introduction

Since the first observation of scalar coupling in liquid samples [4.1], NMR has been able to provide a great deal of information about molecular structure. Scalar coupling constants along with chemical shifts reflect the electronic and spatial character of molecular structure. In simple systems chemical shift and coupling information can often lead to an unambiguous assignment of the spectrum. This is possible when there is no overlap of spin multiplets that would obscure the identification of coupling patterns. Most commercial NMR spectrometer manufacturers provide computer programs which can calculate and iteratively fit high resolution spectra of up to 6 or 7 spins so chemical shifts and coupling constants can be determined to within experimental error. In more complex systems double resonance techniques for specific spin decoupling allow the system to be probed and coupling patterns mapped. In large molecules which have crowded spectra, it is often impossible to decouple only one spin because of multiplet overlap. This makes the information obtained by double resonance techniques difficult to interpret.

Several approaches have been taken to overcome the problems of assignment in crowded spectra. Recently there has been an effort to construct spectrometers with stronger static magnetic fields. As the magnitude of the field increases the chemical shift difference between coupled spins increases linearly with the field while the coupling

remains the same. This reduces strong coupling effects and minimizes overlap of multiplet structure. This approach has made possible the study of molecules as large as small proteins [4.2]. However with the field strengths currently available many systems still present difficulties in interpreting crowded spectra with a great deal of multiplet overlap.

The introduction of two-dimensional Fourier transform spectroscopy [4.3,4.4] has provided perhaps the greatest advantage in separating complex coupling patterns in crowded NMR spectra. The two-dimensional technique spreads the chemical shift and coupling information over a surface in two frequency dimensions while maintaining the same basic resolution as a one-dimensional Fourier transform spectrum. In the case of the two pulse sequence originally proposed by Jeener [4.3], the coupling pattern of a homonuclear spin system is mapped out in one experiment by correlating single quantum coherences among coupled spins. In most cases this allows direct assignment of even complex coupling patterns by examination of the two-dimensional spectrum. Problems are encountered when the chemical shift difference between coupled spins is small for in this case spin multiplets of the Jeener spectrum can be obscured by peaks on the main diagonal. Also ambiguities can occur when two or more pairs of coupled spins have overlapping multiplets centered around the same frequency in F_2. These could continue to overlap in the two-dimensional spectrum making specific assignment difficult.

Bax and Freeman have recently shown that a modification of the basic sequence proposed by Jeener can simplify the assignment of correlations and furnish information on the relative signs of coupling constants [4.5]. By reducing the tip angle of the second pulse in a Jeener sequence from $\frac{\pi}{2}$ to $\frac{\pi}{4}$ the amount of coherence transfer is decreased. As discussed in chapter 3, this change in the tip angle

minimizes transfer to peaks within a multiplet lying on the main diagonal thus allowing correlation of coupled spins closer together. The main diagonal peaks are still the same magnitude as cross peaks among coupled spins so correlations close to the diagonal can be somewhat obscured by overlap with diagonal peaks.

It is possible to remove 'diagonal' peaks entirely from two-dimensional correlation spectrum of homonuclear spin systems. This can be accomplished by correlating multiple quantum coherences with detectable single quantum coherences in a two-dimensional spectrum [4.6]. The spectrum resulting from the Jeener sequence will contain diagonal peaks corresponding to autocorrelation of spins or peaks from solvents such as water. The multiple quantum correlation spectrum contains no autocorrelation peaks or peaks from solvents that cannot be excited into states containing multiple quantum coherence so no 'diagonal' peaks will appear. This alleviates the problem of assigning a coupling between spins separated by a small chemical shift differences which would lie close to the main diagonal in a Jeener spectrum.

In previous applications of multiple quantum correlation [4.6,4.7], the coherences of interest have been excited by appling two $\frac{\pi}{2}$ pulses separated by a delay to allow J-modulation. The amount of multiple quantum coherence created by this method will depend on both the chemical shifts and coupling constants so the technique may not provide broadband excitation. Also a pulse of $\frac{\pi}{2}$ has been used to indirectly detect multiple quantum coherences after a period of evolution. A $\frac{\pi}{2}$ pulse will transfer coherence evenly to all the spins forming a coupled system. In this case all the spins will 'see' all the multiple quantum coherences of a particular order thus no specific correlation with particular spins is possible in a complex system. Specific deuterium enrichment [4.7] has been used to allow correlation of zero quantum

coherences in a proton system by isolating pairs of spins. However this is not a practical approach to take with all molecular systems. Also it is not possible to discriminate between observable magnetization derived from zero quantum coherence and z-magnetization by cycling the phases of pulses and receiver. In the two-dimensional spectrum, z-magnetization present during evolution will appear parallel to F_2 at $F_1 = 0$. Zero quantum peaks lying close to $F_1 = 0$ can be obscured by peaks from z-magnetization making assignment difficult.

In this chapter the correlation of single and double quantum coherences in a homonuclear spin system will be studied in detail for the modified INADEQUATE pulse sequence [4.8] which provides broadband excitation of double quantum coherences. It will be shown that with a proper choice of tip angle for the detection pulse it is possible to correlate double quantum coherences with only the two spins which flip in the double quantum transition. Thus it will be possible to assign correlations in a coupled spin system based on the indirectly detected double quantum transition for two spins. Let the double quantum coherence between two spins, say A and M, be denoted as double quantum coherence AM. A notation of this form will also be used for zero quantum coherence. Also denote the order of a coherence 'rs' as $\Delta m_{rs} = m_r - m_s$. Thus coherences which involve the flip of two spins will be of order zero if $\Delta m_{rs} = 0$ and of double quantum order if $\Delta m_{rs} = 2$.

Correlation through double quantum coherences also has the advantage of reducing the fine structure due to coupling in the two-dimensional spectrum thus reducing the amount of multiplet overlap in a crowded spectrum. For example there would be 144 possible peaks observable in a Jeener spectrum of an AMX spin system. The corresponding double quantum correlation spectrum can have a maximum of

only 72 peaks. Both spectra contain the same amount of information about coupling within the spin system so the double quantum experiment has the potential of simplifying the assignment of complex coupling patterns in homonuclear spin systems.

Double quantum correlation has already proved useful for ^{13}C–^{13}C correlation in natural abundance [4.9]. The INADEQUATE sequence [4.9] allows the mapping of connectivity of the carbon skeleton in organic molecules. A modified INADEQUATE sequence [4.8] has been discussed in chapter 3 which allows discrimination of the sign of the double quantum frequency and improves sensitivity in the two-dimensional carbon-carbon experiment.

In this chapter the modified INADEQUATE sequence,

$$(\tfrac{\pi}{2})_x - \tau - (\pi)_y - \tau - (\tfrac{\pi}{2})_x - t_1 - (\alpha)_\phi - \text{detect}_\xi$$

will be applied to the study of more complicated homonuclear spin systems. The detection pulse and receiver phase are cycled to suppress all signals except those transferred from double quantum order [4.9]. An additional $\frac{\pi}{4}$ z-pulse at the beginning of evolution will be used to provide sign discrimination of the double quantum frequencies [4.10]. The excitation and detection of double quantum coherence in an AMX spin system will be considered in detail and the results illustrated for a proton AMX spin system. The AMX system exhibits important properties of a system of coupled nonequivalent spin-1/2 nuclei and the basic ideas can be extended to more complicated systems. Practical application to a spin system with more complex coupling is considered for proton-proton correlation in the spectrum of a tricyclodecane derivative.

energy level diagram

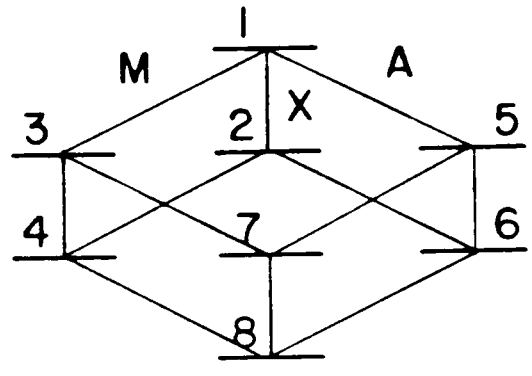

single quantum transitions

spin A	spin M	spin X
15, $\omega_A + \pi(J_{AM}+J_{AX})$;	13, $\omega_M + \pi(J_{AM}+J_{MX})$;	12, $\omega_X + \pi(J_{AX}+J_{MX})$
26, $\omega_A + \pi(J_{AM}-J_{AX})$;	24, $\omega_M + \pi(J_{AM}-J_{MX})$;	34, $\omega_X + \pi(J_{AX}-J_{MX})$
37, $\omega_A - \pi(J_{AM}-J_{AX})$;	57, $\omega_M - \pi(J_{AM}-J_{MX})$;	56, $\omega_X - \pi(J_{AX}-J_{MX})$
48, $\omega_A - \pi(J_{AM}+J_{AX})$;	68, $\omega_M - \pi(J_{AM}+J_{MX})$;	78, $\omega_X - \pi(J_{AX}+J_{MX})$

zero quantum transitions

AM	AX	MX
35, $\omega_A-\omega_M + \pi(J_{AX}-J_{MX})$;	25, $\omega_A-\omega_X + \pi(J_{AM}-J_{MX})$;	23, $\omega_M-\omega_X + \pi(J_{AM}-J_{AX})$
46, $\omega_A-\omega_M - \pi(J_{AX}-J_{MX})$;	47, $\omega_A-\omega_X - \pi(J_{AM}-J_{MX})$;	67, $\omega_M-\omega_X - \pi(J_{AM}-J_{AX})$

double quantum transitions

AM	AX	MX
17, $\omega_A+\omega_M + \pi(J_{AX}+J_{MX})$;	16, $\omega_A+\omega_X + \pi(J_{AM}+J_{MX})$;	14, $\omega_M+\omega_X + \pi(J_{AM}+J_{AX})$
28, $\omega_A+\omega_M - \pi(J_{AX}+J_{MX})$;	38, $\omega_A+\omega_X - \pi(J_{AM}+J_{MX})$;	58, $\omega_M+\omega_X - \pi(J_{AM}+J_{AX})$

triple quantum transitions

AMX

18, $\omega_A+\omega_M+\omega_X$

combination line transitions

27, $\omega_A+\omega_M-\omega_X$; 36, $\omega_A-\omega_M+\omega_X$; 45, $-\omega_A+\omega_M+\omega_X$

Figure 4.1 Energy level diagram and transition frequencies for an AMX spin system of three nonequivalent spin-1/2 nuclei.

4.2. Excitation of double quantum coherence in an AMX spin system

The energy level diagram and transition frequencies for an AMX spin system are illustrated in figure 4.1. The numbering scheme follows the lexicographical ordering [4.11]. The homonuclear AMX spin system provides a good model for study of the excitation of double quantum coherence in a system of nonequivalent spin-1/2 nuclei. The ideas developed for the AMX system can be extended to any number of nonequivalent spins in a straight forward fashion. If the spins are weakly coupled, the X-approximation [4.11] allows decomposition of the system into a number of two spin subsystems. Each pair of spins can be represented by a four level subsystem for every possible state of the other spins in the system. For example in the AMX system any pair of spins can be represented by two subsystems of four levels, one for each possible state of the third spin. Each four level subsystem forms a face of the energy level diagram cube represented in figure 4.1.

It was shown in section 2.5 that operator combinations of transverse coherence associated with different spins forming a coupled pair commute unless one of the operator combinations is in antiphase. The operator combinations which do not commute form a cyclic commutation relationship and can be interpreted in a vector picture of the type shown in figure 2.6. The vector rotation properties can be used to follow the excitation of a spin system initially in a state containing coherences in antiphase. The rotations represent a transformation among orders of coherence hence a pulse to single quantum coherences in antiphase would transform these coherences to a combination of coherences with zero and double quantum order.

The modulation of a spin echo by scalar coupling following a Carr-Purcell pulse sequence [4.12] can be used to prepare the system into a state with coherences in antiphase. The spin echo is independent of

offset frequency and static field inhomogeneity so the modulation is only dependent on the value of the coupling constants among the spins. All three spins of an AMX system are modulated in a similar fashion so consider only the A spin coherences of figure 4.1 following a Carr-Purcell sequence,

$$(\frac{\pi}{2})_x - \tau - (\pi)_y - \tau.$$

If the system is assumed initially to be in thermal equilibrium, the A spin part of the density operator at time 2τ can be written as,

$$\begin{aligned}\rho(2\tau) = a\,[&- (I_y^{15} + I_y^{26} + I_y^{37} + I_y^{48})\cos(2\pi J_{AM}\tau)\cos(2\pi J_{AX}\tau) \\ &+ (I_y^{15} - I_y^{26} - I_y^{37} + I_y^{48})\sin(2\pi J_{AM}\tau)\sin(2\pi J_{AX}\tau) \\ &- (I_x^{15} + I_x^{26} - I_x^{37} - I_x^{48})\sin(2\pi J_{AM}\tau)\cos(2\pi J_{AX}\tau) \\ &- (I_x^{15} - I_x^{26} + I_x^{37} - I_x^{48})\cos(2\pi J_{AM}\tau)\sin(2\pi J_{AX}\tau)\,] \qquad (4.1)\end{aligned}$$

The coefficient 'a' includes the appropriate Boltzmann population factors. The first line in square brackets represents the total y-component of spin A, $(I_y)_A$, amplitude modulated by the product of the cosines of the coupling constants of spin A to the other spins. The final three lines have coherences in antiphase. When a particular combination of two coherences appear in antiphase the combination is amplitude modulated by the sine of the coupling constant between the appropriate two spins. The two coherences are modulated by the cosine of the coupling constant if they are in phase. The last two lines are modulated by the product of a sine and cosine term because the antiphase components are associated with one coupling constant and the in-phase components with the other. The modulation in the third line is opposite to the modulation in the fourth hence the order of sine and cosine is

reversed. Finally, the second line is modulated by sine terms because both possible combinations are in antiphase. For a system of more than three nonequivalent spins the modulation would include multiplicative factors involving the sine or cosine of the coupling constants to additional spins dependent of the relative phases of the coherence.

At time 2τ a $(\frac{\pi}{2})_x$ pulse is applied to the J-modulated system. The pulse can be considered as a cascade of pulses [4.13] to each spin individually as discussed in chapter 2. The first line in equation 4.1 is unaffected by a pulse to the M and X spins. A rotation of $\frac{\pi}{2}$ about $(I_x)_A$ transforms this line into $(I_z)_A$. The third and fourth lines in equation 4.1 are unchanged by a pulse to the A spin. In addition the third line is not rotated by a pulse to the X spin because coherences 15 and 26 are in phase as are 37 and 48. The fourth line is not affected by a pulse to the M spin because the coherences 15, 37 and 26, 48 which are affected by the pulse are in phase. Therefore the third line is only rotated about $(I_x)_M$ and the fourth only rotated about $(I_x)_X$. The result of these rotations can be predicted from figure 2.6. The A spin coherences of the third and fourth lines are rotated into zero and double quantum y-coherences. The second line is affected by a pulse to all three spins and the method is to consider first a pulse to the A spin followed by a pulse to the M then X spin. Figure 2.6a shows that the y-components of coherence are rotated into z-components. From equation 2.151 these z-components can be written in terms of z-components for the M spin. Now a pulse to the M spin rotates these M spin z-components into M spin y-coherences. A pulse to the X spin rotates the M spin y-coherences into x-components of zero and double quantum coherence. Finally the density operator after the pulse can be written as,

$$\rho_+(2\tau) = a\,[\,-(I_z^{15} + I_z^{26} + I_z^{37} + I_z^{48})\cos(2\pi J_{AM}\tau)\cos(2\pi J_{AX}\tau)$$

$$-(I_x^{14} - I_x^{58} - I_x^{23} + I_x^{67})\sin(2\pi J_{AM}\tau)\sin(2\pi J_{AX}\tau)$$

$$+(I_y^{17} + I_y^{28} - I_y^{35} - I_y^{46})\sin(2\pi J_{AM}\tau)\cos(2\pi J_{AX}\tau)$$

$$+(I_y^{16} + I_y^{38} - I_y^{25} - I_y^{47})\cos(2\pi J_{AM}\tau)\sin(2\pi J_{AX}\tau)] \qquad (4.2)$$

Similar results can be obtained for the M and X spins. For spin A, the $(\frac{\pi}{2})_x$ pulse creates the y-component of double quantum coherences AM and AX and x-component of double quantum coherence MX. In general for a particular spin the pulse creates y-components of double quantum coherence associated with that spin and x-components of the double quantum coherence between the other two spins. Without considering the J dependent amplitude factors for the moment, calculations for the other spins show that the y-component of a particular double quantum coherence is created with the same sign on each spin.

The result shown in equation 4.2 indicates that the double quantum coherences 14 and 58 between spin M and X can be created even though the coupling constant, J_{MX}, may be vanishingly small. For correlation based on double quantum coherences to be meaningful it must reflect the coupling pattern within the spin system. It will be shown in the next section that the MX double quantum coherences will be indirectly observable through the M and X spin single quantum coherences only if there is a resolvable coupling between the M and X spins in the F_2 spectrum. Thus a false correlation will not appear on these spins. Even in the absence of a resolvable coupling between the M and X spins the MX double quantum coherence will be observable through the A spin single quantum coherences. This type of indirect correlation can cause confusion in complicated spin systems. However this correlation can be suppressed with a proper choice of tip angle for the detection pulse. Thus no correlation between two spins will appear without a resolvable

coupling constant connecting these spins in the directly detected F_2 spectrum. The dependence of the observable magnetization on the detection pulse will be studied in the next section.

The creation of double quantum coherence has a complicated dependence on the values of the coupling constants. The choice of time 2τ will determine the relative magnitude of the double quantum coherences indirectly observable in a two-dimensional spectrum. If two coupling constants have the same magnitude or are related as integer multiples, it is possible to suppress the corresponding double quantum coherences. If the third coupling constant is sufficiently different from the others only a double quantum coherence for the two spins coupled through the third coupling constant will be observed in the two-dimensional spectrum. In this way it may be possible to reduce the amount of information and thus simplify the assignment of a complicated coupling pattern using the correlation of single and double quantum coherences. An example of J-dependent suppression will be given in the next section after the a discussion of the process of indirect detection.

The third pulse also creates zero quantum coherences with the same dependence on the J-modulation. The y-component of a particular zero quantum coherence is created with opposite phase for each of the two spins of the coherence. In the case where the two contributions to a double quantum element add the corresponding zero quantum element would subtract with a reduction in the amount created. In the limit where two of the spins effectively see no coupling to a third spin, no zero quantum coherence would be created and the system could be described as the isolated two spin system treated at the end of chapter 2. In a system with relatively small coupling to one of the spins, this limit would prevent the assignment of a coupling pattern through zero quantum

coherence for this pulse sequence. Double quantum coherence would be strongly created in this case, providing a good medium for the identification of coupling patterns.

4.3. Indirect detection of double quantum coherence in an AMX spin system

After a period of evolution, double quantum coherence is transferred to observable single quantum coherence by a detection pulse. At this point information about the evolution of the double quantum coherences is reflected in amplitude and phase modulation of the observable magnetization. Two-dimensional Fourier transformation of the detected signal allows the correlation of double and single quantum coherences to be mapped in a two-dimensional spectrum.

For an AMX spin system each double quantum transition frequency involves the sum of the offset frequencies for two nonequivalent spins plus or minus the sum of the coupling constants of these two spins to the other spin in the system. There are a total of six double quantum transitions, two for each pair of spins. Coherence transfer from each of the two double quantum transitions associated with a pair of spins is the same for each of the possible spin pairings. Hence only one exemplary pair of double quantum coherences will be treated to illustrate the result.

Consider the two spins A and M. The pair of double quantum coherences associated with these two spins are denoted 17 and 28 in the numbering scheme of figure 4.1. The result of the coherence transfer to observable single quantum coherence can be calculated directly using equation 3.35. However it is instructive to study in detail the transfer process using a more indirect approach and then use equation 3.35 to obtain the final result. This will aid in the interpretation of

the direct calculation using equation 3.35. With the pulse cascade approach, transfer of the I_x^{17} component to observable single quantum coherence can be written as follows for a detection pulse of tip angle α applied to the x-axis.

$$\left(e^{-i\alpha F_x} I_x^{17} e^{i\alpha F_x} \right)_{obs.}$$

$$= \frac{1}{2} \sin\alpha \cos\alpha \left[(-I_y^{15} + I_y^{37})\cos^2(\tfrac{\alpha}{2}) + (-I_y^{26} + I_y^{48})\sin^2(\tfrac{\alpha}{2}) \right.$$

$$\left. + (-I_y^{13} + I_y^{57})\cos^2(\tfrac{\alpha}{2}) + (-I_y^{24} + I_y^{68})\sin^2(\tfrac{\alpha}{2}) \right]$$

$$+ 2 \sin^3(\tfrac{\alpha}{2})\cos^3(\tfrac{\alpha}{2}) \; (I_y^{12} - I_y^{34} - I_y^{56} + I_y^{78}). \qquad (4.3)$$

The I_x^{17} component is transferred to the A and M single quantum coherences in the same manner. The coherence transfer to either spin A or M can be seen to depend on the state of spin X. For the X spin in the state with $(m_z)_X = +\frac{1}{2}$ the 17 double quantum transition is directly associated with a two spin energy level diagram involving only levels 1, 3, 5 and 7. This association is analogous to the relationship of the double quantum coherence to single quantum coherences for a system of two coupled spins in isolation. The 17 coherence transfers to coherences of the system of levels 1, 3, 5 and 7 in the same way for both spins with the A coherences in antiphase and the M coherences in antiphase. The 17 coherence also transfers to the coherences of the other two-spin energy level diagram for $(m_z)_X = -\frac{1}{2}$ formed by levels 2, 4, 6 and 8. The 17 coherence is indirectly associated with this system and transfer to the single quantum coherences has a different tip angle dependence compared to the system with $(m_z)_X = +\frac{1}{2}$. Again the coherences of spin A and M are in antiphase. The I_x^{17} component transfers to the X spin single quantum coherences with the same tip angle dependence for all elements. It was pointed out in the last

section that the x-component of 17 coherence could be created even in the absence of a resolvable AM coupling. However the result in equation 4.3 shows that this coherence would not be detectable through the A or M single quantum coherences without a resolvable coupling constant, J_{AM}. Hence a false correlation will not occur. Since the 17 x-component is transferred to the X spin independently of J_{AM} this double quantum will be observable on spin X.

The complete specification of the transfer process will require consideration of double quantum coherence transfer to three types of single quantum coherence. Two are associated with either the A or M spins which contribute their offset frequencies to the double quantum precession frequency. The first has $(m_z)_X = +\frac{1}{2}$ and consider coherence 15 as an example. The second has $(m_z)_X = -\frac{1}{2}$ and consider the 26 coherence to illustrate the result. The third type of single quantum coherence involves the X spin which does not contribute its offset frequency to the rate of double quantum precession. Coherence 12 will be used to illustrate the third type of coherence transfer.

The coherence transfer for the I_y^{17} component can also be calculated using the technique of a pulse cascade. The result for observable single quantum coherences is given by,

$$\left(e^{-i\alpha F_x} I_y^{17} e^{i\alpha F_x} \right)_{obs.}$$

$$= \frac{1}{2}\sin\alpha \left[(I_x^{15} - I_x^{37})\cos^2(\tfrac{\alpha}{2}) + (I_x^{26} - I_x^{48})\sin^2(\tfrac{\alpha}{2}) \right.$$

$$\left. + (I_x^{13} - I_x^{57})\cos^2(\tfrac{\alpha}{2}) + (I_x^{24} - I_x^{68})\sin^2(\tfrac{\alpha}{2}) \right]. \qquad (4.4)$$

The I_y^{17} component is transferred to the single quantum coherence associated with only spin A and M. The transfer process for I_y^{17} can be consider^ed as of two types for either the A or M spin with $(m_z)_X = +\frac{1}{2}$ or

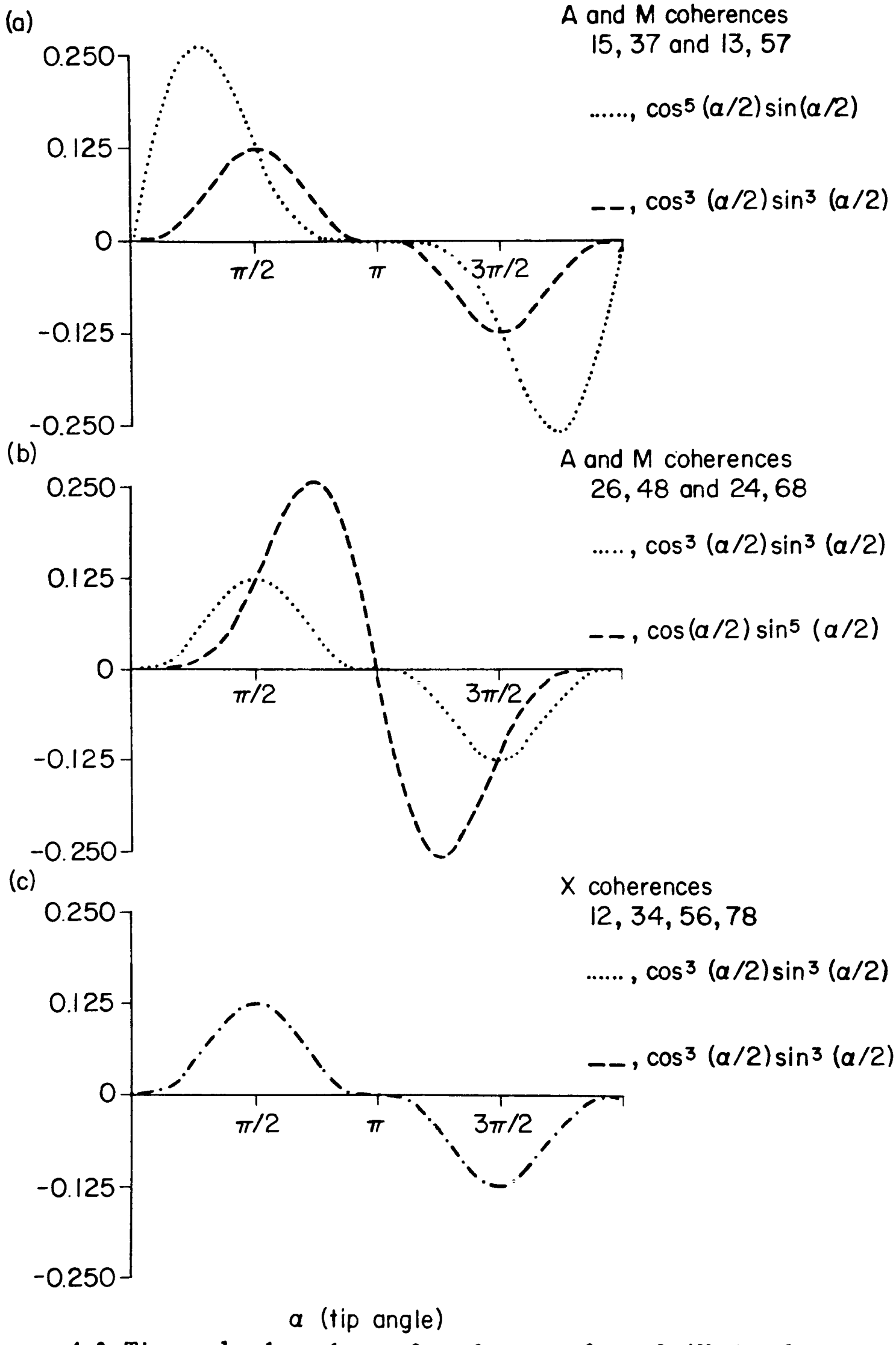

Figure 4.2 Tip angle dependence for the transfer of AM double quantum coherence 17 to single quantum coherences in an AMX spin system. (a) Transfer to A and M coherences with $(m_z)_X = +1/2$. (b) Transfer to A and M coherences with $(m_z)_X = -1/2$. (c) Transfer to X coherences. For each graph, the echo portion is represented by the dashed curve and the antiecho by the dotted curve.

$(m_z)_X = -\frac{1}{2}$ as outlined above.

After the coherence transfer process the observable magnetization due to each element of single quantum coherence can be written directly using equation 3.35. The results of equations 4.3 and 4.4 provide a general guide to the transfer process for specific single quantum coherences. Since both x- and y-components of double quantum coherence are created by the INADEQUATE sequence, let ε denote the initial phase angle of the 17 coherence at the beginning of the evolution period. Assume the detector phase ξ is set to zero and that the detection pulse is applied along the x-axis so the pulse phase, $\emptyset$, is equal to zero.

Using equation 3.35 with the above results, the observable magnetization due to the A spin coherence 15 can be written as,

$$M_{15,17}(t_1,t_2)$$

$$= \gamma\hbar ai \left[\cos^5(\tfrac{\alpha}{2}) \sin(\tfrac{\alpha}{2}) \, e^{i(\omega_{15}t_2 + \omega_{17}t_1 + \varepsilon)} \right.$$

$$\left. - \cos^3(\tfrac{\alpha}{2}) \sin^3(\tfrac{\alpha}{2}) \, e^{i(\omega_{15}t_2 - \omega_{17}t_1 - \varepsilon)} \right]. \qquad (4.5)$$

This represents coherence transfer to the A spin states with the X spin in the state $(m_z)_X = +\frac{1}{2}$. The tip angle dependence of the antiecho and echo portions of equation 4.5 are plotted in figure 4.2.a.

The observable magnetization due to the A spin coherence 26 is given by,

$$M_{26,17}(t_1,t_2)$$

$$= \gamma\hbar ai \left[\cos^3(\tfrac{\alpha}{2}) \sin^3(\tfrac{\alpha}{2}) \, e^{i(\omega_{26}t_2 + \omega_{17}t_1 + \varepsilon)} \right.$$

$$\left. - \cos(\tfrac{\alpha}{2}) \sin^5(\tfrac{\alpha}{2}) \, e^{i(\omega_{26}t_2 - \omega_{17}t_1 - \varepsilon)} \right]. \qquad (4.6)$$

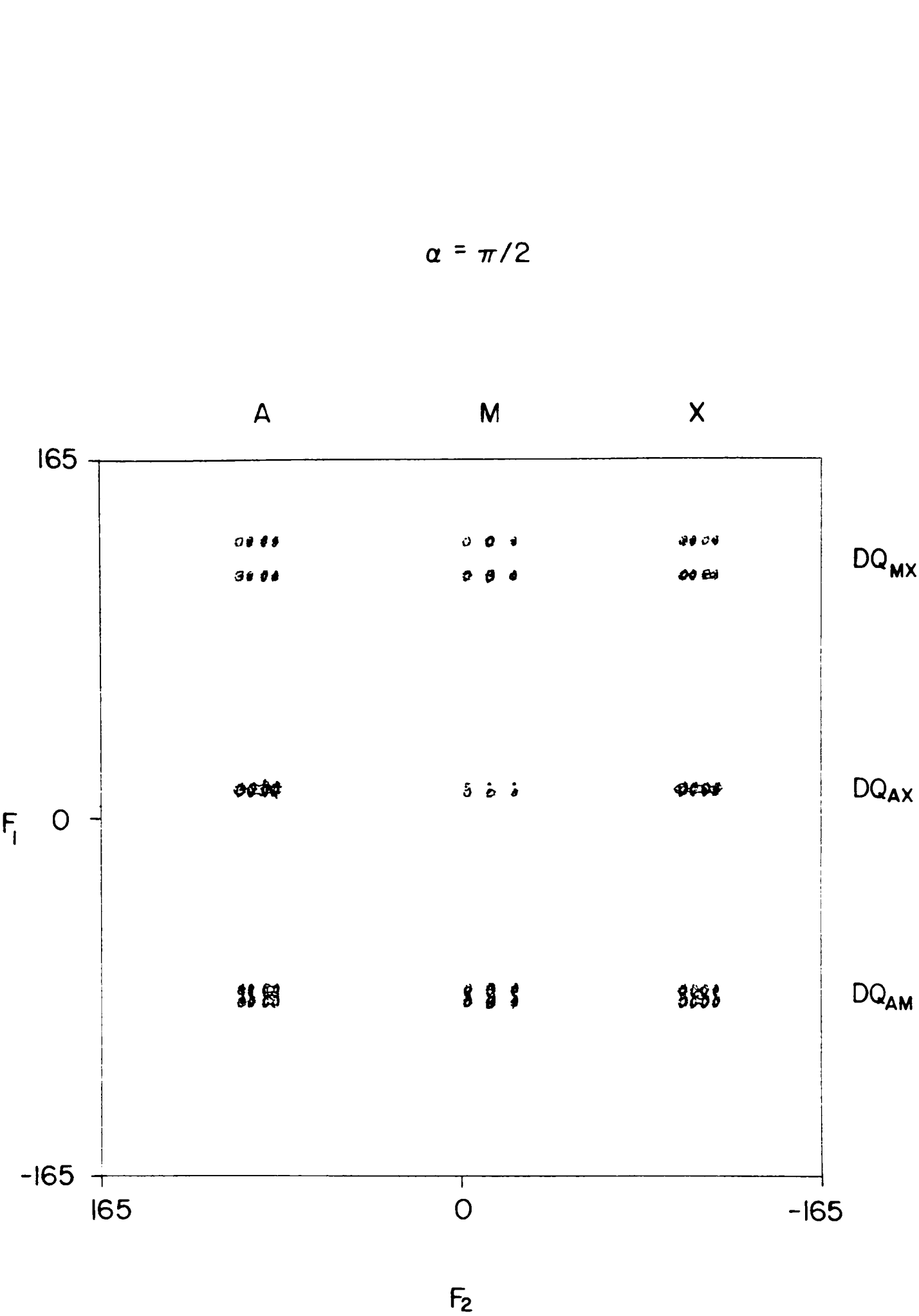

Figure 4.3 Contour plot of the two-dimensional spectrum for the proton AMX spin system 2,3-dibromopropionic acid in benzene-d_6. Tip angle of the detection pulse set equal to $\pi/2$. Single quantum frequencies are in the F_2 dimension and double quantum frequencies lie parallel to the F_1 axis.

The antiecho and echo portions are plotted in figure 4.2.b. This represents coherence transfer to A spin states with spin X in the state $(m_z)_X = -\frac{1}{2}$.

Finally for the X spin, the observable magnetization due to coherence 12 can be expressed as,

$$M_{12,17}(t_1,t_2)$$

$$= -\gamma\hbar ai \left[\cos^3(\tfrac{\alpha}{2}) \sin^3(\tfrac{\alpha}{2}) \, e^{i(\omega_{12}t_2 + \omega_{17}t_1 + \varepsilon)} \right.$$

$$\left. + \cos^3(\tfrac{\alpha}{2}) \sin^3(\tfrac{\alpha}{2}) \, e^{i(\omega_{12}t_2 - \omega_{17}t_1 - \varepsilon)} \right]. \qquad (4.7)$$

The tip angle dependence of the antiecho and echo is plotted in figure 4.2.c.

The initial phase, ε, of the double quantum coherence is represented in the final results as an overall phase factor. In the display of two-dimensional spectra in absolute value mode the peak height is independent of the relative phase of the resonance so the x- and y-components of the double quantum elements will contribute equally.

In general the coherence transfer process for the other double quantum coherence, 28, is identical to that for coherence 17 except that the results for transfer to coherence 15 and 26 are reversed.

For α equal to an odd integer multiple of $\frac{\pi}{2}$, figure 4.2 indicates that the double quantum coherence is transferred evenly to all the single quantum coherences of the coupled system. A specific identification of a double quantum coherence with a particular spin pair is not possible in a two-dimensional spectrum for these values of the tip angle because double quantum coherence is transferred evenly to all spins forming a coupling pattern. As an example the result for an AMX

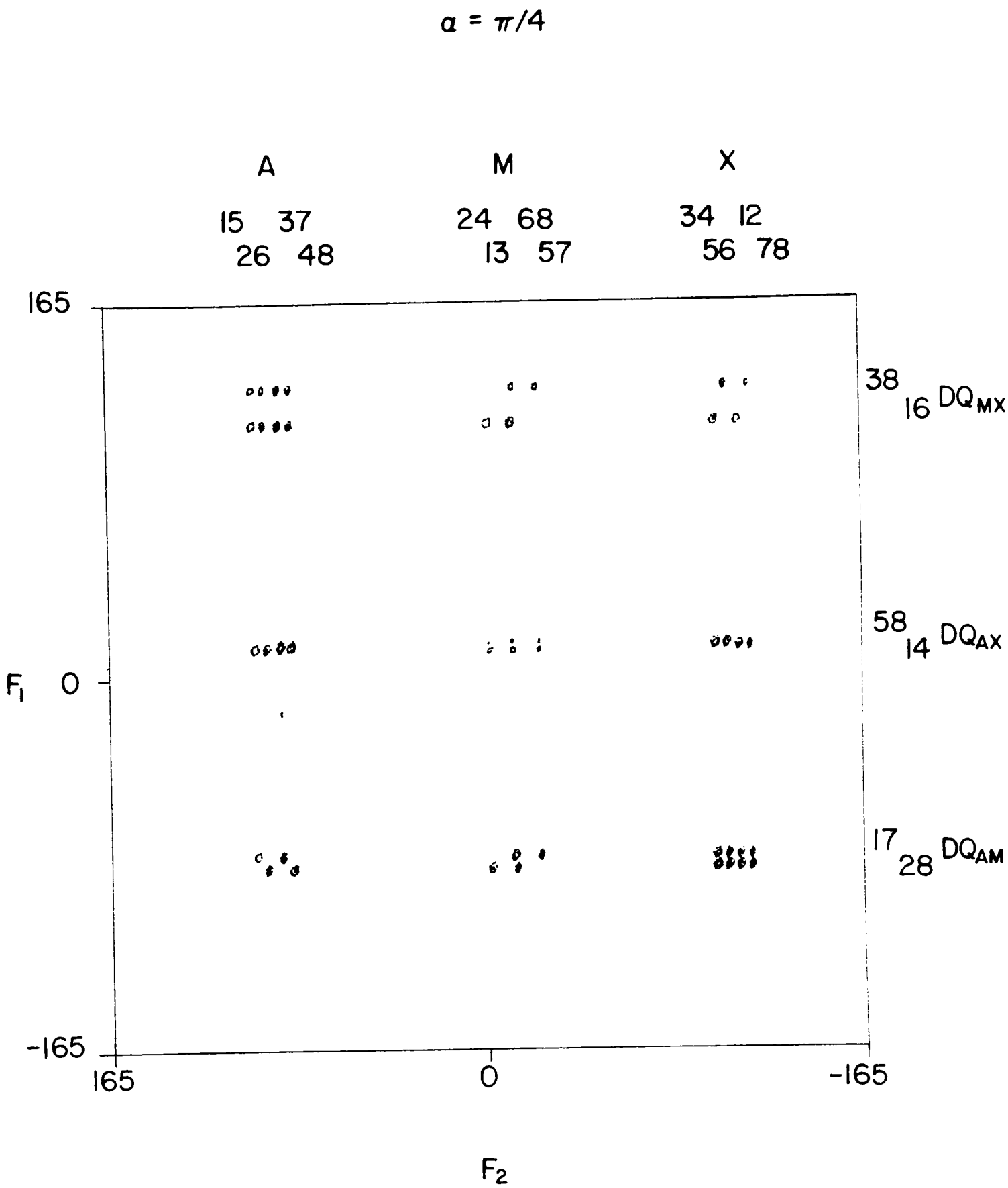

Figure 4.4 Same conditions as described in figure 4.3 except the tip angle of the detection pulse is equal to π/4.

spin system with α set to $\frac{\pi}{2}$ is shown in figure 4.3. The double quantum coherences in the proton AMX spin system 2,3-dibromopropionic acid in benzene-d_6 have been indirectly detected using the modified INADEQUATE pulse sequence. In all the experimental results of this chapter, phase cycling has been used to detect only the echo portion of the observable magnetization derived from double quantum coherence in the manner outlined in the chapter 3. All six possible double quantum transitions are present in the contour plot. Each is correlated with all three spins in the AMX system. A spectrum of this type contains too much information to allow correlation of a given double quantum frequency with a particular pair of spins in a complicated spin system. This situation can be improved because the tip angle effect can be used to reduce the information content and correlate the double quantum frequencies with the appropriate spin pairs.

Specific coherences can be enhanced or suppressed by chosing α other than an odd integer multiple of $\frac{\pi}{2}$. For $\alpha = \frac{\pi}{4}$ the echo portion of the magnetization for the proton AMX system is shown in figure 4.4. The tip angle dependence illustrated in figure 4.2 indicates that the double quantum coherence would be transferred with equal intensity to some single quantum coherences for all three spins. An intensity variation within the coherences associated with a spin appears for the pair of spins of a particular double quantum coherence. For example the intensity of the AM double quantum coherences 17 and 28 is greatest for the directly connected single quantum coherences of the A and M spins. Both of the AM double quantum coherences are transferred equally to all the X spin single quantum coherences thus a distinction can be made between the pair of spins contributing their offsets to the double quantum frequency and the third spin in the coupling system. However the AM double quantum coherence would be observed on the X spin even in the absence of a resolvable coupling between the A and M spins. This

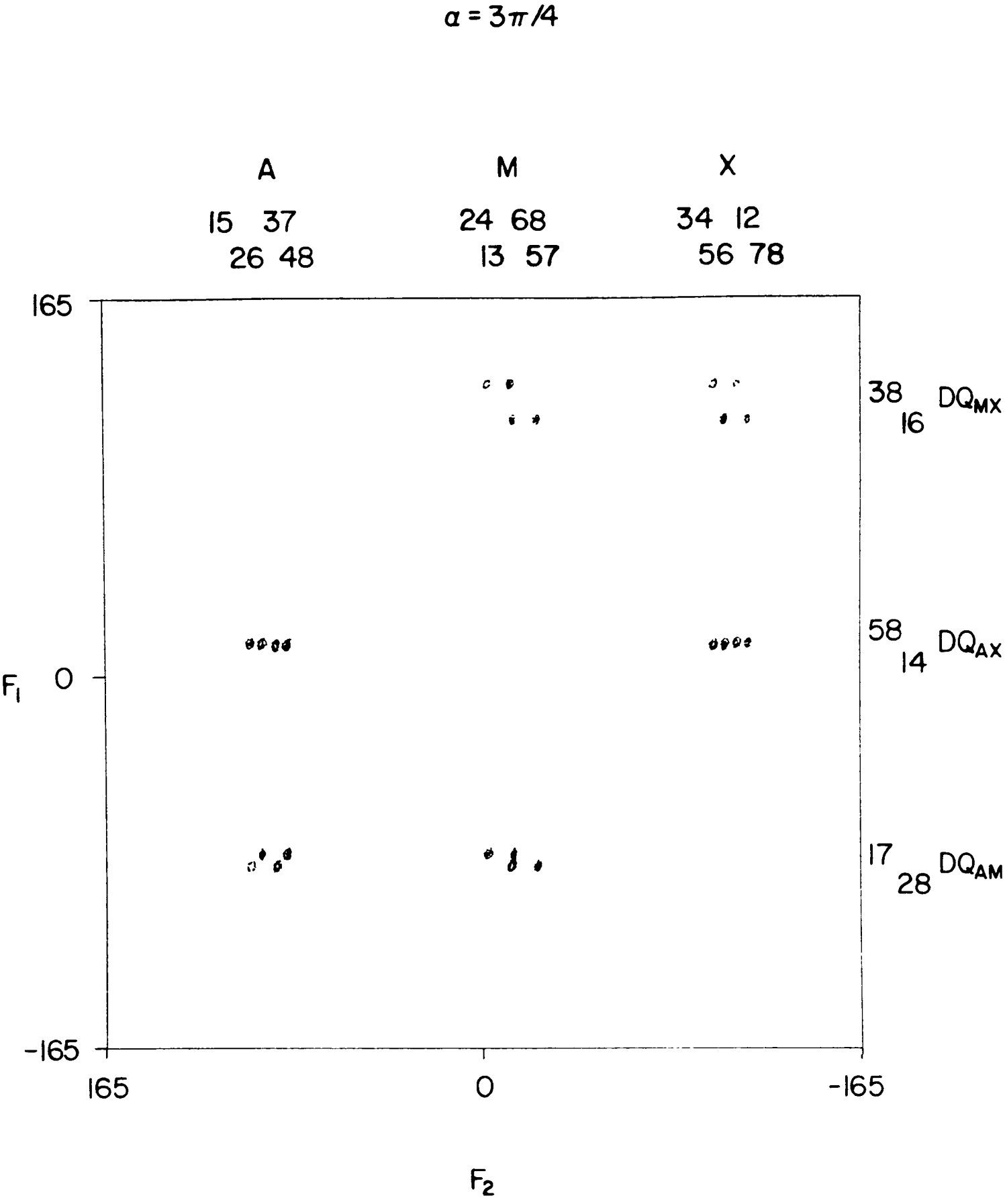

Figure 4.5 Same conditions as described in figure 4.3 except the tip angle of the detection pulse is equal to $3\pi/4$.

could lead to ambiguities in the assignment of complicated coupling patterns.

A further simplification in the appearance of the two-dimensional spectrum is possible with other choices for the value of the tip angle. For α such that $\frac{\pi}{2} < \alpha < \pi$, figure 4.2 shows that transfer of double quantum coherence 17 will be greatest to the indirectly connected A and M single quantum coherences with a maximum at $\alpha \sim 132^{o}$. Transfer to the X spin single quantum coherences will be reduced and all of the same intensity. A contour plot of the spectrum for the proton AMX spin system is shown in figure 4.5 with α set to 135°. At this vertical scale the double quantum coherences only appear correlated to the pair of spins that contribute their offset frequencies to the double quantum precession frequency. Thus for this setting of α it is possible to correlate the double quantum coherences directly with pairs of spins in the coupled spin system. The spectrum of figure 4.3 contains the maximum possible number of 72 peaks in the contour plot. By using the tip angle effect for $\alpha = 135^{o}$ it is possible to reduce the number of intense peaks to 24 and increase the useful information content of the two-dimensional spectrum by allowing correlation of the double quantum coherences with the appropriate spin pair.

The dependence of the creation of double quantum coherences on the coupling constants can be used to enhance or suppress peaks in the two-dimensional spectrum. With the proper choice of delay time τ the amount of J-modulation can be manipulated to select certain antiphase states which will be converted into double quantum coherences by the third pulse of the INADEQUATE sequence. As an example consider the situation where one spin has two coupling constants of nearly equal magnitude. If τ is chosen so that the sine terms for these coupling constants are approximately equal to zero no double quantum coherence will be created

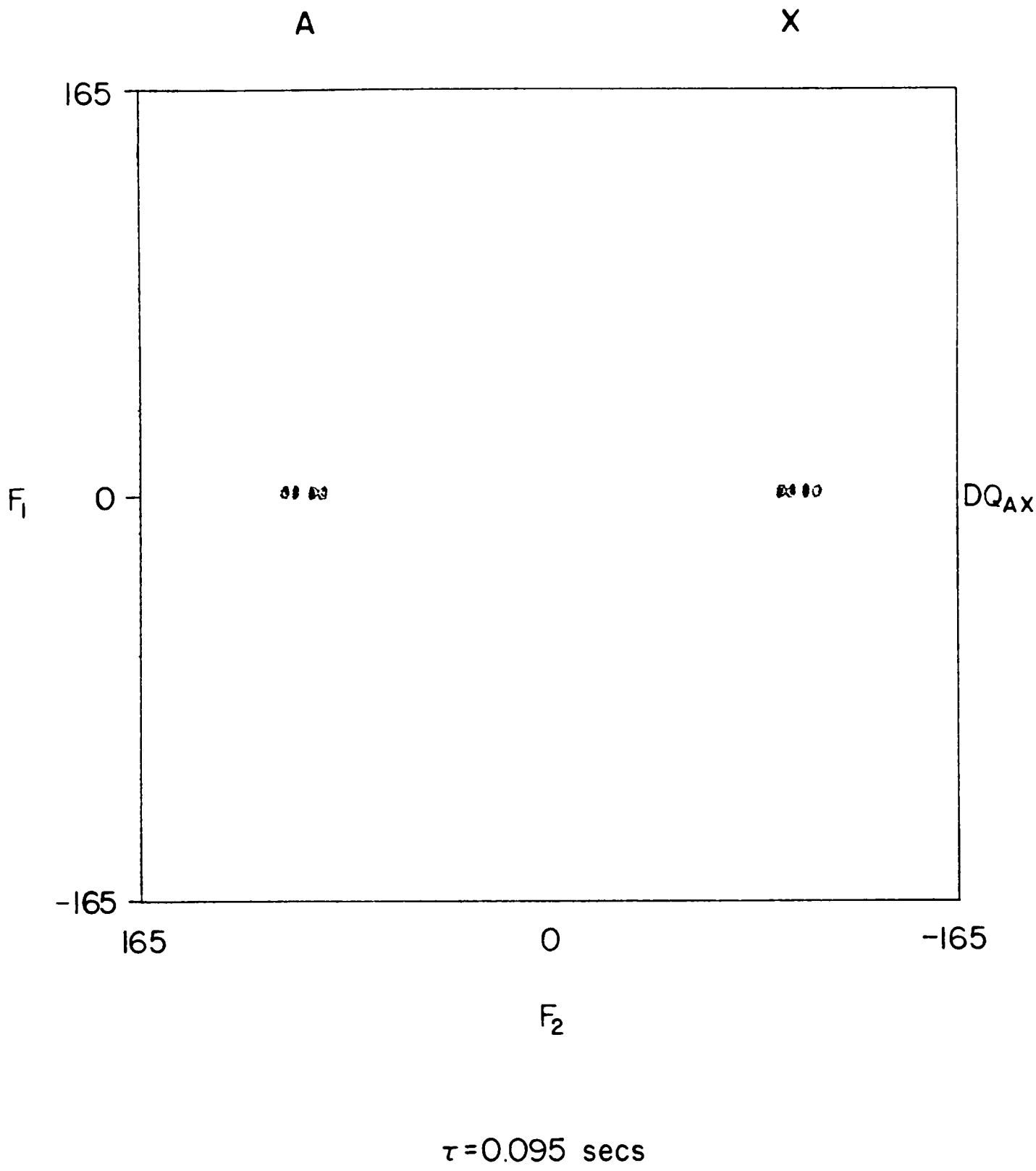

Figure 4.6 Same conditions as described in figure 4.5 except the creation delay, τ set to 0.095 secs to suppress the double quantum coherences, AM and MX, while retaining the coherence AX.

that will allow correlation of this spin to the spins with which it has equal coupling. For the proton AMX spin system, spin M has couplings to spin A and X of $J_{AM} = \pm 11.1$ Hz and $J_{MX} = \mp 10.0$ Hz with opposite sign [4.14]. If τ is chosen to be the reciprocal of twice the average magnitude of these couplings the double quantum peaks correlating spins A to M and M to X will be suppressed. The choice of $\tau = 0.095$ secs is illustrated in figure 4.6. The detection pulse tip angle has been set to 135° to enhance only direct correlations. With these values of tip angle and creation delay the resulting spectrum has been simplified to show only one correlation, spin A to spin X.

4.4. Folding for optimum use of data space

In the two-dimensional spectrum double quantum peaks lie on lines parallel to the F_2 axis centered on a diagonal line of slope 2 which represents the average of the chemical shifts of the two coupled spins. To observe all possible correlations without folding along the F_1 axis, the spectral width in F_1 should be set to twice the spectral width in F_2. For this choice of spectral widths the double quantum peaks will be centered on a line that runs from the bottom left to the top right of the two-dimensional as oriented in figure 4.7. As can be seen for the five coupled idealized spins in the figure, only half the available data space is used to display the information. Spectra with large dispersion will cause difficulties in providing adequate digitization in F_1. This is because increases in digital resolution in F_1 require more increments in t_1 and hence more time to perform the experiment and more computer memory space.

It is possible to allow the spectrum to fold along the F_1 axis by setting the spectral width equal in both dimensions. The dashed line in figure 4.7 represents the folded double quantum diagonal. This choice

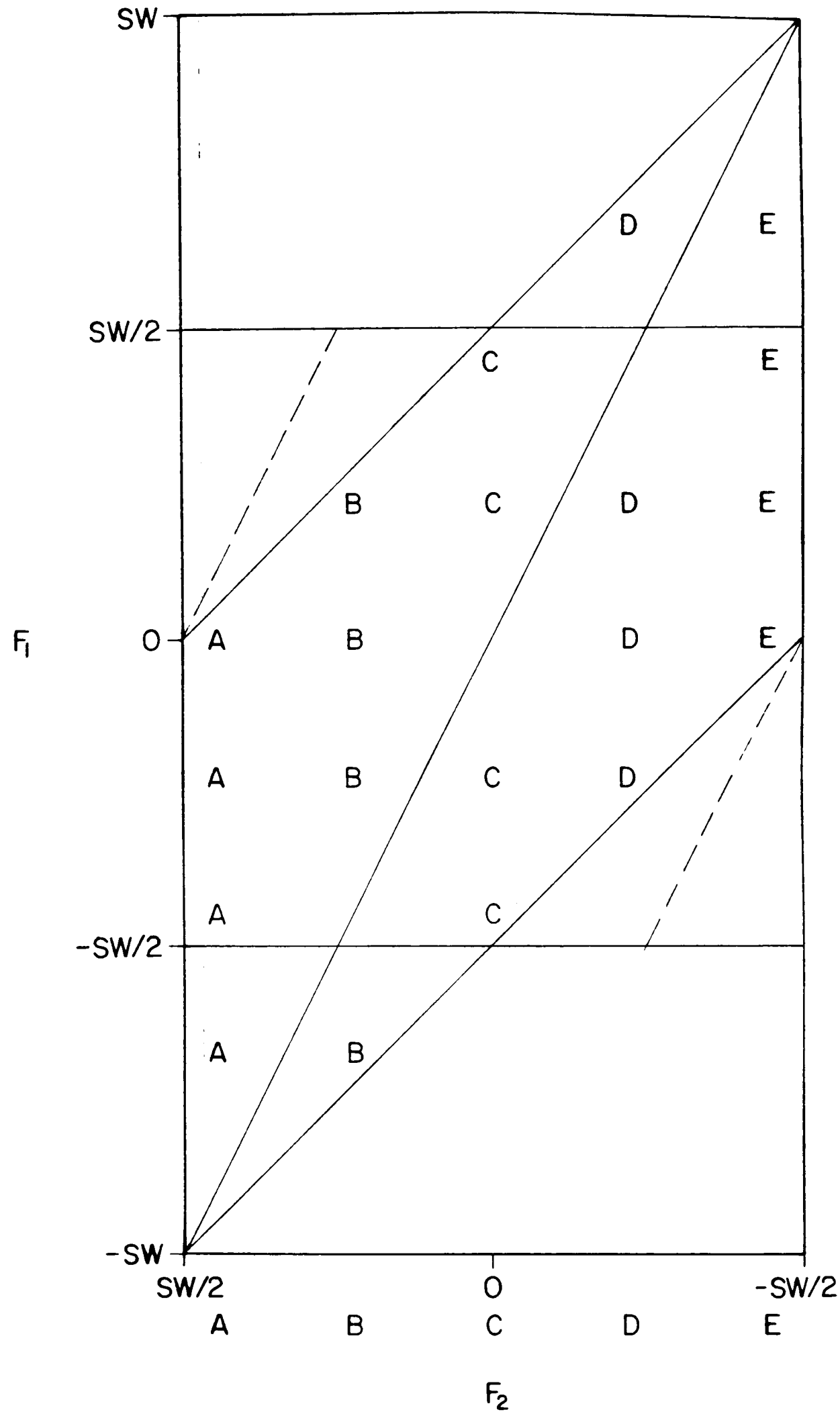

Figure 4.7 Idealized spectrum for five coupled spins representing all possible coupling pairs. The double quantum 'diagonal' runs from the bottom left to the top right of the spectrum with a slope of 2. The dashed line represents the position of the folded double quantum 'diagonal' if the spectral widths are equal in both dimensions.

of spectral widths makes optimum use of the data space and provides the best possible digitization in the available time for the experiment. The spectra of figure 4.3-6 have been acquired with equal spectral widths in both dimensions. The folded portion of the matrix for this spin system contains no peaks so no distortion is observed. Ambiguities along the folded edges of the spectrum can be cleared up by shearing the spectrum parallel to the F_1 axis [4.15]. Data in F_1 can be shifted point by point in each spectrum unfolding the corners. Data is shifted as a function of the frequency in F_2 with the maximum shift at each end. In this way the informative part of the data fills the square matrix exactly.

4.5. Broadband decoupling in the F_1 dimension

The double quantum coherences of a system of more than two spins rotate at different frequencies dependent upon the coupling constants of a particular pair of spins to the other spins in the system. Now consider that the time between creation and detection pulses is held constant and a $(\pi)_x$ refocussing pulse introduced during this interval after a variable delay of $\frac{1}{2}\, t_1$ after the creation pulse. J-modulation will continue during the fixed time, T, independent of the position of the refocussing pulse. Since T is held constant no J-modulation will be transferred as a function of t_1. The offset frequency contribution to the double quantum precession rate will be sensitive to the position of the refocussing pulse so a Fourier transformation with respect to t_1 will produce a frequency spectrum parallel to the F_1 axis which has no fine structure due to coupling constants. This technique effectively decouples the double quantum spectrum parallel to the F_1 axis. Since the refocussing pulse effects all the spins equally, the method provides broadband decoupling in the F_1 dimension. The above method of decoupling has been applied to the Jeener pulse sequence to decouple

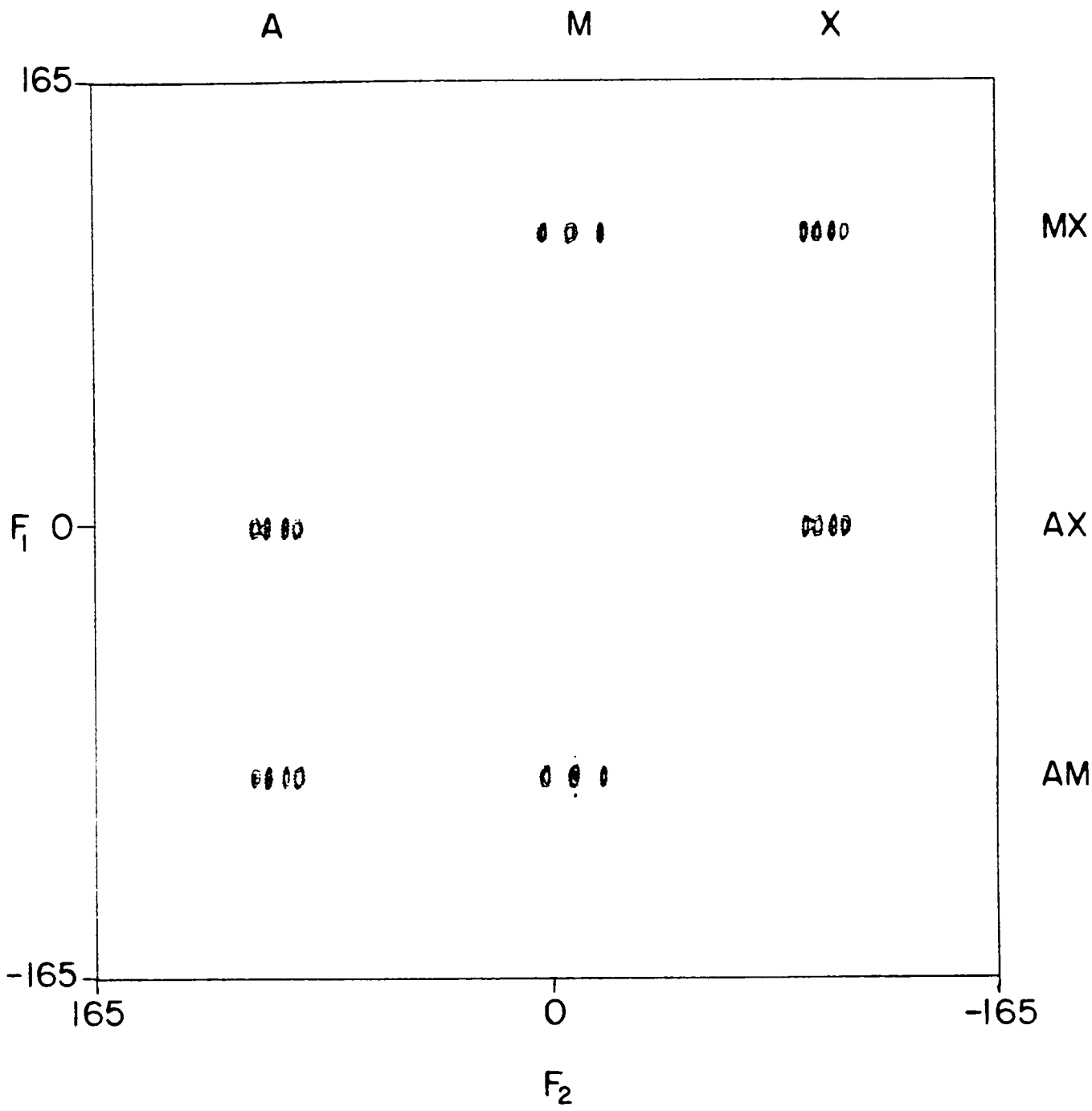

Figure 4.8 Double quantum correlation spectrum of 2-3-dibromopropionic acid in acetone-d_6 decoupled in the F_1 dimension. Parameters as described in text.

single quantum coherences in the F_1 dimension [4.5].

The INADEQUATE sequence for double quantum correlation can be further modified to decouple double quantum coherences in the F_1 dimension as follows,

$$(\tfrac{\pi}{2})_x - \tau - (\pi)_y - \tau - (\tfrac{\pi}{2})_x - \tfrac{1}{2}t_1 - (\pi)_x - (\ T - \tfrac{1}{2}t_1\ ) - (\alpha)_\phi - \text{detect}_\xi .$$

The usual phase cycling of the detection pulse and receiver will be used to observe only double quantum coherence along F_1. Also a $\frac{\pi}{4}$ z-pulse at the beginning of evolution will allow sign discrimination of the double quantum precession. The effective sense of precession during t_1 is reversed by the refocussing pulse for as t_1 increases the amount of precession decreases thus reversing the sense of precession determined by the Fourier transformation process. To allow direct comparison with spectra determined without decoupling in the F_1 dimension it is possible to calculate the complex conjugate of the interferograms before transforming with respect to t_1. The sign of precession is reversed by this calculation and the resulting two-dimensional spectrum can be compared to spectra without F_1 decoupling.

An example of decoupling along F_1 is shown in figure 4.8. The double quantum coherences for the proton AMX spin system 2,3-dibromothiophene have been detected with a tip angle of 135°. The complex conjugate of the interferograms has been calculated to allow comparison with figure 4.3 to 4.6. In more complex systems the correlation of single and double quantum coherences will be simplified by the decoupling process where multiplet overlap will be minimized.

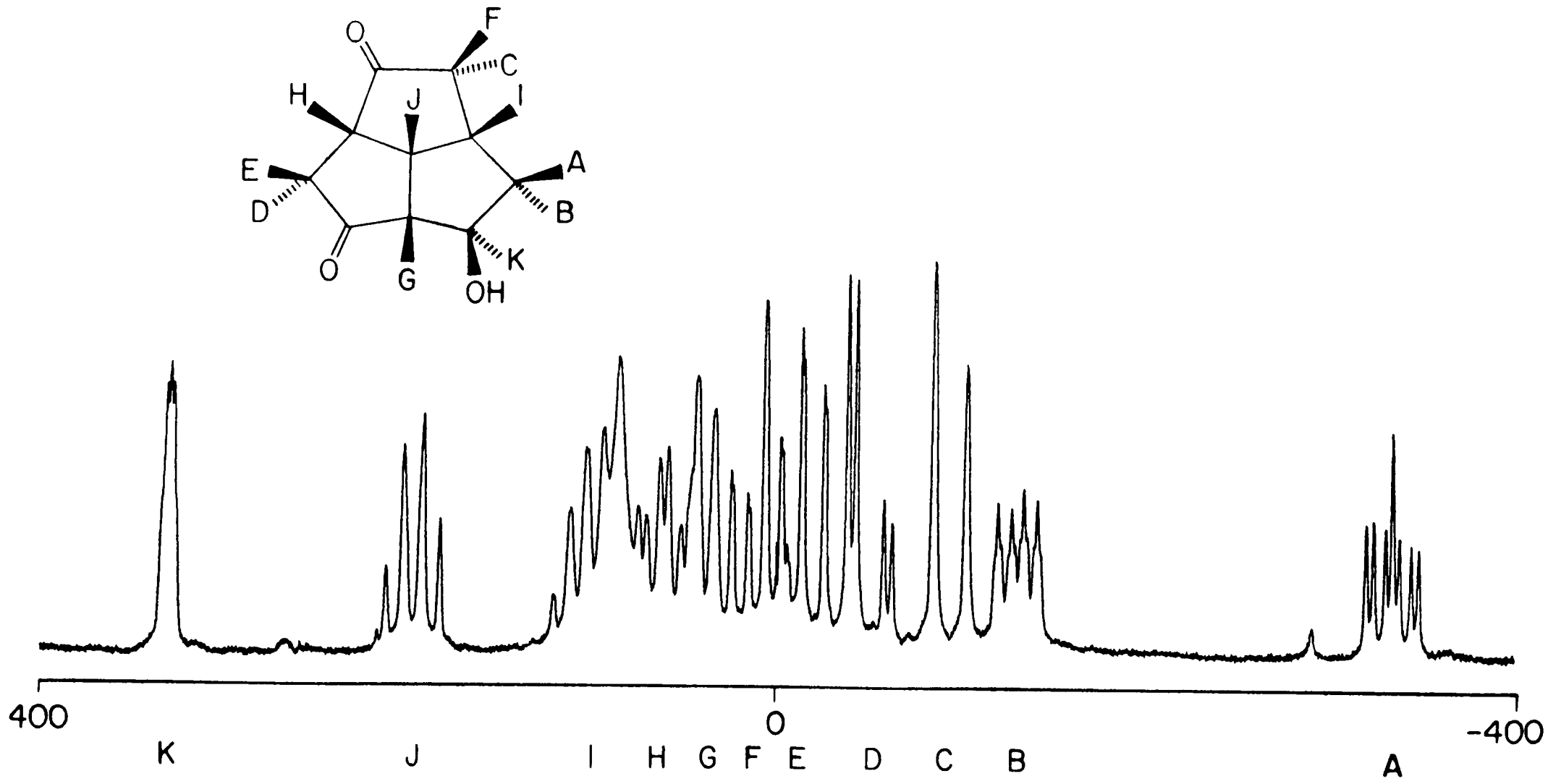

Figure 4.9 High resolution proton spectrum of the tricyclodecane derivative, 9-hydroxytricyclodecan-2,5-dione in $CDCL_3$. Specific proton shift assignments are indicated for the lettering scheme of the molecule at the top of the figure.

4.6. Practical application of correlation through double quantum coherences

As an example of a practical spin system consider the proton spectrum of the tricyclodecane derivative, 9-hydroxytricyclodecan-2,5-dione shown in figure 4.9 which has a wealth of proton-proton couplings spread over a narrow 4 ppm range. Direct correlation through double quantum coherences in shown in figure 4.10 with the spectral width in both dimensions set equal to make optimum use of the data space. The coupling pattern is mapped out clearly through the double quantum transitions excited for this choice of τ. Several are indicated on the spectrum. To suppress indirect correlations a detection pulse of $\sim 157.5^{\circ}$ has been chosen. A few small indirect correlations appear with some of the more intense peaks; for example, the low intensity peak on spin G for the BK double quantum transition. However in general the discrimination is very good. It proved necessary to increase the tip angle of the detection pulse because of the large dynamic range in intensities of the double quantum peaks for different spin pairs. In the spectrum of figure 4.10 the correlations of spins lying close together are clearly visible with no obstruction due to autocorrelation peaks of the type seen near the diagonal for the sequence proposed by Jeener [4.3,4.4]. Also there is less overlap in adjacent spin multiplets than would be seen for the correlation of single quantum coherences [4.5].

A potential source of ambiguity arises when spins are strongly coupled. In this case the tip angle effect for coherence transfer effected by the detection pulse cannot be used to distinguish between direct and indirect correlations because the X-approximation breaks down [4.11]. The energy levels of coupled spins are mixed by the strong coupling which results in transfer to all the strongly coupled spins

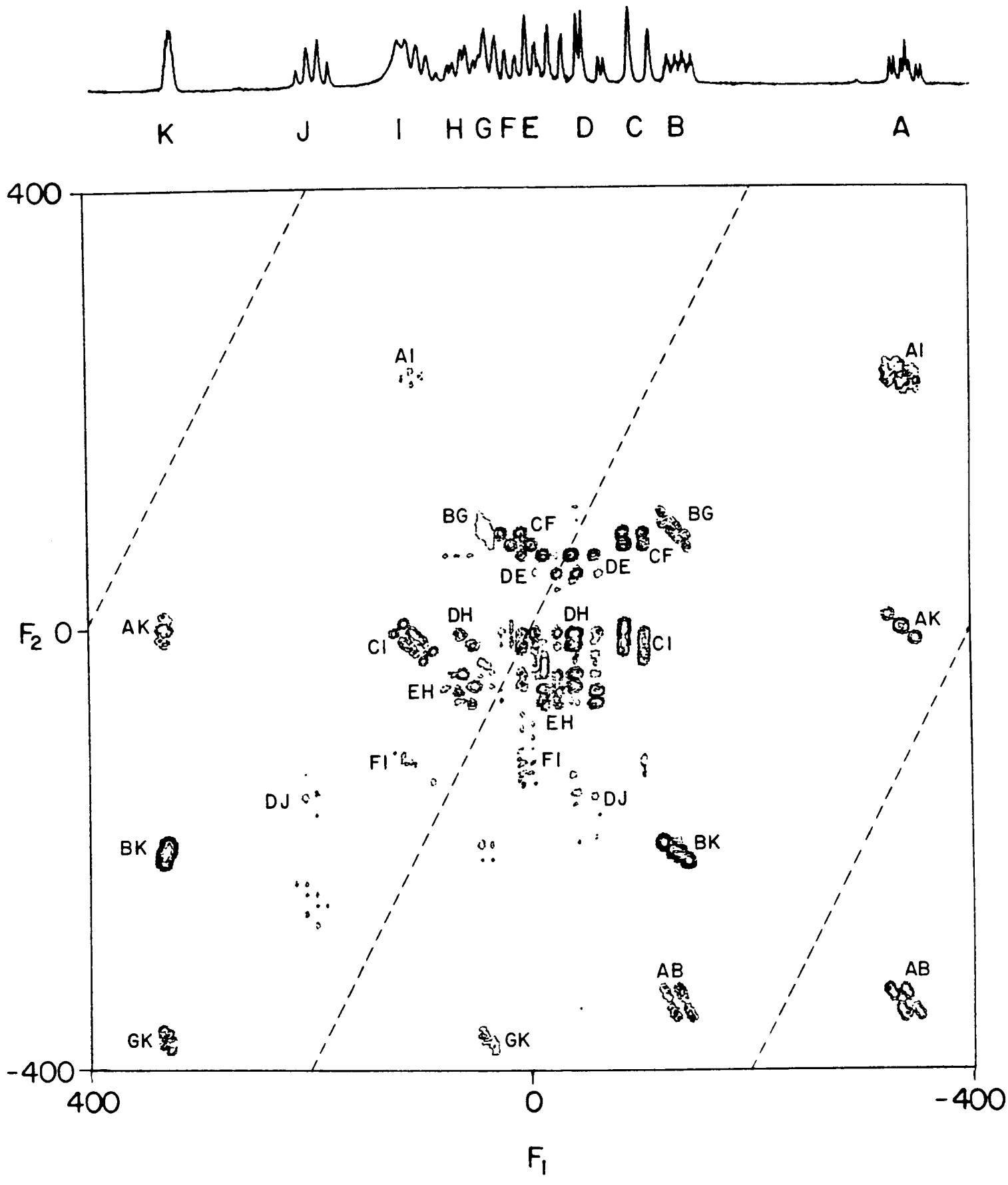

Figure 4.10 Double quantum correlation spectrum of 9-hydroxytricyclodecan-2,5-dione in $CDCL_3$. The detection pulse was set to 135° and creation delay, τ, to 0.150 secs. Double quantum coherences are labeled by the appropriate spin pairs. The double quantum 'diagonal' has been indicated by the dashed line.

without adequate distinction so additional indirect correlation peaks are observable. In the tricyclodecane spectrum of figure 4.10 this effect is seen quite clearly for the D and E spins which are strongly coupled. The effect is strongest when one of this pair of spins is correlated through a double quantum transition to another spin. The transfer of coherence is then quite strong to both D and E spins.

The two-dimensional spectrum obtained with broadband decoupling in the F_1 dimension is shown in figure 4.11. Decoupling separates double quantum multiplets which overlap without decoupling thus simplifying the assignment. Again strong coupling can confuse the results somewhat by the presence of extra peaks due to mixing by the refocussing pulse and by the indirect correlation as described above.

Even with the problems of strong coupling the correlation of proton-proton coupling interactions through double quantum coherence provides a method of reducing overlap in crowded spectra and allows some control over the enhancement or suppression of correlations by the variation of the creation delay, τ.

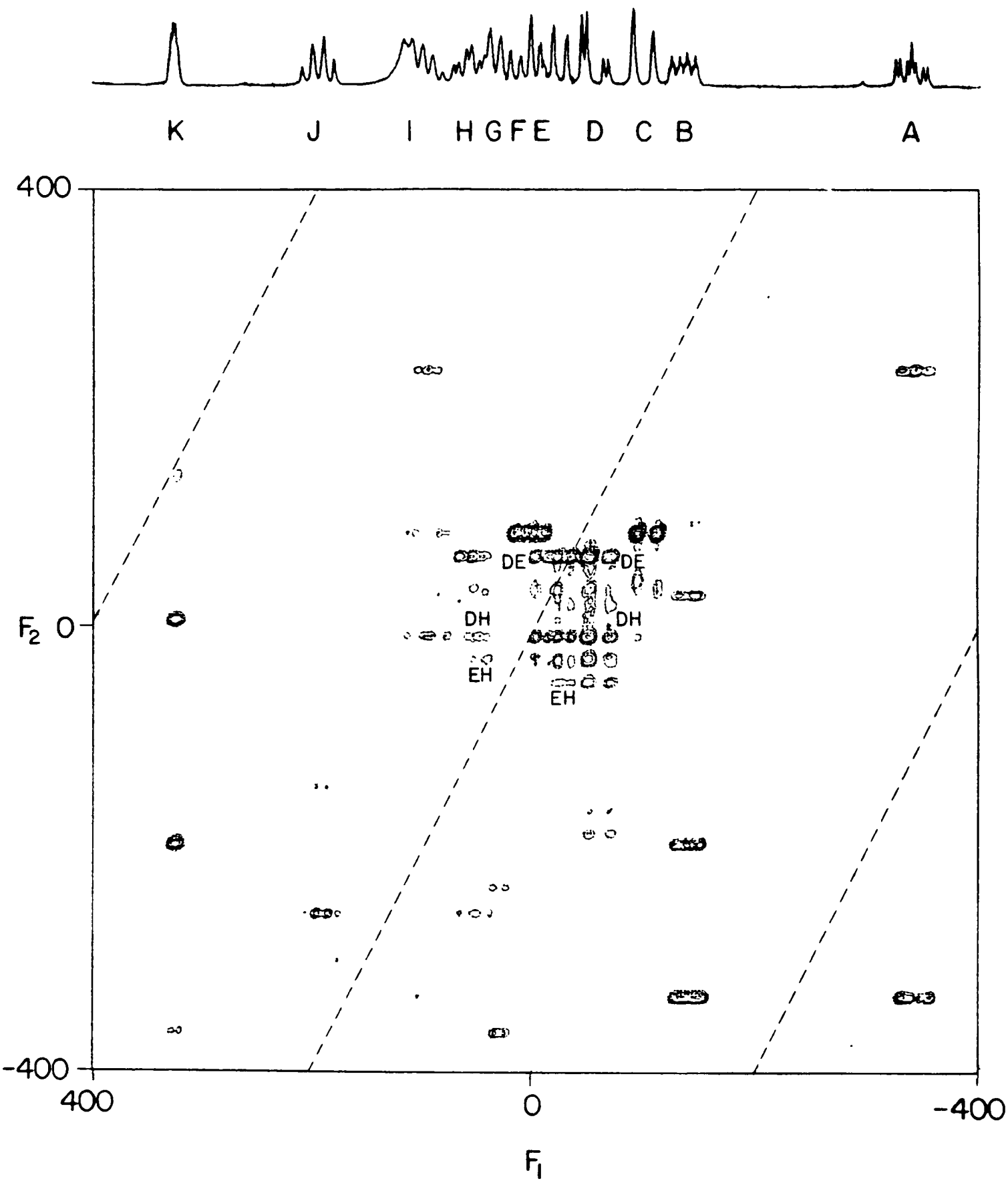

Figure 4.11 Same parameters as described in figure 4.10 with broadband decoupling in the F_1 dimension. The fixed delay, T, during evolution was set to 0.2 secs. The double quantum 'diagonal' has been indicated by the dashed line.

References

[4.1] H. S. Gutowsky, D. W. McCall and C. P. Slichter, Phys. Rev. 84, 589 (1951) E. B. McNeil, C. P. Slichter and H. S. Gutowsky, Phys. Rev. 84, 1245 (1951) E. L. Hahn and D. E. Maxwell, Phys. Rev. 84, 1246 (1951)

[4.2] O. Jardetzky and G. C. K. Roberts, NMR in Molecular Biology, Academic Press, New York (1981)

[4.3] J. Jeener, Ampere International Summer School, Basko Polje, Yugoslavia, 1971

[4.4] W. P. Aue, E. Bartholdi and R. R. Ernst, J. Chem. Phys. 64, 2229 (1976)

[4.5] A. Bax and R. Freeman, J. Magn. Reson. 44, 542 (1981), A. Bax, Two-Dimensional Nuclear Magnetic Resonance in Liquids, Delft University Press, Dordrecht Holland, 1982

[4.6] A. Wokaun and R. R. Ernst, Chem. Phys. Lett. 52, 407 (1977)

[4.7] G. Pouzard, S. Sukumar and L. D. Hall, J. Amer. Chem. Soc. 103, 4209 (1981)

[4.8] T. H. Mareci and R. Freeman, J. Magn. Reson. 48, 158 (1982)

[4.9] A. Bax, R. Freeman and S. P. Kempsell, J. Amer. Chem. Soc. 102, 4849 (1980)

[4.10] R. Freeman, T. A. Frenkiel and M. H. Levitt, J. Magn. Reson. 44, 409 (1981)

[4.11] P. L. Corio, Structure of High Resolution NMR Spectra, Academic Press, New York (1966)

[4.12] H. Y. Carr and E. M. Purcell, Phys. Rev. 94, 630 (1954) S. Meiboom and D. Gill, Rev. Sci. Instr. 29, 688 (1958)

[4.13] G. Bodenhausen and R. Freeman, J. Magn. Reson. 36, 221 (1979)

[4.14] R. Freeman, K. A. McLauchlin, J. I. Musher and K. G. R. Pachler, Mol. Phys. 5, 321 (1962)

[4.15] L. Muller, J. Magn. Reson. 36, 301 (1979), K. Nagayama, A. Kumar, K. Wuthrich and R. R. Ernst, J. Magn. Reson. 40, 321 (1980)

Chapter 5

Heteronuclear coupling constants measured in proton spectra

5.1. Introduction

In organic molecules, chemical shifts of carbon-13 and nitrogen-15 are determined with broadband decoupling from protons. Decoupling collapses multiplets and allows nuclear Overhauser enhancements to build so that the sensitivity is increased. The measurement of heteronuclear coupling constants is more difficult. When the decoupling field is removed so that spin-spin coupling is observed, the signal-to-noise ratio drops dramatically due to the splitting of the resonance by coupling and possible loss of nuclear Overhauser enhancement.

Some advantage in measuring coupling constants can be gained by retaining the nuclear Overhauser enhancement through gating the decoupler field so that it is on at all times except when the spectrum is obtained in the presence of coupling [5.1]. In organic molecules the gated decoupling technique can be used to enhance the signals from carbon-13 or nitrogen-15 spins directly bonded to protons. The technique will not significantly enhance spins not directly bonded to protons hence the measurement of long range couplings will still present a difficult problem. Also the decoupler duty cycle must be kept high to retain the enhancement. For well digitized spectra of small widths this will require longer delays between acquisitions to maintain the same duty cycle and hence less efficient use of experiment time [5.2].

It is possible to observe heteronuclear coupling with increased sensitivity in proton spectra; the heteronuclear coupling information is

present as weak satellites centred about the much stronger 'parent' line. The intensity of the satellites will be smaller than the parent proton signal by a factor of 1/2 times the natural abundance of the heteronuclei. For carbon-13, the satellites would be reduced by a factor of ~ 200, and ~ 540 for nitrogen-15. With a sufficient signal-to-noise ratio one bond coupling constants can be observed directly, however long range couplings can be obscured by the parent proton line.

An estimate of the sensitivity gained by observing heteronuclear coupling in the proton spectra can be made with the following rather crude arguments. Considering only factors involving frequency, gyromagnetic ratio and populations of states, the signal voltage, V, generated in the detection coil by the precessing magnetic moment can be written in an approximate form as [5.3],

$$V \sim \omega M \sim \omega\langle\mu\rho\rangle \sim \omega^2\gamma/kT$$

$$\sim \gamma^3 B_0{}^2/kT. \qquad (5.1)$$

Where γ is the gyromagnetic ratio of the spin and B_0 is the applied magnetic field. With a noise voltage of $V_N \sim (\omega\, kT)^{1/2}$, the observed signal-to-noise ratio in the X spectrum can be written as,

$$\xi = \frac{V}{V_N} \sim \gamma^{5/2} B_0{}^{3/2}/(kT)^{3/2}. \qquad (5.2)$$

With the maximum possible heteronuclear Overhauser enhancement of $(1 + \frac{\gamma_p}{2\gamma_X})$ [5.4] from protons to spins of species X, the signal-to-noise ratio can be written as,

$$\xi \sim \gamma_X^{5/2} B_0{}^{3/2}(1 + \frac{\gamma_p}{2\gamma_X})/(kT)^{3/2}. \qquad (5.3)$$

The ratio, ξ, would be made dimensionless by all the other factors ignored in this rough calculation. As estimate of the gain in sensitivity for measuring H-X coupling in the proton spectrum instead of in the X spectrum is given by the ratio of the signal-to-noise factors in each spectrum. Assume that all other factors are identical such as the coil geometry, filling factor, quality factor Q, etc.

$$\frac{\xi_p}{\xi_X} \sim (\frac{\gamma_p}{\gamma_X})^{5/2}(1 + \frac{\gamma_p}{2\gamma_X})^{-1}. \qquad (5.4)$$

For carbon-13 the value of this ratio is ~ 10 and nitrogen-15 ~ 80. These are worst case estimates, for much larger gains are possible when the nuclear Overhauser enhancement is less than maximum. Clearly observation of heteronuclear couplings in the proton spectrum offers a great sensitivity advantage once a way has been devised to suppress the parent proton line.

In this chapter, several methods of observing heteronuclear couplings in proton spectra will be studied [5.5,5.6]. All the techniques rely on a difference method to suppress the parent proton line and retain the heteronuclear satellites. When good suppression can be achieved, it is possible to observe long range heteronuclear coupling.

5.2. Heteronuclear satellites in proton spectra

In this section two simple pulse sequences suitable for observation of satellite lines in proton spectra are studied. In practice these were carbon-13 satellites, but the same principles are applicable to other species in low isotope abundance. The first method utilizes the fact that proton spin echoes are modulated by a heteronuclear coupling J_{CH} if a π pulse is applied to the carbon-13 spins at the same time as

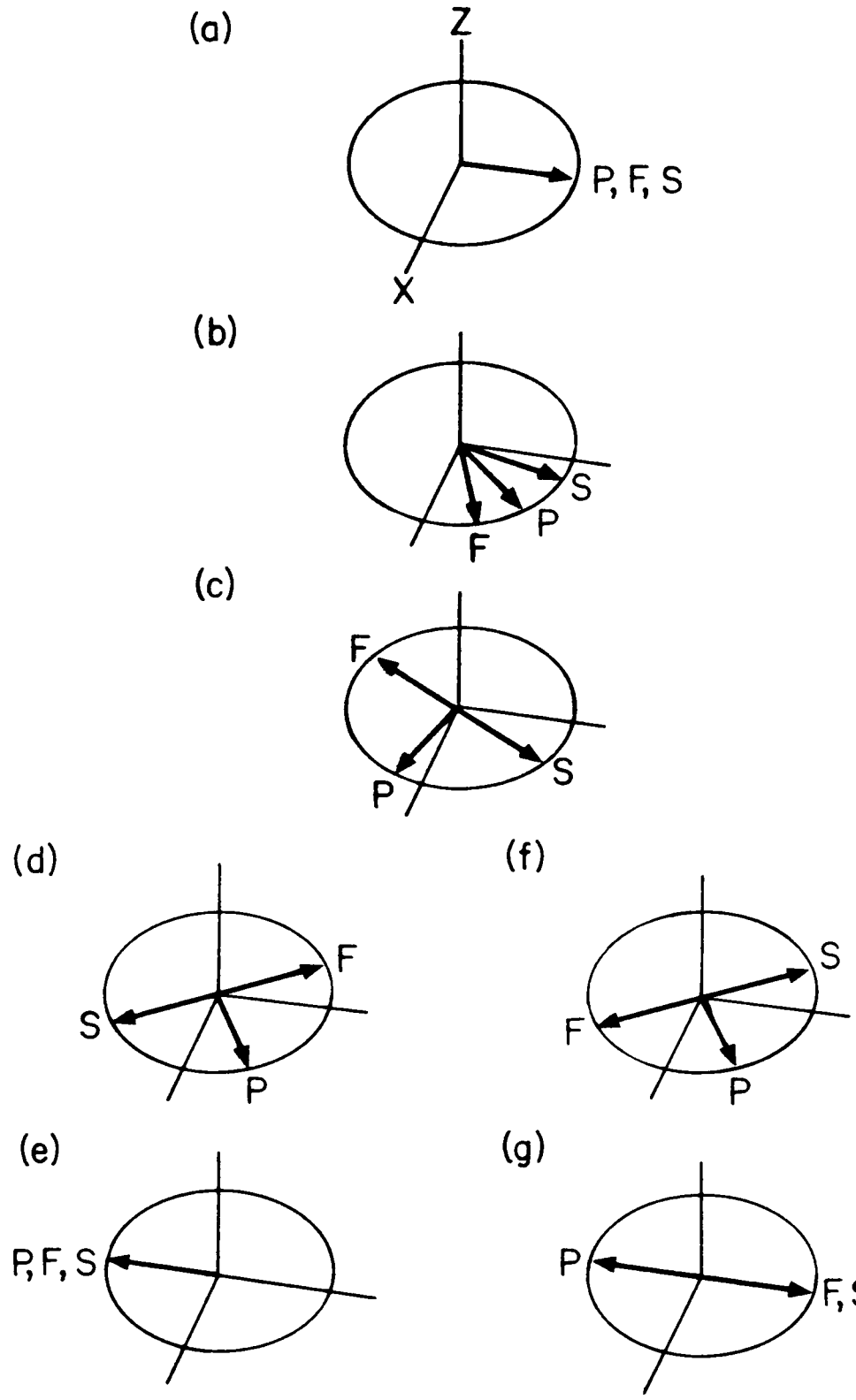

Figure 5.1 Detection of satellite spectra by spin echo difference spectroscopy. (a) Three proton magnetization vectors, representing the strong parent (P) and the fast (F) and slow (S) satellites, are initially aligned along the +y axis. (b) They precess for a time τ until F and S lie antiparallel (c). In the first sequence (a), (b), (c), (d), (e), the π proton pulse flips the vectors to mirror-image positions (d). No pulse is applied to the carbon-13 spins. (e) At time 2τ all three vectors are aligned along the -y axis. In the second sequence (a), (b), (c), (f), (g), the introduction of a carbon-13 π pulse at time τ interchanges the F and S labels (f), with the result that the F and S vectors become aligned along the +y axis at time 2τ, whereas the P vector is still returned to the -y axis. Subtraction of the responses from the two different sequences suppresses the strong parent signal by reinforces the satellites F and S.

the proton π refocussing pulse [5.7]. The pulse sequence for this 'spin echo difference spectroscopy' may be written as

Protons $\quad (\frac{\pi}{2})_x - \tau - (\pi)_x - \tau - \text{Acquisition}(\pm)$

Carbon-13 $\quad (\frac{\pi}{2})_x (\frac{\pi}{2})_{\pm x}$

The delay τ is chosen to equal $1/(2J_{CH})$ so that the two proton vectors in question build up a relative phase difference of 180° in this interval. The two $\frac{\pi}{2}$ pulses applied to carbon-13 act together to give a π or 0 pulse in successive experiments. This combination appears to work rather better than the simpler method of appling a π pulse in alternate experiments since applying two pulses with and without opposing phase minimizes timing differences between the two parts of the experiment and provides the same amount of perturbation to the system. The evolution of the proton magnetization vectors is set out in figure 5.1. In one sequence a π pulse is applied to the carbon-13 spins, which interchanges the spin state labels on the proton vectors so that they continue to diverge during the second τ period, ending up aligned along the + y axis at time 2τ, whereas the vector corresponding to the protons in carbon-12 molecules is aligned along - y. Repetition of the entire sequence 'without' the π pulse to carbon-13 leaves the proton satellite vectors aligned along the - y axis. Subtraction of the acquired signal in alternate experiments suppresses the parent signal but reinforces the satellite signals.

The presence of the very strong parent signal poses some practical difficulties. An extremely high degree of field/frequency stabilization is required if the subtraction process is to achieve high suppression ratios. Since the proton probe on the XL-200 had no coil suitable for irradiation at the carbon-13 frequency, it was necessary to use the 10-mm carbon-13 probe, protons being detected through the Helmholtz coils

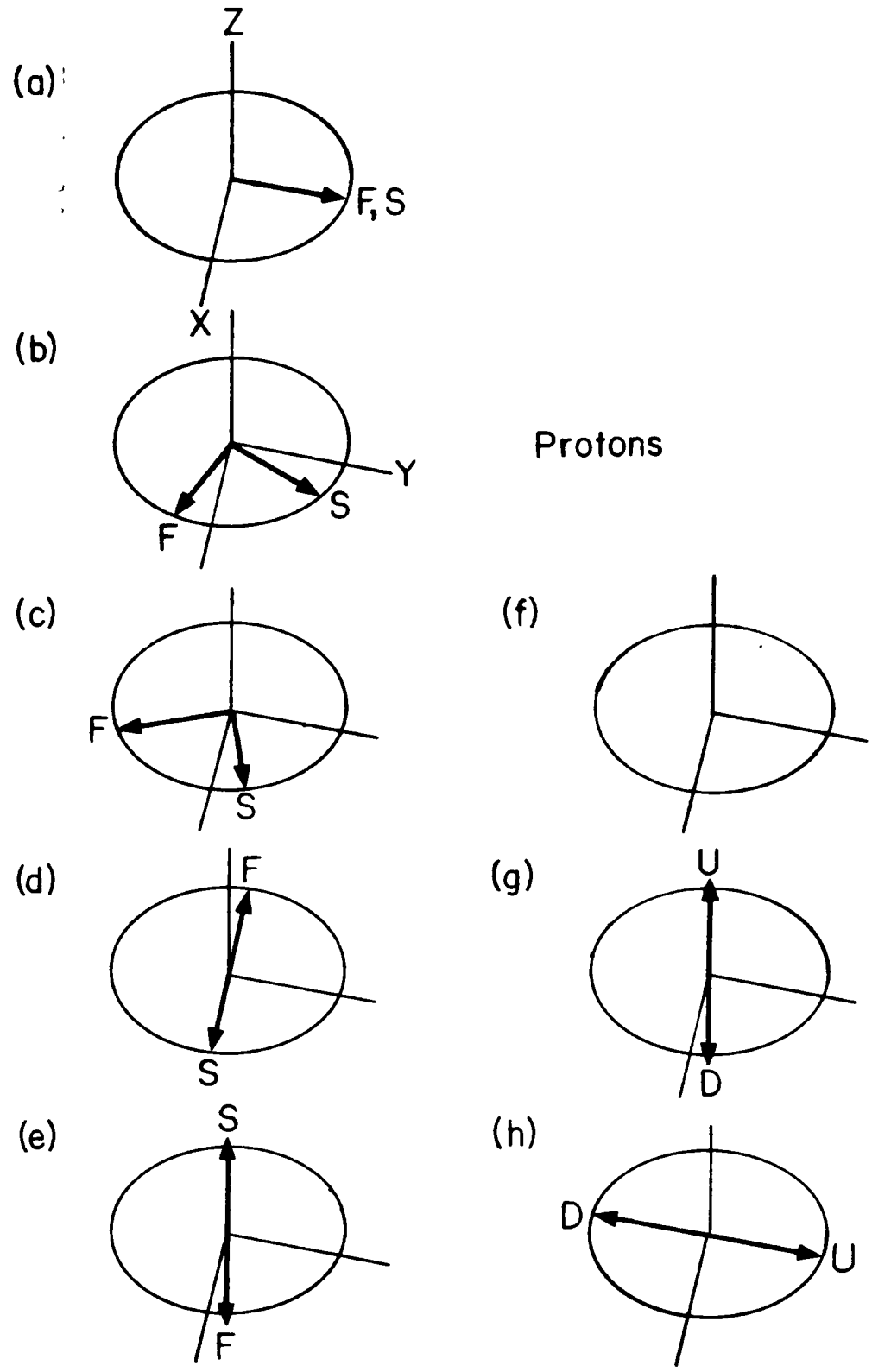

Figure 5.2 Detection of satellite spectra by the reverse INEPT experiment. (a) Two carbon-13 magnetization vectors labeled F (fast) and S (slow) are aligned along the +y axis of the carbon rotating frame. (b) They precess for a time τ until they make an angle of 90° with respect to each other. (c) Simultaneous proton and carbon π pulses interchange F and S labels and flip the vectors into mirror-image positions. (d) Further precession of a period τ leaves F and S opposed along the $\pm$x axes. (e) A $\pi/2$ carbon pulse about the +y axis turns the vectors into the z-direction, S representing equilibrium populations but F corresponding to a population inversion. (f) The proton magnetization is initially zero due to a presaturation sequence. (g) Because of the population disturbances, it acquires longitudinal magnetization from carbon-13, labeled U (up) and D (down). (h) A final $\pi/2$ pulse on the protons creates transverse magnetizations along the $\pm$y axes. In a second pulse sequence, the S and F vectors are reversed in (a) but since the last proton pulse is also reversed, the vectors D and U remain as shown in (h). Any residual parent signal is inverted and hence canceled at the end of the second sequence.

normally used as decoupling coils. The observed proton signal is very strong in all but very low concentration solutions, hence clipping of the signal at the detector had to be prevented by inserting an attenuator between the preamplifier and the amplifier. It is of course necessary to ensure that the analogue-to-digital conversion stage has sufficient dynamic range to carry both the weak and strong signal components. The overall effect is a loss of sensitivity and resolution. It should be possible to improve the situation using a probe specifically designed to observe protons with a coil for heteronuclear decoupling.

However, there is another method available which does not involve the acquisition of the strong parent signal. This is a direct application of the 'insensitive nuclei enhanced by polarization transfer' (INEPT) technique [5.8], used with the roles of the two nuclear species reversed. The pulse sequence may be written as

Protons (presaturation) $\quad (\pi)_x - \tau - (\frac{\pi}{2})_{\pm x}$ - Acquisition

Carbon-13 $\quad (\frac{\pi}{2})_{\pm x} - \tau - (\pi)_x - \tau - (\frac{\pi}{2})_y$

In this method attention must be focussed on the time evolution of the carbon-13 spins as illustrated in figure 5.2. For simplicity, consider first the case of a CH group. Using the form of equation 2.158, the initial density operator can be written as,

$$\rho_0 = \beta_H (I_z)_H + \beta_C (I_z)_C$$
$$= \beta_H (I_z^{13} + I_z^{24}) + \beta_C (I_z^{12} + I_z^{34}), \qquad (5.5)$$

where the β's are the appropriate population factors. Since the protons are presaturated $\beta_H \sim 0$. The τ delay is chosen to equal $1/(4J_{CH})$ so

that the two carbon-13 vectors (referred to as fast (F) and slow (S)) precess during τ to give a relative phase angle of 90°. The π pulse to carbon-13 refocusses the chemical shift effects but the π pulse to protons causes the two vectors to continue to diverge until they are aligned along the $\pm$ x axes. The $(\frac{\pi}{2})_y$ pulse to carbons converts these to $\pm$ z magnetization. The density operator at time 2τ can be written as,

$$\rho(2\tau) = \pm \beta_C(I_z^{12} - I_z^{34}). \qquad (5.6)$$

This corresponds to a disturbance of the spin state populations, and since the proton transitions share the same energy levels, they are also affected. Using the identity in equation 2.151, the above equation can be rewritten in terms of proton z-magnetization as,

$$\rho(2\tau) = \pm \beta_C(I_z^{13} - I_z^{24}). \qquad (5.7)$$

A subsequent proton 'read' pulse excites satellite responses, one positive-going and one inverted [5.9]. Following the pulse the system can be described by the density operator,

$$\rho_+(2\tau) = -\beta_C(I_y^{13} - I_y^{24}). \qquad (5.8)$$

Phase alternation of the first $\frac{\pi}{2}$ carbon pulse and the last $\frac{\pi}{2}$ proton pulse ensures that the satellite signals reinforce after two complete pulse sequences, but that the parent proton signals cancel. In fact this parent signal is greatly attenuated by a presaturation sequence, consisting of a train of $\frac{\pi}{2}$ pulses separated by intervals of 3 msec. This not only eliminates the majority of the signals not generated by magnetization from carbon-13, but also establishes a nuclear Overhauser enhancement of the initial carbon-13 polarization. If CH_2 and CH_3 groups are also present, a slightly shorter setting for τ is used, a

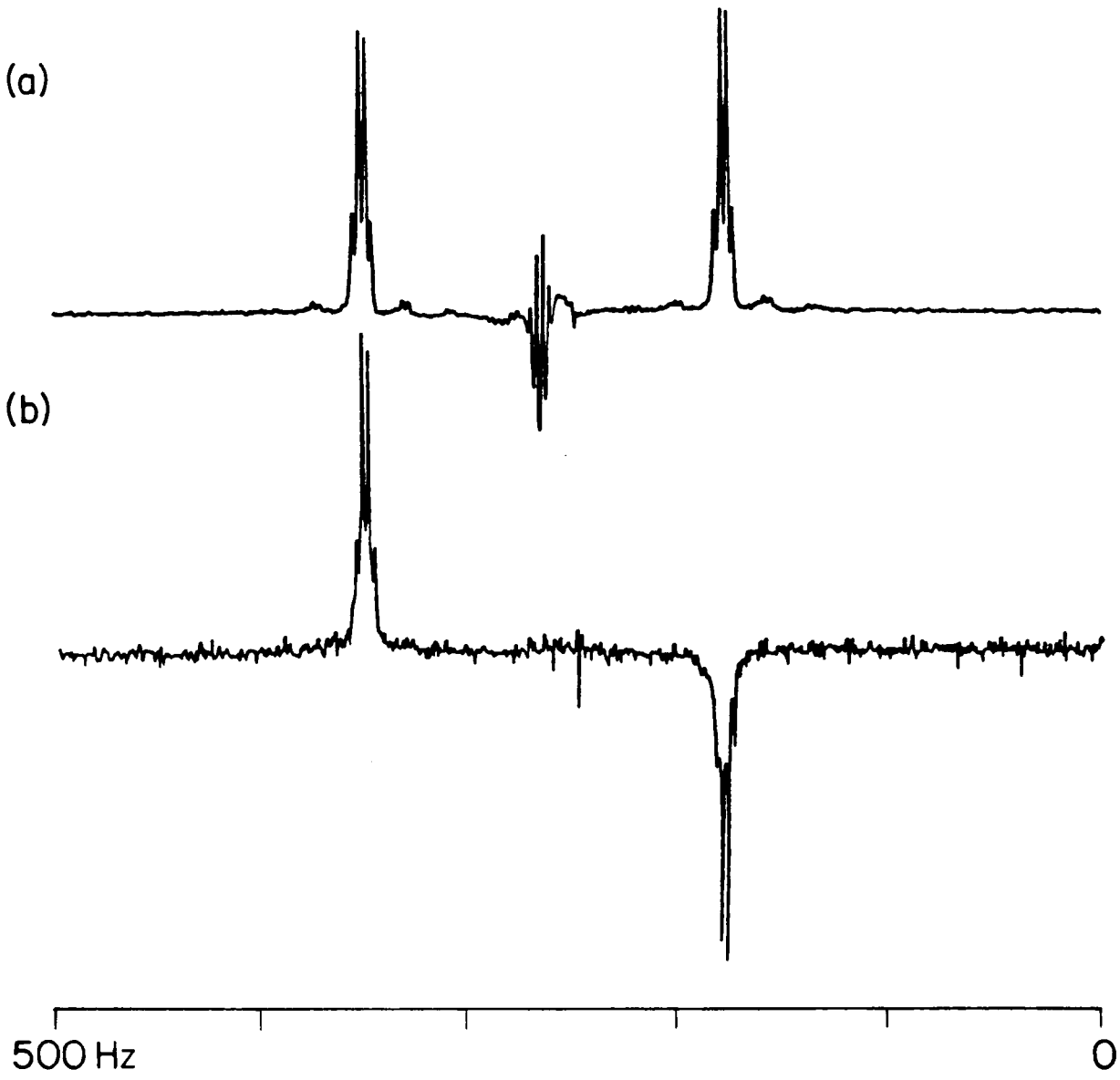

Figure 5.3 The carbon-13 satellite spectra of the aldehyde proton of acetaldehyde in a sample of natural carbon-13 abundance. (a) Observed by the method of spin echo difference spectroscopy (2048 transients), (b) observed by the method of reverse INEPT (64 transients). The direct CH coupling is 172 Hz.

compromise which gives a near-optimum signal intensity for all three cases [5.9].

Figure 5.3.a shows the satellite spectrum of the aldehyde proton of acetaldehyde obtained by the first of the two methods, spin-echo difference spectroscopy. Since it relies on subtraction to suppress the large parent signal, even a very small displacement of this signal in successive experiments leaves a residual signal in the centre. This suppression ratio on the order of 300 for the spectrum of figure 5.3.a is disappointing in view of the much better results obtained for carbon-13 satellites in carbon-13 spectroscopy [5.10].

Figure 5.3.b illustrates the better suppression obtainable with the reverse INEPT experiment, where only very weak signals from the parent resonance ever reach the receiver. The suppression ratio is of the order of 800. The antiphase nature of the two sides of the satellite spectrum is a distinctive feature of INEPT spectra; the two signals can be made to point in the same sense by a simple extension of the pulse sequence [5.10].

Using the type of argument introduced in the first section of this chapter, the relative sensitivity of the two experiments can be estimated. The signal-to-noise ratio for the reverse INEPT experiment with full nuclear Overhauser enhancement can be written as,

$$\xi_p' \sim \gamma_p^{3/2}\gamma_X B_0^{3/2}(1 + \frac{\gamma_X}{2\gamma_p})/(kT)^{3/2}. \qquad (5.9)$$

The spin echo difference experiment should have higher sensitivity by a factor,

$$\frac{\xi_p}{\xi_p'} \sim (\frac{\gamma_p}{\gamma_X})(1 + \frac{\gamma_X}{2\gamma_p})^{-1}. \qquad (5.10)$$

For carbon-13 this factor will be ~ 4/3 but for nitrogen-15 it will have the value ~ 10/4. So spin echo difference would have a significant advantage in signal-to-noise for the observation of nitrogen-15 satellites. In some molecular systems the longitudinal relaxation time, T_1, is shorter for protons than for either carbon-13 of nitrogen-15. This is especially true for quaternary carbons where long range couplings are of interest. In this situation because the spin echo difference experiment can be repeated at a rate determined by proton T_1's, it will have an advantage in efficiency over the reverse INEPT experiment which is repeated at a rate limited by the relaxation times of the heteronuclear spin of interest.

Both methods can be applied to weak long-range couplings by an appropriate increase in the τ delay. Direct and long-range couplings may be observed in the same spectrum by judicious choice of a long τ delay. However the results can be difficult to interpret in complex spectra where H-X and H-H coupling constants are of comparable magnitude. In the spin echo difference spectrum the satellite peaks will appear with positive intensity but will be modulated as a function of the H-H coupling constants leading to a complicated phase relationship for each pair of satellites. The reverse INEPT spectrum will not have problems from a phase distortion due to modulation by H-H coupling but the satellites will appear in antiphase on each side of the parent peak. For spectra with overlapping satellites, some signals might cancel making assignment difficult. If the antiphase satellites are refocussed, modulation by H-H coupling introduces phase distortion. These problems can be overcome with a technique in two-dimensional spectroscopy.

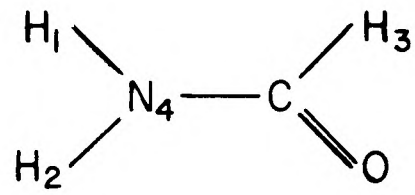

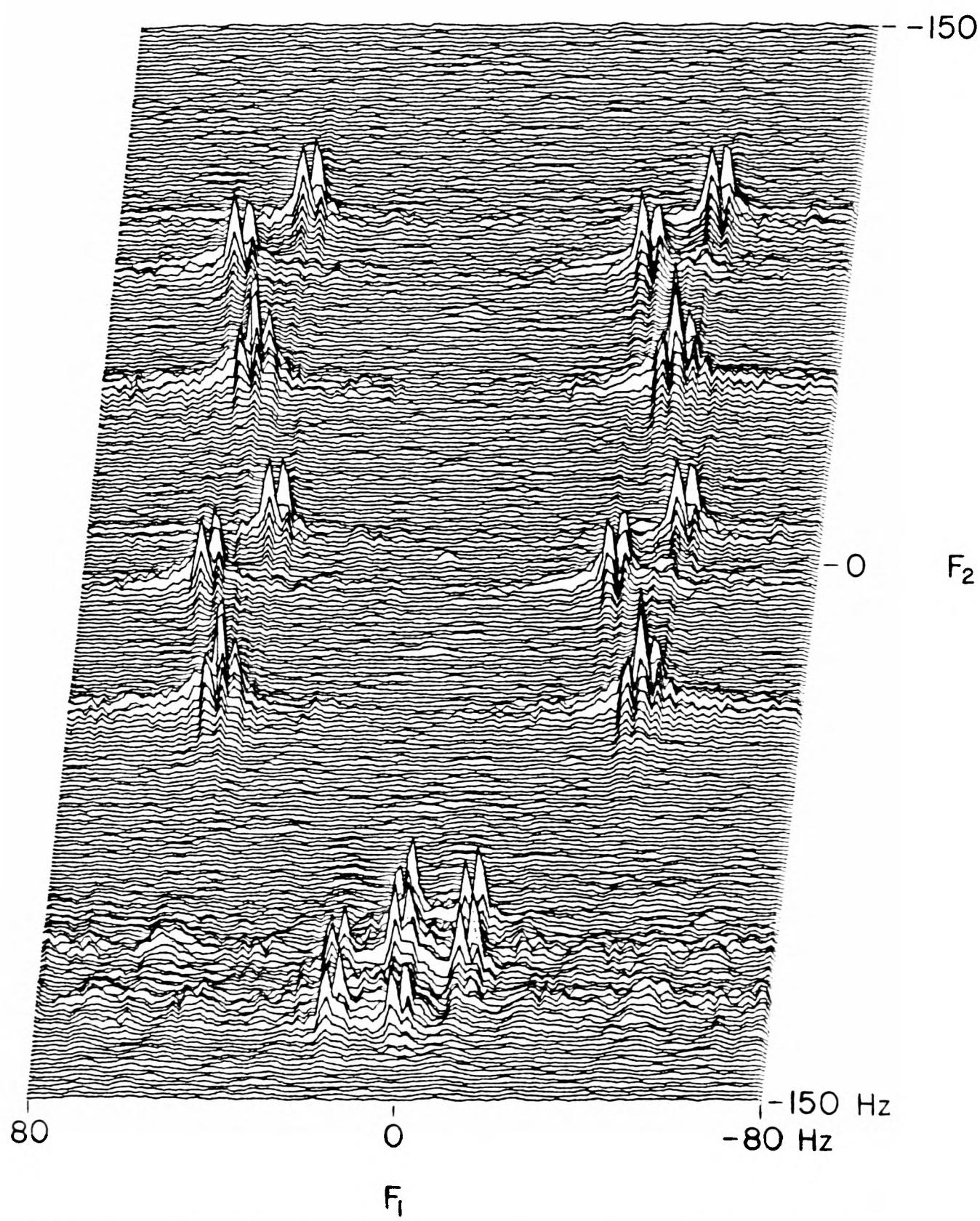

Figure 5.4 The two-dimensional proton spectrum of formamide (containing 20% dimethyl sulfoxide-d_6) obtained as described in the text. The structure of formamide is illustrated at the top of the figure. The total period of data acquisition was 20 hr. Note the high degree of suppression of the proton signals from the molecules containing nitrogen-14.

5.3. Two-dimensional observation of satellites in proton spectra

The interpretation of satellite spectra can be complicated when the X-H coupling constants are comparable in magnitude with the H-H coupling constants, which is usually the case for long-range X-H couplings. In this section a method for discriminating between the H-H and X-H splittings by a form of two-dimensional Fourier transform spectroscopy is examined. The procedure is illustrated by reference to nitrogen-15 satellites, but it is of course equally applicable to other heteronuclei, for example, carbon-13. The low natural abundance of nitrogen-15 provides a stringent test of the method, but it turns out that the shorter spin-spin relaxation times of protons attached to the quadrupolar nucleus nitrogen-14 make it somewhat easier to achieve a high degree of cancellation of the parent proton signals.

Proton spin echoes are excited by the usual $\frac{\pi}{2} - \pi -$ echo sequence [5.11] and are modulated through the effect of a π pulse applied to nitrogen-15 in synchronism with the proton refocussing pulse. Just before the acquisition of the second half of the spin echo, a similar π pulse is applied to nitrogen-15, once again interchanging the spin state labels on the proton satellites. The sequence is diagrammed below.

Proton	$(\frac{\pi}{2})_x - \frac{1}{2}t_1 - (\pi)_y - \frac{1}{2}t_1$	Acquisition($\pm$)
Nitrogen-15	$\frac{1}{2}t_1 - (\pi)_x - \frac{1}{2}t_1 - (\frac{\pi}{2})_{\pm x}(\frac{\pi}{2})_x$	

The entire sequence is then repeated 'without' the last π pulse , and with the receiver phase inverted in order to generate the difference spectrum in which the parent proton signals are suppressed. In actual practice, the alternation between π pulse and 0 pulse is effected by two $\frac{\pi}{2}$ pulses either in the same sense or in opposite senses; this introduced less interference with the deuterium field/frequency lock.

H-H couplings		N-H couplings	
J_{12}	= 2.5	J_{14}	= 90.4
J_{13}	= 2.0	J_{24}	= 87.7
J_{23}	= 13.7	J_{34}	= 14.4

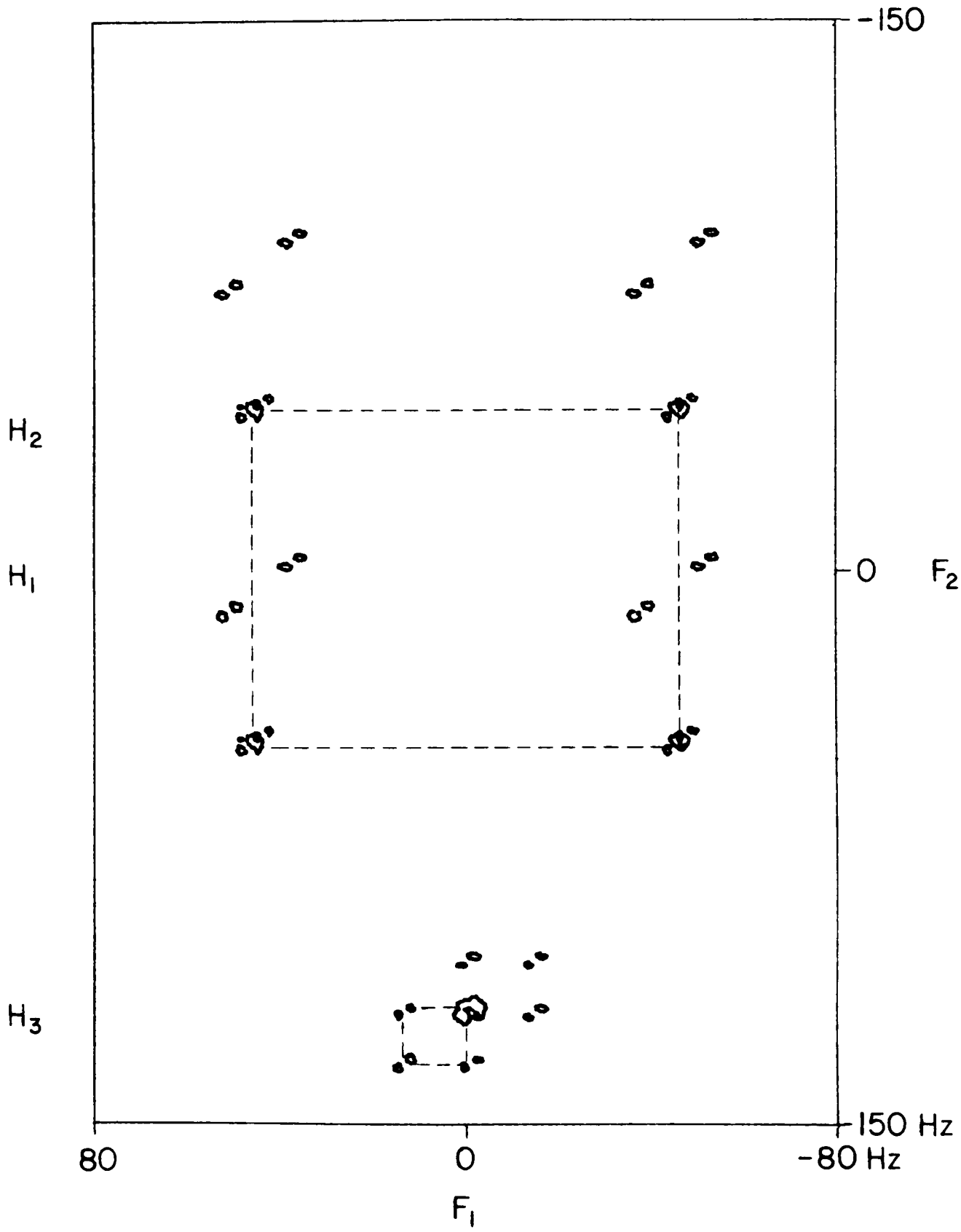

Figure 5.5 The data of figure 5.4 displayed as an intensity contour plot. All the H-H splittings lie on 45° diagonals, whereas N-H splittings form square patterns. Two such squares are sketched in, corresponding to couplings J_{14} = 90.4 Hz and J_{34} = 14.4 Hz. Analysis of this spectrum gives the coupling constants listed at the top of this figure for the numbering scheme of figure 5.4.

This dual sequence is then repeated at a series of different settings of the evolution period t_1 and a two-dimensional Fourier transformation is carried out, generating a two-dimensional spectrum. The frequency ordinates in the F_2 dimension are determined by proton chemical shifts, proton-proton and proton-nitrogen-15 coupling constants, the projection on this axis being the conventional nitrogen-15 satellite spectrum with the parent proton signals suppressed. In the F_1 dimension the spectrum contains no proton shift information, and in principle, field inhomogeneity broadening is greatly reduced by the refocussing effect of the proton π pulse. In practice, this resolution improvement is masked by the relatively coarse digitization in the F_1 dimension.

The method is illustrated by the nitrogen-15 satellite spectrum of the protons in formamide in figure 5.4 and 5.5. Proton-proton coupling acts in both frequency dimensions, generating spin multiplets which lie on a 45° diagonal. This is best appreciated in the contour diagram of figure 5.5. In contrast, nitrogen-proton multiplets lie on 45° diagonals but are also reflected in the vertical axis $F_1 = 0$. This is because the two-dimensional spectrum is essentially the superposition of two spectra, in one of which the precession attributable to N-H coupling has been effectively reversed [5.12] through the influence of the second π pulse applied to the nitrogen-15. Consequently, N-H splittings form a square pattern readily distinguished from the 45° slope of the H-H splittings. Such a distinction turns out to be very useful when the two types of splitting are of the same order of magnitude.

If the nuclei in formamide are labeled as shown at the top of figure 5.4, the coupling constants found by this method are as shown at the top of figure 5.5, in good agreement with earlier determinations [5.13], bearing in mind that these couplings are known to be

significantly dependent on the solvent.

In situations where the interest is in the large N-H coupling between directly bonded atoms, the pulse sequence described above can be employed in a one-dimensional mode by fixing t_1 equal to $1/(2J_{NH})$. At this time the two proton magnetization vectors corresponding to states of nitrogen-15 with $m_z = \pm 1/2$ are aligned along the $\pm$ x axes of the rotating frame, and a $(\frac{\pi}{2})_x$ proton pulse will turn the parent proton signal into the - z axis, leading to better suppression. However, there will be intensity distortions if the H-H couplings are of magnitudes comparable to those of the N-H couplings, or if there is a variation in the magnitudes of the N-H couplings.

The determination of N-H coupling constants can be very useful for the assignment of the conformation of biologically important molecules. The N-H couplings in nucleotides, within amino acid residues and across peptide linkages can be used to indicate the three-dimensional structure [5.14]. The present techniques allows these coupling constants to be more readily extracted from the proton spectrum.

References

[5.1] J. Feeney, D. Shaw and P. J. S. Pauwels, J. Chem. Soc. Chem. Comm., 554 (1970), R. Freeman and H. D. W. Hill, J. Magn. Reson. 5, 278 (1971)

[5.2] J. S. Waugh, J. Mol. Spectrosc. 35, 298 (1970)

[5.3] A. Abragram, The Principles of Nuclear Magnetism, Oxford University Press, London and New York (1961)

[5.4] J. H. Noggle and R. E. Schirmer, The Nuclear Overhauser Effect, Academic Press, New York (1971)

[5.5] R. Freeman, T. H. Mareci and G. A. Morris, J. Magn. Reson. 42, 341 (1981)

[5.6] T. H. Mareci and R. Freeman, J. Magn. Reson. 44, 572 (1981)

[5.7] M. Emschwiller, E. L. Hahn and D. Kaplan, Phys. Rev. 118, 414 (1960) R. Freeman and H. D. W. Hill, J. Chem. Phys. 54, 301 (1971)

[5.8] G. A. Morris and R. Freeman, J. Amer. Chem. Soc. 101, 760 (1979)

[5.9] R. Freeman and G. A. Morris, Bull. Magn. Reson. 1, 5 (1979)

[5.10] R. Freeman, Proc. Roy. Soc. London A373, 149 (1980)

[5.11] G. Bodenhausen, R. Freeman, R. Neidermeyer and D. L. Turner, J. Magn. Reson. 26, 133 (1977)

[5.12] P. Bachmann, W. P. Aue, L. Muller and R. R. Ernst, J. Magn. Reson. 28, 29 (1977)

[5.13] B. Sunners, L. H. Piette and W. G. Schneider, Can. J. Chem. 38, 681 (1960) R. J. Chuck, D. G. Gillies and E. W. Randall, Mol. Phys. 16, 121 (1969)

[5.14] G. C. Levy and R. L. Lichter, Nitrogen-15 Nuclear Magnetic Resonance Spectroscopy, Wiley-Interscience, New York, 1979

Appendix A

1. General density operator at thermal equilibrium in the high temperature limit

The general density operator in the high temperature limit can be developed from the operator form of the density matrix. First write the density matrix in the operator form as,

$$\rho = Z^{-1} e^{-H_0/kT} \tag{A.1}$$

where the partition function is given by, $Z = Tr(e^{-H_0/kT}) = \sum_n e^{-E_n/kT}$ and $H_0|\xi_n\rangle = E_n|\xi_n\rangle$. The sum is over all possible states, n, of the spin system. The Hamiltonian, H_0, for coupled spins in an external applied field, B_0, can be written as the sum of a Zeeman term, H_Z, and a coupling term, H_J,

$$H_0 = H_Z + H_J. \tag{A.2}$$

If the coupling is sufficiently weak compared to the Zeeman interaction the coupling term can be neglected when considering equilibrium populations of the energy levels. Therefore at thermal equilibrium the density operator can be written as,

$$\rho \simeq Z^{-1} e^{-H_Z/kT} \tag{A.3}$$

where explicitly $H_Z = -\sum_{j=1}^{N} \mu_j . B_0 = -\hbar \sum_{j=1}^{N} \gamma_j (I_z)_j B_0$ and the sum runs over all nuclei, j, of the spin system. Also define $\omega_j = -\gamma_j B_0$, therefore

the density operator becomes,

$$\rho = Z^{-1} e^{-\sum_{j=1}^{N} \hbar\omega_j (I_z)_j / kT} \tag{A.4}$$

and

$$Z = \sum_n \exp[-(\sum_{j=1}^{N} \hbar\omega_j (m_z)_j)_n / kT]. \tag{A.5}$$

The sum over the states, $\sum_n$, runs from total z-component of spin angular momentum equal to -I to I, where $I_z = (I_z)_1 + (I_z)_2 + \ldots + (I_z)_n$. In the high temperature limit the exponential in the density operator can be expanded and only terms to first order in temperature retained provided $[\sum_{j=1}^{N} \hbar\omega_j (m_z)_j] \ll kT$. In this limit the exponential term becomes,

$$\exp[-\sum_{j=1}^{N} \hbar\omega_j (m_z)_j / kT] \simeq 1 - \sum_{j=1}^{N} \frac{\hbar\omega_j}{kT} (m_z)_j. \tag{A.6}$$

The partition function, Z, can be written in this limit as,

$$Z = \sum_{n=-I}^{I} [1 - \sum_{j=1}^{N} \frac{\hbar\omega_j}{kT} (m_z)_j]. \tag{A.7}$$

The sum can be evaluated as follows,

$$Tr(1) = \sum_{n=-I}^{I} 1 = (2I + 1) \tag{A.8}$$

and

$$\sum_{n=-I}^{I} \left[\sum_{j=1}^{N} \frac{\hbar\omega_j}{kT} (m_z)_j \right]_n$$

$$= \frac{1}{kT} \hbar[\omega_1(m_z)_1 + \omega_2(m_z)_2 + \ldots + \omega_N(m_z)_N]_{-I}$$

$$+ \frac{1}{kT} \hbar[\omega_1(m_z)_1 + \omega_2(m_z)_2 + \ldots + \omega_N(m_z)_N]_{-I+1}$$

$$+ \ldots +$$

$$+ \frac{1}{kT} \hbar[\omega_1(m_z)_1 + \omega_2(m_z)_2 + \ldots + \omega_N(m_z)_N]_{I}. \qquad (A.9)$$

It can be seen that terms with total spin angular momentum of equal but opposite signs cancel hence this sum equals zero and the partition function in this limit becomes

$$Z = \mathrm{Tr}(\ 1\ ) = (2I + 1) \qquad (A.10)$$

and the density operator can be written in the high temperature limit as

$$\rho = (2I + 1)^{-1}\left(1 - \sum_{j=1}^{N} \frac{\hbar\omega_j}{kT} (I_z)_j\right). \qquad (A.11)$$

2. Reduced density operator

In the density operator formulation an observable of a system is calculated by taking the trace of the product between the operator for the observable and the density operator.

$$\langle O \rangle = \mathrm{Tr}\ (O\rho) = \sum_{i} \langle i|O\rho|i\rangle. \qquad (A.12)$$

The observables in magnetic resonance experiments are the components of magnetic moment, μ, which is proportional to the spin angular momentum, I. An observable arbitrary component of magnetic moment, μ_α, is given by

$$\langle \mu_\alpha \rangle \sim \mathrm{Tr}(I_\alpha \rho). \tag{A.13}$$

In the high temperature limit the density operator can be written as

$$\rho = \rho_0 + \rho_r \tag{A.14}$$

where $\rho_0 = (2I + 1)^{-1}$ and $\rho_r = f(I_\beta)$. This defines a reduced density operator as $\rho_r = \rho - \rho_0$ where ρ_r is a function, $f(I_\beta)$, of spin angular momentum components, I_β. In thermal equilibrium,

$$\rho_r = -(2I + 1)^{-1} \sum_{j=1}^{N} \frac{\hbar\omega_j}{kT} (I_z)_j \tag{A.15}$$

In the high temperature limit, the observable component of magnetic moment becomes,

$$\begin{aligned} \langle \mu_\alpha \rangle &\sim \mathrm{Tr}(I_\alpha \rho_0) + \mathrm{Tr}(I_\alpha \rho_r) \\ &= (2I + 1)^{-1} \mathrm{Tr}(I_\alpha) + \mathrm{Tr}(I_\alpha f(I_\beta)). \end{aligned} \tag{A.16}$$

The first term can be shown to be equal to zero for any component of spin so the observable reduces to

$$\begin{aligned} \langle \mu_\alpha \rangle &\alpha \mathrm{Tr}(I_\alpha f(I_\beta)) \\ &= \mathrm{Tr}(I_\alpha \rho_r). \end{aligned} \tag{A.17}$$

Experiments in high resolution NMR performed at room temperature will satisfy the condition for the high temperature limit to apply so that it is only necessary to calculate the reduced density operator, ρ_r to determine the state of the spin system.

The system evolves according to the equation of motion of the

density operator,

$$\frac{\partial \rho}{\partial t} = \frac{\partial \rho_r}{\partial t} = \frac{i}{\hbar} [H , \rho_r] \qquad (A.18)$$

so that in the high temperature limit all the time dependence is contained in the reduced density operator and all calculations can be carried out using the density operator in this form.